A Thesis Entitled

# Biogeochemical Controls on Productivity and Particle Flux in the Coastal Antarctic Sea Ice Environment

A Thesis Submitted for the Degree of
Doctor of Philosophy

by

Damien Stuart Carson, *BSc (Hons)*


School of Geosciences
Faculty of Science and Engineering
The University of Edinburgh
2009

## Declaration

I certify that the work described in this thesis is my own, except where otherwise stated, and has not been previously submitted for any other degree at this, or any other university.

Damien Stuart Carson

**Abstract**

In order to trace modern processes in the ocean and reconstruct past oceanic conditions, reliable tracers of oceanic processes such as productivity, nutrient utilisation and export production need to be developed. This study therefore assessed a suite of geochemical proxies in the coastal Antarctic sea ice environment over two growing seasons (2004-2006). Time series measurements of productivity and export production were carried out over two contrasting growing seasons in Ryder Bay, a coastal embayment on the Western Antarctic Peninsula with a heavy sea ice influence. Ryder bay exhibits intense primary production during the short ice-free spring and summer months and particle export occurs as an intense period of sedimentation following surface water productivity, similar to many other coastal Antarctic environments. The two growing seasons were preceded by different sea ice regimes, with lighter sea ice cover during winter 04 and extended sea ice cover during winter 05. This resulted in a dynamic water column during the 04/05 growing season with frequent nutrient inputs to the surface, and a more stable, stratified water column during the 05/06 season with a few minor nutrient inputs to the surface. In response to these changes in the water column, higher mass fluxes occurred during the 04/05 season due to higher nutrient availability, with much lower fluxes occurring during the 05/06 season after the extended sea ice cover during the preceding winter.

Variability of $\delta^{13}C_{POC}$ at this site is not caused by changes in $[CO_{2(aq)}]$ or $\delta^{13}C$-$CO_2$, but appears to be affected by changes in diatom assemblages with different surface area to volume ratios and biochemical pathways for C fixation. Although the $\delta^{13}C_{POC}$ signal in surface waters is transferred to depth, these findings preclude the use of $\delta^{13}C$ as a tracer of paleo-$pCO_2$ concentration. $\delta^{15}N$, the proxy for nitrate utilisation in the Southern Ocean shows a predicted response to nutrient utilisation and the physical properties of the water column in each season, with each season displaying a different evolution of $\delta^{15}N$ over the course of spring and summer. However, this proxy for utilisation of nitrate does not reflect the absolute changes in C flux. It is

therefore necessary to consider this scenario when making connections between nitrate utilisation and changes in atmospheric $CO_2$ in sediment cores.

This study also better constrained the biogeochemical cycling of Ba in the coastal Antarctic sea ice environment. $Ba_{XS}$ formation in surface waters appears related to productivity, but appears to peak during periods of early decay of phytoplankton when barite is formed. Standing stocks of $Ba_{XS}$ in sea ice are consistently an order of magnitude higher than surface waters and display higher than average Ba:POC ratios than surface waters. The formation of barite in the water column appears to be linked to the decay of organic matter and precipitation of barite in supersaturated micro-environments. Finally, the flux of $Ba_{XS}$ relative to carbon in the coastal Antarctic sea ice environment is consistent with algorithms published for the open ocean.

This study has successfully identified mechanisms that affect the attenuation of proxy signatures in coastal Antarctic sediments. However, extreme inter-annual variability also highlights the need for further long-term monitoring of elemental and isotopic tracers in the coastal Antarctic sea ice environment, in order to establish longer term trends and truly establish the effect of differences in sea ice extent.

In addition to the work in Ryder Bay, this thesis also includes a case study on the Antarctic sediment core MD03-2601 from Adélie Land, East Antarctica. This 40 m Holocene core has an exceptionally high sedimentation rate and is heavily influenced by sediment focusing. Using careful corrections to remove the influence of lateral input of material, and redox sensitive tracers to identify any anoxic sections of the core, paleoproductivity reconstructions were carried out using carbon, opal and Ba tracers of export production. The results are consistent with the climatic phases of the Holocene and present a valuable case study suggesting that these proxies are useful, either

quantitatively or qualitatively, for reconstructing paleoproductivity on a core heavily affected by focusing and containing periods of sedimentary oxygen deficiency.

**Acknowledgements**

Firstly, I would like to thank Dr. Raja Ganeshram for providing me with the opportunity to work towards a PhD, and for trusting me with such an exciting project which required significant time away in the field, unsupervised! His constant enthusiasm, geochemical prowess, and guidance, inspired me to prepare a thesis I am proud of. Thank you also to my co-supervisors, Dr. Bryne Ngwenya, Prof. Tim Jickells, Prof. Harry Elderfield, and my advisor Dr. Mary Elliot.

My sincerest gratitude is given also to the British Antarctic Survey and the staff of Rothera Research Station from 2004-2006. In particular, I would like to thank (in no particular order) Paul Mann, Andy Miller, Dan Smale, Matt Brown, John Withers, Kate Hendry, Joanna Coldron, Keith Weston, Andy Wilson, Bernard Meehan and Andy Barker. Not only do I appreciate your assistance with my work, but also your friendship during the long seasons on the frozen continent.

Completing the amount of laboratory analysis required for this project would not have been possible without the following people: Colin Chilcott (Edin), Amber Annett (Edin), Nic Odling (Edin), Tony Fallick (SUERC), Andrew Tait (SUERC), Julie Douggans (SUERC), Xavier Crosta (Bordeaux), Delphine Denis (Bordeaux), and Prof. Daniel Sigman (Princeton). Special thanks is also reserved for Jim Smith and Alan Pike, two of the most useful and undervalued members of the School of GeoSciences at the University of Edinburgh.

A big thank you to my partners in oceanographic crime: Elsa Arrelano-Torres, Laetitia Pichevin, Tom Russon, Amber Annett and Kevin Welsh. The office(s) wouldn't have been the same without you.

I would especially like to thank my mum, Lynda, and my dad, Gary, for guiding me safely to trainee adulthood. Finally, Fiona, your love and support made this thesis possible, and knowing you were always there, especially during my long seasons in Antarctica, kept me sane.

**Table of Contents**

**Declaration** ..... **i**

**Abstract** ..... **ii**

**Acknowledgements** ..... **v**

**Table of Contents** ..... **vi**

**1 Introduction** ..... **1**

1.1 Overview ..... 1

1.2 Rationale and Motivation for this Study ..... 1

1.3 Sea Ice ..... 3

1.4 Coastal Antarctic Sea ice Environment ..... 5

1.5 Stable Isotopes of Carbon and Nitrogen ..... 7

1.6 $\delta^{13}C$ in the Southern Ocean ..... 9

1.7 $\delta^{15}N$ in the Southern Ocean ..... 11

1.8 Barium ..... 13

1.9 Thesis Outline ..... 17

1.10 References ..... 18

**2 Field Work** ..... **25**

2.1 Introduction ..... 25

2.2 Field Seasons ..... 26

2.3 Surface Water Sampling ..... 26

2.4 Sea Ice Sampling ..... 27

2.5 Measured Parameters ..... 28

2.6 Research Cruises Aboard the RRS James Clark Ross ..... 28

2.7 Sediment Trap Mooring Arrays ..... 28

2.8 Box Coring ..... 33

2.9 References ..... 34

**3 Inter-Annual Variability of Productivity and Particle Flux in Ryder Bay, Antarctica** ..... **35**

3.1 Introduction ..... 36

3.2 Materials and Methods ..... 37

3.2.1 Sea Ice Sample Collection ..... 38

3.2.2 Surface Water Sample Collection ..... 39

3.2.3 Sample Analysis ..... 39
3.2.4 Sediment Trap Deployments ..... 40
3.3 Results ..... 41
3.3.1 Sea Ice ..... 43
3.3.2 Surface Waters ..... 44
3.4 Discussion ..... 52
3.5 Conclusions ..... 56
3.6 References ..... 56
**4 Factors Influencing $\delta^{13}C$ of suspended and sinking Organic Matter in the Coastal Antarctic Sea Ice Environment ..... 61**
4.1 Introduction ..... 63
4.2 Materials and Methods ..... 64
4.2.1 Study Area ..... 64
4.2.2 Sea ice Sampling ..... 66
4.2.3 Surface Water Sampling ..... 67
4.2.4 $[CO_{2(aq)}]$ Analysis ..... 67
4.2.5 $\delta^{13}C$-$CO_2$ Determination ..... 68
4.2.6 POC, PON and $\delta^{13}C_{POC}$ Analysis ..... 68
4.2.7 Diatom Census Counts ..... 69
4.2.8 Sediment Trap Deployments ..... 69
4.2.9 Sediment Organic Carbon and $\delta^{13}C_{org}$ Analysis ..... 70
4.2.10 Sedimentary Diatom Census Counts ..... 70
4.3 Results ..... 71
4.3.1 Seasonal Sea Ice Cover and Productivity ..... 71
4.3.2 $[CO_{2(aq)}]$ and $\delta^{13}C$-$CO_2$ ..... 72
4.3.3 Suspended Particulate Organic Carbon (POC) ..... 73
4.3.4 Surface water $\delta^{13}C_{POC}$ and $[CO_{2(aq)}]$ ..... 75
4.3.5 Sinking Particulate Organic Carbon and $\delta^{13}C_{org}$ ..... 80
4.3.6 Sediment Trap Diatom Assemblages ..... 81
4.4 Discussion ..... 86
4.4.1 $\delta^{13}C$ in Surface Waters and Sea Ice ..... 86
4.4.2 Sinking Particulate Carbon ..... 91

4.4.3 Potential Implications for $\delta^{13}C$-based $pCO_2$ Reconstructions in the Southern Ocean ..... 93
4.5 Conclusions ..... 94
4.6 References ..... 95
**5 $\delta^{15}N$ of Nutrients and Organic Matter as Proxies for Productivity and Export Production in the Coastal Antarctic Sea Ice Environment . 100**
5.1 Introduction ..... 101
5.2 Materials and Methods ..... 103
5.2.1 Study Area ..... 103
5.2.2 Sea Ice Sampling ..... 105
5.2.3 Surface Water Sampling ..... 105
5.2.4 $NO_3$, $NH_4$ and $pCO_2$ Determination ..... 106
5.2.5 $\delta^{15}N$-$NO_3$ Determination ..... 107
5.2.6 Bulk POC/PON and $\delta^{15}N_{PON}$ Determination ..... 108
5.2.7 Sediment Trap Deployments ..... 108
5.2.8 Box Cores ..... 109
5.2.9 Sediment Organic Carbon Nitrogen and $\delta^{15}N_{org}$ Determination ..... 109
5.3 Results ..... 110
5.3.1 Growing Seasons 2004-2006 ..... 110
5.3.2 Sea Ice ..... 111
5.3.3 Surface Waters ..... 112
5.3.4 Sinking Particulate C/N and $\delta^{15}N$ ..... 119
5.4 Discussion ..... 124
5.4.1 Sea Ice Nitrogen Isotope Biogeochemistry ..... 125
5.4.2 Surface Water Nitrogen Isotope Biogeochemistry ..... 127
5.4.3 Nutrient Sources ..... 129
5.4.4 $NO_3$ Utilisation and $CO_2$ Drawdown ..... 130
5.4.5 Sinking Particulate $\delta^{15}N$ and Export Fluxes ..... 132
5.4.6 Open versus Closed System $\delta^{15}N$ ..... 133
5.5 Conclusions ..... 136
5.6 References ..... 136

**6 Particulate Barium Transformations and Fluxes in the Continental Shelf Antarctic Sea Ice Environment ..... 141**

6.1 Introduction ..... 142

6.2 Materials and Methods ..... 145

6.2.1 Dissolved Ba Determination ..... 146

6.2.2 Particulate Barium and Aluminium ..... 147

6.2.3 Sequential Leaching of Barium ..... 147

6.2.4 HF Digestion of Material ..... 148

6.2.5 Sediment Trap Material and Surface Sediments ..... 148

6.2.6 Analysis of Barium and Aluminium ..... 149

6.2.7 $Ba_{XS}$ Determination ..... 149

6.2.8 Suspended Particulate Organic Carbon ..... 150

6.3 Results ..... 151

6.3.1 Crustal Ba:Al Determination ..... 151

6.3.2 Surface Waters and Sea Ice ..... 152

6.3.3 Sediment Traps ..... 162

6.3.4 Box Cores ..... 167

6.4 Discussion ..... 167

6.4.1 Sea Ice Associated Particulate $Ba_{XS}$ ..... 167

6.4.2 Surface Water Barium Seasonality ..... 170

6.4.3 Sinking Particulate $Ba_{XS}$ ..... 172

6.4.4 Conclusions ..... 177

6.5 References ..... 177

**7 Reconstructing paleoproductivity throughout the Holocene: A case study from Adélie Land, East Antarctica ..... 182**

7.1 Introduction ..... 183

7.2 Proxies ..... 184

7.3 Materials and Methods ..... 186

7.3.1 Age Model ..... 187

7.3.2 Diatom Census Counts ..... 187

7.3.3 Organic Carbon and Biogenic Opal Measurements ..... 187

7.3.4 Elemental Analysis ..... 188

7.3.5 Sediment fluxes normalisation ..... 188
7.4 Results ..... 191
7.5 Discussion ..... 195
7.5.1 Biogenic Flux Reconstructions ..... 195
7.5.2 Preservation Versus Export/Production Changes ..... 199
7.5.3 $Ba_{XS}$ Proxy Sensitivity ..... 200
7.5.4 Opal:$C_{org}$ Decoupling ..... 201
7.6 Conclusions ..... 202
7.7 References ..... 203
**8 Conclusions ..... 211**
8.1 Productivity and Particle Flux ..... 211
8.2 Carbon and $\delta^{13}C$ in the Coastal Antarctic Sea Ice Environment ..... 213
8.3 Nitrogen and $\delta^{15}N$ in the Coastal Antarctic Sea Ice Environment ..... 214
8.4 Barium Biogeochemistry in the coastal Antarctic Sea Ice Environment 215
8.5 Summary of Proxy Findings in Ryder Bay ..... 217
8.6 Reconstructing Paleoproductivity in Core MD03-2601 ..... 219
8.7 Future Considerations ..... 220
**9 Appendices ..... 221**
9.1 Appendix 1. Full list of sampling events during the 2004/2005 field season. ..... 221
9.2 Appendix 2. Full list of sampling events during the 2005/2006 field season. ..... 222
9.3 Appendix 3. List of sea ice sampling events during the 2004/2005 and 2005/2006 field seasons. ..... 223
9.4 Appendix 4. List of Measured Parameters out with the RaTS programme measured for surface water and sea ice samples. ..... 224
9.5 Appendix 5. Sea ice time-series N data from the 04/05 and 05/06 growing season. ..... 225
9.6 Appendix 6. Surface water time series N data for the 04/05 growing season. ..... 226

9.7 Appendix 7. Surface water time-series N data for the 05/06 growing season. ..... 227

9.8 Appendix 8. Sediment Trap flux data and $\delta^{15}N_{org}$ from the RaTS Site throughout the duration of this study. ..... 228

9.9 Appendix 9. Sediment Trap flux data and $\delta^{15}N_{org}$ from the Deep Site throughout the duration of this study. ..... 229

# 1 Introduction

## 1.1 Overview

This thesis investigates the key biogeochemical mechanisms controlling productivity and particle flux in the coastal Antarctic sea ice environment. High resolution time series analysis of sea ice, surface waters and sediment traps over two growing seasons coupled with analysis of sediment cores, opened up the coastal sea ice environment to thorough geochemical inspection. Using the data sets the key mechanisms that control the stable isotope and elemental composition of organic matter were identified. The data have important implications regarding the interpretation of Southern Ocean sediment records and relating them to past surface water conditions, which are discussed in detail throughout the forthcoming chapters.

## 1.2 Rationale and Motivation for this Study

Understanding modern day cycling of nutrients, organic matter, stable isotopes and other elements in the ocean and how this information is transferred during sinking of suspended particles and sedimentation, has allowed us to develop an understanding of what the Southern Ocean was like during different periods of earth's history. Information locked up in sediment cores has the potential to give a quantitative and chronological insight into the conditions of the ocean in the past. The information provided by cores can relate to variables such as nutrient utilisation, export production, phytoplankton assemblages, ocean circulation, ocean temperature, and ocean alkalinity to give some examples. Paleoceanographic investigation of the Southern Ocean have uncovered vast quantities of data that are used to form hypotheses of how the Southern Ocean influenced, or was influenced by, glacial to interglacial cyclicity e.g.(Anderson, et al., 2002; Anderson, et al., 1998; Crosta, et al., 1998; Crosta, et al., 2002; De La Rocha, et al., 1998; Ellwood and Hunter, 2000; Falkowski, 1997; Francois and Altabet, 1992; Francois, et al., 1997; Kumar, et al., 1995; Rau, et al., 1991; Robinson, et al., 2004; Robinson, et al., 2005; Rosenthal, et al., 2000; Schneider-Mor, et al.,

2005; Sigman and Boyle, 2000; Sigman, et al., 2004). There are a variety of theories that attempt to explain how the Southern Ocean influenced atmospheric $CO_2$ during glacial/interglacial cycles, for example;

- An increase in Southern Ocean carbon export, resulting in more carbon dioxide being sequestered in sediments to help lower atmospheric $CO_2$, this may have been caused by iron fertilisation;
- Changes in stratification that resulted in the reduction of $CO_2$ outgassing from ocean to atmosphere through a decrease in vertical mixing;
- Increased sea ice cover, both spatially and temporally, reducing the area of Southern Ocean that could exchange with the atmosphere, again reducing $CO_2$ outgassing.

Paleoproductivity reconstructions of the Southern Ocean are hampered by contradictions between the different proxies. For example, the stable isotopic composition of nitrogen ($\delta^{15}N_{org}$), a proxy for nitrate utilisation, suggests that a higher proportion of available nitrate was consumed during glacial periods (Francois and Altabet, 1992; Robinson, et al., 2005), consistent with the theory that higher nutrient utilisation promoted $CO_2$ drawdown and sequestered this carbon in sediments. However, studies applying other proxies inferred no change or a reduction in nutrient utilisation (De La Rocha, et al., 1998; Elderfield and Rickaby, 2000; Ellwood and Hunter, 2000). Francois et al., (1997) proposed the theory that Southern Ocean stratification was heightened during glacial periods, hypothesising that this was consistent with lowering of atmospheric $CO_2$ as the deeper waters rich in $CO_2$ were not exposed to the atmosphere. The stratification theory also implies the upper mixed layer of the glacial Southern Ocean would have a reduced supply of nutrients, thus explaining the high $\delta^{15}N_{org}$ of glacial Southern Ocean Sediments, as a higher proportion of the reduced nutrient supply would have been utilised. With the examples given above, more research is essential in order to develop new paleoceanographic proxies and to constrain exactly

how classic proxies, such as $\delta^{15}N$, applied to sediment cores should be interpreted.

Therefore this study was designed to test the validity of a suite of stable isotope and elemental proxies in the coastal Antarctic sea ice environment. Most proxy algorithms are based on open water conditions in the deep ocean, here we conduct a high resolution time-series analysis of biogeochemical cycling in sea ice and surface waters and monitor the export of these geochemical signals to depth and sedimentation. This was done with the hypothesis that proxy signals in the coastal sea ice environment are affected by different processes (extended sea ice cover, grazing, glacial melt, intra-seasonal variability, etc) than the rest of the Southern Ocean and therefore interpretation of sedimentary geochemical signals will not conform to broader scale open ocean relationships.

### 1.3 Sea Ice

Sea ice cover around Antarctica is one of the most seasonal geophysical parameters on the Earths surface, with coverage ranging from $18.8 \times 10^6$ km$^2$ during austral winter to $3.6 \times 10^6$ km$^2$ during austral summer (Comiso et al., 1998). Sea ice acts as a blanket, covering the ocean surface and affects the fluxes of heat and moisture across the ocean-atmosphere boundary (Wu et al., 1997). Sea ice presence also strongly increases the albedo of the Southern Ocean, acting as a reflector of heat (Ebert et al., 1995), especially during the spring and summer months. Rejection of brine (super saline water) during sea ice formation, and freshwater input to the ocean during sea ice melting are also considered to strongly affect thermohaline circulation (Keeling and Stevens, 2001). In addition to the physical affects, sea ice also strongly influences the timing, magnitude and species composition of primary production in Southern Ocean waters (Arrigo et al., 1998; Crosta et al., 2007; Kim et al., 2005; McMinn, 1996) as well as playing a major role in structuring the Antarctic food web (Ducklow et al., 2006; Eicken, 1992). The sea ice covered Southern Ocean promotes a stable surface water environment

during spring and summer growing seasons. Freshwater delivery to the ocean surface after sea ice melting stratifies the ocean surface and strongly favours diatoms as the main phytoplankton group growing in sea ice and surface waters (Wright and Van Der Enden, 2000). Diatoms within sea ice may also account for a significant proportion of Southern Ocean primary production (Arrigo et al., 1997), which may account for up to 5 % of total Southern Ocean biogenic carbon production, and can account for up to 25 % of total primary production in heavily ice covered areas (Arrigo et al., 1995).

Sea ice is strongly influenced by climate, and changes in sea ice are thought to have been significant during previous glacial to interglacial cycles (Crosta et al, 1998) and during the different climatic periods of the Holocene (Crosta et al., 2007).

Most geochemical proxies used to reconstruct productivity, nutrient utilisation and export production have been developed studying the open ocean (e.g. De La Rocha et al., 1998; Francois et al., 1992; Rau, 1994). It is therefore essential to understand how changes in sea ice cover may affect the geochemical composition of organic matter exported from the surface ocean in response to productivity.

Sea ice has the potential to affect the elemental and stable isotopic composition of organic matter produced in the surface ocean both directly and indirectly. Growth of phytoplankton within the sea ice matrix (mainly diatoms) often occurs within a closed or semi-closed system, which can lead to high levels of nutrient utilisation if phytoplankton growth is abundant. Previous studies have shown that increases in the stable isotopic composition of organic carbon ($\delta^{13}C$) and nitrogen ($\delta^{15}N$) of organic material within the sea ice matrix are a result of high nutrient utilisation (Fischer et al., 1991; Gibson, et al., 1999). In addition changes in the elemental composition of organic matter (C:N ratio) have also been observed in the ice matrix (Kennedy et al., 2002). If the composition of this material is faithfully

exported to the sea floor after sea ice decay and melting, this may have a notable influence on the composition of the seasonal flux compared to the open water produced material alone.

The seasonality of sea ice can also significantly affect the dominant phytoplankton species that compose the spring and summer growing season (e.g. Crosta et al., 2005; Crosta et al., 2007). Evolution of Southern Ocean diatom assemblages in response to sea ice change can lead to marked variations in the elemental composition of the exported flux, e.g. opal:C (Armand et al., 2008) and the $\delta^{13}C$ composition of organic matter (Burkhardt et al., 1999; Cassar et al., 2006; Popp et al., 1998).

One of the goals of this study is to identify the key mechanisms that give sea ice associated organic material such different geochemical characteristics that open water associated organic material, and whether the sea ice material significantly influences annual flux in the coastal Antarctic sea ice environment.

### 1.4 Coastal Antarctic Sea ice Environment

The Antarctic continental shelves are regions of intense biological activity and biogeochemical cycling, and constitute high levels of primary production (Arrigo et. al., 1998; Vernet, et. al., in-press), drawdown of $pCO_2$ (Arrigo et. al., 1999) and intense "pulses" of sedimentation (Ducklow et al., in-press). In addition the continental shelves surrounding Antarctica are one of the global oceans richest reservoirs of biogenic opal, due to high primary productivity that is dominated by diatoms (Broecker, 1982)

Ryder Bay, the main study area for this thesis, is located south of Alexander Island and west of the mainland on the Western Antarctic Peninsula (WAP) (Clarke et al., *in-press*). Ryder Bay is a coastal embayment adjoining Marguerite Bay and the main study site is situated in open water at a maximum depth of 520 m. The WAP is unusual compared with most regions of Antarctica because of it's proximity to the Antarctic Circumpolar Current

(ACC) (Martinson, et al., *in-press*). Waters from the ACC can intrude directly onto the WAP continental shelf, with Circumpolar Deep Water (CDW), the water mass that occupies the mid-levels of the ACC being the most common. This is usually divided into Upper (shallower) and lower components (UCDW and LCDW respectively), with UCDW being characterised by a maximum in potential temperature and high nutrient content (Meredith et al., 2004). Incursions of UCDW, the most common water mass supplying heat and nutrients to the surface in the WAP continental shelf. UCDW floods large areas of the WAP, including Ryder Bay and Marguerite Bay almost every year, and appears to be a consistent feature of shelf oceanography in this region (Ducklow et al., 2007).

The uppermost waters over the continental shelf are typically very much colder and fresher than UCDW, because of interaction with the atmosphere and cryosphere. Traditionally termed Antarctic Surface Waters (AASW), they typically cool and gain salt from sea ice formation as summer moves to winter, then warm and freshen from winter to summer (Klinck 1998). The AASW is thus thermally highly variable and solar heating can lead to strong stratification with relatively warm surface layers in summer (Meredith et al., 2004). The creation of a relatively warm and fresh surface layer during summer leads to isolation of the remnant cold winter mixed layer from the atmosphere, termed Winter Water (WW). The coastal oceanography of this region is thus dominated by the AASW at depths down to 100 m, including WW at lower levels.

A second important factor in the oceanography of the WAP is annual sea ice retreat and its proximity to large quantities of glacial ice on land, and hence the influence of meltwater (Meredith et al., *in-press*). It is known that the seasonal variability in the volume and spatial extent of glacial meltwater plays a critical role in oceanic ecosystem processes, particularly primary production (Dierssen et al., 2002), and also that water column stability and a shallow mixed layer are essential to phytoplankton bloom development (Mitchell and

Holm-Hansen, 1991). The addition of a thin lens of freshwater to the ocean surface will greatly increase it's stability, thereby retaining phytoplankton within a favourable light environment by preventing mixing to depths where light is limiting.

Despite many years of investigation, most biological and biogeochemical studies of the Southern Ocean concerning productivity, $CO_2$ variations and export production, especially in continental shelf regions, have been limited to ice free seasons and very few studies go beyond a single year. Recently, there have been two very useful studies documenting long-term monitoring of regions of the Western Antarctic Peninsula (WAP) (Clarke et. al., in-press; Ducklow, et. al., in-press), but many observations remain without explanation, for example why the peak flux period in the WAP is now roughly 40 days later than in 1993. The WAP is a very important region of Antarctica to climate and ocean scientists, as it has experienced the highest rate of warming (3°C) over the last 50 years (Turner et. al., 2005), so understanding the mechanisms affecting sea ice seasonality, primary production and particle export are essential in order to understand how future warming or other aspects of climate change may affect this ecosystem.

The high inter-annual variability observed in the continental shelf, Antarctic sea ice environment makes generalisation about annual primary production and export production very difficult. More long-term monitoring programmes are required to identify the mechanisms affecting sea ice extent, changes in circulation and mixing of water masses, phytoplankton assemblages, primary production and export production.

### 1.5 Stable Isotopes of Carbon and Nitrogen

The stable isotope composition of carbon and nitrogen in organic and inorganic forms is a common technique used to trace processes occurring in the carbon and nitrogen cycle in the marine environment, such as nutrient utilisation. Carbon and nitrogen each have two stable isotopes, with $^{12}C$ and $^{13}C$ comprising 98.89 % and 1.11 % and $^{14}N$ and $^{15}N$ comprising 99.64 % and

0.36 % of the total natural abundance respectively (Faure et al., 1986). Because of the size of this abundance gap, the ratios of $^{13}C$ to $^{12}C$ and $^{14}N$ to $^{15}N$ in carbon or nitrogen compounds are expressed in the delta notation as per mil" (‰) differences relative to reference standards, where;

$$\delta^{13}C = [\{(^{13}C/^{12}C)_{sample} - (^{13}C/^{12}C)_{standard}\} / (^{13}C/^{12}C)_{standard}] \times 1000; \text{ and}$$
$$\delta^{15}N = [\{(^{15}N/^{14}N)_{sample} - (^{15}N/^{14}N)_{standard}\} / (^{15}N/^{14}N)_{standard}] \times 1000$$

In general, isotopic proxies of nutrient utilisation work on the principle that, in a reservoir of finite size, the preferential removal of one isotope over another result in an increasing enrichment of the remaining isotope as the reservoir is depleted, a process known as Rayleigh distillation. The interpretation of stable isotope values hinges on accurate measurements of kinetic isotope effects, where the isotopic composition of the product varies as a result of reaction rate. Rayleigh Distillation is calculated by;

$$R_f / R_o = f^{(\alpha-1)}$$

Where $f$ is the fraction of remaining reactant, $R_f$ is the del value of the reactant at an $f$ value and $R_o$ is the del value when $f$=1 (i.e. prior to the removal of any reactant).

The marine carbon and nitrogen cycles are largely controlled by biological processes and are regulated by kinetic fractionations. Fractionation is caused by the slight physicochemical differences that exist amongst the isotopes of an element ($^{12}C$ and $^{13}C$, and $^{14}N$ and $^{15}N$), the slight mass difference causes the activation energies of molecules and their chemical bonds to differ (Galimov, 1985). As a result, the chemical bonds in the lighter isotopes of an element react relatively faster, so phytoplankton preferentially uptake the lighter isotope of an element causing the products to become enriched in the lighter isotope and the remaining pool of reactants to become enriched in the heavier isotope (Wada and Hatori, 1978; Burkhardt et al, 1999).

The extent of isotopic fractionation is highly dependant on environmental variables including temperature, the size of the reservoirs of various compounds involved in the reactions and the number of intermediate steps in the reaction(s). Interpreting changes to the stable isotopic (C and N) composition of nutrients and organic matter relative to productivity in the marine environment is complicated by the effects of changes to the fractionation factor ($\varepsilon_p$) during both physical and biological processes. Understanding the mechanisms that may affect such changes in fractionation are essential in order to use stable isotopes as tracers of oceanic processes, and are discussed herein.

### 1.6 $\delta^{13}C$ in the Southern Ocean

The stable carbon isotopic composition of sedimentary organic carbon ($\delta^{13}C_{org}$) was initially developed as a tracer for changes in $pCO_2$ of surface waters (Rau et al, 1991; Rau et al., 1994) and was used to infer changes in atmospheric $CO_2$ over glacial to interglacial cycles. Higher $\delta^{13}C_{org}$ in low latitude ocean sediments during the last glacial maximum (LGM) was attributed to the lowering of atmospheric $CO_2$ and the 1-2 ‰ change in $\delta^{13}C_{org}$ was consistent with the 80 ppmv change in glacial atmospheric $CO_2$ inferred from Antarctic ice cores (Barnola et al., 1987). The transition into the current interglacial period was then mirrored by an equivalent decrease in $\delta^{13}C_{org}$ consistent with the increase in atmospheric $CO_2$ observed during this transition. However, results from such paleo-observations in low latitude systems are not consistent with similar paleoceanographic studies in the Southern Ocean, with the Southern Ocean displaying different altercations in $\delta^{13}C_{org}$ during glacial to interglacial cycles.

Paleoceanographic studies of the Southern Ocean observed that the glacial $\delta^{13}C$ of diatom bound organic matter were lower than during interglacials and the Holocene (Crosta and Shemesh, 2002; Rosenthal, et al., 2000; Schneider-Mor, et al., 2005; Singer and Shemesh, 1995). The reasons for

these isotopic shifts remain unclear but suggested causes include higher concentrations of dissolved molecular carbon dioxide ($[CO_2]_{aq}$), lower growth rates and changes in diatom abundance or size effects. Documenting processes that decouple carbon isotopes from the classic $\delta^{13}C$ versus $pCO_2$ relationship used for paleo-$CO_2$ reconstructions is important in understanding the influence or response of the Southern Ocean in glacial-interglacial transitions in the earth's climate.

Indeed, recent lab and field studies highlight that the isotopic composition of suspended particulate organic carbon ($\delta^{13}C_{POC}$) in phytoplankton can be affected by cell size or shape (Burkhardt, et al., 1999; Popp, et al., 1998; Trull and Armand, 2001), non diffusive carbon uptake through carbon concentration mechanisms (Cassar, et al., 2004; Rau, 2001) and other environmental and physiological factors such as $CO_2$ concentration, light levels and growth rates (Cassar, et al., 2006). These processes affect carbon isotopic fractionation ($\varepsilon_p$) and loosen the relationship between $\delta^{13}C_{org}$ and $[CO_2]_{aq}$ and may account for the observed discrepancy between marine $\delta^{13}C_{org}$ based $pCO_2$ reconstructed from low-latitude records and Vostok $CO_2$ (Kienast, et al., 2001).

In the Southern Ocean, $[CO_2]_{aq}$ is generally very high and growth rates are relatively low, so it is likely that Antarctic phytoplankton acquire their inorganic carbon by diffusion, negating the need for active carbon uptake. A recent paleo-study in Adelie Land, East Antarctica (Crosta, et al., 2005), also highlighted how past climate-driven changes in diatom assemblages affect the $\delta^{13}C_{org}$ signature of Holocene sediments. Given that the size and shape of phytoplankton and the growth conditions are seemingly a very important factor in shaping the $\delta^{13}C_{org}$ of Southern Ocean sediments, a detailed time-series of Antarctic phytoplankton species or groups and concurrent information on their effects on carbon isotopes fractionation is essential in order to make $\delta^{13}C_{org}$ a reliable paleo-$CO_2$ proxy.

## 1.7 $\delta^{15}N$ in the Southern Ocean

The nitrogen stable isotope composition ($\delta^{15}N$) of organic matter in sediments has been used as a proxy for surface water nitrate utilisation in an attempt to understand the role of Southern Ocean in glacial/interglacial changes in atmospheric $CO_2$ (e.g Francois and Altabet, 1992; Francois, et al., 1997; Sigman, et al., 1999). The High Nutrient Low Chlorophyll (HNLC) nature of the Southern Ocean leaves the majority of $NO_3$ and $PO_4$ in surface waters unutilised during the spring and summer months, believed to be due to iron limitation (Martin, et al., 1990; Timmermans, et al., 1998). Increased nutrient utilisation in the Southern Ocean has be linked to lower atmospheric $CO_2$ concentrations through changes in the efficiency of the biological pump (possibly as a result of increased iron fertilisation), or reduced nutrient ($CO_2$) supply to the ocean surface and release to the atmosphere (Francois, et al., 1997; Kumar, et al., 1995), perhaps due to increased stratification of surface waters. It is therefore essential to be able to understand the balance between changes in export production and the physical oceanographic processes affecting nutrient delivery to the surface to determine changes in the drawdown of $CO_2$.

Natural abundance measurements of $\delta^{15}N$ are useful as tracers of changes in nutrient utilisation in HNLC regions. Drawdown of $NO_3$ in surface waters results in increasing $\delta^{15}N$ of $NO_3$ ($\delta^{15}N$-$NO_3$) due to isotopic fractionation during utilisation by phytoplankton (Sigman, et al., 1999; Wada and Hattori, 1978; Wu, et al., 1997). Increasing $\delta^{15}N$-$NO_3$ is then transferred to the $\delta^{15}N$ of suspended particulate organic nitrogen ($\delta^{15}N_{PON}$), and subsequently sinking particulate organic nitrogen ($\delta^{15}N_{org}$) (Altabet, 1996; Altabet, et al., 1991; Wu, et al., 1999). Preservation of this isotopic signal in sediments facilitates the study of present and past changes in nutrient drawdown. High $\delta^{15}N$ in Antarctic sediments has thus been used to infer increased nutrient utilisation and drawdown of $NO_3$ and $CO_2$ from surface waters in a normally HNLC region, assuming that high $\delta^{15}N$ was pertinent to increased export production (e.g. Robinson, et al., 2005; Sigman, et al., 1999).

There are still, however, uncertainties regarding the use of $\delta^{15}N$ in sediments as a tracer of $NO_3$ utilisation in the Southern Ocean and whether high $\delta^{15}N$ in sediments can indeed be linked to increased carbon drawdown (Altabet and Francois, 2001; Crosta and Shemesh, 2002; Lourey et al., 2003). This uncertainty is linked to observations of higher $\delta^{15}N_{PON}$ and $\delta^{15}N_{org}$ during winter than the spring months, (Lourey et al., 2003), which has the potential to skew interpretation of sediment core records leading to overestimation of $NO_3$ utilisation. This is believed to be caused by a high residence time of dead or slow growing winter phytoplankton that are highly degraded, which increases their $\delta^{15}N_{PON}$ composition. Thus sinking $\delta^{15}N_{org}$ from this material may be significantly higher than material observed in the growing season and skew interpretation of sediment core records leading to overestimation of $NO_3$ utilisation.

Growth of phytoplankton in sea ice, which can reach high standing stocks comparable to open water may also display high $\delta^{15}N$ values compared to surface water phytoplankton. High levels of productivity in the closed or semi-closed sea ice matrix has the potential to exhaust nutrients and produce particulate organic material with anomalously high $\delta^{15}N$ composition (Fischer, et al., 2002; Gibson, et al., 1999; Kennedy, et al., 2002). Similar to winter surface water material, sinking material from sea ice with high $\delta^{15}N_{org}$ may also skew interpretation of sediment core records leading to overestimation of $NO_3$ utilisation.

Other studies have also suggested that the fractionation factor (εp) may change in response to phytoplankton assemblages (Needoba, et al., 2006) light levels (Difiore, et. al., 2006) or the concentration of iron in surface waters (Karsh et al., 2003), as a cause for changes in Southern Ocean sediment $\delta^{15}N$. Nitrogen εp in the Southern Ocean has been estimated to be between 4-8 ‰ (Altabet and Francois, 2001; Difiore, et al., 2006; Sigman, et al., 1999) based on models used for a steady state system (continuous

nutrient supply) and a closed system (no nutrient supply), and this value may be even lower when physical mixing of water masses and remineralisation of nitrogen occur (Needoba, et al., 2006).

Making connections between high $\delta^{15}N$ (nutrient utilisation) and $CO_2$ drawdown may not be relevant in many scenarios as the C and N systems can be severely decoupled in surface waters (Crosta and Shemesh, 2002; Lourey et al, 2003). This may occur not only from sea ice and winter surface water material, but from the total cumulative levels of nutrients utilised in a single growing season. Seasonally integrated sediment $\delta^{15}N$ may be comparable to the relative utilisation of $NO_3$ in surface waters, but does not capture the amount of inorganic carbon and nitrogen that can be assimilated and exported over the duration of a growing season (Francois, et al., 1997).

### 1.8 Barium

Barite formation in the marine water column and its flux to the seafloor appear linked to surface productivity and carbon export (Bishop, 1988; Dehairs et al., 1992; Dehairs et al., 2000; McManus et al., 1998). Thus the reconstruction of carbon export based on barium content of sediments may provide quantitative information about past changes in primary production (Francois et al., 1997; Ganeshram and Pedersen, 1998; Ganeshram et al., 1995). A host of previous studies utilising sediment traps monitoring fluxes of carbon and barium have produced preliminary algorithms linking the flux of biogenic barium to carbon export production (Dymond et al., 1992; Francois et al., 1995; McManus et al., 2002; Nurnberg et al., 1997).

Barite crystals are common in the suspended matter of the water column (Dehairs et al, 1980) despite the fact that the water column is usually undersaturated with respect to barium (Monin et al, 1999). Studies of the global ocean based on water column profiles of dissolve barium have shown that barium is recycled like nutrients, with lower concentrations at the surface and enrichment at depth. This distribution results from the bio-intermediate

nature of barium, with formation of particulate barium at the surface with dissolution at depth, but the exact mechanism of this process is still debated (Bernstein and Byrne, 2004; Bertram and Cowen, 1997; Ganeshram *et al.*, 2003). There is evidence supporting the idea that biogenic microenvironments in settling detritus provide favourable conditions for barite precipitation through supersaturation resulting from barium and sulphur release from decaying organic matter (Ganeshram *et al.*, 2003; Monnin *et al.*, 1999) and that processes such as trophic processing, faecal pellet packaging and particle aggregation may significantly enhance barite formation.

Biologically mediated barite formation has been demonstrated in culture experiments (Ganeshram et al, 2003). Using axenic and coastal plankton samples, barite precipitation in decaying phytoplankton was unambiguously demonstrated to increase with time. Further leaching experiments showed that a large proportion of the particulate barium in surface waters is very labile and readily released during decay. While most of this barium is released into the surrounding waters, a small fraction is converted to barite. These findings suggest the following mechanism for barite formation in seawater;

1. Biological uptake of dissolved Ba by plankton or abiotic adsorption onto organic matter, resulting in high particulate Ba concentration in surface waters that is mostly very labile
2. Rapid release of dissolved Ba from labile particulate Ba during the early stages of plankton decomposition either by cell lysis or decay of labile organic matter
3. Most of the released Ba is returned to the dissolved Ba pool in surrounding water, but a small fraction precipitates as barite in supersaturated microenvironments created as a result of rapid Ba release.
4. Barite and Ba bound to more refractory organic matter flux to the deep sea as sinking particles.

In laboratory experiments 2-4 % of the barium pool was converted to barite (Ganeshram et al, 2003), it is very difficult to calculate or model this precipitation in open marine systems but it is feasible that a relatively small amount of barite is produced. As with stable isotopes, barium based productivity estimated are also affected by various physical, chemical and biological processes while sinking and upon deposition on the sea floor before preservation (e.g. Fagel et al, 1999; Cardinal et al, 2001; Schenau et al, 2001). For instance, the availability of this supersaturated microenvironment is believed to be the limiting factor for barite precipitation (Ganeshram et al, 2003) so processes such as fecal-pellet packaging marine snow aggregation, although not prerequisite may enhance barite formation. Studies have shown that the relationships between barium and carbon fluxes vary in different oceanic regions (Francois et al., 1995), especially between continental shelf seas, continental margin environments and the open oceans (Dehairs et al., 2000; Francois et al., 1995; McManus et al., 2002).

In the polar oceans, little attention has been paid to document the effects of seasonal sea ice cover on the relationship between barium and carbon fluxes. In these environments, ice cover can extend over large proportions of the year and controls the timing of the growing season (Eicken, 1992), often resulting in short, episodic spring blooms in association with the melting sea ice. It is unclear how spring blooms and flux of material occurring in episodic 'pulses' may affect the yield of barite per unit carbon in sinking organic matter, but it has been suggested that it may reduce barite fluxes as the organic matter export in these environments occurs too rapidly to allow barite precipitation to attain completion (McManus *et al.*, 2002). Other reported cases where the excess Ba does not correlate with particulate organic carbon (e.g. Fagel et al, 1999) highlight that more research needs to be carried out to assess the environmental factors that may affect the quantitative relationship between the export of carbon and barite.

There are no published studies investigating the behaviour of barium in Antarctic sea ice to date, which is surprising considering the influence sea ice has over productivity and particle flux (Arrigo et al., 1997; Garrity et al., 2005; Kim et al., 2005) and the use barium as a paleoproductivity proxy in the Southern Ocean. Productivity within the sea ice matrix has the potential to produce a Ba:Corg relationship very different to that seen in surface waters. Primary production in sea ice often occurs in a closed or a semi-closed system within brine pockets and brine channels. This closed system effect can retain and degrade large quantities of organic matter produced within the ice matrix, a lot of which may be recycled for further production. Thus the relatively small brine channels and gap layers in sea ice are excellent candidates for barite formation, where barium and sulphur may reach levels high enough for barite precipitation during decay of organic matter. It is therefore essential to understand the biogeochemical cycling of barium in sea ice and monitor the release of barium from decaying and melting sea ice, bearing in mind that sea ice particle can account for a significant proportion of mass flux in the Southern Ocean (Arrigo et al., 1997).

The method developed by Ganeshram, et al., (2003) is a useful sequential leaching method for monitoring the behaviour of barium in decaying phytodetritus. This method uses sequential extractions of dilute $HNO_3$ for labile particulate barium, 30 % HCl for barite and hot conc. $HNO_3$ for particulate barium associated with refractory organic matter. This method was applied to monitor barite growth and behaviour relative to other Ba phases in laboratory phytoplankton decay experiments. The results from the experiments revealed the presence of large pool of labile Ba in the fresh phytoplankton, which during decay was readily released and a proportion converted to barite (see Figure 2.1).

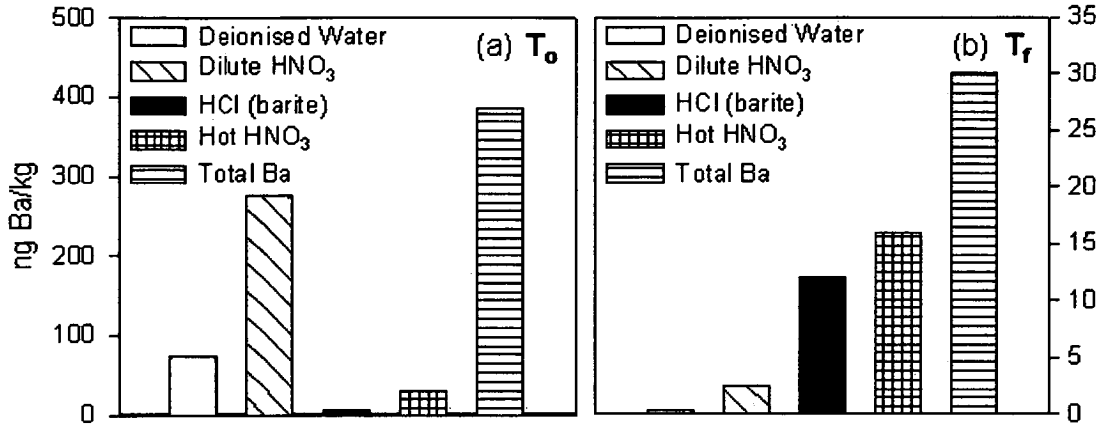


**Figure 1.1. Sequential leaching data showing particulate Ba transformations during decay of phytodetritus, courtesy of Ganeshram et al., (2003). Panels show Ba phases in freshly collected coastal phytoplanktom bloom (a) and after 8 weeks of decay in the dark (b). Note that most Ba resides in the labile fraction (Deionised water + Dilute $HNO_3$ extraction) in the bloom material but mainly in the barite (HCl) and refractory fraction (Hot $HNO_3$) after decay indicating the loss of labile Ba and the production of barite during the decay process.**

This method can easily be transferred to time-series analysis of suspended particulate samples from sea ice and the surface ocean, to monitor the behaviour of barite and other particulate Ba phases over seasonal timescales. Using this method in the field may identify the transformations of particulate Ba in surface waters and sinking material in order to gain a more detailed understanding of the biogeochemical cycling of Ba in relation to productivity and particle flux.

## 1.9 Thesis Outline

This thesis is organised into 8 further chapters following this general introduction. The next chapter (chapter 2) gives a detailed account of the field work conducted in Antarctica, along with general information about sampling procedures, dates and locations. Detailed methodologies of sample analysis are not given in chapter 2, these are presented in the following data chapters. The following 6 chapters (chapters 3-8) present the data and intellectual arguments put forward as a result of the work and are organised in "paper format", which have been or are soon to be submitted to peer reviewed

journals. The final chapter (chapter 8) summarises the thesis as a whole and the implications of this work in the more general aspects of Southern Ocean biogeochemistry and Paleoceanography.

The main body of this work, i.e. the 5 paper-chapters address some of the key issues raised in sections 1.3 through to 1.7. The arguments put forward not only complement the biological time series work of the British Antarctic Survey but also give insight into biogeochemical processes that are poorly constrained in the coastal Antarctic sea ice environment. This adds depth to existing data sets and provides further insight into the application of stable isotope and elemental proxies in the Souther Ocean.

In addition, the last data chapter of this thesis (chapter 7) documents a case study on a sediment core from the continental shelf Antarctic sea ice environment. This core covering the Holocene is quite unique in that it has an average mass accumulation rate of 0.4 $cm.yr^{-1}$ and was heavily influenced by sediment focusing. I was invited to carry out some geochemical analysis on this core by Dr. Xavier Crosta from Bordeaux University. The results were used to assess the suitability of applying a suite of geochemical proxies (C, N, opal and Ba) of paleoproductivity on this core. This involved correcting for the effects of sediment focusing, and assessing the reliability of these proxies to reconstruct past productivity and export production over the Holocene.

## 1.10 References

Anderson, R. F., et al. (1998), Late-Quaternary changes in productivity of the Southern Ocean, Journal of Marine Systems, 17, 497-514.

Anderson, R. F., et al. (2002), The Southern Ocean's biological pump during the Last Glacial Maximum, Deep-Sea Research Part Ii-Topical Studies in Oceanography, 49, 1909-1938.

Armand, L. K., Cornet-Barthaux, V., Mosseri, J. and Queguiner, B. (2008) Late summer diatom biomass and community structure on and around the

naturally iron-fertilised Kerguelen Plateau in the Southern Ocean. Deep-Sea Research II, 55, 653-676.

Arrigo, K. R., Worthen, D., Schnell, A. and Lizotte, M. P. (1998) Primary production in Southern Ocean waters. Journal of Geophysical Research, 103, 15,587-15,600.

Barnola, J. M., Raynaud, D., Korotkevich, Y. S. and Lorius, C. (1987) Vostok ice cores provides 160, 000-year record of atmospheric CO2. Nature 329, 408-413.

Bernstein, R. E., Byrne, R. H., Betzer, P. R. and Greco, A. M. (1992) Morphologies and transformations of celestite in seawater: the role of acantharians in strontium and barium geochemistry. Geochimica et Cosmochimica Acta, 56, 3273-3279.

Bishop, J.K.B., (1988). The Barite-Opal-Organic Carbon Association in Oceanic Particulate Matter. Nature 332 (6162), 341-343.

Broecker, W. S. and Peng, T. H. (1982) Tracers in the sea. Eldigio Press, Palisades.

Cassar, N., et al. (2004), Bicarbonate uptake by Southern Ocean phytoplankton, Global Biogeochemical Cycles, 18, GB2003, doi:2010.1029/2003GB002116.

Cassar, N., et al. (2006), Carbon isotopic fractionation by the marine diatom Phaeodactylum tricornutum under nutrient- and ligh-limited growth conditions, Geochimica et Cosmochimica Acta.

Clarke, A., et al. (2008), Seasonal and interannual variability in temperature, chlorophyll and macronutrients in northern Marguerite Bay, Antarctica, Deep Sea Research Part II: Oceanographic Research Papers, in press.

Crosta, X., et al. (1998), Application of modern analog technique to marine Antarctic diatoms: Reconstruction of maximum sea-ice extent at the last glacial maximum, Paleoceanography, 13, 284-297.

Crosta, X., et al. (2002), Late quaternary variations of elemental ratios (C/Si and N/Si) in diatom-bound organic matter from the Southern Ocean, Deep-Sea Research Part Ii-Topical Studies in Oceanography, 49, 1939-1952.

Crosta, X., and A. Shemesh (2002), Reconciling down core anticorrelation of diatom carbon and nitrogen isotopic ratios from the Southern Ocean, Paleoceanography, 17.

Crosta, X., et al. (2005), Major factors controlling Holocene d13Corg changes in a seasonal sea-ice environment, Adelie Land, East Antarctica, Global Biogeochemical Cycles, 19, doi:10.1029/2004GB002426.

Crosta, X., Debret, M., Denis, D., Courty, M.A. and Ther, O. (2007) Holocene long- and short-term climate changes off Adélie Land, East Antarctica. Geochemistry, Geophysics, Geosystems, 8(11), Q11009, doi: 10.1029/2007GC001718.

Dehairs, F., Baeyens, W., Goeyens, L., (1992). Accumulation of Suspended Barite at Mesopelagic Depths and Export Production in the Southern-Ocean. Science 258 (5086), 1332-1335.

Dehairs, F., Fagel, N., Antia, A.N., Peinert, R., Elskens, M., Goeyens, L., (2000) Export production in the Bay of Biscay as estimated from barium - barite in settling material: a comparison with new production. Deep-Sea Research Part I-Oceanographic Research Papers 47 (4), 583-601.

De La Rocha, C. L., et al. (1998), Silicon-isotope composition of diatoms as an indicator of past oceanic change, Nature, 395, 680-683.

Difiore, P. J., Sigman, D. M., Trull, T. W., Lourey, M. J., Karsh, K., Cane, G. and Ho, R (2006) Nitrogen isotope constraints on subantarctic biogeochemistry. Journal of Geophysical Research, 111, C08016, doi:10.1029/2005JC003216.

Ducklow, H. W., Erickson, M., Kelly, J., Smith, R. C., Stammerjohn, S. E., Vernet, M. and Karl, D. M. (2008) Particle export from the upper ocean over the continental shelf of the west Antarctic Peninsula: A long-term record, 1992-2006. Deep Sea Research Part II: Oceanographic Research Papers, in press.

Dymond, J., Suess, E., Lyle, M., (1992) Barium in deep-sea sediment: A geochemical proxy for paleoproductivity. Paleoceanography 7 (2), 163-181.

Ebert, E. E., et al. (1995) Disposition of solar radiation in sea ice and upper ocean. Journal of Geophysical Research, 100, 15965-15975.

Elderfield, H., and R. E. M. Rickaby (2000), Oceanic Cd/P ratio and nutrient utilization in the glacial Southern Ocean, Nature, 405, 305-310.

Ellwood, M. J., and K. A. Hunter (2000), Variations in the Zn/Si record over the last interglacial glacial transition, Paleoceanography, 15, 506-514.

Fagel, N., Andre, L., Dehairs, F., 1999. Advective excess Ba transport as shown from sediment and trap geochemical signatures. Geochimica et Cosmochimica Acta 63 (16), 2353-2367.

Faure, G. (1986) Principles of isotope geology. John Wiley & Sons

Fisher, G. (1991), Stable carbon isotope ratios of plankton carbon and sinking organic matter from the Atlantic sector of the Southern Ocean, Marine Chemistry, 35, 581-596.

Francois, R., and M. A. Altabet (1992), Glacial to interglacial changes in surface nitrate utilisation in the Indian sector of the Southern Ocean as recorded by sediment d15N, Paleoceanography, 7, 589-606.

Francois, R., Honjo, S., Manganini, S.J., Ravizza, G.E., (1995) Biogenic Barium Fluxes to the Deep-Sea - Implications for Paleoproductivity Reconstruction. Global Biogeochemical Cycles 9 (2), 289-303.

Francois, R., et al. (1997), Contribution of Southern Ocean surface-water stratification to low atmospheric CO2 concentrations during the last glacial period, Nature, 389, 929-935.

Galimov, E. M. (1985) The biological fractionation of isotopes. Acedemic Press.

Ganeshram, R.S., Pedersen, T.F., Calvert, S.E., Murray, J.W., (1995) Large Changes in Oceanic Nutrient Inventories from Glacial to Interglacial Periods. Nature 376 (6543), 755-758. Ganeshram, R.S., Francois, R., Commeau, J., Brown-Leger, S.L., (2003) An experimental investigation of Barite formation in seawater. Geochimica et Cosmochimica Acta 67 (14), 2599-2605.

Garrity, C., Ramseier, R.O., Peinert, R., Kern, S., Fischer, G., (2005) Water column particulate organic carbon modeled fluxes in the ice-frequented Southern Ocean. Journal of Marine Systems 56 (1-2), 133-149.

Gibson, J. A. E., et al. (1999), Sedimentation of C-13-rich organic matter from Antarctic sea-ice algae: A potential indicator of past sea-ice extent, Geology, 27, 331-334.

Karsh, K. L., Trull, T. W., Lourey, M. J. and Sigman, D. M. (2003) Relationship of nitrogen isotope fractionation to phytoplankton size and iron availability during the Southern Ocean Iron RElease Experiment (SOIREE), Limnology and Oceanography, 48(3), 1058-1068.

Keeling, R. F. and Stephens, B. B. (2001) Antarctic sea ice and the control of Pleistocene instability. Paleoceanography, 16(1), 112-131.

Kennedy, H., Thomas, D. N., Kattner, G., Haas, C. and Dieckmann, G. S. (2002) Particulate organic matter in Antarctic summer sea ice: concentration and stable isotopic composition. Mar. Ecol. Prog. Ser., 238, 1-13.

Kienast, M., et al. (2001), A critical review of marine sedimentary delta C-13(org)-pCO(2) estimates: New palaeorecords from the South China Sea and a revisit of other low-latitude delta C-13(org)-pCO(2) records, Global Biogeochemical Cycles, 15, 113-127.

Kim, D., Kim, D., Park, J. and Kim, Y., (2005) Interannual variation of particle fluxes in the eastern Branfield Straight, Antarctica: A response to the sea ice distribution. Deep-Sea Research Part I

Kumar, N., et al. (1995), Increased Biological Productivity and Export Production in the Glacial Southern-Ocean, Nature, 378, 675-680.

Lourey, M. J., et al. (2003), Sensitivity of delta N-15 of nitrate, surface suspended and deep sinking particulate nitrogen to seasonal nitrate depletion in the Southern Ocean, Global Biogeochemical Cycles, 17.

McManus, J., Berelson, W.M., Klinkhammer, G.P., Johnson, K.S., Coale, K.H., Anderson, R.F., Kumar, N., Burdige, D.J., Hammond, D.E., Brumsack, H.J., McCorkle, D.C., Rushdi, A., 1998. Geochemistry of barium in marine sediments: Implications for its use as a paleoproxy. Geochimica et Cosmochimica Acta 62 (21-22), 3453-3473.

McManus, J., Dymond, J., Dunbar, R.B., Collier, R.W., 2002. Particulate barium fluxes in the Ross Sea. Marine Geology 184 (1-2), 1-15.

Meiners, K., Gradinger, R., Fehling, J., Civitarese, G., Spindler, M., 2003. Vertical distribution of exopolymer particles in sea ice of the Fram Strait (Arctic) during autumn. Marine Ecology-Progress Series 248, 1-13.

McMinn, A. (1996) Preliminary investigation of the contribution of fast-ice algae to the spring phytoplankton bloom in Ellis Fjord, eastern Antarctica. Polar Biology, 16, 301-307.

Monnin, C., Jeandel, C., Cattaldo, T., Dehairs, F., (1999) The marine barite saturation state of the world's ocean. Marine Chemistry 65, 253-261.

Needoba, J. A., Marchetti, A., Henry, M. F., Harrison, P. J., Wong, C., Johnson, K. W. and Pedersen, T. F. (2006) Stable nitrogen isotope dynamics of a mesoscale iron enrichment experiment in the NE Subarctic Pacific. Deep Sea Research II, 53, 2214-2230.

Nurnberg, C.C., Bohrmann, G., Schluter, M., Frank, M., (1997) Barium accumulation in the Atlantic sector of the Southern Ocean: Results from 190,000-year records. Paleoceanography 12 (4), 594-603.

Robinson, R. S., et al. (2005), Diatom-bound N-15/N-14: New support for enhanced nutrient consumption in the ice age subantarctic, Paleoceanography, 20.

Rosenthal, Y., et al. (2000), Southern Ocean contributions to glacial-interglacial changes of atmospheric pCO(2): An assessment of carbon isotope records in diatoms, Paleoceanography, 15, 65-75.

Sigman, D. M., and E. A. Boyle (2000), Glacial/interglacial variations in atmospheric carbon dioxide, Nature, 407, 859-869.

Singer, A. J., and A. Shemesh (1995), Climatically Linked Carbon-Isotope Variation During the Past 430,000 Years in Southern-Ocean Sediments, Paleoceanography, 10, 171-177.

Popp, B. N., et al. (1998), Effect of phytoplankton cell geometry on carbon isotopic fractionation, Geochimica Et Cosmochimica Acta, 62, 69-77.

Schenau, S.J., Prins, M.A., De Lange, G.J., Monnin, C., (2001) Barium accumulation in the Arabian Sea: Controls on barite preservation in marine sediments. Geochimica et Cosmochimica Acta 65 (10), 1545-1556.

Sigman, D. M., et al. (1999a), The isotopic composition of diatom-bound nitrogen in Southern Ocean sediments, Paleoceanography, 14, 118-134.

Sigman, D. M., et al. (1999b), The delta N-15 of nitrate in the Southern Ocean: Consumption of nitrate in surface waters, Global Biogeochemical Cycles, 13, 1149-1166.

Trull, T. W., and L. Armand (2001), Insights into Southern Ocean carbon export from the [delta]13C of particles and dissolved inorganic carbon during the SOIREE iron release experiment, Deep Sea Research Part II: Topical Studies in Oceanography, 48, 2655-2680.

Turner, J., Colwell, S. R., Marshall, G. J., Lachlan-Cope, T. A., Carleton, A. M., Jones, P. D., Lagun, V., Reid, P. A. and Iagovinka, S. (2005) Antarctic climate change during the last 50 years. International Journal of Climatology, 25, 279-294.

Wu, X.., et al. (1997) Modelling of Antarctic sea-ice in a General Circulation Model. Journal of Climatology, 10(4), 593-609.

# 2 Field Work

## 2.1 Introduction

This short chapter is designed to give a detailed description of events during field work conducted at Rothera Research Station to collect samples for this research project. The information presented details sampling events (e.g. dates, locations, sample types taken) and any analyses performed by the authors or The British Antarctic Survey that are considered general analyses (e.g. CTD casts, sea ice observations) that are used throughout this thesis.

The majority of samples for this project were taken at the Rothera Time Series Site (See Figure 2.1), or 'RaTS site' as it will be referred to herein for surface water samples.

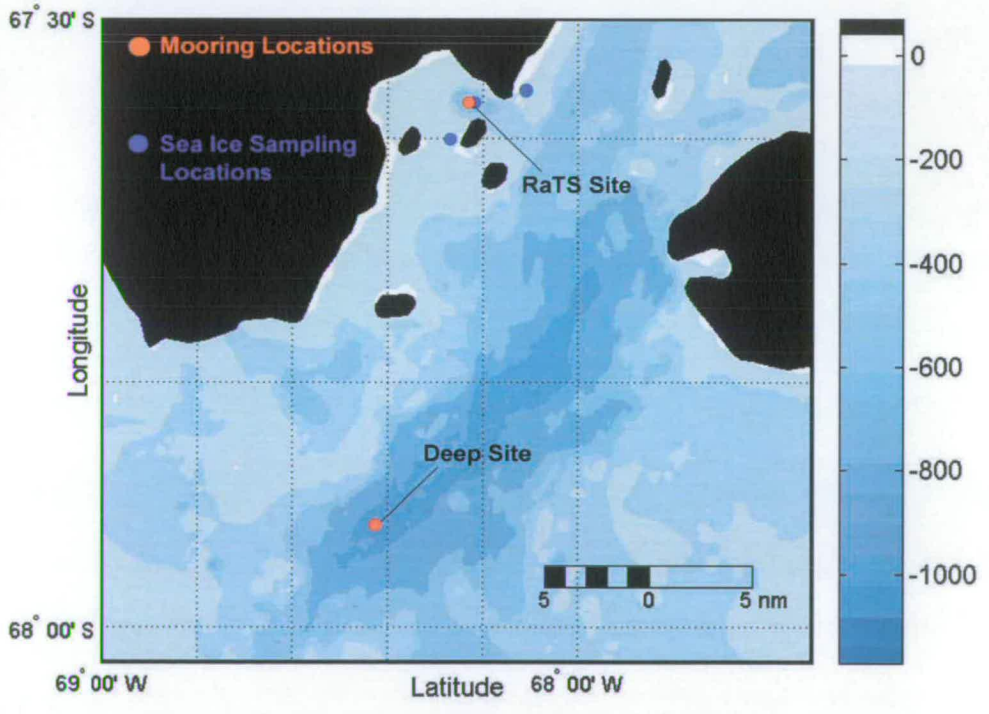


**Figure 2.1. Location of sea ice sampling, RaTS site of time series water sampling and mooring deployment and mooring deployment at the deep site.**

The British Antarctic Survey has been conducting a year round oceanographic time series study at this site since 1997 (Clarke, et al., 2007).

The RaTS site is located in Ryder Bay, Antarctica (67°34.02'S, 68°14.02'W), although there is a site nearby, referred to as 'RaTS site 2' that is used whenever the RaTS site is unavailable due to ice cover. The RaTS programme frequently measures depth profiles of conductivity, temperature and depth as well as measurements of chlorophyll, nutrients and other biochemical components at 15 m. Sea ice samples were taken in the surrounding area of the RaTS site, but were limited to where the ice was deemed safe to walk on by the resident Field Assistants at Rothera Research Station.

## 2.2 Field Seasons

The 2004/2005 field season commenced in early December 2004 and ran until March 2005. Upon arrival at Rothera Research Station, most of the sea ice had retreated in Ryder Bay, with only areas of land-fast ice available to sample. The spring bloom was already underway, so the ice cover to open water transition was missed. A total of 5 sea ice brine samples and 22 surface water samples were taken during the 2004/2005 field season The 2005/2006 field season commenced in early November 2005 and ran until March 2006. Upon arrival, the whole of Ryder Bay was still covered in sea ice and it remained until the 25$^{th}$ December, allowing a more detailed time series sampling of sea ice and surface waters during ice cover and the transition to open water spring bloom conditions. A total of 10 sea ice samples and 19 surface water samples were taken during the 2005/2006 field season.

## 2.3 Surface Water Sampling

Surface water sampling was conducted at 15 m depth at the RaTS site, the same depth as the RaTS programme. Sampling was conducted aboard an inflatable boat with a custom built CTD winch on board. CTD casts were taken to 500 m depth using a Sea Bird Electronics 19 Plus SEACAT CTD module. For measurements of conductivity, temperature and depth a Wet Labs Wetstar module was used. Water samples were taken using a 5 L Niskin bottle for chlorophyll analysis. Temperature at 15 m was measured using a Sensoren Instrumente Systeme GmbH reversible thermometer; the

thermometer was lowered to 15 m and left to equilibrate for 2 min before sending the messenger down to intitate temperature recording. For geochemical analysis, water was either collected using the 5 L Niskin bottle or was pumped from 15 m depth using a 12 V dolphin pump and silicon tubing into acid cleaned 10 L polypropylene carboys.

Water samples were stored in a cold room in the dark at 0°C until processed in the laboratory. Samples were never left for longer than 2 h after collection before processing. During the winter and early spring 2005 when sea ice was covering the bay, CTD casts and Niskin sampling were conducted at the RaTS site from a winch attached to a sledge, through a hole cut in the ice. Water samples for geochemical analysis were taken at the RaTS site below the ice during September and October 2005. Samples taken under the ice during November and December 2005 were located closer to the shore where the ice was deemed safe to walk on. Using dive holes, British Antarctic Survey divers took empty closed carboys under the ice and opened them immediately below the ice. Water samples were stored in a cold room in the dark at 0°C until processed in the laboratory. Samples were never left for longer than 2 h after collection before processing. Sampling frequency was aimed to occur twice weekly, but due to the weather this was not always possible. Refer to Appendix 1 for a full list of all sampling events during field season 2004/2005 and Appendix 2 for a full list of sampling events during field season 2005/2006.

## 2.4 Sea Ice Sampling

Sea ice sampling was conducted at three locations during both field seasons. During the first season where sparse land fast ice was remaining during December 2005, 5 sea ice samples were taken on ice floes attached to lagoon island (67' 35.6° S, 68' 14.5° W). During austral winter 2005 (September and October), 2 sea ice samples were taken at the RaTS site (67° S, 68° W). During early spring 2005 (November and December) a further 8 sea ice samples were taken at a near shore site (67' 33.85° S, 68' 07.52°

W). Sea ice sampling events were conducted using the same stepwise process each time. Thin sack holes were firstly drilled into the ice and allowed to fill with brine. Firstly, samples for dissolved gases (alkalinity and stable isotopes of dissolved inorganic carbon) were taken followed by measurements of temperature and conductivity using a YSI 85 multi-parameter. A larger hole was then drilled and samples for nutrients, particulates and dissolved constituents were taken. Sea ice brine was transferred from the sack hole to clean polypropylene carboys using an acid clean 500 ml HDPE beaker. Brine samples were stored in a cold room in the dark at 0°C until processed in the laboratory. Samples were never left for longer than 2 h after collection before processing. Refer to Appendix 3 for a list of sea ice sampling events during the 200/2005 and 2005/2006 field seasons.

## 2.5 Measured Parameters

For a list of parameters measured in surface waters and sea ice, refer to Appendix 4 (detailed methods of sampling and analysis for each parameter are given in subsequent chapters).

## 2.6 Research Cruises Aboard the RRS James Clark Ross

A total of 3 cruises aboard the RRS James Clark Ross were conducted during field work for this project (Brandon, 2005; Walker and Weston, 2006; Weston and Brandon, 2007). The purpose of these cruises were to deploy and/or retrieve sediment trap mooring arrays that were located at the RaTS site in Ryder Bay (67' S, 68' W) and a deeper site in Marguerite Bay (68' W, 68' S) (exact locations described for each deployment), to conduct CTD casts at each mooring site and a transect across the mouth of Marguerite Bay and to take box core samples below each mooring site.

## 2.7 Sediment Trap Mooring Arrays

Two sediment trap mooring arrays were deployed at the RaTS site and the deeper site in Marguerite Bay to catch sinking particles in concert with the time series water sampling programme. Each mooring consisted of two time-

series sediment traps, which were situated at 200 m and 500 m for the RaTS mooring and 123 m and 745 m for the deep site mooring. The moorings were also equipped with an ADCP at 200 m, current meters and CTD's directly below each sediment trap and temperature loggers and CTD's in between each sediment trap. For schematic diagrams of each mooring array, refer to Figures 2.2 and 2.3.

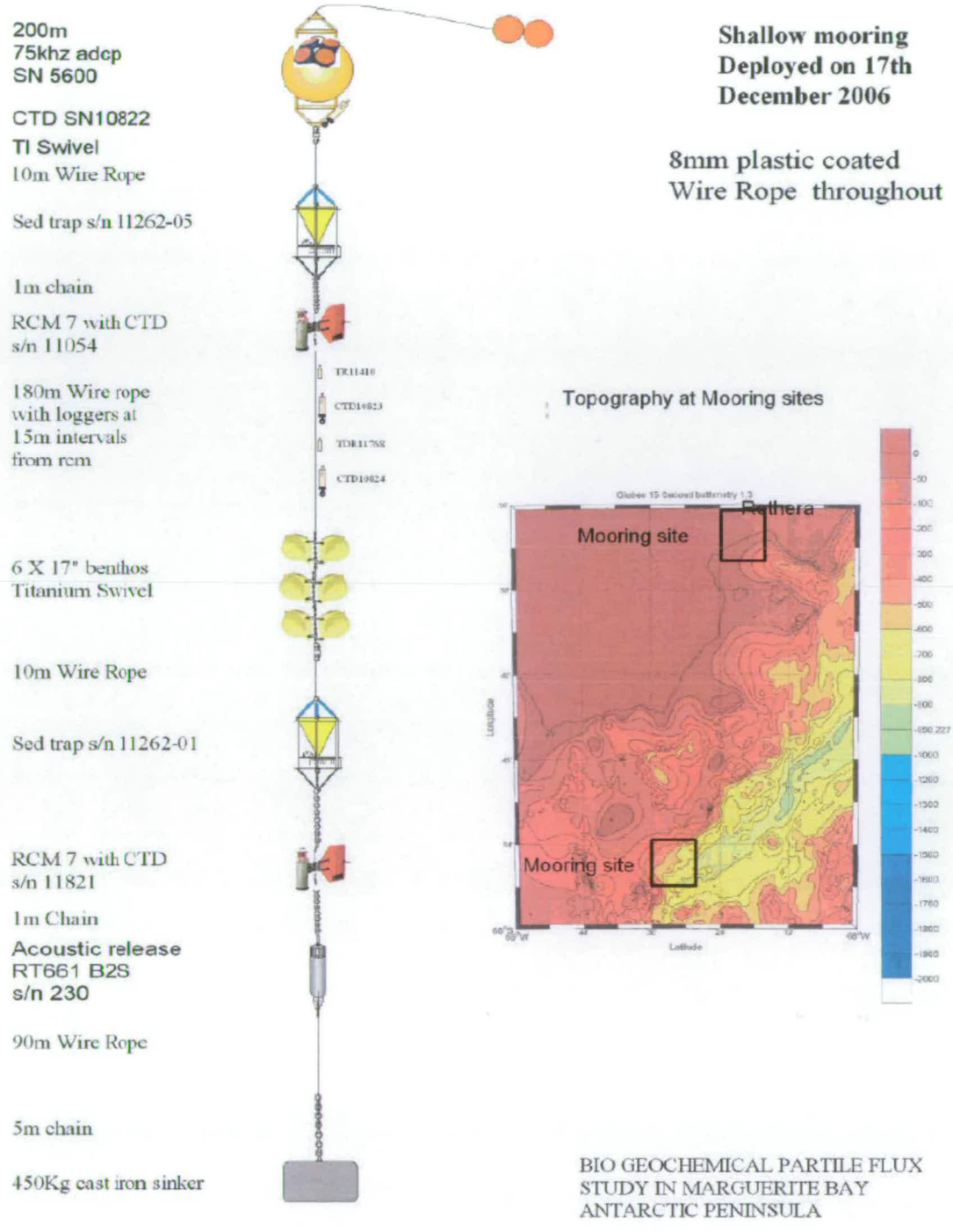


**Figure 2.2. Schematic diagram of the RaTS mooring array showing the instruments and construct and detailing depth and serial numbers. Diagram also shows topography of the deployment sites for both moorings. Diagram taken from Weston and Brandon, (2007).**

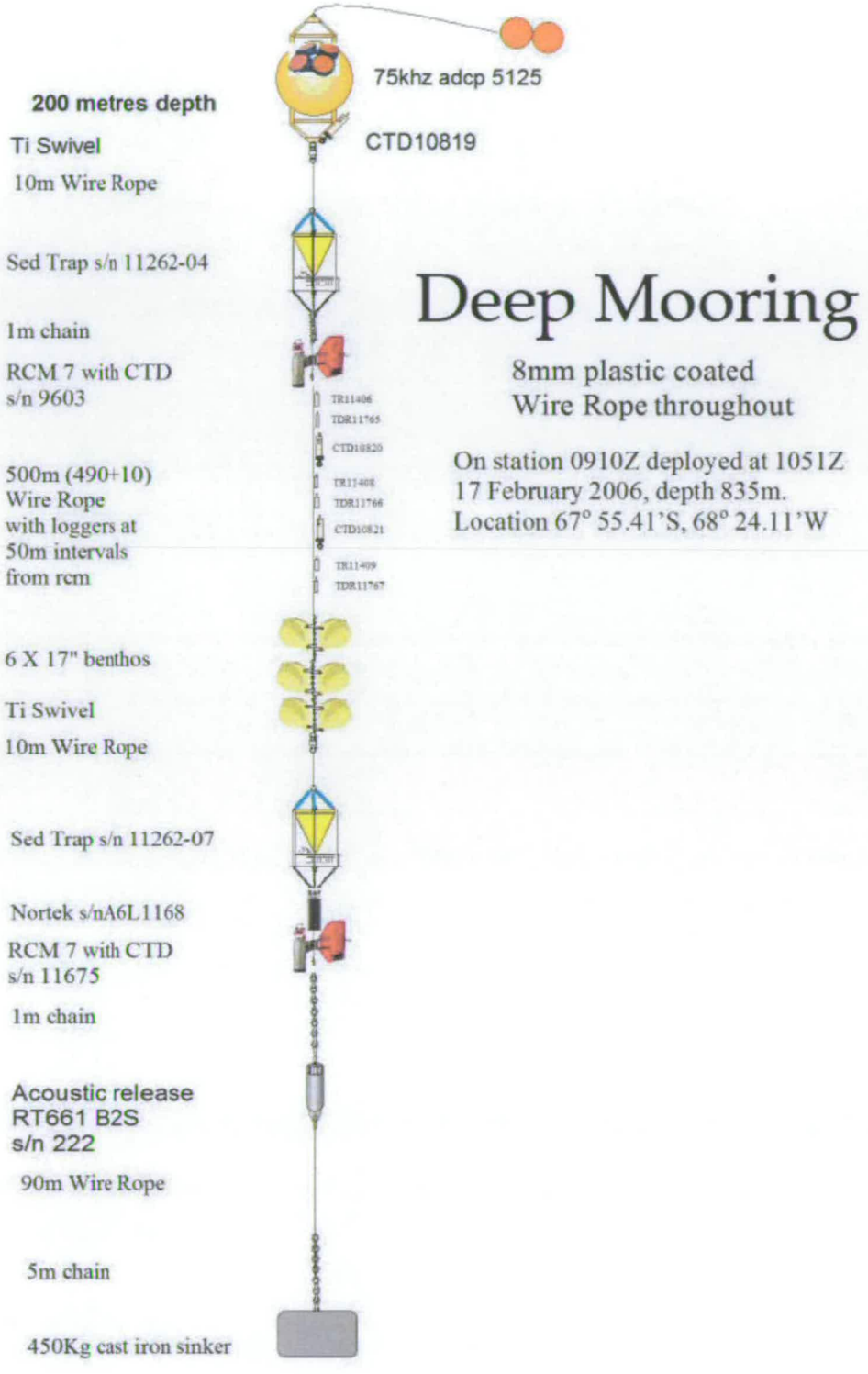


**Figure 2.3. Schematic diagram of the deep mooring array showing the instruments and construct and detailing depth and serial numbers.**

Each sediment trap was equipped with 21 rotating for cups, which were programmed to rotate at predefined intervals. The strategy employed for cup rotation utilised higher resolution cup turnover during periods of potential sea ice melt and the spring bloom with lower resolution cup rotation during the low flux winter periods. Mooring arrays were initially deployed during JCR cruise 112/113. The RaTS site mooring was deployed on the 25th January 2005 in 502 m water at 67'34.02°S, 68' 14.02°W). The deep site mooring was deployed on the 24th January 2005 in 841 m water at 67' 55.39°S, 68' 24.15° W. For a table of sediment trap bottle rotations, refer to Table 2.1.

**Table 2.1. Dates for sediment trap cup rotation during the first deployment between January 2005 and February 2006.**

| Trap | Dates | Trap | Dates |
|---|---|---|---|
| 1 | 26/01/05 – 07/02/05 | 13 | 29/11/05 – 06/12/05 |
| 2 | 07/02/05 – 21/02/05 | 14 | 06/12/05 – 13/12/05 |
| 3 | 21/02/05 – 01/03/05 | 15 | 13/12/05 – 20/12/05 |
| 4 | 01/03/05 – 01/04/05 | 16 | 20/12/05 – 27/12/05 |
| 5 | 01/04/05 – 01/05/05 | 17 | 27/12/05 – 03/01/06 |
| 6 | 01/05/05 – 01/06/05 | 18 | 03/01/06 – 18/01/06 |
| 7 | 01/06/05 – 15/07/05 | 19 | 18/01/06 – 01/02/06 |
| 8 | 15/07/05 – 01/09/05 | 20 | 01/02/06 – 15/02/06 |
| 9 | 01/09/05 – 01/10/05 | 21 | Not Used |
| 10 | 01/10/05 – 01/11/05 | | |
| 11 | 01/11/05 – 15/11/05 | | |
| 12 | 15/11/05 – 29/11/05 | | |

Moorings were retrieved for the first time during JCR cruise 136/137. The RaTS mooring and deep mooring were recovered on the 15th February 2006 and the sediment trap bottles were removed and replaced with fresh ones. Both moorings were redeployed on the 17th February 2006. The RaTS mooring was redeployed at a water column depth of 522m at 67' 34.00°S, 68' 14.00°W. The deep mooring was redeployed at a water column depth of 835m at 67' 55.41°S, 68'24.11°W. For a table of sediment trap bottle

rotations during the second deployment, refer to Table 2.2. The moorings were further recovered on 17th December 2006 aboard JCR Cruise 155. The RaTS mooring was successfully turned over, but unfortunately the deep mooring was lost. The same cup rotation dates in Table 2.2 were used after the RaTS mooring was redeployed in December 2006, so no further tables have been included for the third deployment. Final recovery of the RaTS mooring was conducted in April 2007 aboard JCR Cruise 174.

**Table 2.2. Dates for sediment trap cup rotation during the second deployment between February and December 2006.**

| Trap | Dates | Trap | Dates |
|---|---|---|---|
| 1 | 18/02/06 – 03/03/06 | 13 | 01/12/06 – 10/12/06 |
| 2 | 03/03/06 – 17/03/06 | 14 | 10/12/06 – 17/12/06 |
| 3 | 17/03/06 – 31/03/06 | 15 | 17/12/06 – 24/12/06 |
| 4 | 31/03/06 – 01/05/06 | 16 | 24/12/06 – 07/01/07 |
| 5 | 01/05/06 – 01/06/06 | 17 | 07/01/07 – 20/01/07 |
| 6 | 01/06/06 – 01/07/06 | 18 | 20/01/07 – 01/02/07 |
| 7 | 01/07/06 – 01/08/06 | 19 | 01/02/07 – 21/02/07 |
| 8 | 01/08/06 – 01/09/06 | 20 | 21/02/07 – 08/03/07 |
| 9 | 01/09/06 – 01/10/06 | 21 | 08/03/07 – 01/04/07 |
| 10 | 01/10/06 – 01/11/06 | | |
| 11 | 01/11/06 – 15/11/06 | | |
| 12 | 15/11/06 – 01/12/06 | | |

## 2.8 Box Coring

During JCR Cruise 155, box core samples were taken at both the RaTS site and the deep site. The box core at the RaTS site was retrieved on 15th December 2006 at 67'34.15°S, 68'13.44°W. A total of 4 sub-cores were taken from the box core by pushing plastic sleeves through the main core of sediment. The RaTS box core measured 31 cm in length and each was sectioned at 0.5 cm intervals for the first 2 cm, at 1 cm intervals between 2 and 10cm and at 2cm intervals between 10 and 30 cm. The box core at the deep site was retrieved on the 15th December 2006 at 67'55.28°W 68'24.34°W. A total of 4 sub-cores were taken from the box core by pushing

plastic sleeves through the main core of sediment. The deep site box core measured 29 cm in length and each was sectioned at 0.5 cm intervals for the first 2 cm, at 1 cm intervals between 2 and 10cm and at 2cm intervals between 10 and 28 cm.

## 2.9 References

Brandon, M. (2005), JR112/113 Cruise Report, 12pp.

Clarke, A., et al. (*in-press*), Seasonal and interannual variability in temperature, chlorophyll and macronutrients in northern Marguerite Bay, Antarctica. *Deep Sea Research.*

Walker, D., and K. Weston (2006), JR 136/137 Cruise Report, 27pp.

Weston, K., and M. Brandon (2007), JR 174 Cruise Report, 9pp.

# 3 Inter-Annual Variability of Productivity and Particle Flux in Ryder Bay, Antarctica


## Abstract

This study reports time series measurements of productivity in sea ice and surface waters and export production over two contrasting growing seasons in Ryder Bay, Antarctica. Ryder Bay is a region of intense primary production during the short ice-free spring and summer months and particle export occurs as an intense period of sedimentation following surface water productivity. Standing stocks of organic C and N in sea ice are high and each season exhibited a spring bloom lasting 4 months and both showed a two peak profile of productivity, which is believed to be a result of intense grazing pressure and was accompanied by elevated concentrations of NH4. Primary production measurements also show that regenerated production levels were elevated during the latter stages of the 05/06 season after the mid-season decline in biomass. Differences in the sea ice regime over the two growing seasons had a major effect on the characteristics of each growing season, leading to a dynamic water column with several nutrient inputs during the 04/05 season and a more stable water column during the 05/06 season. Nutrient utilisation reached similar levels over each season, suggesting that there was more productivity during the 04/05 season. This was evident in the amount of sinking material being much lower in the 05/06 season compared to the 04/05 season. The stable water column during 05/06 would also have retained more material at the surface for recycling and regenerated production. Export efficiency estimates during 05/06 were very low (<10 %), consistent with other measurements in the region, and suggest a food web structure efficient at retention and recycling of the net community production. C:N ratios of surface water material was low (5.7), with the sinking material C:N ratio increasing to 6.3 at the sediment surface, values much lower than other studies in the region. These ratios do, however, suggest that recycling of material occurred from the increase of 0.6 from surface waters to the sediment surface.

## 3.1 Introduction

The Antarctic continental shelves are regions of intense biological activity and biogeochemical cycling, and constitute high levels of primary production (Arrigo et. al., 1998; Vernet, et. al., in-press), drawdown of pCO2 (Arrigo et. al., 1999) and intense "pulses" of sedimentation (Ducklow et al., in-press). In addition the continental shelves surrounding Antarctica are one of the global oceans richest reservoirs of biogenic opal, due to high primary productivity that is dominated by diatoms (Broecker, 1982)

Despite many years of investigation, most biological and biogeochemical studies of the Southern Ocean concerning productivity, $CO_2$ variations and export production, especially in continental shelf regions, have been limited to ice free seasons and very few studies go beyond a single year. Recently, there have been two very useful studies documenting long-term monitoring of regions of the Western Antarctic Peninsula (WAP) (Clarke et. al., in-press; Ducklow, et. al., in-press), but many observations remain without explanation, for example why the peak flux period in the WAP is now roughly 40 days later than in 1993. The WAP is a very important region of Antarctica to climate and ocean scientists, as it has experienced the highest rate of warming ($3^{o}C$) over the last 50 years (Turner et. al., 2005), so understanding the mechanisms affecting sea ice seasonality, primary production and particle export are essential in order to understand how future warming or other aspects of climate change may affect this ecosystem.

The high inter-annual variability observed in the continental shelf, Antarctic sea ice environment makes generalisation about annual primary production and export production very difficult. More long-term monitoring programmes are required to identify the mechanisms affecting sea ice extent, changes in circulation and mixing of water masses, phytoplankton assemblages, primary production and export production.

In this study we compare two contrasting growing seasons in Ryder Bay Antarctica, the site of the Rothera Biological Time Series (RaTS), a long-term monitoring programme that has been running since 1997 (Clarke et al., in-press). The growing seasons presented have two very different sea ice regimes and subsequent hydrographic properties, primary productivity and export production.

### 3.2 Materials and Methods

This study was conducted between 2004 and 2006 in Ryder Bay and Marguerite Bay located south of Alexander Island and west of the mainland on the Western Antarctic Peninsula (see Figure 3.1). Ryder Bay is a coastal embayment adjoining Marguerite Bay and the study site is situated in open water at a depth of 520 m.

Sea ice brine was sampled when sea ice was present at three locations, with a total of 15 sea ice samples taken during this study. Sea ice had receded from Ryder Bay upon arrival at in December 2004, however there was still land fast ice located around Lagoon Island (see Figure 3.1 for Lagoon Island sampling site), with 5 samples taken at the Lagoon Island site during December 2004. A further 10 samples were taken during the 05/06 season. During winter 2005, two sea ice samples were taken in September and October at the RaTS site and during early spring 2005 (Nov-Dec), a further eight sea ice samples were taken at a site north of Rothera Point (See Figure 3.1). A high resolution time series of surface water samples were taken in Ryder Bay, at the Rothera Time Series study site at 67°34.02'S, 68°14.02'W (Clarke, et al., 2007) during austral spring and summer 2004/2005 and austral spring and summer 2005/2006 (Figure 3.1). All surface water samples were taken at 15 m. Two water samples were taken during September and October 2005 through a hole cut in the ice.

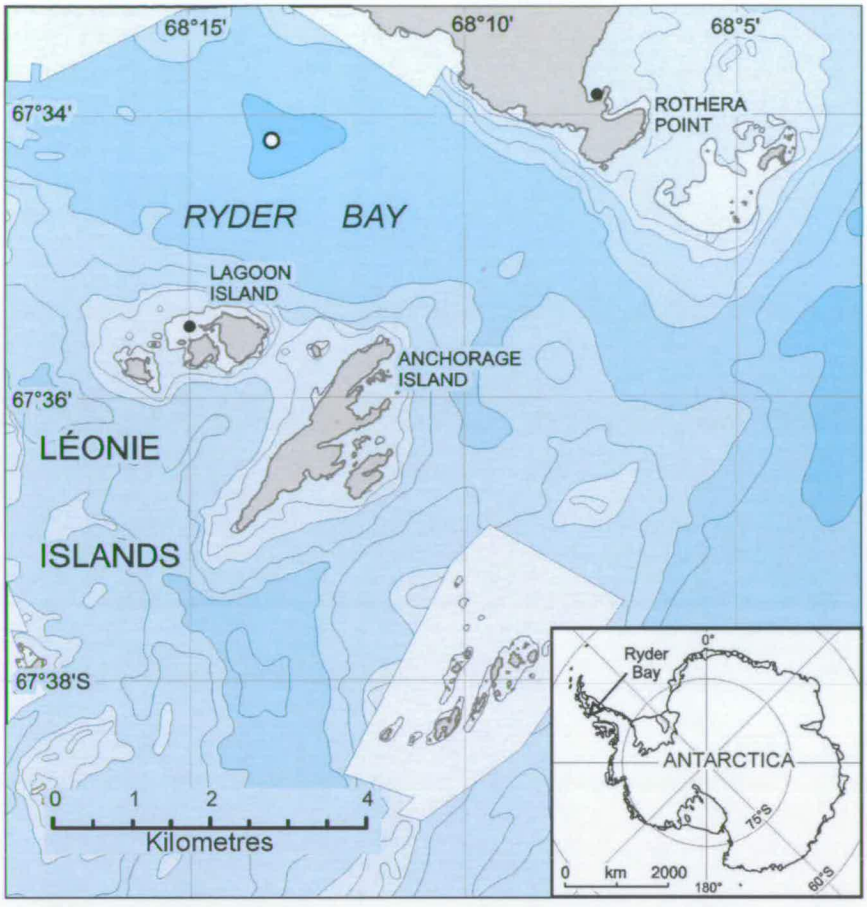


**Figure 3.1. Map of Ryder Bay showing the RaTS site (white circle) and the two other sites used for sea ice sampling (black circles). Map courtesy of the British Antarctic Survey.**

### 3.2.1 Sea Ice Sample Collection

Sea ice brine was sampled using a sack hole drilling method, with samples for [$CO_{2(aq)}$] taken first to minimise atmospheric contamination. Alkalinity samples for [$CO_{2(aq)}$] determination were taken by immersing a 250 ml BOD bottle in the sack hole and sealing the bottle with a plastic stopper ensuring no air bubbles were present. Salinity and temperature were measured using a YSI-500 multi-parameter meter.

For particulate carbon and nitrogen measurements, sea ice brine was transferred to acid-clean HDPE carbuoys and taken back to the laboratory for filtration. Sea ice brine samples were filtered through muffle-furnaced (400°C for 4 h) 47 mm GF/F filters, within 2 h of collection. The filters were then dried

at 50°C overnight, and stored frozen until analysis. Filtered water was transferred to 50 ml HDPE tubes and frozen at -20°C until analysis for major nutrients.

### 3.2.2 Surface Water Sample Collection

CTD casts were taken to 500 m depth using a Sea Bird Electronics 19 Plus SEACAT CTD module. For depth profile measurements of conductivity, temperature and depth a Wet Labs Wetstar module was used for mixed layer depth (MLD) determination. For measurement of temperature at 15 m, a Sensoren Instrumente Systeme GmbH reversible thermometer was lowered to 15 m, allowed to equilibrate for 2 min and a brass messenger was sent down to initiate temperature recording.

Surface water samples were taken using a 5 L Niskin bottle for chlorophyll a, and $[CO_{2(aq)}]$ measurements. Alkalinity samples for $[CO_{2(aq)}]$ determination were transferred from the Niskin straight into a 250 ml BOD bottle and sealing the bottle with a plastic stopper ensuring that no air bubbles were present.

Particulate samples were retrieved using a 12 V dolphin pump and 15 m of silicone tubing weighted down at the end. Water from 15 m was pumped into 10 L HDPE carbuoys for transfer back to the laboratory. Surface water samples were filtered through muffle-furnaced (400°C for 4 h) 47 mm GF/F filters. The filters were then dried at 50°C overnight and stored frozen until analysis. Filtered water was transferred to 50 ml HDPE tubes and frozen at -20°C until analysis.

### 3.2.3 Sample Analysis

Determination of $[CO_{2(aq)}]$ was conducted utilising measurements of salinity, temperature, pH and alkalinity. Salinity measurements were taken from the CTD profiles, temperatures were measured using a Sensoren Instrumente Systeme GmbH reversible thermometer. Alkalinity was determined by titration with 0.05 M HCl and the Gran plot method (Almgren, et al., 1983).

[$CO_{2(aq)}$] was calculated using constants from (Dickson and Millero, 1987), (Hannson, 1973) and (Mehrbach, et al., 1973) with the CO2SYS programme (Lewis and Wallace, 1998). $NO_3$ concentrations were measured using a Skaler San $^{plus}$ nutrient autoanalyser employing standard colorimetric techniques (Strickland and Parsons, 1972). Ammonium concentrations were measured on the filtered sea ice and surface water samples using the standard addition method described in Holmes, et al., (1999) on the day of sample collection. Bulk POC and PON analyses were conducted using a method similar to (Lourey, et al., 2004). Prior to analysis, the filters were decarbonated by wetting the filter with Milli-Q water and fuming with HCl for 48h and then drying at 50°C. Filters were analysed for elemental POC and PON using a Carlo Erba NA 2500 elemental analyser.

### 3.2.4 Sediment Trap Deployments

Two sediment trap mooring arrays were deployed, with one at the RaTS site and the other at a deeper site in Marguerite Bay (67' 55.39°S, 68' 24.15° W) to catch sinking particles in concert with the time series water sampling programme. Each mooring consisted of two time-series sediment traps, which were situated at 200 m and 500 m for the RaTS mooring and 123 m and 745 m for the deep site mooring. Each sediment trap was equipped with 21 rotating for cups, which were programmed to rotate at predefined intervals, with higher resolution cup turnover during periods of potential sea ice melt and the spring bloom with lower resolution cup rotation during the low flux winter periods. Each cup was filled with filtered seawater spiked with an extra 5 ‰ NaCl to increase its density to above that of the surrounding seawater and also spiked with formaldehyde to have an overall concentration of 2 % (v/v) to prevent bioturbation. After recovery, the solution in each cup was allowed to settle, the supernatant siphoned off and the swimmers were removed. Each sample cup was then split into 10 fractions using a rotary splitter at the National Oceanography Centre (NOC), Southampton, UK.

The RaTS site mooring was initially deployed on the 25$^{th}$ January 2005 in 502 m water at 67'34.02°S, 68' 14.02°W. The deep site mooring was

deployed on the 24th January 2005 in 841 m water at 67' 55.39°S, 68' 24.15° W. The RaTS mooring and deep mooring were recovered on the 15th February 2006 and the sediment trap bottles were removed and replaced with fresh ones. Both moorings were redeployed on the 17th February 2006. The RaTS mooring was redeployed at a water column depth of 522m at 67' 34.00°S, 68' 14.00°W. The deep mooring was redeployed at a water column depth of 835m at 67' 55.41°S, 68'24.11°W. The moorings were further recovered on 17th December 2006 aboard JCR Cruise 155. The RaTS mooring was successfully recovered, but unfortunately the deep mooring was lost. For full details of mooring deployment and sediment cup rotation, refer to Chapter 2. One sediment trap cup split and the surface sediment from the box core were freeze-dried and ground for analysis of particulate components. For POC and PON analysis, duplicate 10 mg aliquots of dried sediment were weighed into silver capsules and were acidified with 50 % HCl to remove carbonates and dried at 60°C overnight. Decarbonated samples were then analysed for elemental POC/PON using a Carlo Erba NA 2500 elemental analyser. Opal analysis was conducted using the method described in Mortlock and Froelich (1989).

### 3.3 Results

The two growing seasons sampled during this study are summarised in Figure 3.2. Sea ice covered Ryder Bay from mid-June 2004 until it receded in November with the onset of the spring and summer growing season, which lasted for around 4 months until March 2005. During the autumn of 2005, sea ice began to form and was fully covering Ryder Bay again in June 2005. The sea ice persisted until late December 2005 with the onset of the growing season, which lasted 4 months until April 2006. During the 04/05 growing season, the growth of phytoplankton (chlorophyll a) did not start until the sea ice had almost fully receded in November, whereas growth began underneath the sea ice during the 05/06 season about 1 month before the ice disappeared. Each growing season (as well as many previous growing seasons samples in Ryder Bay since 1997 (Clarke, et. al., in-press) shows two peaks in chlorophyll a, with a mid-season decline in chlorophyll occurring

about 2 months into each 4 month growing season. Chlorophyll a concentrations peak at 30-35 mg/m$^3$ during each growing season, which are very high concentrations for the Western Antarctic Peninsula region (Ducklow et. al., in press) and are likely a result of the shallow (500 m) coastal nature of Ryder Bay.

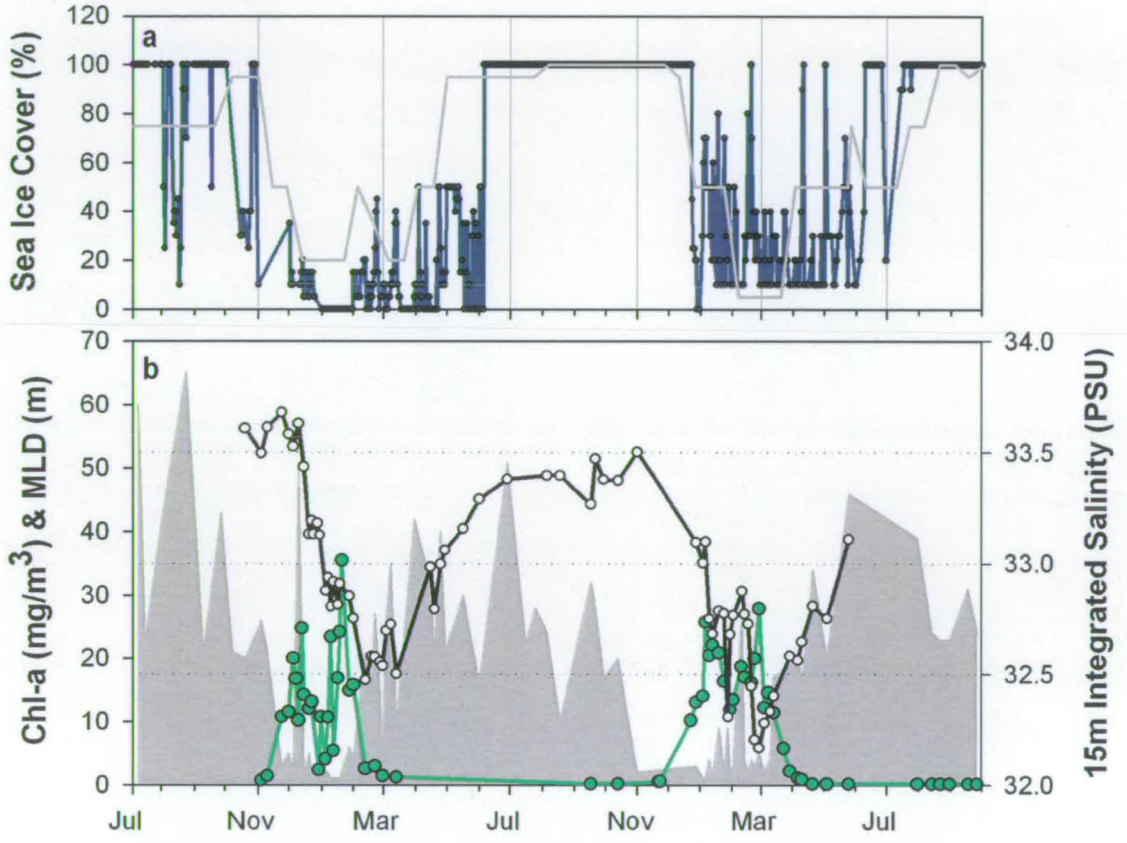


**Figure 3.2. (a) Sea ice cover for the region (grey line) taken from the NOAA archive and daily observations of Ryder Bay (blue line), and (b) Chl-a (green line), 15m integrated salinity (black line) and MLD (grey shaded area).**

The mixed layer depth (MLD) shows a typical seasonal cycle (Clarke, et. al., in-press), with a deep MLD of up to 65 m during winter, when sea ice is present and the water column is well mixed, to a shallow MLD during summer, as a result of the freshwater "lens" created by sea ice and glacier melt. This shallow MLD in summer protects the water column from wind induced mixing and stabilises the water column, promoting the growth of diatoms which dominate in Ryder Bay (Clarke et al., in-press; Garibotti, et.

al., 2006). There is a much more persistent shallow MLD during the 05/06 season compared to the 04/05 season, indicating that there was higher freshwater input to Ryder Bay during that season. The average salinity value in the upper 15 m of the water column also exhibits lower values during the 05/06 growing season, indicating higher freshwater input contributing to the consistently low MLD.

### 3.3.1 Sea Ice

Time series measurements of POC, [$CO_{2(aq)}$], PON and NO3 in sea ice are presented in Figure 3.3.

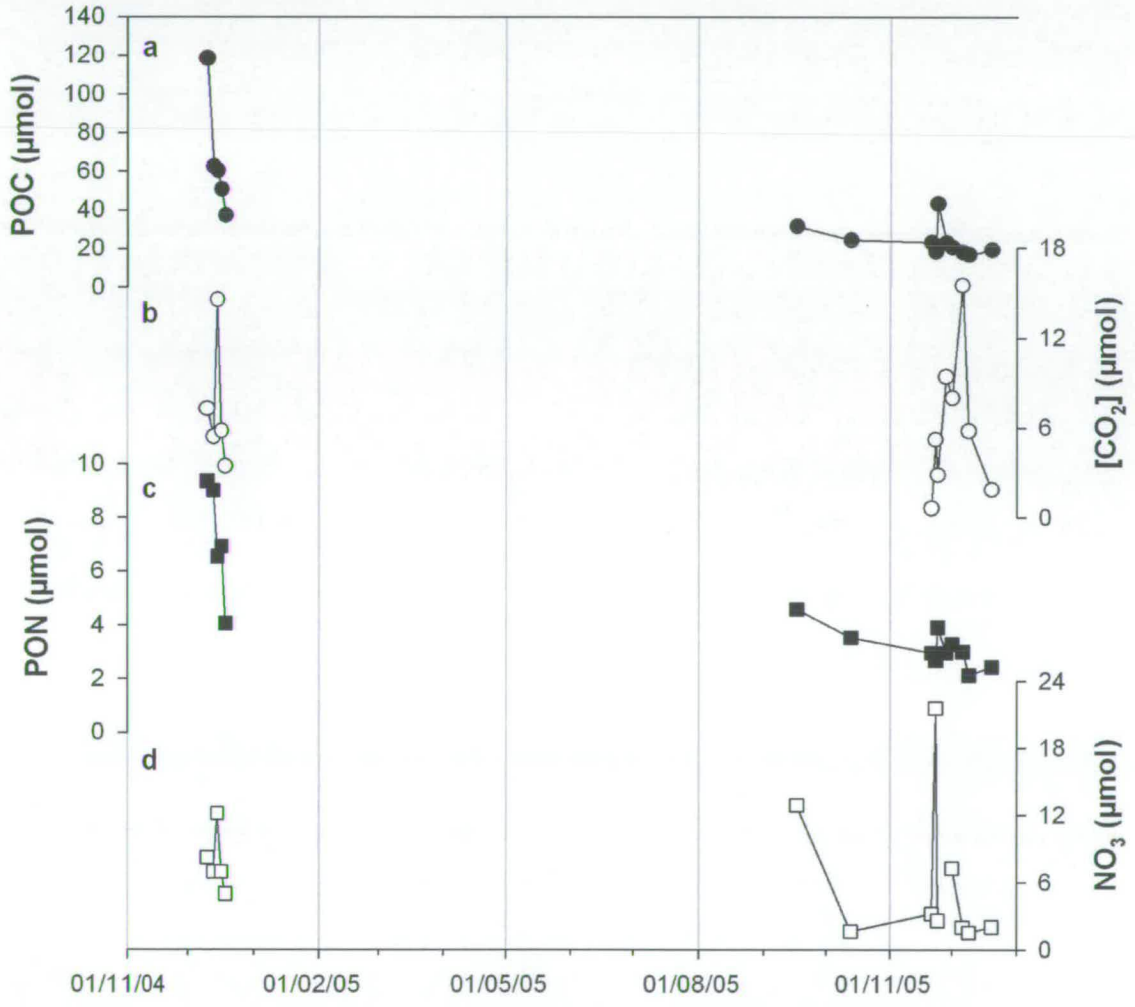


**Figure 3.3. Time series measurements of sea ice (a) particulate organic carbon (b) dissolved carbon dioxide (c) particulate organic nitrogen and (d) nitrate.**

Although both temporally and spatially sparse, these measurements indicate high standing stocks of phytoplankton in sea ice with POC concentrations reaching as high as 118 µmol.l-1. For both the 04/05 and 05/06 season, levels of POC and PON were in decline, probably as a result of the rate of degradation exceeding the rate of production as the sea ice ages and starts to decay prior to breaking up and melting. Both [$CO_{2(aq)}$] and NO3 concentrations are highly variable, but do show a general decreasing trend over time indicating utilisation. There is however evidence of nutrient injections during the 05/06 season, but this may just be an artefact of the high spatial and temporal variability of the sea ice matrix (Gleitz et. al., 1995; Kennedy et. al., 2002), and each sample was taken from a slightly different location, varying by up to $10m^2$ at the sites chosen.

### 3.3.2 Surface Waters

Time series measurements of POC, [$CO_{2(aq)}$], PON, $NO_3$ and $NH_4$ from the RaTS site at 15 m over the two growing seasons show high seasonality and are presented in Figure 3.4. POC and PON profiles resemble that of chlorophyll, reaching maxima of 72 and 13 $\mu mol.l^{-1}$ respectively during the 04/05 season and 61 and 10 $\mu mol.l^{-1}$ respectively during the 05/06 season.

During winter, when sea ice was present, concentrations of POC and PON drops to around 1.4 and 0.2 $\mu mol.l^{-1}$ respectively. The time series profiles of [$CO_{2(aq)}$] and $NO_3$ indicate high levels of nutrient utilisation in Ryder Bay. [$CO_{2(aq)}$] reaches minimum values of 5.2 and 11.1 µmol during the 04/05 and 05/06 seasons respectively, and NO3 reaches minimum values of 3.3 and 2.3 µmol during the 04/05 and 05/06 seasons respectively. Winter values of [$CO_{2(aq)}$] were not measured, but winter values of $NO_3$ were ~34 µmol as expected from the Upper Circumpolar Deep Water source for the region (Sigman et. al., 1999).

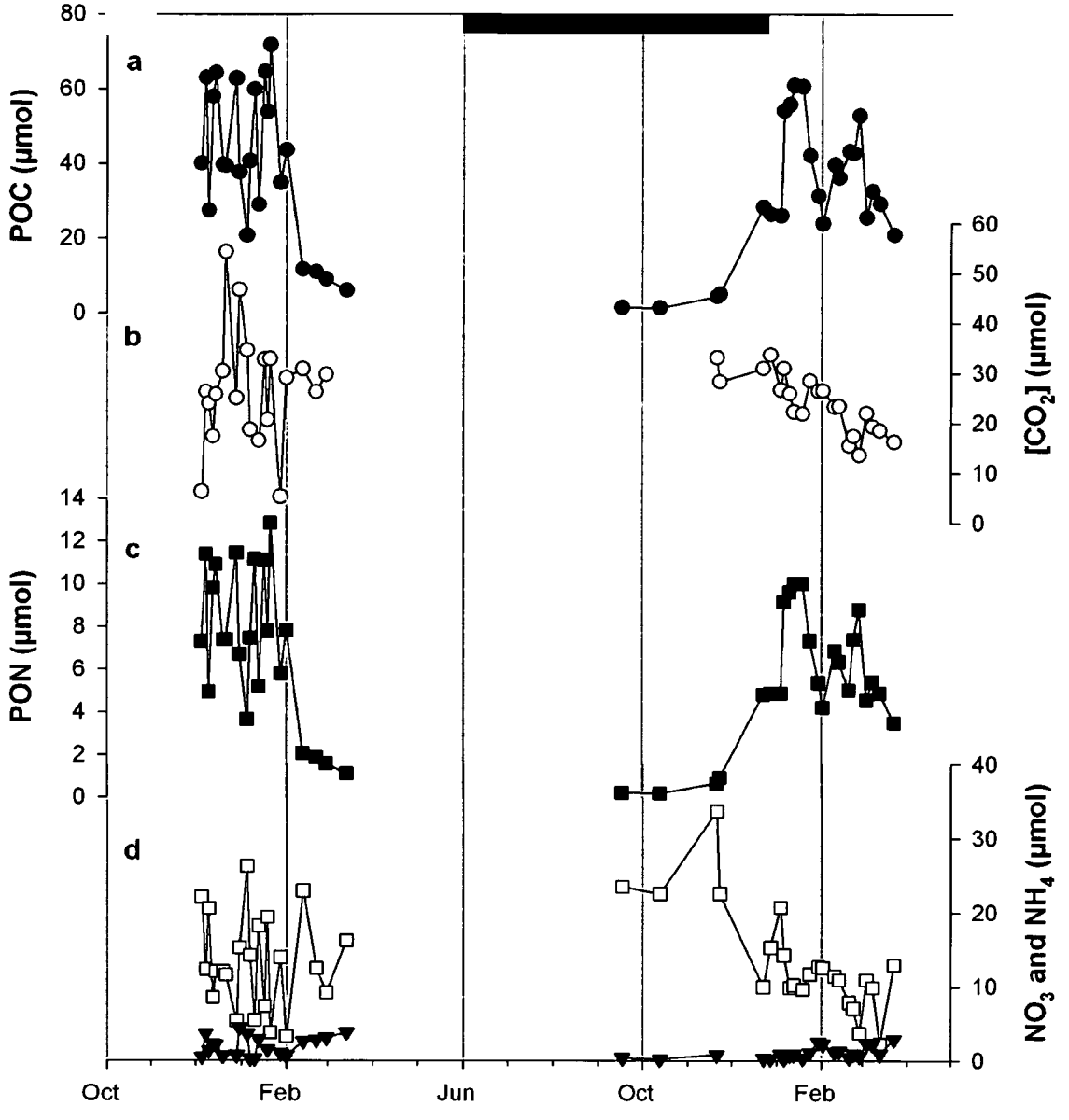


**Figure 3.4. Time series measurements of surface water (a) particulate organic carbon (b) dissolved carbon dioxide (c) particulate organic nitrogen and (d) nitrate (squares) and ammonium (triangles). Black bars indicate sea ice cover.**

The $NH_4$ profile shows generally low concentrations during the growing season that elevate during events where biomass (POC, PON) declines during mid-season and end of season, reaching values as high as 4 µmol. Higher values and more peaks in $NH_4$ concentration were observed during the 04/05 season.

There are high amplitude variations in the POC, PON, $[CO_{2(aq)}]$ and $NO_3$ profiles during the 04/05 season, showing significant declines in particulate organic material and increases in nutrient concentrations. This may be a product of vertical mixing of water masses, bringing nutrient rich water to the surface. The 05/06 season POC and PON profiles are much more stable, with nutrients also showing more of a monotonic decrease as they are utilised, with fewer and low magnitude inputs of nutrients occurring. This is consistent with the data in Figure 3.2 showing more stable water column characteristics during the 05/06 season, compared to 04/05.

The fluxes of organic carbon, organic nitrogen and biogenic opal exported from the surface waters to depth for Ryder Bay and nearby Marguerite Bay (Deep Site) are presented in Figure 3.5.

Although the initial flux from 2004 was not captured, we believe this occurred during December 2004, based on CTD fluorescence measurements that were taken at every sampling time point (Andy Clarke, pers. Comm.; Chapter 5). Biogenic fluxes show typical seasonality for the coastal Antarctic setting, with high fluxes occurring during the ice free spring and summer months, with very low fluxes during the ice covered autumn and winter.

Even though the initial flux from 2004 is unknown, based on the available data it is clear that there was a larger seasonal flux at the RaTS site during the 04/05 season compared to the 05/06 season, with the recorded fluxes at the Deep Marguerite Bay site being fairly similar. A summary of C and fluxes N for each growing season are presented in Table 3.1.

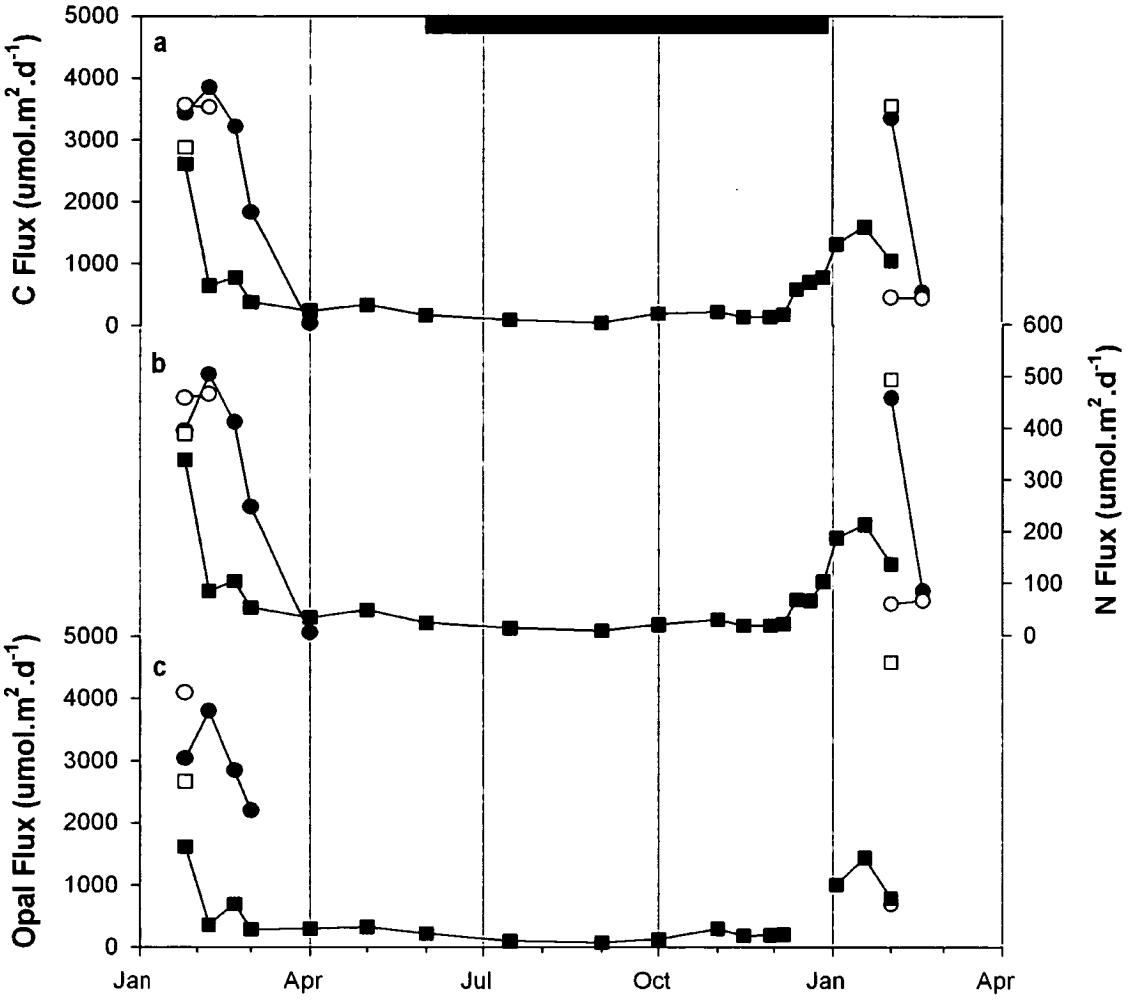


**Figure 3.5. Sediment trap fluxes of (a) organic carbon (b) organic nitrogen and (c) biogenic opal for the RaTS 200m trap (closed circles), the RaTS 512m trap (open circles), the Deep Site 123 m trap (closed squares) and the Deep Site 745 m trap (open squares).**

At the RaTS site, the data covering the latter part of the 04/05 season exhibit fluxes of 2.73 mmol C.m$^{-2}$.d$^{-1}$ and 0.35 mmol N. m$^{-2}$.d$^{-1}$ at 200 m and 1.42 mmol C.m-2.d$^{-1}$ and 0.18 mmol N. m$^{-2}$.d$^{-1}$ at 512 m. The fluxes were much lower during the 05/06 season at 1.99 mmol C. m$^{-2}$.d$^{-1}$ and 0.28 mmol N. m$^{-2}$.d$^{-1}$ at 200 m and 0.45 mmol C. m$^{-2}$.d$^{-1}$ and 0.06 mmol N. m$^{-2}$.d$^{-1}$ at 512 m.

At the Deep Site in Marguerite Bay, the trap fluxes were a little more consistent between seasons, although it is difficult to make conclusions for this trap as the initial flux in 2004 and the latter season flux in 2005 were not collected. During the partial coverage of the latter period of the 04/05 season

there were fluxes of 0.90 mmol C. $m^{-2}.d^{-1}$ and 0.12 mmol N. $m^{-2}.d^{-1}$ at 123 m and 0.53 mmol C. $m^{-2}.d^{-1}$ and 0.07 mmol N. $m^{-2}.d^{-1}$ at 745 m. During the early part of the 05/06 season (as the mooring was lost after the redeployment) the fluxes were 1.32 mmol C. $m^{-2}.d^{-1}$ and 0.18 mmol N. $m^{-2}.d^{-1}$ at 123 m and 1.15 mmol C. $m^{-2}.d^{-1}$ and 0.16 mmol N. $m^{-2}.d^{-1}$ at 745 m.

**Table 3.1. Summary of spring and summer fluxes during the sediment trap mooring deployments in Ryder Bay and Marguerite Bay (2005-2006).**

| Sediment Trap | C Flux ($mmol.m^{-2}.d^{-1}$) 04/05 | C Flux ($mmol.m^{-2}.d^{-1}$) 05/06 | N Flux ($mmol.m^{-2}.d^{-1}$) 04/05 | N Flux ($mmol.m^{-2}.d^{-1}$) 05/06 |
|---|---|---|---|---|
| RaTS 200 m | 2.73* | 1.99 | 0.35* | 0.28 |
| RaTS 500 m | 1.42* | 0.45 | 0.18* | 0.06 |
| Deep Site 123 m | 0.90* | 1.32* | 0.12* | 0.18* |
| Deep Site 745 m | 0.53* | 1.15* | 0.07* | 0.16* |

* - Partial values for the season as the initial flux was not captured for 04/05 and the Deep Site mooring was lost after redeployment in Feb 06.

The annually integrated flux calculated from both sites from 26th January 05 until 26th January 06 are presented in Table 3.2. The fluxes were higher at the RaTS site, and at both the RaTS and Deep Site, the levels of flux decreased with depth.

**Table 3.2. Annually integrated fluxes calculated for sediment trap mooring deployments in Ryder Bay and Marguerite Bay (2005-2006).**

| Annualy Integrated Flux | RaTS Site 200 m | RaTS Site 512 m | Deep Site 123 m | Deep Site 745 m |
|---|---|---|---|---|
| C Flux ($mmol.m^{-2}$) | 212.67 | 93.43 | 150.98 | 79.90 |
| N Flux ($mmol.m^{-2}$) | 27.64 | 12.19 | 20.34 | 10.97 |

Linear regression plots used to determine POC:PON ratios of material collected in sea ice and surface waters is presented in Figure 3.6. In sea ice, there was high variability in POC:PON ratios and using linear regression the POC:PON ratio was calculated as 10.5, although there may be error in this calculation as the Y-intercept is at -9, if forcing the intercept to 0, the POC:PON ratio calculation is still high at 8.8.

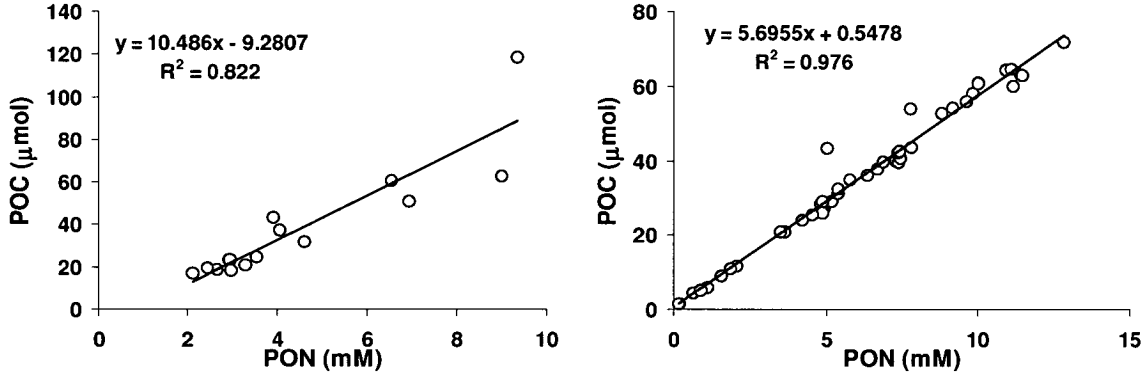


**Figure 3.6. Particulate organic carbon plotted against particulate organic nitrogen in (a) sea ice samples and (b) surface water samples.**

In surface waters there is considerably less variability in POC:PON ratio, with the higher values occurring during winter. The calculated POC:PON ratio is 5.7. Both of these ratios differ from the classic Redfield Ratio of 6.6, with sea ice exhibiting a much higher value and surface waters a slightly lower value.

The C:N ratio of sinking particulate organic matter in sediment traps is presented in Figure 3.7. Calculated ratios using linear regression are presented for both the shallow and deeper traps at each site. There is considerable variation in the C:N ratios, with the shallower traps showing slightly higher values than the deeper ones, which would be unexpected considering that C:N is expected to increase with depth as a result of faster degradation of organic nitrogen.

These plots, however, may be misleading as there was no material for analysis in the deeper traps during the lower flux periods when the POC:PON ratios in surface waters were higher. The C;N ratio of surface sediments collected at each site in 2005 were 6.3 for the RaTS site and 6.4 for the deep site.

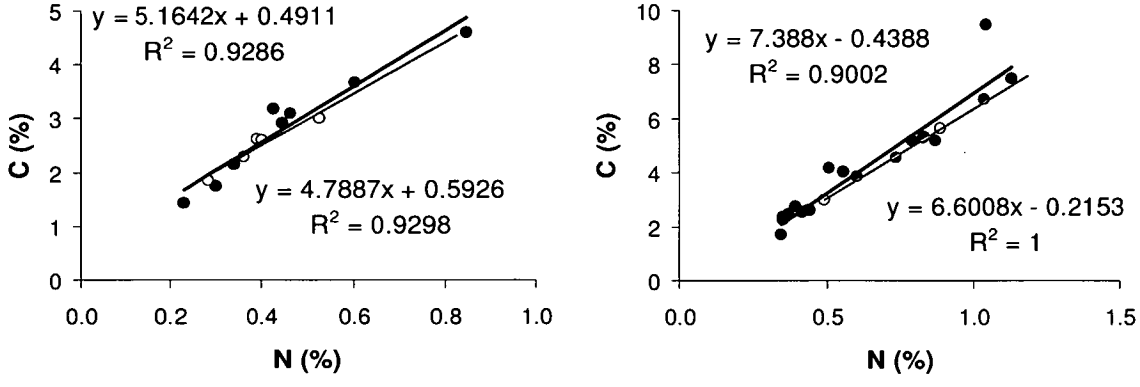


**Figure 3.7. % organic carbon plotted against % organic nitrogen in (a) The RaTS 200 m trap (closed circles, black line) and the RaTS 512 m trap (open circles, grey line) and (b) The deep site 123 m trap (closed circles, black line) and the Deep Site 745 m trap (open circles, grey line).**

Due to the limited number of opal measurements in the sediment traps, similar plots for the opal:carbon ratios were not made as they would not have been representative.

Time series measurements of the C:N ratio and opal:C ratio in sediment traps are presented in Figure 3.8 and show the seasonal progression of the

elemental composition of organic matter. The C:N ratios are fairly consistent during the growing seasons, but elevate to values as high as 9.1 during the winter when sea ice is present.

Although there is higher variability, there is a similar pattern observed in the opal:C ratios in sinking particles, reaching values as high as 7.6 during winter. There are also increases in the opal:C ratios observed with depth during the spring and summer months, when material was available for analysis, reaching values as high as 7.6 in the RaTS 512 m trap.

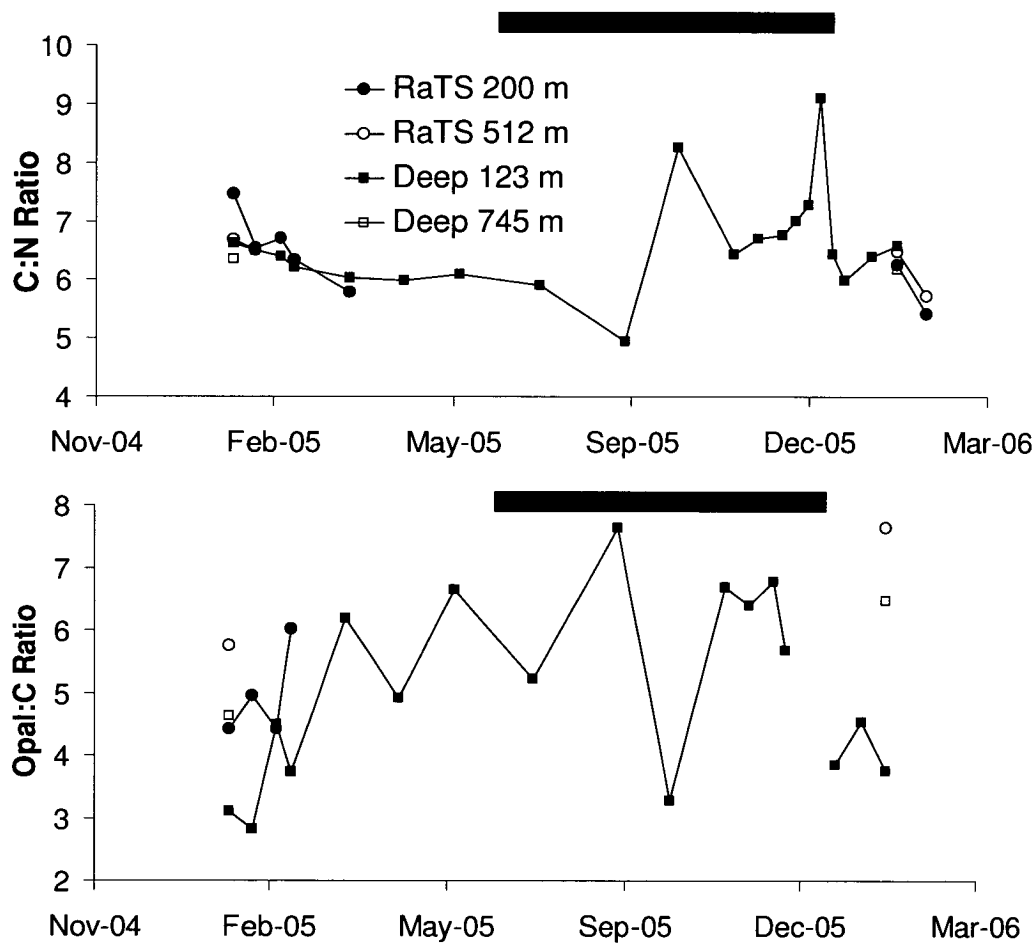


**Figure 3.8. Time series C:N ratios and opal:C ratios for the RaTS 200 m trap (closed circles) and the RaTS 512 m trap (open circles) and (b) The deep site 123 m trap (closed squares) and the Deep Site 745 m trap (open squares).**

## 3.4 Discussion

This study identifies some of the key controls on near shore Antarctic primary production and particle export, and potential mechanisms that may drive the high inter-annual variability in such ecosystems. Defining the root cause or any long term trend, however, is not in the scope of this paper as the study only lasted for two years.

The data emphasises the strong influence sea ice presence has on the timing of the spring bloom in coastal Antarctic environments, evident in previous studies (Clarke and Leakey, 1996; Ducklow et. al., In-press; Eicken, 1992; Villinski et. al., 2000; Wefer et. al., 1988). The data also provide evidence from discrete sea ice samples of the high standing stocks of organic matter that are released into the water column and may seed the phytoplankton bloom (Garrison et. al., 1983; Wilson et. al., 1986) and/or contribute to the annual export of organic material to depth (Arrigo et. al., 1997).

The two peak characteristics of chlorophyll profiles during both seasons studied are surprisingly similar in their timing and magnitude (Figure 3.4). Interestingly they are each accompanied by elevated concentrations of NH4, which suggests significant phytoplankton decay. It is possible these declines in biomass are a product of intense grazing, followed by secondary production. However, considering the low levels of $NH_4$ and observed $NO_3$ utilisation, secondary production is not thought to have dominated over primary production. This hypothesis is supported by primary production data (Weston, et al., unpublished), showing that primary production remains dominant throughout most of the season, although levels of secondary production are elevated during latter periods of the growing season.

One of the significant findings of this study is the differences in the sea ice regime of the winter preceeding each growing season. During winter 2004 sea ice cover lasted for 5 months (June to November), and during winter

2005 lasted for 6 months, and was considerably thicker than in 2004 (Andy Clarke pers. comm.) There are many possible causes for this significant difference in sea ice coverage of Ryder Bay, but this paper is not intended to investigate such reasons, it is intended to identify the effects such differences in sea ice will have on seasonal primary production. This sea ice effect did not seem to alter the duration of spring phytoplankton growth (~4 months), with both seasons exhibiting similar bloom characteristics and standing stocks of chlorophyll and POC.

These differences in sea ice seemed, however, to significantly affect the stability of the water column and thus the frequency of nutrient inputs to the system. During the 04/05 season, there were several $NO_3$ injections to the system (Figure 3.4), believed to have occurred due to a less stable water column. During the 05/06 season, the water column was more stable (Figure 2) and tended towards a closed system with fewer, low magnitude nutrient inputs. These contrasting conditions had a major impact on the quantity of material exported to depth at the RaTS site. In the RaTS 200 m trap, 177 mmol $C.m^{-2}$ was exported during the partial coverage of spring and summer 04/05 and only 54 mmol $C.m^{-2}$ exported during the full coverage of spring and summer 05/06. In the RaTS 512 m trap 92 mmol $C.m^{-2}$ was exported during 04/05 and only 12 mmol $C.m^{-2}$ was exported during 05/06.

Annually integrated fluxes were determined from January 05 to January 06 (Table 3.2) and were similar to levels quoted by Ducklow, et. al., (in-press), for the open continental shelf on the Western Antarctic Peninsula. Although this approach splits the flux peak between two succeeding years, this was the only way to estimate annual flux during this study. In-situ determination of primary production measured from December 05 to March 06 at the RaTS site (Weston et. al., unpublished) compared to the calculated sedimentation for that period gives an export efficiency of about 10 % at 200 m. This is likely an overestimate, however, as the in-situ primary production measurements were only carried out from late December, whereas primary

production began in early December, so the real export efficiency is more likely to be considerably <10 %, consistent with the estimate of Ducklow et al., (in-press) of 3-6 %. This is very low compared to the BATS site or the North Atlantic. In addition, there are no primary production data for sea ice communities, which were assumed to be negligible for the purpose of export efficiency estimation. The low export efficiency in continental shelf ecosystems suggests that they are composed of planktonic systems with relatively high regeneration efficiency and low f-ratios, a characteristic observed in this study during the secondary peak of production after the mid-season decline during the 05/06 season where such data were available.

Without the relevant primary production data to compare export efficiency in 05/06 to the 04/05 season, it is unclear whether there was increased export efficiency during the 04/05 growing season where the surface water was not as stable, and the absolute quantity of available nutrients was higher. This type of data would be useful to identify whether surface water stability is a potential control on export efficiency in this environment.

In contrast to Ducklow et al., (in-press) the exported material in this study did not show highly elevated C:N:P ratios, with such elevated values attributed to efficient remineralisation of N and P (note there were no P measurements conducted during this study). Ducklow et. al., (in-press) measured C:N ratios of 7.81, whereas summer flux values in Ryder Bay tended to be closer to the Redfield ratio of 6.6, as was the surface sediment sample C:N ratio (6.3).

There was an increase in C:N ratio in this study, when comparing the surface water POC:PON ratio of 5.7 to the surface sediment C:N ratio of 6.3. This suggests that the efficiency organic matter recycling is perhaps not as great in Ryder Bay as it is further out on the continental shelf of the Western Antarctic Peninsula. In this study, we also observe elevated C:N ratios of sinking particles during winter (Figure 3.8), a trait observed elsewhere in the continental shelf Southern Ocean (Collier et. al., 2000) that is consistent with

the longer retention time of organic material in surface waters during the ice covered winter, and more efficient degradation of such particles (Lourey et. al., 2003).

The high variability of opal:C in sediment traps may also be influenced by diatom assemblages as diatoms dominate production in Ryder Bay and the neighbouring Marguerite Bay (Clarke, et. al., in-press; Garibotti et. al., 2003; Garibotti et. al., 2005). Without surface water biogenic silica data it is difficult to determine the exact cause of the increase in opal:carbon in sediment traps, but similarly to carbon, it may be due to the degradation of the diatomaceous organic matter. The smaller, pennate or needle like, diatom species that are abundant in the surface waters of this region are often prone to remineralisation before they are exported to depth, and tend to have a lower opal:carbon ration than the larger diatoms that have a more robust opal frustule and export more opal per unit carbon than the smaller diatoms (Armand et al., 2008). Therefore the increase in opal:carbon ratio with depth in this region may be a result of the larger diatoms being more efficiently exported to depth than smaller diatoms. During winter, the higher opal:carbon ratio is likely caused by more efficient remineralisation of suspended organic material (similar to C:N ratios). Higher retention time of diatoms during winter would lead to a more rapid recycling of carbon compared to opal, in a senescent population of diatoms possibly leaving many the diatom frustules empty (Queguiner et al., 1997). This would explain the vast increases in the opal:carbon ratio of organic material caught in sediment traps over winter in this study. Again, without surface water biogenic silica data to compare with carbon, it is difficult to determine the exact nature of the opal:carbon enrichment observed in these traps.

## 3.5 Conclusions

The following conclusions can be drawn from this study:

- Sea ice not only exerts control on the timing of the spring bloom, but in conjunction with glacier melt, the freshwater input appears to significantly affect the stability of the water column and the characteristics of the growing season (i.e. total production and export).
- The two peak characteristic of each growing season may be explained by grazing pressures during the mid-season decline in biomass and elevation of $NH_4$. This leads to elevated levels of regenerated production during the latter period of the growing season.
- Estimated export efficiency at this site is very low, consistent with other studies in this region.
- Seasonal progression of C:N ratios and opal:C ratios in sinking particles show an increase with depth and elevated levels during winter. This is a result of increased remineralisation of sinking diatoms with depth and increased retention time of particles in the surface water during winter leading to more efficient recycling of N relative to C and C relative to opal.

## 3.6 References

Armand, L. K., Cornet-Barthaux, V., Mosseri, J. and Queguiner, B. (2008) Late summer diatom biomass and community structure on and around the naturally iron-fertilised Kerguelen Plateau in the Southern Ocean. *Deep-Sea Research II*, 55, 653-676.

Arrigo, K. R., Worthen, D. L., Lizotte, M. P., Dixon, P. and Dieckmann, G. (1997) Primary production in Antarctic sea ice. Science, 276, 394-397.

Arrigo, K. R., Worthen, D., Schnell, A. and Lizotte, M. P. (1998) Primary production in Southern Ocean Waters. Journal of Geophysical Research, 103, 15587-15600.

Arrigo, K. R., Robinson, D. H., Worthen, D. L., Dunbar, R. B., DiTullio, G. R., VanWoert, M. and Lizotte, M. P. (1999) Phytoplankton community structure and the drawdown of CO2 in the Southern Ocean. Science, 283, 365-367.

Broecker, W. S. and Peng, T. H. (1982) Tracers in the sea. Eldigio Press, Palisades.

Carson, D. S., Ganeshram, R. S., Difiore, P. J., Sigman, D. M. and Clarke, A. (in-prep) δ15N of nutrients and organic matter as proxies for productivity and export production in the coastal Antarctic Sea Ice Environment. For submission to Deep Sea Research Part II: Oceanographic Research Papers.

Clarke, A. and Leakey, R. J. G. (1996) The seasonal cycle of phytoplankton, macronutrients, and the microbial community in a nearshore Antarctic ecosystem. Limnology and Oceanography, 41(6), 1281-1294.

Clarke, A., et al. (2008), Seasonal and interannual variability in temperature, chlorophyll and macronutrients in northern Marguerite Bay, Antarctica, Deep Sea Research Part II: Oceanographic Research Papers, in press.

Collier, R., Dymond, J., Honjo, S., Manganini, S., Francois, R. and Dunbar, R. (2000) The vertical flux of biogenic and lithogenic material in the Ross Sea: moored sediment trap observations 1996-1998. Deep Sea Research II, 47, 3491-3520.

Dickson, A. G., and F. J. Millero (1987), A comparison of the equilibrium constants for the dissociation of carbonic acid in seawater media, Deep Sea Research Part I: Oceanographic Research Papers, 34, 1733-1743.

Ducklow, H. W., Erickson, M., Kelly, J., Smith, R. C., Stammerjohn, S. E., Vernet, M. and Karl, D. M. (2008) Particle export from the upper ocean over the continental shelf of the west Antarctic Peninsula: A long-term record, 1992-2006. Deep Sea Research Part II: Oceanographic Research Papers, in press.

Eicken, H. (1992) The role of sea ice in structuring Antarctic ecosystems. Polar Biology, 12, 3-13.

Garibotti, I. A., Vernet, M., Ferrario, M. E., Smith, R. C., Ross, R. S. and Quetin, L. B. (2003) Phytoplankton spatial distribution patterns along the

western Antarctic Peninsula (Southern Ocean). Marine Ecology Progress Series, 261, 21-39.

Garibotti, I. A., et al. (2005), Annually recurrent phytoplanktonic assemblages during summer in the seasonal ice zone west of the Antarctic Peninsula (Southern Ocean), Deep-Sea Research Part I-Oceanographic Research Papers, 52, 1823-1841.

Garrison, D. L., Ackley, S. F. and Buck, K. R. (1983) A physical mechanism for establishing algal populations in frazil ice. Nature, 306, 363-365.

Gleitz, M., et al. (1995), Comparison of Summer and Winter Inorganic Carbon, Oxygen and Nutrient Concentrations in Antarctic Sea-Ice Brine. Marine Chemistry, 51, 81-91.

Hannson, I. (1973), A new set of activity constants for carbonic acid and boric acid in seawater, Deep Sea Research, 20, 461-478.

Holmes, R. M., et al. (1999), A simple and precise method for measuring ammonium in marine and freshwater ecosystems, Canadian Journal of Fisheries and Aquaculture Sciences, 56, 1801-1808.

Kennedy, H., Thomas, D. N., Kattner, G., Haas, C. and Dieckmann, G. S. (2002) Particulate organic matter in Antarctic summer sea ice: concentration and stable isotopic composition. Marine Ecology Progree Series, 238, 1-13.

Lewis, E., and D. W. R. Wallace (1998), Program developed for CO2 system calculations. ORNL/CDIAC-105. Carbon dioxide information analysis center, Oak Ridge National Laboratory, U.S. Department of Energy, Oak Ridge, Tenesee.

Lourey, M. J., et al. (2003), Sensitivity of delta N-15 of nitrate, surface suspended and deep sinking particulate nitrogen to seasonal nitrate depletion in the Southern Ocean. Global Biogeochemical Cycles, 17(3), 1081, doi:10.1029/2002GB001973.

Lourey, M. J., et al. (2004), Sensitivity of delta C-13 of Southern Ocean suspended and sinking organic matter to temperature, nutrient utilization, and atmospheric CO2. Deep-Sea Research Part I-Oceanographic Research Papers, 51, 281-305.

Mehrbach, C., et al. (1973), Measurement of the apparent dissociation constant of carbonic acid in seawater at atmospheric pressure, Limnology and Oceanography, 18, 897-907.

Mortlock, R. A. and Froelich, P. N. (1989) A simple method for the rapid determination of biogenic opal in pelagic marine sediments. Deep Sea Research, 36(9), 1415-1426.

Queguiner, B., Treguer, P., Peeken, I. and Scharek, R. (1997) Biogeochemical dynamics and the silicon cycle in the Atlantic sector of the Southern Ocean during austral spring 1992. *Deep-Sea Research II*, 44, 69-89.

Sigman, D. M., et al. (1999), The delta N-15 of nitrate in the Southern Ocean: Consumption of nitrate in surface waters. Global Biogeochemical Cycles, 13, 1149-1166.

Strickland, J. D. H., and T. R. Parsons (1972), A Practical Handbook of Seawater Analysis, pp. 311. Fisheries Research Board of Canada.

Turner, J., Colwell, S. R., Marshall, G. J., Lachlan-Cope, T. A., Carleton, A. M., Jones, P. D., Lagun, V., Reid, P. A. and Iagovinka, S. (2005) Antarctic climate change during the last 50 years. International Journal of Climatology, 25, 279-294.

Villinski, J. C., et al. (2000), Carbon 13 Carbon 12 ratios of sedimentary organic matter from the Ross Sea, Antarctica: A record of phytoplankton bloom dynamics, Journal of Geophysical Research-Oceans, 105, 14163-14172.

Vernet, M., Martinson, D. G., Iannuzzi, R. A., Stammerjohn, S. E., Kozlowski, W. A., Sines, K. and Smith, R. C. (2008) Control on primary production by sea ice dynamics in the Western Antarctic Peninsula. Deep Sea Research, in-press.

Wefer, G., Fischer, G., Futterer, D. and Gersonde, R. (1988) Seasonal particle flux in the Bransfield Strait, Antarctica. Deep Sea Research, 35, 891-898.

Wilson, D. L., Smith, W. O. and Nelson, D. M. (1986) Phytoplankton bloom dynamics of the western Ross Sea ice edge. I. Primary productivity and species-specific production. Deep Sea Research, 33, 1375-1387.

# 4 Factors Influencing $\delta^{13}C$ of suspended and sinking Organic Matter in the Coastal Antarctic Sea Ice Environment

A version of this chapter has been submitted to Deep Sea Research Part I and is currently under review.

Citation: Carson, DS, Annett, AL, Ganeshram, RS, Weston, K, Crosta, X, Tait, A, Dougans, J, Fallick AE and Clarke A (in review) Factors influencing $\delta^{13}C$ of suspended and sinking organic matter in the coastal Antarctic sea ice environment.

## Abstract

This study presents the first high-resolution time series analysis of the $\delta^{13}C$ of dissolved inorganic carbon, suspended and sinking particulate organic carbon and diatom assemblages in the near shore Antarctic sea ice environment, Ryder Bay, Antarctica. The study spans a period of two growing seasons from 2004 to 2006. Our results show on average higher $\delta^{13}C$ in sea ice samples compared to surface waters, possibly brought on by post-production decomposition processes. In addition a very large ~10 ‰ negative shift in surface water $\delta^{13}C_{POC}$ is observed during the growing seasons, which was not accompanied by a similar change in $[CO_{2(aq)}]$ or $\delta^{13}C\text{-}CO_2$. Analysis of diatom assemblages shows that the negative shifts in $\delta^{13}C_{POC}$ are accompanied by distinct changes in diatom assemblages with a higher surface area to volume ratio (SA:V). Thus the higher fractionation factor associated with carbon fixation ($\varepsilon_p$) with increasing SA:V appears to be primary cause for the significant negative excursions in $\delta^{13}C_{POC}$. Other processes involving internal cell biochemistry may also have contributed to changes in $\varepsilon_p$, but these processes are not well constrained for most diatom species and cannot be fully assessed. $\delta^{13}C_{org}$ of particles collected in sediment traps in Ryder Bay show that the negative $\delta^{13}C$ shifts are transferred to the deep waters by sinking particles. These findings document the potential importance of diatom assemblage changes and sea ice-derived material in influencing sedimentary $\delta^{13}C_{POC}$ in Antarctic sea ice environments

and highlights potential weaknesses in the utility of using diatom-based $\delta^{13}C$ in reconstructing paleo-$pCO_2$.

## 4.1 Introduction

Paleoceanographic studies of the Southern Ocean have observed that the glacial $\delta^{13}C$ of diatom bound organic matter were lower than during interglacials and the Holocene (Crosta and Shemesh, 2002; Rosenthal, et al., 2000; Schneider-Mor, et al., 2005; Singer and Shemesh, 1995). The reasons for these isotopic shifts remain unclear but suggested causes include higher concentrations of dissolved molecular carbon dioxide ($[CO_2]_{aq}$), lower growth rates and changes in diatom abundance or size effects. Documenting processes that decouple carbon isotopes from the classic $\delta^{13}C$ versus $pCO_2$ relationship used for paleo-$CO_2$ reconstructions is important in understanding any influence the Southern Ocean may have had during glacial-interglacial climate transitions.

Indeed, recent lab and field studies highlight that the isotopic composition of suspended particulate organic carbon ($\delta^{13}C_{POC}$) in phytoplankton can be affected by cell size or shape (Burkhardt, et al., 1999; Popp, et al., 1998; Trull and Armand, 2001), non diffusive carbon uptake through carbon concentration mechanisms (Cassar, et al., 2004; Rau, 2001) and other environmental and physiological factors such as $CO_2$ concentration, light levels and growth rates (Cassar, et al., 2006). These processes affect carbon isotopic fractionation ($\varepsilon_p$) and loosen the relationship between $\delta^{13}C_{org}$ and $[CO_2]_{aq}$ and may account for the observed discrepancy between marine $\delta^{13}C_{org}$ based $pCO_2$ reconstructed from low-latitude records and Vostok $CO_2$ (Kienast, et al., 2001).

In the Southern Ocean, $[CO_2]_{aq}$ is generally very high and growth rates are relatively low, so it is likely that Antarctic phytoplankton acquire their inorganic carbon by diffusion, negating the need for active carbon uptake. A recent paleo-study in Adelie Land, East Antarctica (Crosta, et al., 2005), also highlighted how past climate-driven changes in diatom assemblages affect the $\delta^{13}C_{org}$ signature of Holocene sediments. Given that the size and shape

of phytoplankton and the growth conditions are seemingly a very important factor in shaping the $\delta^{13}C_{org}$ of Southern Ocean sediments, a detailed time-series of Antarctic phytoplankton species or groups and concurrent information on their effects on carbon isotopes fractionation is essential in order to make $\delta^{13}C_{org}$ a reliable paleo-$CO_2$ proxy.

This study provides one of the first high resolution time-series measurements of geochemical parameters coupled with diatom assemblages in coastal Antarctic surface waters, covering two growing seasons and one full winter of sea ice cover. We present results from Ryder Bay, Antarctica; a coastal, seasonally sea ice covered Southern Ocean environment. Diatoms dominate the summer assemblages in this region, with biomass of other phytoplankton such as prymnesiophytes and cryptophytes more than an order of magnitude lower (Garibotti, et al., 2005). We compare levels of productivity biomass (chlorophyll and POC) in sea ice and surface waters with $[CO_{2(aq)}]$, the stable carbon isotopic composition of dissolved inorganic carbon ($\delta^{13}C$-$CO_2$) of surface water and sea ice, diatom assemblages, the stable carbon isotope composition of suspended POC ($\delta^{13}C_{POC}$) and the stable carbon isotopic composition of sinking particulate organic carbon ($\delta^{13}C_{org}$) in an effort to understand the major factors that may control $\delta^{13}C_{POC}$ signatures in this environment on a seasonal timescale.

## 4.2 Materials and Methods

### 4.2.1 Study Area

This study was conducted between 2004 and 2006 in Ryder Bay and Marguerite Bay located south of Alexander Island and west of the mainland on the Western Antarctic Peninsula (see Figure 4.1). Ryder Bay is a coastal embayment adjoining Marguerite Bay and the study site is situated in open water at a depth of 520 m.

Sea ice brine was sampled when sea ice was present at three locations, with a total of 15 sea ice samples were taken during this study. Sea ice had

receded from Ryder Bay upon arrival at in December 2004, however there was still land fast ice located around Lagoon Island (see Figure 4.1 for Lagoon Island sampling site), with 5 samples taken at the Lagoon Island site during December 2004. A further 10 samples were taken during the 05/06 season. During winter 2005, two sea ice samples were taken in September and October at the RaTS site and during early spring 2005 (Nov-Dec), a further eight sea ice samples were taken at a site north of Rothera Point (See Figure 1).

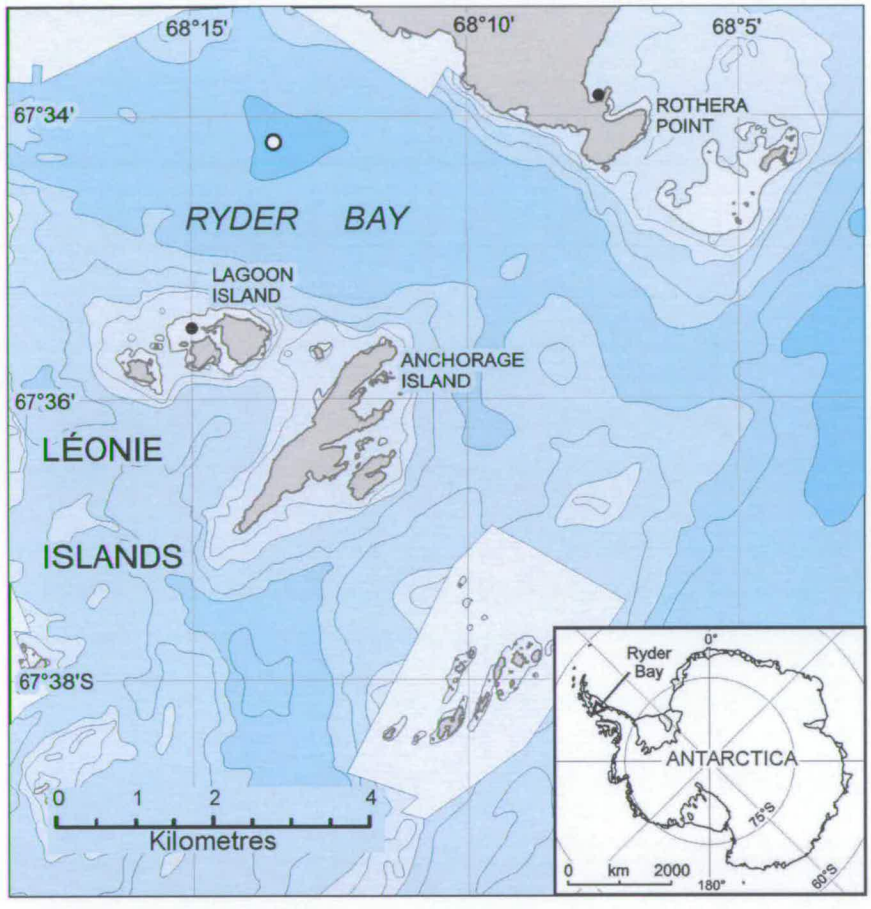


**Figure 4.1. Map of Ryder Bay showing the RaTS site (white circle) and the two other sites used for sea ice sampling (black circles). Map courtesy of the British Antarctic Survey.**

A high resolution time series of surface water samples were taken in Ryder Bay, at the Rothera Time Series study site at 67°34.02'S, 68°14.02'W (Clarke, et al., 2007) during austral spring and summer 2004/2005 and austral spring and summer 2005/2006 (Figure 4.1). Low resolution time

series sampling was conducted during winter 2005. Sea ice brine and surface water samples at 15 m depth (the average depth of the chlorophyll maximum in Ryder Bay (Clarke, et al., 2007) were taken measuring: temperature, salinity, chlorophyll-*a*, $[CO_{2(aq)}]$, $\delta^{13}C\text{-}CO_2$, suspended POC, $\delta^{13}C_{POC}$ and diatom assemblages. Routine CTD measurements were also taken at every surface water sampling event to monitor changes in the mixed layer depth (MLD). Sinking particulate $\delta^{13}C$ and associated diatom assemblages were collected in time-series sediment traps located at two depths at both the RaTS site and a deeper site in Marguerite Bay during the study (see section 4.8). Finally, surface sediments and shallow sediment box cores were taken at the RaTS site in January 2005 and December 2006 and the deep site in December 2006 (see section 3.2.9), and were analysed for both $\delta^{13}C$ and diatom assemblages.

### 4.2.2 Sea ice Sampling

Sea ice brine was sampled using a sack hole drilling method, with samples for $\delta^{13}C\text{-}CO_2$ and $[CO_{2(aq)}]$ taken first to minimise atmospheric contamination. Samples for $\delta^{13}C\text{-}CO_2$ were taken using a 50 ml syringe and gently injected into a 12 ml glass exetainer vial preloaded with 50 µL of 35 $g.L^{-1}$ copper sulphate to suppress bacterial activity (Winslow, et al., 2001). Alkalinity samples for $[CO_{2(aq)}]$ determination were taken by immersing a 250 ml BOD bottle in the sack hole and sealing the bottle with a plastic stopper ensuring no air bubbles were present. Salinity and temperature were measured using a YSI-500 multi-parameter meter. For particulate carbon measurements, sea ice brine was transferred to acid-clean HDPE carbuoys and taken back to the laboratory for filtration. Sea ice brine samples were filtered through muffle-furnaced (400°C for 4 h) 47 mm GF/F filters, within 2 h of collection. The filters were then dried at 50°C overnight, and stored frozen until analysis. For diatom census counts, sea ice brine was filtered through 37 mm polycarbonate filter (0.45 µm). Filters were dried overnight at 50°C and stored in clean plastic Petri-slides until analysis.

### 4.2.3 Surface Water Sampling

In surface waters, CTD casts were taken to 500 m depth using a Sea Bird Electronics 19 Plus SEACAT CTD module. For depth profile measurements of conductivity, temperature and depth a Wet Labs Wetstar module was used. For measurement of temperature at 15 m, a Sensoren Instrumente Systeme GmbH reversible thermometer was lowered to 15 m, allowed to equilibrate for 2 min and a brass messenger was sent down to initiate temperature recording. Surface water samples were taken using a 5 L Niskin bottle for chlorophyll *a*, $\delta^{13}C\text{-}CO_2$ and $[CO_{2(aq)}]$ measurements. For $\delta^{13}C\text{-}CO_2$, water was drawn from the Niskin bottle using a 50 ml syringe and gently injected into a 12 ml glass exetainer vial preloaded with 50 µL of 35 $g.L^{-1}$ copper sulphate to suppress bacterial activity (Winslow, et al., 2001). Alkalinity samples for $[CO_{2(aq)}]$ determination were taken from the Niskin straight into a 250 ml BOD bottle and sealing the bottle with a plastic stopper ensuring that no air bubbles were present. Particulate samples were retrieved using a 12 V dolphin pump and 15 m of silicone tubing weighted down at the end. Water from 15 m was pumped into 10 L HDPE carbuoys for transfer back to the laboratory. Surface water samples were filtered through muffle-furnaced (400°C for 4 h) 47 mm GF/F filters. The filters were then dried at 50°C overnight and stored frozen until analysis. For diatom census counts, water was filtered through 37 mm polycarbonate filter (0.45 µm). Filters were dried overnight at 50°C and stored in clean plastic Petri-slides until analysis.

### 4.2.4 $[CO_{2(aq)}]$ Analysis

Determination of $[CO_{2(aq)}]$ was conducted utilising measurements of salinity, temperature, pH and alkalinity. Salinity measurements were taken from the CTD profiles, temperatures were measured using a Sensoren Instrumente Systeme GmbH reversible thermometer. Alkalinity was determined by titration with 0.05 M HCl and the Gran plot method (Almgren, et al., 1983). $[CO_{2(aq)}]$ was calculated using constants from (Dickson and Millero, 1987),

(Hannson, 1973) and (Mehrbach, et al., 1973) with the CO2SYS programme (Lewis and Wallace, 1998).

### 4.2.5 $\delta^{13}C$-$CO_2$ Determination

$\delta^{13}C$-DIC analysis was conducted by GC-IRMS using a method similar to Assayag, et al., (2006). The 12 ml glass exetainer vial containing 12 ml of water sample spiked with $CuSO_4$ to surpress biological activity was split into two samples by inserting a closed syringe through the septum of the vial and injecting 6 ml of He into the sample vial using a separate needle and syringe. The 6 ml of sample extracted was then injected into a clean 12 ml exetainer vial that had been placed under vacuum for 30 min to remove all gases that were inside. Each sample was then injected with 0.6 ml of concentrated $H_3PO_4$ in order to convert the DIC into aqueous and gaseous $CO_2$ for analysis. Three sets of isotopic standards were prepared (MAB2, $CaCO_3$ and $NaHCO_3$) using a range of final DIC concentrations. The standards were weighed into 12 ml glass exetainer vials and then placed on a vacuum to remove all gases. 6 ml of 10 % $H_3PO_4$ was then injected into each standard vial to reproduce the same conditions in the sample vials. $\delta^{13}C$-DIC was analysed using a custom built GC-IRMS system and raw $\delta^{13}C$ values were corrected using the isotopic standards, which also included any fractionation of the standards in the correction. Precision of $\delta^{13}C$-DIC values was generally better than 0.2 ‰. The isotopic composition of $CO_{2(aq)}$ ($\delta^{13}C$-$CO_2$) was determined from $\delta^{13}C$-DIC and absolute temperature ($T_k$ in Kelvin) using the following equation from (Rau, et al., 1996):

$$\delta^{13}C\text{-}CO_2 = \delta^{13}C\text{-DIC} + 23.644 - 9701.5/T_k$$

### 4.2.6 POC, PON and $\delta^{13}C_{POC}$ Analysis

Bulk POC, PON and $\delta^{13}C_{org}$ analyses were conducted using a method similar to (Lourey, et al., 2004). Prior to analysis, the filters were decarbonated by wetting the filter with Milli-Q water and fuming with HCl for 48h and then drying at 50°C. Filters were analysed for elemental POC and $\delta^{13}C_{POC}$ using a Carlo Erba NA 2500 elemental analyser in-line with a VG PRISM III isotope

ratio mass spectrometer. $\delta^{13}C_{org}$ results are presented in the delta notation versus PDB.

### 4.2.7 Diatom Census Counts

To count diatoms, a sub sample of the polycarbonate filter was coated in gold and analysed using secondary electron imaging on a Philips XL 30 CP scanning electron microscope. Thirty fields of view were counted at each magnification, 500X for large cells, and 1000X for small cells. Calculations of cell concentrations were adapted from the Űtermohl method (Utermohl, 1958) using the volume of seawater filtered, and assuming even distribution of cells on the filter. Cell volumes and surface area were estimated from average measurements of 30 cells of each species where possible. Total volume contribution of each species was calculated using average cell volume. SA:V for collective diatom assemblages were calculated using a weighted average of the SA:V for each species and the proportion of the diatom assemblage the species made up at each time point.

### 4.2.8 Sediment Trap Deployments

Two sediment trap mooring arrays were deployed, with one at the RaTS site and the other at a deeper site in Marguerite Bay (67' 55.39°S, 68' 24.15° W) to catch sinking particles in concert with the time series water sampling programme. Each mooring consisted of two time-series sediment traps, which were situated at 200 m and 400 m for the RaTS mooring and 123 m and 745 m for the deep site mooring. Each sediment trap was equipped with 21 rotating for cups, which were programmed to rotate at predefined intervals. The strategy employed for cup rotation utilised higher resolution cup turnover during periods of potential sea ice melt and the spring bloom with lower resolution cup rotation during the low flux winter periods (see chapter 2 for exact dates of cup rotation). Each cup was filled with filtered seawater spiked with an extra 5 ‰ NaCl to increase its density to above that of the surrounding seawater and finally spiked with formaldehyde to have an overall concentration of 2 % (v/v) to prevent bioturbation.

After recovery, the solution in each cup was allowed to settle, the supernatant siphoned off and the swimmers were removed. Each sample cup was then split into 10 fractions using a rotary splitter at the National Oceanography Centre (NOC), Southampton, UK. The RaTS site mooring was initially deployed on the 25th January 2005 in 502 m water at 67'34.02°S, 68' 14.02°W. The deep site mooring was deployed on the 24th January 2005 in 841 m water at 67' 55.39°S, 68' 24.15° W. The RaTS mooring and deep mooring were recovered on the 15th February 2006 and the sediment trap bottles were removed and replaced with fresh ones. Both moorings were redeployed on the 17th February 2006. The RaTS mooring was redeployed at a water column depth of 522m at 67' 34.00°S, 68' 14.00°W. The deep mooring was redeployed at a water column depth of 835m at 67' 55.41°S, 68'24.11°W. For a table of sediment trap bottle rotations during the second deployment, refer to Table 6. The moorings were further recovered on 17th December 2006 aboard JCR Cruise 155. The RaTS mooring was successfully recovered, but unfortunately the deep mooring was lost.

### 4.2.9 Sediment Organic Carbon and $\delta^{13}C_{org}$ Analysis

One sediment trap cup split and sub-section of the box core were freeze-dried and ground for analysis of particulate components. For POC, PON and $\delta^{13}C_{org}$ analysis, duplicate 10 mg aliquots of dried sediment were weighed into silver capsules and were acidified with 50 % HCl to remove carbonates and dried at 60°C overnight. Decarbonated samples were then analysed for elemental POC, PON and $\delta^{13}C_{org}$ using a Carlo Erba NA 2500 elemental analyser in-line with a VG PRISM III isotope ratio mass spectrometer. $\delta^{13}C_{org}$ results are presented in the delta notation versus PDB.

### 4.2.10 Sedimentary Diatom Census Counts

Diatoms were taxonomically identified in all sediment trap cups where enough material was available. Diatom analysis, sediment treatment and slide preparation followed a technique adapted from the one described by (Rathburn, et al., 1997). Diatom counts followed (Schrader and Gersonde, 1978) and (Laws, 1983). Roughly 350 diatom valves were counted in each

sample at a magnification of 1000 on a phase contrast Olympus BX51. Diatoms were identified to species or species group level, and the relative abundance of each was calculated as the fraction of diatom species against total diatom abundance in each sample. More detailed information about slide preparation, diatom identification and statistical treatment are given by (Crosta, et al., 2004)

## 4.3 Results

### 4.3.1 Seasonal Sea Ice Cover and Productivity

Sea ice cover, mixed layer depth (MLD) and chlorophyll a (chl-a) data from growing seasons (2004/2005 and 2005/2006) sampled during this study are presented in Figure 4.2.

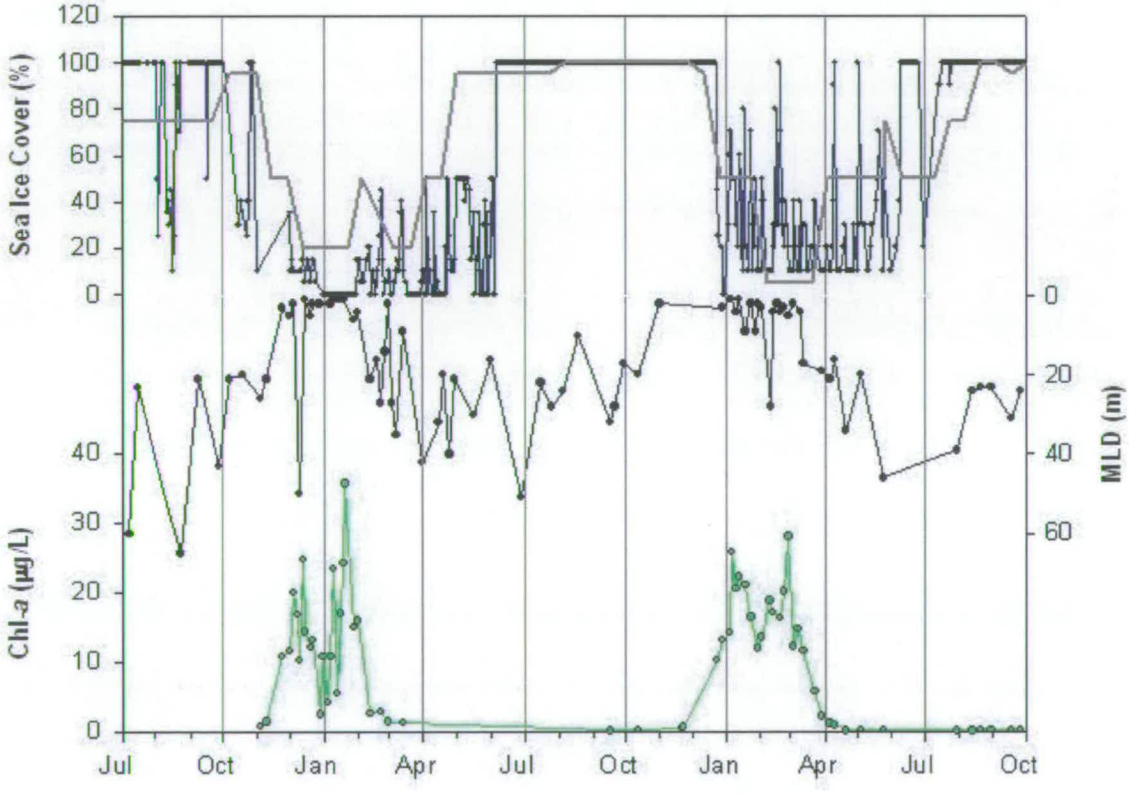


**Figure 4.2. Time-series profiles of (a) Sea ice cover with the grey line representing regional sea ice cover from NOAA satellite data and the blue line representing daily observations of Ryder Bay (b) Mixed layer depth and (c) chlorophyll-a concentrations spanning the growing seasons sampled during this study.**

Total sea ice cover was variable between the two seasons at the RaTS site, occurring from 16th June to 1st November during winter 2004 and 10th June to 25th December during winter 2005. The mixed layer depth (MLD) data in Figure 4.2 show typical seasonality for Ryder Bay, with a deep winter mixed layer and a shallow surface layer in summer, influenced heavily by freshwater melt from sea ice and glaciers (Clarke, et al., 2007). The freshwater melt layer stabilises the surface waters and prevents wind-induced upwelling, providing a stable environment for diatom blooms to grow and promoting nutrient drawdown (Clarke, et al., 2007).

The presence and retreat of ice over this period and the physical aspects of the water column resulted in growing seasons that lasted ~4 months during both growing seasons. However, the growing season of 05/06 began and finished ~1 month later due to sea ice cover lasting one extra month during winter of 2005.

### 4.3.2 $[CO_{2(aq)}]$ and $\delta^{13}C\text{-}CO_2$

The concentration of $[CO_{2(aq)}]$ and $\delta^{13}C\text{-}CO_2$ in surface waters are presented in Figure 4.3 and show a general trend of $[CO_{2(aq)}]$ decrease and $^{13}C$ enrichment during spring and summer, and appears to be largely controlled by biological uptake of carbon. $[CO_{2(aq)}]$ concentrations decreased from values as high as 54.2 µmol to 5.1 µmol with $\delta^{13}C\text{-}CO_2$ values rising from -10.9 to -9.0 ‰ during the 04/05 season. $[CO_{2(aq)}]$ concentrations decreased from a high winter value of 33.7 µmol to 13.6 µmol with $\delta^{13}C\text{-}CO_2$ values rising from -10.9 to -9.2 ‰ during the 05/06 season. $[CO_{2(aq)}]$ and $\delta^{13}C\text{-}CO_2$ can be affected by air-sea carbon fluxes, upwelling of nutrient rich water, lateral input of surface water and organic carbon remineralisation.

The $[CO_{2(aq)}]$ profile in Figure 4.3 shows that inputs of inorganic carbon occurred during both field season, albeit to a greater extent during the 04/05 season. These inputs of $CO_{2(aq)}$ to the system resulted in small negative shifts in $\delta^{13}C\text{-}CO_2$ occurring mid-season, with values falling as low as -10.5 ‰ during December 2004 and February 2006. The $\delta^{13}C\text{-}CO_2$ in sea ice is on

average higher than surface waters and with higher temporal variability, with values ranging from -10.7 to -4.8 ‰. $CO_{2(aq)}$ concentrations in sea ice are very low, with a maximum of 10 µmol.kg$^{-1}$,.and the subsequent higher $\delta^{13}C$-$CO_2$ in sea ice samples is consistent with DIC utilisation within a closed or semi-closed system. The observed high temporal and spatial variability within samples is common in sea ice, due to varying exchange with the atmosphere and underlying water (Gleitz, et al., 1995).

### 4.3.3 Suspended Particulate Organic Carbon (POC)

The surface water $\delta^{13}C_{POC}$ also presented in Figure 4.3 shows high inter-annual variability between the two growing seasons. During the 04/05 season, $\delta^{13}C_{POC}$ increases during the growing season from -21.2 to -17.9 ‰, with a small ~1‰ decrease in $\delta^{13}C_{POC}$ during late December 2004 when chl-*a* declined and [$CO_{2(aq)}$] increased due to injection of nutrients into the system. In February 2005, when chl-*a* began to decline at the end of the growing season, a large ~9 ‰ negative shift is observed in $\delta^{13}C_{POC}$ occurring in concert with an increase in $CO_{2(aq)}$ of ~ 8 µmol and a decrease in $\delta^{13}C$-$CO_2$ of ~ 1.2 ‰. At the end of the growing season, $\delta^{13}C_{POC}$ returned to near winter values of ~ -25 ‰.

The 05/06 season $\delta^{13}C_{POC}$ profile spans winter 2005 (from September 2005) until the end of the growing season (March 2006). $\delta^{13}C_{POC}$ increases from a winter low of ~ -25 ‰ in September 2005 to a season high of -18.8 ‰ in December 2005 just prior to sea ice retreat. Once the open water spring phytoplankton bloom was underway, $\delta^{13}C_{POC}$ were around -21 ‰ until there was an injection of ~ 7 µmol [$CO_{2(aq)}$] into the system during late January resulting in a -0.7 ‰ decrease in $\delta^{13}C$-$CO_2$ and the $\delta^{13}C_{POC}$ dropping to 22 ‰. At the end of January and early February there was then a large negative shift in $\delta^{13}C_{POC}$ reaching values as low as -28.7 ‰ (Figure 4.3). This negative shift in $\delta^{13}C_{POC}$ occurred during the entirety of the second chl-*a* peak and once chlorophyll had declined at the end of the growing season, the $\delta^{13}C_{POC}$ returned to a typical winter value of – 25 ‰ towards the end of March 2006. The large isotopic transition period observed during the 05/06

season contributed significantly to the POC concentration weighted $\delta^{13}C_{POC}$ average of the season, with the 04/05 season average being -20.0 ‰ and the 05/06 season average being -24.51 ‰.

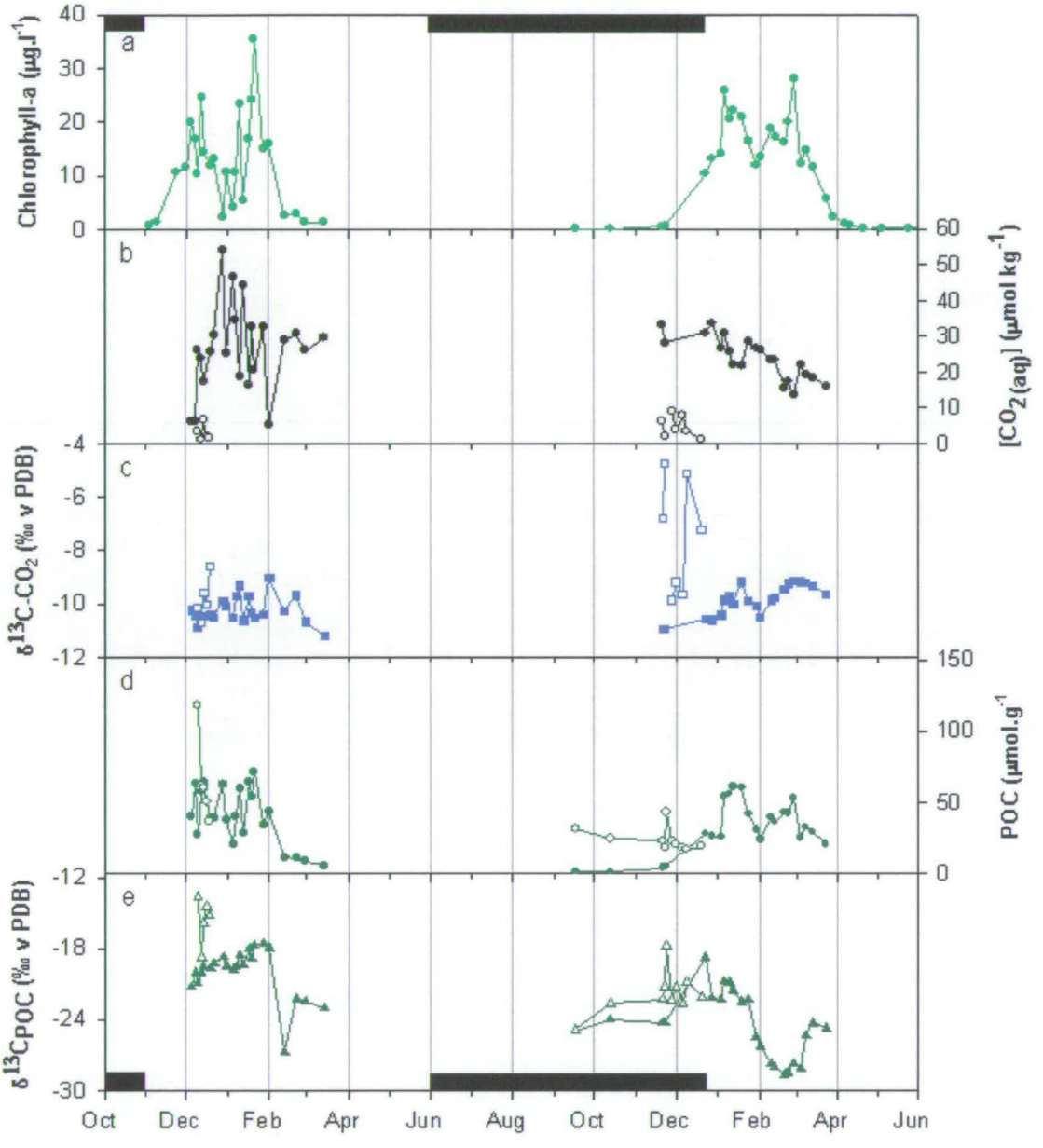


**Figure 4.3. Sea ice (open symbols) and surface water (closed symbols) time-series profiles of (a) Chlorophyll-a (b) $[CO_{2(aq)}]$ (c) $\delta^{13}C$-$CO_2$ (d) POC and (e) $\delta^{13}C_{POC}$. Black bars indicate sea ice coverage.**

The C:N ratios of particulates averaging at 5.7 indicates that suspended material is marine in origin, with few individual spikes observed at a C:N ratio of up to ~8 (see Figure 4.4). Therefore, the large decrease in $\delta^{13}C_{POC}$ (~10 ‰) cannot be due to significant input of terrestrial organic carbon to the system. Although highly variable, the C:N ratio of particulate matter is generally much higher in sea ice (Figure 4.4) and averages 8.0, compared to the average of 5.8 in surface waters.

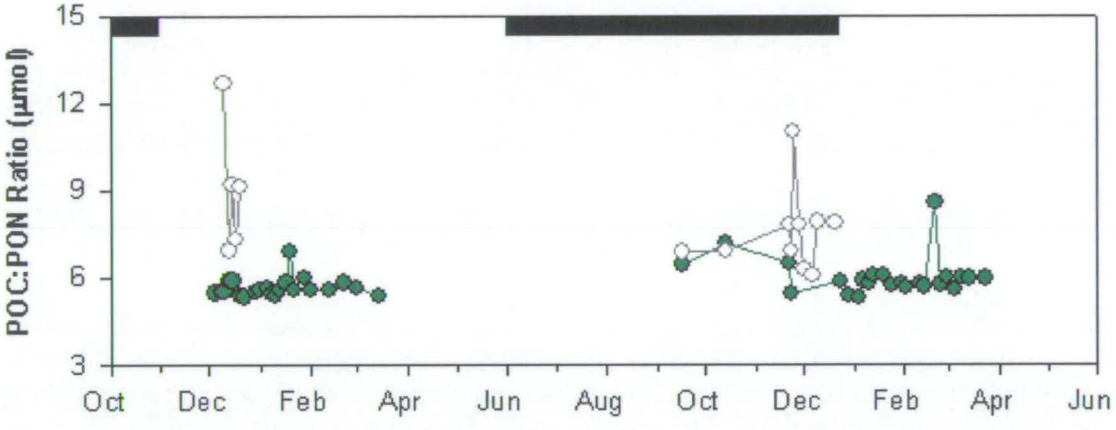


**Figure 4.4. Sea Ice (open symbols) and surface waters (green closed symbols) POC:PON ratios over the study period. Black bars indicate sea ice coverage.**

### 4.3.4 Surface water $\delta^{13}C_{POC}$ and $[CO_{2(aq)}]$

Concurrent $\delta^{13}C_{POC}$ and $[CO_{2(aq)}]$ measurements are presented in Figure 4.5, to investigate the influence of changing $[CO_{2(aq)}]$ on the isotopic composition of organic carbon. Good correlations have been observed between $\delta^{13}C_{POC}$ and $[CO_{2(aq)}]$ and $\delta^{13}C_{POC}$ and $1/[CO_{2(aq)}]$ in open-ocean studies in the Southern Ocean (Lourey, et al., 2004), but we see no clear correlation in either of these two comparisons for sea ice or surface waters. Although some of the more subtle changes in $\delta^{13}C_{POC}$ are consistent with minor changes to $[CO_{2(aq)}]$ and $\delta^{13}C\text{-}CO_2$ during nutrient utilisation and nutrient injections as described in section 4.3.3. $[CO_{2(aq)}]$ and $\delta^{13}C\text{-}CO_2$ do not account for the large change in $\delta^{13}C_{POC}$ during the 04/05 season and the more marked $\delta^{13}C_{POC}$ decrease during the 05/06 season. This suggests that factors other

than $[CO_{2(aq)}]$ must be influencing the $\delta^{13}C_{POC}$ in sea ice and surface waters in Ryder Bay.

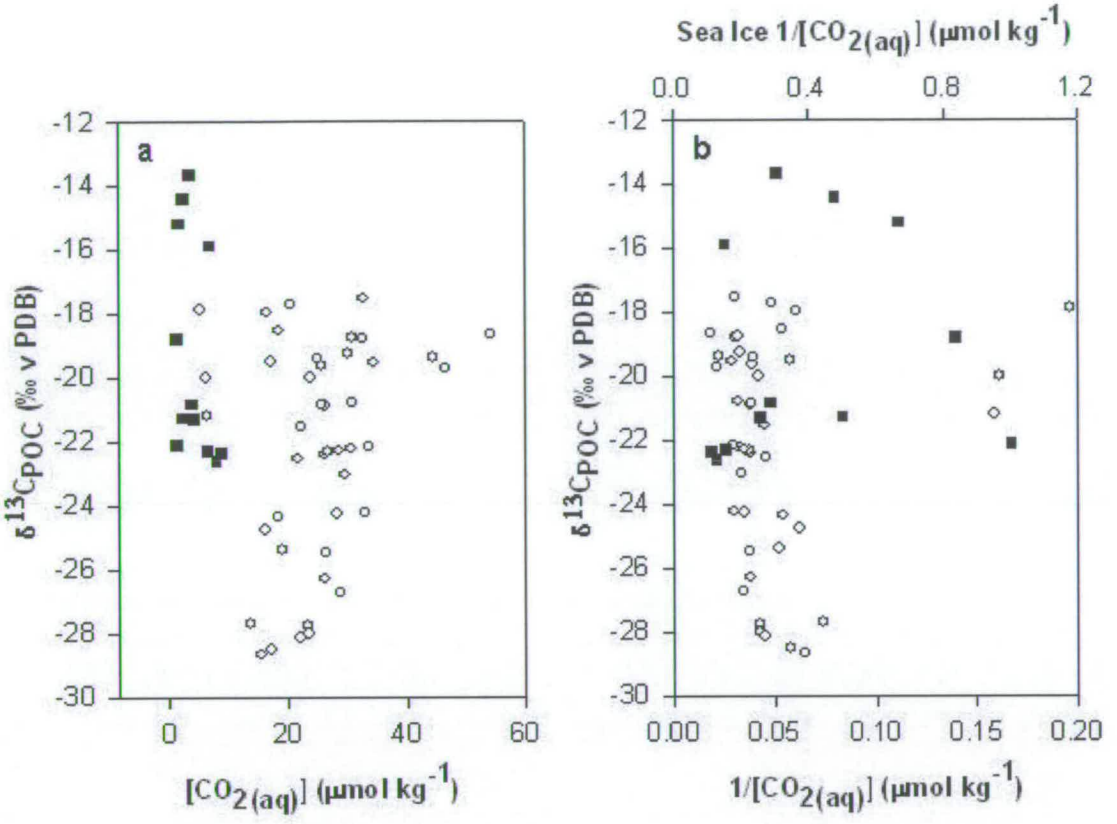


**Figure 4.5. Comparative plots of (a) $[CO_{2(aq)}]$ versus $\delta^{13}C_{POC}$ in sea ice (closed symbols) and surface waters (open symbols) and (b) $1/[CO_{2(aq)}]$ versus $\delta^{13}C_{POC}$ in sea ice (closed symbols) and surface waters (open symbols).**

Figure 4.6 presents diatom assemblages in sea ice and Figure 4.7 presents time series measurements of chlorophyll-*a*, total diatom abundances and the % biomass of the major diatom groups that dominated the surface water diatom blooms and their average surface area to volume ratio. The diatom groups used for sea ice and surface water diatom assemblages are presented in Table 4.1.

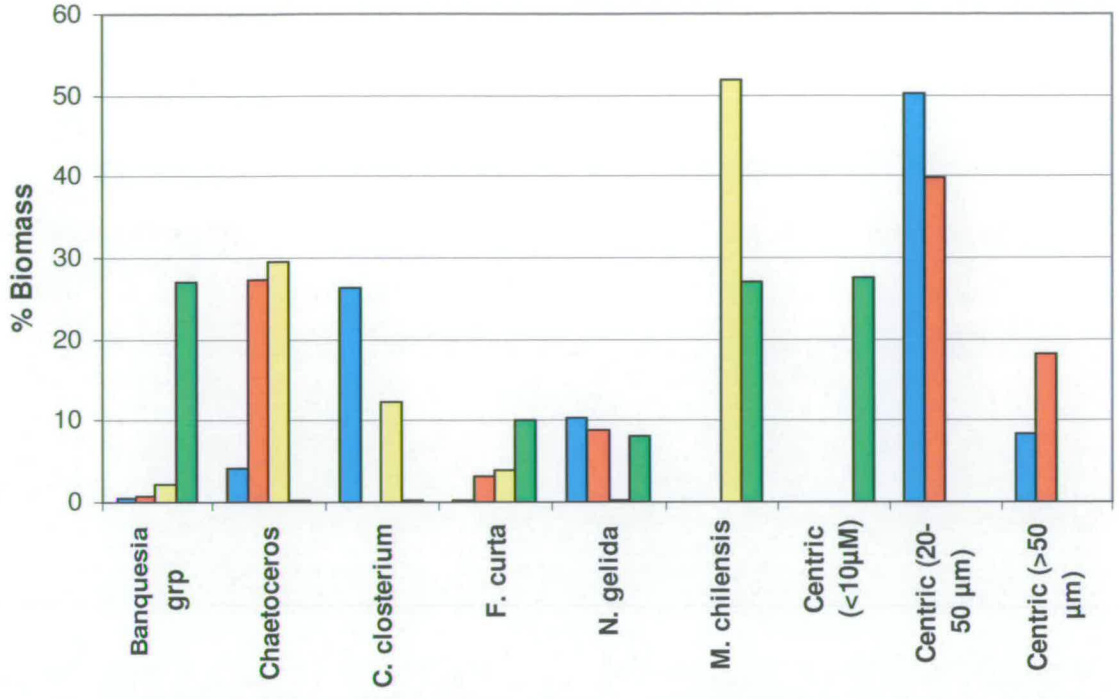


**Figure 4.6. Dominant diatom groups from sea ice samples that were analysed by SEM presented as the % of total biomass. Each colour represents the same sea ice sample for comparison.**

Size fractionated chlorophyll (not presented) shows the >20 µM fraction dominates throughout the summer growing season, indicating that diatoms dominate over the smaller nanoplankton and picoplankton (Clarke, et al., 2007).

Diatom assemblages show distinct changes throughout the growing seasons, occurring in concert with the changes observed in $\delta^{13}C_{POC}$. In sea ice samples the diatom biomass was dominated by the *Banquesia* group, the *Chaetoceros* group, *Cylindrotheca closterium*, the *Fragilariopsis curta* group, the *Navicula* group, *Minidiscus chilensis* and small, medium and large centric groups, presented in Figure 4.6.

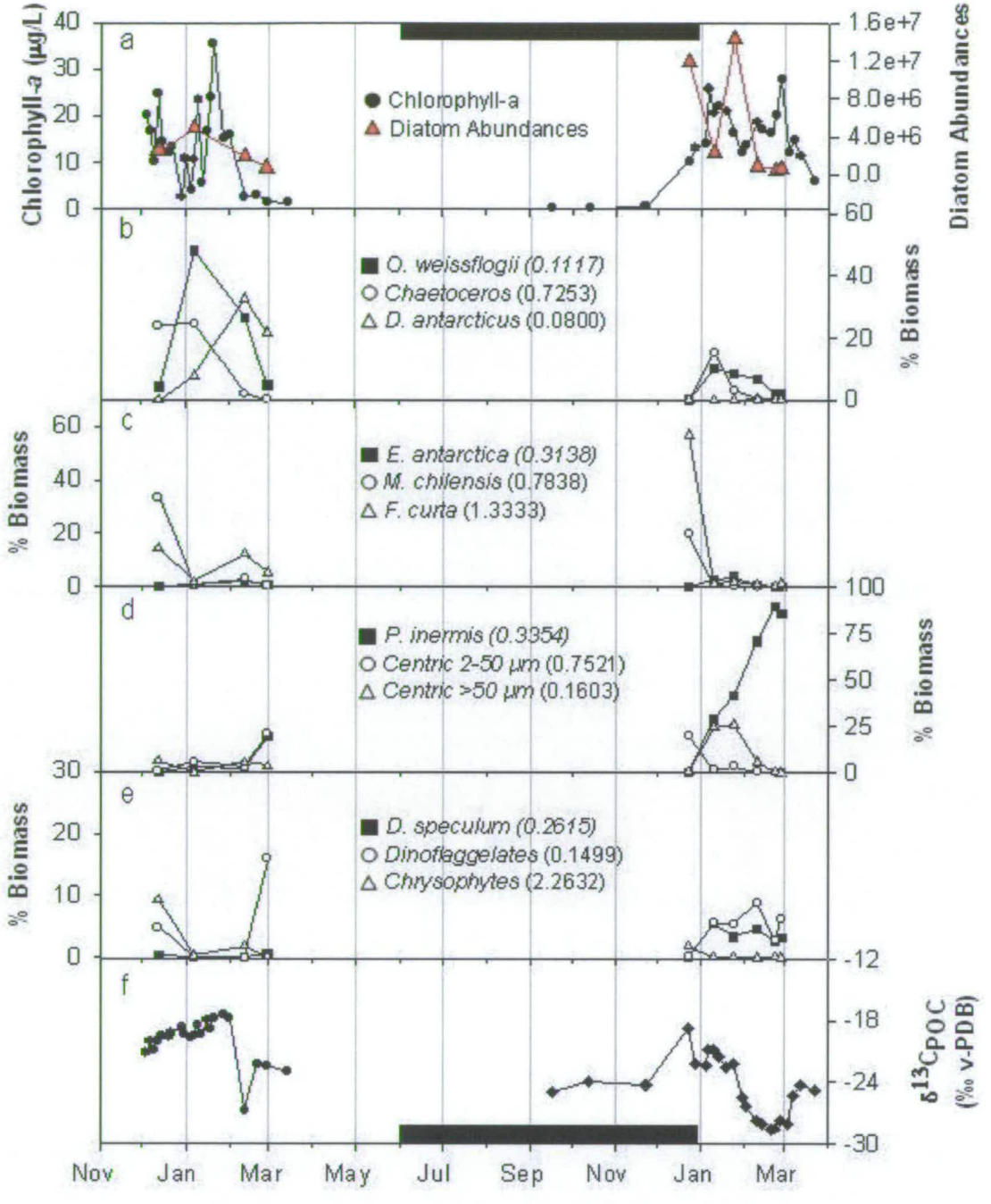


**Figure 4.7. (a-e) Diatom, Dinoflaggelate and Chrysophyte abundances and species data from surface water samples at the RaTS site including the average SA:V (given in parentheses) of the species group and (f) $\delta^{13}C_{POC}$ of organic matter at the RaTS site during the study period. Black bars represent sea ice cover.**

Surface water productivity can be categorised into different phases of the growing season, these phases consist of: growth under the ice, early bloom, isotopic transition periods and the late bloom. Diatom biomass under the ice

is dominated by the *F. curta* group, *M. chilensis* and the medium sized centric group. Early bloom conditions are dominated by the *Chaetoceros* group, *M. chilensis*, the *F. curta* group and medium sized centrics. The isotopic transition period observed in January 2005 covering one sampling event occurs with emergence of the chain-forming diatom *Dactyliosolen antarcticus*, composing ~30% of the biomass. The more pronounced isotopic transition period in January and February 2006 is mirrored by near total dominance of the pennate diatom, *Proboscia inermis*; a species only really seen at the end of the first season. *Proboscia inermis* was present throughout the 2005/2006 season after the retreat of the sea ice. The late bloom phases consist of diatom assemblages dominated by *Odontella weissflogii*, *D. antarctica*, *P. inermis*, and medium sized centrics during the 2004/2005 season and dominance of *P. inermis* during the last diatom counted sample from the 2005/2006 season.

**Table 4.1. List of species associated with diatom groups used in this study.**

| Group | Species |
|---|---|
| *Banquesia* group | *Banquesia belgicae, Berkleya rutilans, Haslea trompii, Amphiprora kufferathii, Membraneis challengeri.* |
| *Chaetoceros* (sub-group Hyalochaeta) | *C. neglectus, C. simplex, C. socialis* |
| *Fragilariopsis curta* group | *F. curta, F. cylindrus, F. vanheurkii.* |
| *Navicula* group | *N. directa, N. gelida, N. glaciei* |
| Small Centrics (< 20 µm) | *Thalassiosira ambigua, Thalassiosira dichotomica, Thalassiosira frenguelli, Thalassiosira gracilis, Thalssiosira gravida.* |
| Medium Centrics (20 – 50 µm) | *Actinocyclus actinochilus, Porosira glacialis, Porosira pseudodenticulata, Thalassiosira Antarctica.* |
| Large Centrics (>50 µm) | *Asteromphalus hookeri, Stellarima microtrias, Thalassiosira antarctica, Thalassiosira lentiginosa.* |

### 4.3.5 Sinking Particulate Organic Carbon and $\delta^{13}C_{org}$

Figure 4.8 presents $\delta^{13}C_{org}$ data from the time-series sediment traps deployed at the RaTS site in Ryder Bay and nearby at the deeper site in Marguerite Bay and Table 4.2 presents a summary of the trap flux data. Carbon fluxes were highly variable between traps and between seasons, during the 04/05 season, flux rates during the growing seasons were 2731 µmol $C.m^{-2}.d^{-1}$ in the 200 m RaTS trap, 1418 µmol $C.m^{-2}.d^{-1}$ in the RaTS 512 m trap, 899 µmol $C.m^{-2}.d^{-1}$ in the deep site 123 m trap and 532 µmol $C.m^{-2}.d^{-1}$ in the deep site 745 m trap. During the 05/06 season, flux rates during the growing season were 1993 µmol $C.m^{-2}.d^{-1}$ in the RaTS 200 m trap, 453 µmol $C.m^{-2}.d^{-1}$ in the RaTS 512 m trap, 1316 µmol $C.m^{-2}.d^{-1}$ in the deep site 123 m trap and 1155 µmol $C.m^{-2}.d^{-1}$ in the deep site 745 m trap.

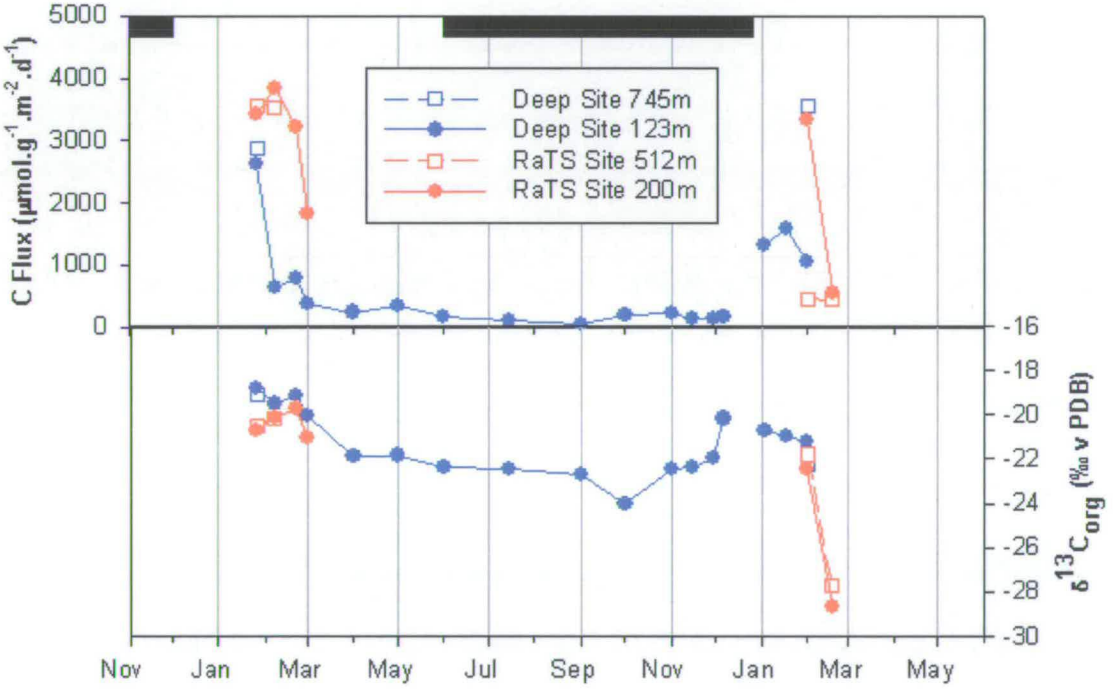


**Figure 4.8. Carbon fluxes in sediment traps at both the RaTS and deep site and $\delta^{13}C_{org}$ of organic matter in sediment traps.**

Flux weighted average $\delta^{13}C_{org}$ values were fairly consistent between traps on the same mooring (Table 4.2). During the 04/05 growing season, flux weighted $\delta^{13}C_{org}$ values were -20.32 ‰ in the RaTS 200 m trap, -20.35 ‰ in

the RaTS 512 m trap, -19.06 ‰ in the deep site 123 m trap and -19.12 ‰ in the deep site 745 m trap. During the 05/06 season, flux weighted $\delta^{13}C_{org}$ values were -23.32 ‰ in the RaTS 200 m trap, -24.72 ‰ in the RaTS 512 m trap, -20.46 ‰ in the deep site 123 m trap and -19.12 ‰ in the deep site 745 m trap. In all cases the flux weighted average $\delta^{13}C_{org}$ value grew slightly higher with depth, probably as a product of degradation processes.

**Table 4.2. Sediment trap carbon fluxes, the seasonal flux weighted average $\delta^{13}C_{org}$ of organic matter (C flux is presented in µmol.g.m$^{-2}$.d$^{-1}$ dry weight and $\delta^{13}C_{org}$ is presented in ‰ versus PDB).**

| Trap | C flux (04/05) | C flux (05/06) | $\delta^{13}C_{org}$ (04/05) | $\delta^{13}C_{org}$ (05/06) |
|---|---|---|---|---|
| RaTS 200m | 2731 | 1993 | -20.32 | -23.32 |
| RaTS 512m | 1418 | 453 | -20.35 | -24.72 |
| Deep 123m | 899 | 1316 | -19.06 | -20.46 |
| Deep 745m | 532 | 1155 | -19.12 | -22.28 |

### 4.3.6 Sediment Trap Diatom Assemblages

Diatom abundances and assemblages in the sediment trap samples for the RaTS site and deep site are presented in Figures 4.9 and 4.10 respectively. In the 200 m trap on the RaTS mooring, diatom abundances peaked at 216 million valves per g of sediment during the latter part of the 04/05 season and 55 million valves per g of sediment at the start of the 05/06 season (Figure 4.9). In the 512 m trap on the RaTS mooring, diatom abundances peaked at 212 million valves per g of sediment during the latter part of the 04/05 season and 120 million valves per g sediment at the start of the 05/06 season. In the 123 m trap on the deep site mooring, diatom abundances peaked at 494 million valves per g of sediment during the latter part of the 04/05 season and 868 million valves per g sediment at the start of the 05/06 season (Figure 4.10). In the 745 m on the deep site mooring, diatom abundances peaked at 466 million valves per g sediment during the latter part of the 04/05 season and 339 million valves per g sediment at the start of the 05/06 season.

Diatom assemblages also change on a seasonal timescale. Data from the RaTS mooring are presented in Figure 4.9.

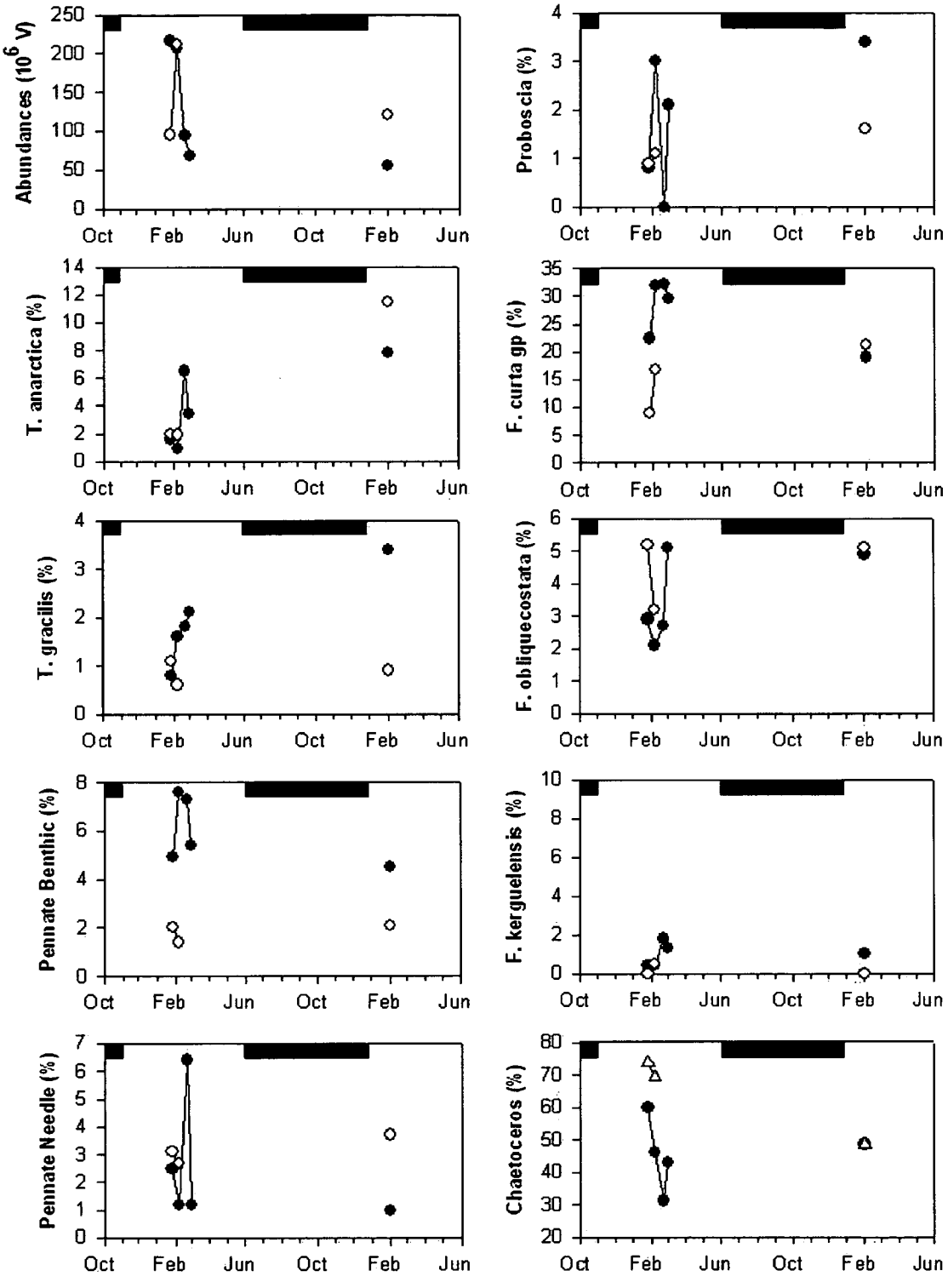


**Figure 4.9. RaTS mooring sediment trap abundances of diatom groups for the shallow 200 m trap (closed symbols) and the deep 500 m trap (open symbols). Black bars indicate sea ice cover.**

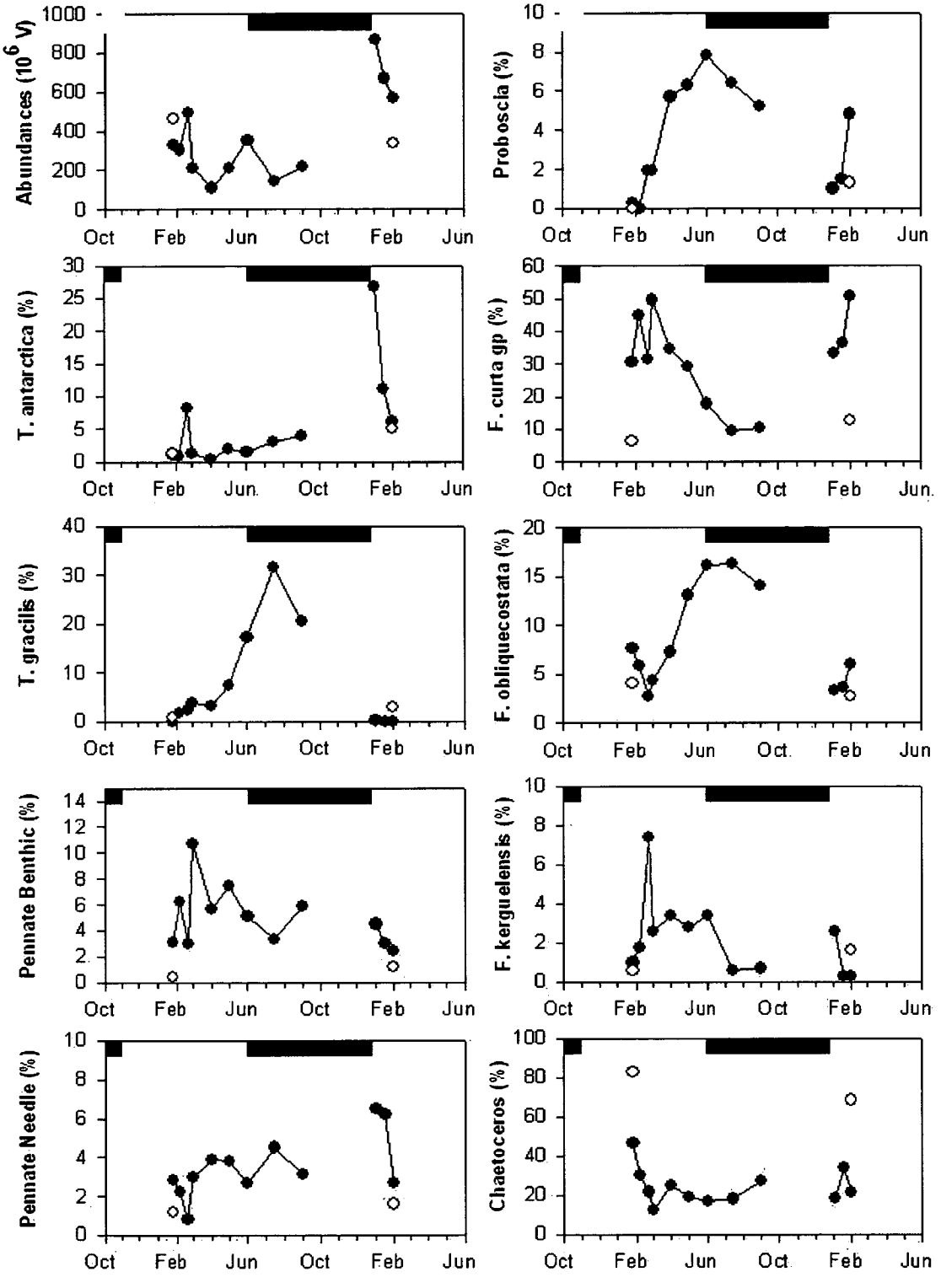


**Figure 4.10. Deep site mooring sediment trap abundances of diatom groups for the shallow 123 m trap (closed symbols) and the deep 745 m trap (open symbols). Black bars indicate sea ice cover.**

During the late 04/05 season when the deployment started, diatom assemblages were dominated by *Chaetoceros* species and *F. curta* with the rest of the assemblages made up of a mixture of pennate and centric species groups. In the 200 m RaTS trap, *Chaetoceros* species composed between 31 % and 60 % of the assemblages and *F. curta* composed between 22 % and 32 % of the assemblage. Other groups such as *Thalassiosira antarctica*, *Thalassiosira* gracilis, pennate benthic, pennate needle and *Fragilariopsis obliquecostata* composed up to ~ 8 % of the assemblage. In the 512 m RaTS trap, *Chaetoceros* composed between 60 % and 74 % of the assemblages where *F. curta* composed between 9 and 17 % of the assemblages. Interestingly, this reduction in the proportion of *F. curta* in the deep trap is also seen in other small pennate species and the pennate benthic group and may indicate inefficiency in their export due to fragility of smaller, thinner cells. Due to the lack of material in the winter trap bottles at the RaTS site, it was not possible to analyse the material for diatom assemblages. After retreat of sea ice and initiation of the spring bloom during the 05/06 growing season, the 200 m RaTS trap was again dominated by flux of *Chaetoceros* and *F. curta* species. *Chaetoceros* species composed 49 % of the assemblages and *F. curta* composed 19 % of the assemblage. Other groups composed up to ~ 8 % of the assemblages. In the 512 m RaTS trap, *Chaetoceros*, *F.* curta and *T. antarctica* dominated the assemblage. *Chaetoceros* composed 49 % of the assemblage, *F. curta* composed 21 % of the assemblage and *T. antarctica* composed 12 % of the assemblage. Interestingly, there are higher abundances in the 512 m trap of the species groups *T. antarctica*, the pennate needle group, *F. curta* and *F. obliquecostata group*, species commonly associated with sea ice material, indicating that sea ice material may have accumulated in the deeper trap prior to the start of the open water spring bloom. This may not be accounted for in previous trap cups, where there was not enough material to conduct diatom assemblage analysis. There are also decreases in the proportion of *T. gracilis*, pennate benthic and *Proboscia* group in the deeper trap, which may also be due to inefficiency in their export due to fragility of smaller, thinner

cells, but may also be partly due to the flux recorded in the shallow trap having not reached 512 m at that time.

Data from the deep mooring are presented in Figure 4.10. During the late 04/05 season when the deployment started, diatom assemblages were generally dominated by *Chaetoceros* and *F. curta* with the rest of the assemblages made up of a mixture of pennate and centric species groups. In the 123 m deep site trap, *Chaetoceros* species composed between 13 % and 47 % of the assemblages and *F. curta* composed between 29 % and 50 % of the assemblage. Other groups composed up to ~ 11 % of the assemblage. In the 745 m deep site trap, *Chaetoceros* compose 83 % of the assemblages where *F. curta* composed only 7 % of the assemblages. The other diatom species groups composed up to ~ 5 % of the assemblage. The reduction in the proportion of *F. curta* in total diatom flux is also seen in other small pennate species groups such as pennate benthic, pennate needle, *F. obliquecostata* and *F. kerguelensis* and may also indicate inefficiency in their export due to fragility of smaller, thinner cells. In the 123 m trap from the deep mooring site, there was sufficint flux during winter to analyse diatom assemblages during the early period of winter sea ice cover (see Figure 9). During the early winter months when sea ice covered the region, the assemblages were dominated by *T. gracilis*, *F. obliquecostata*, and the *Chaetoceros* group. *T. gracilis* composed between 17 and 32 % of the assemblage, *F. obliquecostata* composed between 14 and 16 % of the assemblage and *Chaetoceros* composed between 17 and 28 % of the assemblage. The other individual diatom groups composed up to ~ 8 % of the total assemblage. After retreat of sea ice and initiation of the spring bloom during the 05/06 growing season, the 123 m deep site trap was dominated by flux of *Chaetoceros*, *F. curta* and the very start of the open water season, the *T. antarctica* species group was abundant. *Chaetoceros* species composed between 18 % and 34 % of the assemblages, *F. curta* composed between 33 % and 51 % of the assemblage and *T. antarctica* composed between 6 % and 27 %. The other individual species groups

composed up to ~ 6 % of the assemblages. In the 745 m deep site trap, *Chaetoceros* and *F.* curta dominated the assemblage. *Chaetoceros* composed 68 % of the assemblage and *F. curta* composed 13 % of the assemblage. The other individual species groups composed up to ~ 5 % of the assemblage.

The diatom assemblages in sediment traps are similar in composition to the surface waters, although the exact proportions of each species are somewhat different. Generally the smaller, fragile species exhibit a significantly lower composition in the traps than in the surface waters, suggesting that these species are not efficiently exported to depth compared to others.

## 4.4 Discussion

### 4.4.1 $\delta^{13}C$ in Surface Waters and Sea Ice

One of the significant findings in this study are the large negative shifts in surface water $\delta^{13}C_{POC}$ observed at the end of the 04/05 growing season and a more pronounced and prolonged negative shift during the latter stage of the 05/06 growing season (Figure 4.3). These negative isotopic shifts occur without a similar change in $[CO_{2(aq)}]$ or $\delta^{13}C\text{-}CO_2$, but in parallel with changes in surface water diatom assemblages (Figure 4.7). Marine algae always display lower $\delta^{13}C_{POC}$ than the inorganic carbon source they assimilate due to preferential assimilation of $^{12}C$ during photosynthesis (Hayes, 1993). For the stable isotope composition of the inorganic carbon pool to strongly influence the product $\delta^{13}C_{POC}$, a significant shift in $\delta^{13}C\text{-}CO_2$ would have to take place. In Figure 4.3, $\delta^{13}C\text{-}CO_2$ only changes by 2.19 ‰ in surface waters but the $\delta^{13}C_{POC}$ goes through a ~10 ‰ change. Changes in $[CO_{2(aq)}]$ can also affect $\delta^{13}C_{POC}$, independent of the initial $\delta^{13}C\text{-}CO_2$ (Burkhardt, et al., 1999; Lourey, et al., 2004; Rau, et al., 1996), with increasing $[CO_{2(aq)}]$ resulting in a higher fractionation factor ($\varepsilon_p$) during inorganic carbon assimilation. If this were the primary mechanism, we would expect to see a negative correlation between $[CO_{2(aq)}]$ and $\delta^{13}C_{POC}$, but in Figure 4.5, no

negative correlation was observed. Although there is a small response in $\delta^{13}C\text{-}CO_2$ to injections of $[CO_{2(aq)}]$ into surface waters (see section 3.3) causing subtle changes in $\delta^{13}C_{POC}$, it is clear from comparisons of $[CO_{2(aq)}]$ and $1/[CO_{2(aq)}]$ with $\delta^{13}C_{POC}$ (see Figure 4.4) that variations in $[CO_{2(aq)}]$ were not responsible for the large decreases in $\delta^{13}C_{POC}$ observed during the growing seasons.

In a coastal site such as the Ryder Bay, inputs of terrestrial organic carbon could potentially influence the $\delta^{13}C_{POC}$ in surface waters as terrestrial organic matter source from C3 plant remains are generally more depleted in $^{13}C$ than marine organic matter (Fry and Sherr, 1984). C:N ratios can reach as high as ~20 for terrestrial organic matter and are generally <10 for marine phytoplankton. Therefore C:N ratios of suspended organic matter that average 5.83 over the two growing seasons (Figure 4.4) indicate a wholly marine origin, as no obvious changes were associated with negative shifts in $\delta^{13}C_{POC}$. Thus, we conclude that terrestrial organic inputs are not the mechanism driving the observed negative shifts in $\delta^{13}C_{POC}$.

$\delta^{13}C_{POC}$ in near shore, Antarctic surface waters appears to undergo significant changes on a seasonal timescale in response to changes in diatom assemblages (Figure 4.7). There are several possible mechanisms influencing the observed pattern in the isotope signal. Recent studies have shown that changes in cell size and geometry can affect the $\varepsilon_p$ with cells displaying high Surface Area to Volume ratios (SA:V) exhibiting higher $\varepsilon_p$ (Burkhardt, et al., 1999; Popp, et al., 1998).

In Figure 4.7 we show time series plots of % biomass and the average SA:V ratios of the major diatom species in surface waters and Figure 4.11 shows the estimated SA:V of the entire assemblage plotted against the calculated fractionation factor ($\varepsilon_p$). During the early season open water diatom bloom period, a diverse range of large and small celled species are abundant. During the negative isotopic shifts seen clearly in the second season but less

obviously in the first, the lower $\delta^{13}C_{org}$ values are accompanied by shifts in the diatom assemblages, most notably enrichment of *D. antarcticus* (SA:V of 0.08) in 2005 and near total dominance of *P. inermis* (SA:V of 0.3) in 2006. At the end of the growing season and transition to winter conditions, suspended particles became increasingly enriched in debris, probably due to the effects of grazing by heterotrophs and decomposition. Diatom assemblages then returned to a diverse assortment of large and small cells with an increase in the biomass of dinoflagellates.

Figure 4.11 shows the whole community SA:V ratio of diatom assemblages surface waters plotted against their corresponding $\varepsilon_p$ value. There are positive correlations between SA:V and $\varepsilon_p$ for surface waters ($R^2$=0.46), suggesting that increasing diatom assemblage SA:V increases $\varepsilon_p$, thus influencing the product $\delta^{13}C_{POC}$.

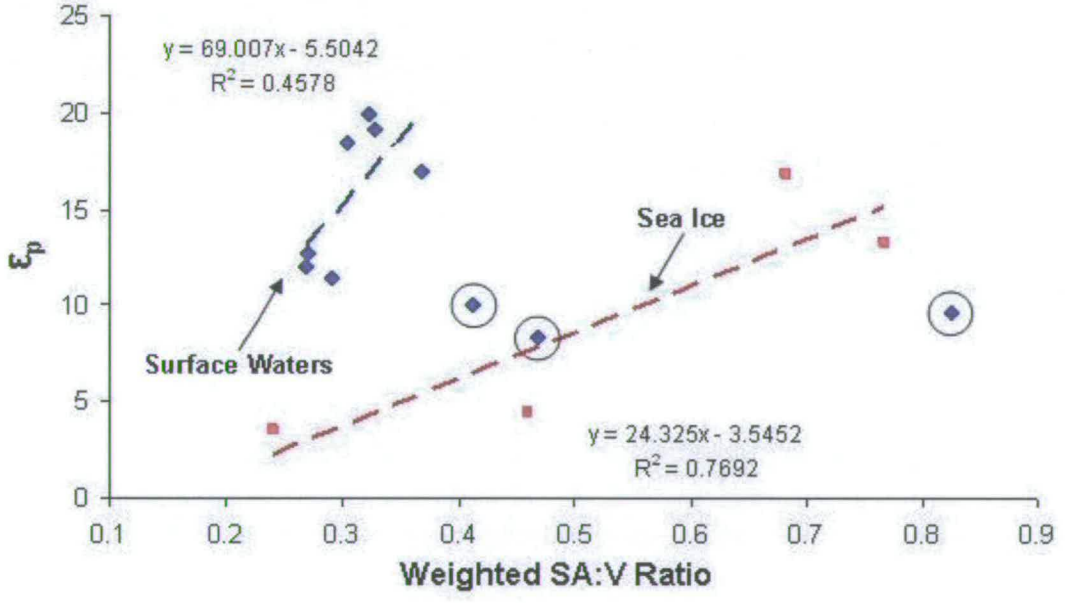


**Figure 4.11. Comparative plots of the weighted SA:V ratio of diatom assemblages and the corresponding $\varepsilon_p$ for sea ice (red squares) and surface water (blue diamonds) samples.**

In the sea ice samples taken from the two field seasons, distinct differences in the diatom assemblages compared to surface waters are clearly observed

(Figure 4.6). Sea ice diatom biomass was dominated by groups that generally display a higher SA:V ratio (i.e. smaller diatoms) than their open water counterparts (see Figures 4.6 and 4.11). These samples also show on average higher $\delta^{13}C$ than surface waters (Figure 3) and in Figure 11 sea ice diatom assemblage SA:V also show a positive correlation with $\varepsilon_p$. ($R^2$=0.77).

In previous work, higher $\delta^{13}C$ in sea ice has been attributed to a higher degree of [$CO_{2(aq)}$] utilisation (Gibson et al., 1999; Villinski et al., 2000), but the lack of consistently higher $\delta^{13}C$-$CO_2$ (Figure 4.3) or a relationship between [$CO_{2(aq)}$] and $\delta^{13}C_{POC}$ (Figure 5) in this study suggest that this is not the causative process. Instead the higher $\delta^{13}C_{POC}$ in sea ice is attributed to post production degradation processes, where the $^{12}C$ material is preferentially degraded, leaving the remaining organic carbon enriched in $^{13}C$. A high rate of organic particle degradation in sea ice is consistent with the high C/N ratios (Figure 4); due to organic nitrogen being preferentially degraded over carbon bearing compounds (Ganeshram et al., 1999; Hedges et al., 1986; Rosenfeld, 1981).

The difference between the surface water and sea ice relationships in Figure 11 may be due to the effect of biodegradation processes in sea ice. As $\varepsilon_p$ was calculated as the difference between $\delta^{13}C$-$CO_2$ and $\delta^{13}C_{POC}$, the material remaining in sea ice after degradation would be enriched in $^{13}C$ and thus be calculated as having a lower $\varepsilon_p$ when compared to the surface water relationship. The differing slopes between the two relationships may also be an effect of biodegradation, where different sea ice samples had undergone different degrees of degradation.

The circled surface water samples outlying the correlated values in Figure 11 were taken from surface waters on 13$^{th}$ December 04, 7$^{th}$ January 05 and 23$^{rd}$ December 05. The similarity between these SA:V versus $\varepsilon_p$ is consistent with these samples containing material from sea ice. While this explanation holds for the sample from 23$^{rd}$ December 05, as the sea ice was still covering

Ryder Bay at the time, not so for the earlier two samples. The low C:N ratios for these samples (5.4 to 5.9), does not suggest significant degradation, as would be expected from sea ice material. It remains unclear what mechanism caused these points to differ from the relationship observed for surface water samples. Other factors must therefore contribute to the $\delta^{13}C_{POC}$ composition of organic matter in Ryder Bay. Other possible factors controlling $\varepsilon_p$ include internal biochemical processes in different diatom species (Cassar, et. al, 2006), growth rates (Burkhardt, et al., 1999; Popp, et al., 1998; Rau, et al., 1996; Villinski et al., 2000) and the presence of the prymnesiophte *Phaeocystis antarctica* (Villinski, et al., 2000).

A recent study has shown that diatom $\varepsilon_p$ may not be a unique function of growth rate, $CO_2$ concentration or SA:V ratio and that other cellular biochemical processes may explain discrepancies in the reported effects of growth conditions on carbon fractionation (Cassar, et al., 2006). Currently, factors such as cell wall permeability, carbon fixation kinetics, carbon to volume content and active uptake of bicarbonate and $CO_2$ through the cell membrane are not sufficiently constrained for most diatom species, especially species from the Southern Ocean to pinpoint the causative processes affecting $\delta^{13}C_{POC}$. Therefore further studies are requires to fully investigate the effects of the aforementioned processes.

Differences in phytoplankton growth rates may also alter the stable carbon isotope $\varepsilon_p$ (Burkhardt, et al., 1999; Popp, et al., 1998; Rau, et al., 1996; Villinski et al., 2000), with lower growth rates generally associated with a higher $\varepsilon_p$ and subsequently lower $\delta^{13}C_{POC}$. Growth rates in the Southern Ocean are generally low, and in the two seasons covered by this study the diatom abundances are particularly low during isotopic transition periods (see Figure 4.7). Any effect this may have had on $\varepsilon_p$, however, remains speculative due to the lack of growth rate measurements and grazing data to ascertain if low diatom abundances are in fact due to changes in growth rate and not a result of grazing pressures.

Our results showing strong influence of diatoms cell sizes on $\delta^{13}C_{POC}$ is in contrast to results from a previous study from the Ross Sea (another continental shelf, sea ice environment) where the prymnesiophyte *Phaeocystis antarctica* and dinoflagellates can dominate the biomass and cause shifts in $\delta^{13}C_{POC}$ to values approaching -30 ‰ (Villinski, et al., 2000), as seen in this study. In Marguerite Bay diatoms dominate phytoplankton biomass in this area and *Phaeocystis* biomass is more than an order of magnitude lower than diatoms during spring blooms (Garibotti, et al., 2005). This contrast may reflect the difference in the dominant phytoplankton group in study areas. In surface waters of Ryder Bay diatom assemblage composition exhibits large changes on a seasonal timescale (Figures 4.6 and 4.7). It therefore appears that in Ryder Bay, species specific SA:V, and internal biochemical pathways associated with seasonal progression of diatom speciation have more of an influence on $\varepsilon_p$, than shifts in phytoplankton assemblages towards prymnesiophytes and/or dinoflagellates.

### 4.4.2 Sinking Particulate Carbon

The time-series $\delta^{13}C_{org}$ of sinking particles presented in Figure 4.8, show similar features to the surface water time-series (Figure 4.3), suggesting that the changing $\varepsilon_p$ and subsequent $\delta^{13}C_{POC}$ produced in surface waters driven by succession of diatom assemblages, is transferred to depth. During the 04/05 growing season, $\delta^{13}C_{POC}$ ranged between -21.2 ‰ to -17.5 ‰ when the transition period occurred in February and $\delta^{13}C_{POC}$ dropped to -26.7 ‰ before returning to -23.0 ‰ after productivity ceased (Figure 4.3). Although the early season flux was missed by the sediment traps during the 04/05 season, we see a progressive increase in $\delta^{13}C_{org}$ in the RaTS 200 m trap from -20.7 ‰ to -19.7 ‰ between late January and February 05, followed by a drop to -22.55 ‰ in March and April (Figure 4.8). Assessing this feature is not possible in the deep site trap as there are only two data points and we have no stable isotope or diatom data for surface waters at this site, but this lack of a similar response may be due to more subtle seasonal changes in

diatom assemblages in the more open ocean site that do not have the same effect on $\delta^{13}C_{POC}$ as the coastal site.

The 05/06 growing season shows very different stable carbon isotope characteristics. In surface waters during winter, $\delta^{13}C_{POC}$ is initially ~ -25 ‰ and then increases to a maximum value of -18.8 ‰ as primary production begins as the sea ice begins to decay (Figure 4.3). During late January, February and early March, we see the isotopic transition period, where $\delta^{13}C_{POC}$ values reach as low as -28.7 ‰ and then rise to a winter value of ~ -25 ‰ when productivity declines. The material in the sediment traps shows very similar features to the surface waters, with $\delta^{13}C$ shifting from -22.5 ‰ in February 06 to -28.7 ‰ in late February and early March in the 200m RaTS trap (Figure 4.8), consistent with the isotopic shift seen in surface water material. This is also seen in the 512m RaTS trap, where $\delta^{13}C_{org}$ changes from -21.8 ‰ in early February to -27.8 ‰ in late February and early March. As the deep site mooring was lost, we do not have coverage of the isotopic transition seen in 2006 at the deep site and thus can not comment on it. The diatom species counts in sediment traps show similar dominant species as in the surface waters (Figures 4.9 and 4.10). Species not observed in the traps that were present in surface waters are assumed to have been subject to grazing and remineralisation and therefore were not exported to depth. While this may have slightly altered the $\delta^{13}C$ of the material, this effect is thought to be negligible as the seasonal progressions of suspended particles and sinking particles $\delta^{13}C$ were very similar.

Thus the $\delta^{13}C_{org}$ of sinking material is highly variable in sediment traps and is directly related to changes in surface water $\delta^{13}C_{POC}$, which is mainly explained by the effects of carbon fixation by different species of diatoms. The flux weighted average of sediment trap material from each season is presented in Table 2 and is consistent with that observed in surface waters. The 04/05 season flux weighted average $\delta^{13}C_{org}$ is -20.3 ‰ for the RaTS 200 m trap and -20.4 ‰ for the RaTS 512 m trap and for the 05/06 season the

flux weighted average $\delta^{13}C_{org}$ is -23.3 ‰ for the RaTS 200 m trap and -24.7 ‰ for the RaTS 512 m trap. The deep site traps also exhibit lower flux weighted average $\delta^{13}C_{org}$ values for the 05/06 season, although not to the same degree. This may be due to a similar mechanism occurring at both sites, but with the changes in diatom assemblages and subsequent $\delta^{13}C_{POC}$ being more subtle at the deep site.

### 4.4.3 Potential Implications for $\delta^{13}$C-based $pCO_2$ Reconstructions in the Southern Ocean

Our results showing carbon isotope transition associated with seasonal changes in diatom assemblages influence in surface waters and conveyance of the signal to depth in sinking particles (Figure 4.7 and Table 4.3) have important implications for the interpretation of carbon isotope signatures in both coastal and open ocean Southern Ocean regions. $\delta^{13}C$ records in the Southern Ocean show depleted glacial values of up to 4 ‰ (Crosta and Shemesh, 2002; Rosenthal, et al., 2000; Schneider-Mor, et al., 2005; Singer and Shemesh, 1995), with various hypotheses put forward for the mechanism(s) controlling these changes in $\delta^{13}C$. The low $\delta^{13}C$ values of the glacial periods have been linked to higher [$CO_{2\ (aq)}$] resulting from wide-spread upwelling. Later studies, using other proxy records such as $\delta^{15}N$ & Ba/Al, indicate a stratified glacial Southern Ocean (Francois, et al., 1997) and lowered productivity, contradicting the upwelling theory. Therefore it was suspected that $\delta^{13}C$ in glacial periods could have been influenced by other factors such as growth rates and changes in diatom abundance or cell size and geometry (Rosenthal, et al., 2000). Crosta and Shemesh (2002) also proposed a scenario of reduced vertical mixing and extended sea ice cover to explain the anti-correlation of low $\delta^{13}C$ and high $\delta^{15}N$ in Southern Ocean sediment records. Reduced vertical mixing and extended sea ice cover were postulated to have kept [$CO_{2\ (aq)}$] at high concentrations inducing lower $\delta^{13}C$ of organic matter, with reduced vertical mixing lowering the $NO_3$ input into the photic zone, causing higher per cent $NO_3$ utilisation and subsequent $\delta^{15}N$ enrichment (Crosta and Shemesh, 2002). Our data suggest that in the coastal Antarctic sea ice environment, extended sea ice coverage and a

more stratified system can result in changes in diatom assemblages that contribute to large negative shifts in $\delta^{13}C_{POC}$. This process may have also contributed to the lighter carbon isotope signatures of the glacial Southern Ocean. Indeed diatom assemblages preserved in glacial Southern Ocean sediments show differences from modern open ocean assemblages reflecting much more extensive sea ice cover and highly stratified conditions as a result of more extensive fresh water contributions from sea ice and iceberg melt (Crosta, et al., 1998a; b; Francois, et al., 1997). Interestingly, the two growing seasons sampled during this study had very different sea ice regimes and hydrography, and very different phytoplankton assemblages. Nonetheless both display the shift to lower $\delta^{13}C_{POC}$, albeit to varying degrees, and were to some extent influenced by SA:V (Figure 4.11). This further loosens the relationship used in the application of a $\delta^{13}C$ versus $pCO_2$ relationship for reconstructing paleo-$pCO_2$ from sediment core $\delta^{13}C_{org}$ in this area.

## 4.5 Conclusions

This study presents a unique insight into the factors affecting the $\delta^{13}C$ of organic matter in the coastal Antarctic sea ice environment. The findings of this time-series investigation lead to the following conclusions:

1. Sea ice $\delta^{13}C_{POC}$ appears to be controlled more by post-production decomposition processes and not a high degree of nutrient utilisation as other studies may have inferred.
2. $[CO_{2(aq)}]$ and $\delta^{13}C\text{-}CO_2$ are not major controlling factors on the $\delta^{13}C$ of suspended particulate organic carbon;
3. The ~10 ‰ shifts seen in surface waters appear driven by seasonal shifts in diatom assemblages and the subsequent shift to lower SA:V ratios of the assemblages during the isotopic shifts, possibly exacerbated by changes to internal diatom biochemical pathways for carbon fixation and changing growth rates.

4. Although much of the surface suspended material (including certain diatom species) are not exported to depth, the $\delta^{13}C$ composition of surface suspended organic carbon is transferred to depth.

5. Sediment $\delta^{13}C$ is therefore not a reliable proxy for $pCO_2$ due to the effects of seasonal changes in $\varepsilon_p$.

## 4.6 References

Ahad, J. M. E. (2005), Evaluating the origins and transformations of organic matter and dissolved inorganic nitrogen in two contrasting North Sea Estuaries, *PhD Thesis, The University of Edinburgh, School of GeoSciences*, 247pp.

Assayag, N., et al. (2006), Improved method for isotopic and quantitative analysis of dissolved inorganic carbon in natural water samples, *Rapid Communications in Mass Spectrometry*, *20*, 2243-2251.

Burkhardt, S., et al. (1999), Effects of growth rate, CO2 concentration, and cell size on the stable carbon isotope fractionation in marine phytoplankton, *Geochimica Et Cosmochimica Acta*, *63*, 3729-3741.

Cassar, N., et al. (2004), Bicarbonate uptake by Southern Ocean phytoplankton, *Global Biogeochemical Cycles*, *18*, GB2003, doi:2010.1029/2003GB002116.

Cassar, N., et al. (2006), Carbon isotopic fractionation by the marine diatom Phaeodactylum tricornutum under nutrient- and ligh-limited growth conditions, *Geochimica et Cosmochimica Acta*.

Clarke, A., et al. (2007), Seasonal and interannual variability in temperature, chlorophyll and macronutrients in northern Marguerite Bay, Antarctica, *Deep Sea Research Part II: Oceanographic Research Papers*, *in press*.

Crosta, X., et al. (2005), Major factors controlling Holocene d13Corg changes in a seasonal sea-ice environment, Adelie Land, East Antarctica, *Global Biogeochemical Cycles*, *19*, doi:10.1029/2004GB002426.

Crosta, X., et al. (1998a), Application of modern analog technique to marine Antarctic diatoms: Reconstruction of maximum sea-ice extent at the last glacial maximum, *Paleoceanography*, *13*, 284-297.

Crosta, X., et al. (1998b), Reappraisal of Antarctic seasonal sea-ice at the Last Glacial Maximum, *Geophysical Research Letters*, *25*, 2703-2706.

Crosta, X., and A. Shemesh (2002), Reconciling down core anticorrelation of diatom carbon and nitrogen isotopic ratios from the Southern Ocean, *Paleoceanography*, *17*.

Crosta, X., et al. (2004), Late Quaternary sea ice history in the Indian sector of the Southern Ocean as recorded by diatom assemblages, *Marine Micropaleontology*, *50*, 209-223.

Dickson, A. G., and F. J. Millero (1987), A comparison of the equilibrium constants for the dissociation of carbonic acid in seawater media, *Deep Sea Research Part I: Oceanographic Research Papers*, *34*, 1733-1743.

Fisher, G. (1991), Stable carbon isotope ratios of plankton carbon and sinking organic matter from the Atlantic sector of the Southern Ocean, *Marine Chemistry*, *35*, 581-596.

Francois, R., et al. (1997), Contribution of Southern Ocean surface-water stratification to low atmospheric CO2 concentrations during the last glacial period, *Nature*, *389*, 929-935.

Fry, B. and Sherr, E. B. (1984) $\delta^{13}C$ measurements as indicators of carbon flow in marine and fresh-water ecosystems. *Contributions to Marine Science*, 27, 13-47.

Ganeshram, R. S., Calvert, S. E., Pedersen, T. F. and Cowie, G. L. (1999) Factors controlling the burial of organic carbon in laminated and bioturbated sediments off NW Mexico: Implications for hydrocarbon preservation. *Geochimica et Cosmochimica acta,* **63**, 1723-1734.

Garibotti, I. A., et al. (2005), Annually recurrent phytoplanktonic assemblages during summer in the seasonal ice zone west of the Antarctic Peninsula (Southern Ocean), *Deep-Sea Research Part I-Oceanographic Research Papers*, *52*, 1823-1841.

Gibson, J. A. E., et al. (1999), Sedimentation of C-13-rich organic matter from Antarctic sea-ice algae: A potential indicator of past sea-ice extent, *Geology*, *27*, 331-334.

Gleitz, M., et al. (1995), Comparison of Summer and Winter Inorganic Carbon, Oxygen and Nutrient Concentrations in Antarctic Sea-Ice Brine, *Marine Chemistry*, *51*, 81-91.

Hannson, I. (1973), A new set of activity constants for carbonic acid and boric acid in seawater, *deep Sea Research*, *20*, 461-478.

Hayes, J. M. (1993), Factors controlling $^{13}C$ contents of sedimentary organic compounds: principles and evidence., *Marine Geology*, *113*, 111-125.

Hedges, J. I., Clark, W. A., Quay, P. D., Richey, J. E., Devol, A. H. and Santos, U. D. (1986) Compositions and fluxes of particulate matter in the Amazon River. *Limnology and Oceanography*, **31**, 717-738.

Kienast, M., et al. (2001), A critical review of marine sedimentary delta C-13(org)-pCO(2) estimates: New palaeorecords from the South China Sea and a revisit of other low-latitude delta C-13(org)-pCO(2) records, *Global Biogeochemical Cycles*, *15*, 113-127.

Laws, R. A. (1983), Preparing strewn slides for quantitative microscopical analysis: A test using calibrated microspheres, *Micropaleontology*, *24*, 60-65.

Lewis, E., and D. W. R. Wallace (1998), Program developed for CO2 system calculations. ORNL/CDIAC-105. Carbon dioxide information analysis center, Oak Ridge National Laboratory, U.S. Department of Energy, Oak Ridge, Tenesee.

Lourey, M. J., et al. (2004), Sensitivity of delta C-13 of Southern Ocean suspended and sinking organic matter to temperature, nutrient utilization, and atmospheric CO2, *Deep-Sea Research Part I-Oceanographic Research Papers*, *51*, 281-305.

Mehrbach, C., et al. (1973), Measurement of the apparent dissociation constant of carbonic acid in seawater at atmospheric pressure, *Limnology and Oceanography*, *18*, 897-907.

Popp, B. N., et al. (1998), Effect of phytoplankton cell geometry on carbon isotopic fractionation, *Geochimica Et Cosmochimica Acta*, *62*, 69-77.

Rathburn, A. E., et al. (1997), Microfossil and stable-isotope evidence for changes in Late Holocene palaeoproductivity and palaeoceanographic

conditions in the Prydz Bay region of Antarctica, *Palaeogeography Palaeoclimatology Palaeoecology*, *131*, 485-510.

Rau, G. H. (2001), Plankton $^{13}C/^{12}C$ variations in Monterey Bay, California: Evidence of non-diffusive inorganic carbon uptake by phytoplankton in an upwelling environment, *Deep Sea Research Part I: Oceanographic Research Papers*, *48*, 79-94.

Rau, G. H., et al. (1996), A model of photosynthetic C-13 fractionation by marine phytoplankton based on diffusive molecular CO2 uptake, *Marine Ecology-Progress Series*, *133*, 275-285.

Rosenfeld, J. K. (1981) Nitrogen diagenesis in Long Island South sediments. *Americal Journal of Science*, **281**, 436-462.

Rosenthal, Y., et al. (2000), Southern Ocean contributions to glacial-interglacial changes of atmospheric pCO(2): An assessment of carbon isotope records in diatoms, *Paleoceanography*, *15*, 65-75.

Schneider-Mor, A., et al. (2005), Diatom stable isotopes, sea ice presence and sea surface temperature records of the past 640 ka in the Atlantic sector of the Southern Ocean, *Geophysical Research Letters*, *32*.

Schrader, H. J., and R. Gersonde (1978), Diatoms and silicoflagellates, in Micropaleontological Counting Methods and Techniques - An Exercise on an Eight Meters Section of the Lower Pliocene of Capo Rossello, edited by E. Zachariasse et al., *Utrecht Micropaleontology Bulletin*, *17*, 129-176.

Singer, A. J., and A. Shemesh (1995), Climatically Linked Carbon-Isotope Variation During the Past 430,000 Years in Southern-Ocean Sediments, *Paleoceanography*, *10*, 171-177.

Trull, T. W., and L. Armand (2001), Insights into Southern Ocean carbon export from the [delta]13C of particles and dissolved inorganic carbon during the SOIREE iron release experiment, *Deep Sea Research Part II: Topical Studies in Oceanography*, *48*, 2655-2680.

Utermohl, H. (1958), Zur vervollkommung der quantitativen phytoplankton-methodik, *Mitt. d. internat. Vereinig. f. Limnologie*, *9*, 1-39.

Villinski, J. C., et al. (2000), Carbon 13 Carbon 12 ratios of sedimentary organic matter from the Ross Sea, Antarctica: A record of phytoplankton

bloom dynamics, *Journal of Geophysical Research-Oceans*, *105*, 14163-14172.

Winslow, S. D., et al. (2001), Microbial inhibitors for US EPA drinking water methods for the determination of organic compounds, *Environmental Science & Technology*, *35*, 4103-4110.

# 5 $\delta^{15}N$ of Nutrients and Organic Matter as Proxies for Productivity and Export Production in the Coastal Antarctic Sea Ice Environment


## Abstract

Higher utilisation of nutrients during the onset of glacial periods in the Southern Ocean, inferred from higher $^{15}N$ in sediments, has been linked to the lowering of atmospheric $CO_2$ due to higher export of carbon to the seafloor. There are, however, still uncertainties regarding the seasonal progression of $^{15}N$ throughout the water column, the usefulness of $^{15}N$ as a proxy for increased nutrient utilisation in surface waters, and whether this tracer is directly linked to carbon export. This study comprises a high resolution time-series investigation of nitrogen biogeochemistry and export production, over a period of two growing seasons with significantly different hydrographical properties, largely controlled by sea ice and other freshwater inputs. The stability of the surface waters over the growing season plays a significant role in the seasonal evolution of surface water $\delta^{15}N_{PON}$ and total export flux. Surface water $\delta^{15}N$ of nutrients and organic matter respond as expected to nutrient utilisation and inputs of nutrients from mixing of water masses, where as $\delta^{15}N$ in sea ice is primarily controlled by post-production decomposition processes rather than from high nutrient utilisation. The annually integrated $\delta^{15}N$ of sinking particulate matter is consistent with the "steady state" nitrate utilisation model during 04/05 and the "closed system" model during 05/06, reflecting the observed oceanographic characteristics of each season. This, however, does not reflect the changes in C flux of the two seasons. These findings therefore weaken the utility of making direct connections between nitrate utilisation and atmospheric $CO_2$ changes during paleoceanographic studies.

## 5.1 Introduction

The nitrogen stable isotope composition ($\delta^{15}N$) of organic matter in sediments has been used as a proxy for surface water nitrate utilisation in an attempt to understand the role of Southern Ocean in glacial/interglacial changes in atmospheric $CO_2$ (e.g Francois and Altabet, 1992; Francois, et al., 1997; Sigman, et al., 1999a). The High Nutrient Low Chlorophyll (HNLC) nature of the Southern Ocean leaves the majority of $NO_3$ and $PO_4$ in surface waters unutilised during the spring and summer months, believed to be due to iron limitation (Martin, et al., 1990; Timmermans, et al., 1998). Increased nutrient utilisation in the Southern Ocean has be linked to lower atmospheric $CO_2$ concentrations through changes in the efficiency of the biological pump (possibly as a result of increased iron fertilisation), or reduced nutrient ($CO_2$) supply to the ocean surface and release to the atmosphere (Francois, et al., 1997; Kumar, et al., 1995), perhaps due to increased stratification of surface waters. It is therefore essential to be able to understand the balance between changes in export production and the physical oceanographic processes affecting nutrient delivery to the surface to determine changes in the drawdown of $CO_2$.

Natural abundance measurements of $\delta^{15}N$ are useful as tracers of changes in nutrient utilisation in HNLC regions. Drawdown of $NO_3$ in surface waters results in increasing $\delta^{15}N$ of $NO_3$ ($\delta^{15}N$-$NO_3$) due to isotopic fractionation during utilisation by phytoplankton (Sigman, et al., 1999; Wada and Hattori, 1978; Wu, et al., 1997). Increasing $\delta^{15}N$-$NO_3$ is then transferred to the $\delta^{15}N$ of suspended particulate organic nitrogen ($\delta^{15}N_{PON}$), and subsequently sinking particulate organic nitrogen ($\delta^{15}N_{org}$) (Altabet, 1996; Altabet, et al., 1991; Wu, et al., 1999). Preservation of this isotopic signal in sediments facilitates the study of present and past changes in nutrient drawdown. High $\delta^{15}N$ in Antarctic sediments has thus been used to infer increased nutrient utilisation and drawdown of $NO_3$ and $CO_2$ from surface waters in a normally

HNLC region, assuming that high $\delta^{15}N$ was pertinent to increased export production (e.g. Robinson, et al., 2005; Sigman, et al., 1999).

There are still, however, uncertainties regarding the use of $\delta^{15}N$ in sediments as a tracer of $NO_3$ utilisation in the Southern Ocean and whether high $\delta^{15}N$ in sediments can indeed be linked to increased carbon drawdown (Altabet and Francois, 2001; Crosta and Shemesh, 2002; Lourey et al., 2003). This uncertainty is linked to observations of higher $\delta^{15}N_{PON}$ and $\delta^{15}N_{org}$ during winter than the spring months, (Lourey et al., 2003), which has the potential to skew interpretation of sediment core records leading to overestimation of $NO_3$ utilisation. This is believed to be caused by a high residence time of dead or slow growing winter phytoplankton that are highly degraded, which increases their $\delta^{15}N_{PON}$ composition. Thus sinking $\delta^{15}N_{org}$ from this material may be significantly higher than material observed in the growing season and skew interpretation of sediment core records leading to overestimation of $NO_3$ utilisation. It has been suggested that reduction of the growing season due to extended sea ice cover may have been a cause of the high $\delta^{15}N_{org}$ in sediments based on these winter observations (Lourey et al., 2003).

Growth of phytoplankton in sea ice, which can reach high standing stocks comparable to open water (Carson et, al., in-prep – Chapter 3) may also display high $\delta^{15}N$ values compared to surface water phytoplankton. High levels of productivity in the closed or semi-closed sea ice matrix has the potential to exhaust nutrients and produce particulate organic material with anomalously high $\delta^{15}N$ composition (Fischer, et al., 2002; Gibson, et al., 1999; Kennedy, et al., 2002). Similar to winter surface water material, sinking material from sea ice with high $\delta^{15}N_{org}$ may also skew interpretation of sediment core records leading to overestimation of $NO_3$ utilisation.

Other studies have also suggested that the fractionation factor ($\varepsilon_p$) may change in response to phytoplankton assemblages (Needoba, et al., 2006) light levels (Difiore, et. al., 2006) or the concentration of iron in surface

waters (Karsh et al., 2003), as a cause for changes in Southern Ocean sediment $\delta^{15}N$. Nitrogen $\varepsilon_p$ in the Southern Ocean has been estimated to be between 4-8 ‰ (Altabet and Francois, 2001; Difiore, et al., 2006; Sigman, et al., 1999b) based on models used for a steady state system (continuous nutrient supply) and a closed system (no nutrient supply), and this value may be even lower when physical mixing of water masses and remineralisation of nitrogen occur (Needoba, et al., 2006).

Making connections between high $\delta^{15}N$ (nutrient utilisation) and $CO_2$ drawdown may not be relevant in many scenarios as the C and N systems can be severely decoupled in surface waters (Crosta and Shemesh, 2002; Lourey et al, 2003). This may occur not only from sea ice and winter surface water material, but from the total cumulative levels of nutrients utilised in a single growing season. Seasonally integrated sediment $\delta^{15}N$ may be comparable to the relative utilisation of $NO_3$ in surface waters, but does not capture the amount of inorganic carbon and nitrogen that can be assimilated and exported over the duration of a growing season (Francois, et al., 1997).

To address these concerns regarding the $\delta^{15}N$ proxy, this study presents a high-resolution time series of nitrogen isotope measurements covering two austral growing seasons (2004-2006) coupled with measurements of carbon and nitrogen export. The goal is to understand nitrogen isotope biogeochemistry in a Southern Ocean sea ice environment (Ryder Bay, Western Antarctic Peninsula) and to test the reliability of using $\delta^{15}N$ as a proxy for nutrient utilisation and export production.

## 5.2 Materials and Methods

### 5.2.1 Study Area

This study took place from 2004 until 2006 and was located in Ryder Bay and Marguerite Bay, which lies south of Alexander Island and west of the mainland on the Western Antarctic Peninsula (see Figure 5.1). Ryder Bay is a coastal embayment adjoining Marguerite Bay and the study site is situated

in open water at a depth of 520 m. Sea ice brine was sampled when sea ice was present at three locations, with a total of 15 sea ice samples taken during this study. Sea ice had receded from Ryder Bay upon arrival in December 2004, however there was still land fast ice located around Lagoon Island (see Figure 5.1 for Lagoon Island sampling site), with 5 samples taken at the Lagoon Island site during December 2004. A further 10 samples were taken during the 05/06 season. During winter 2005, two sea ice samples were taken in September and October at the RaTS site and during early spring 2005 (Nov-Dec), a further eight sea ice samples were taken at a site north of Rothera Point (See Figure 5.1).

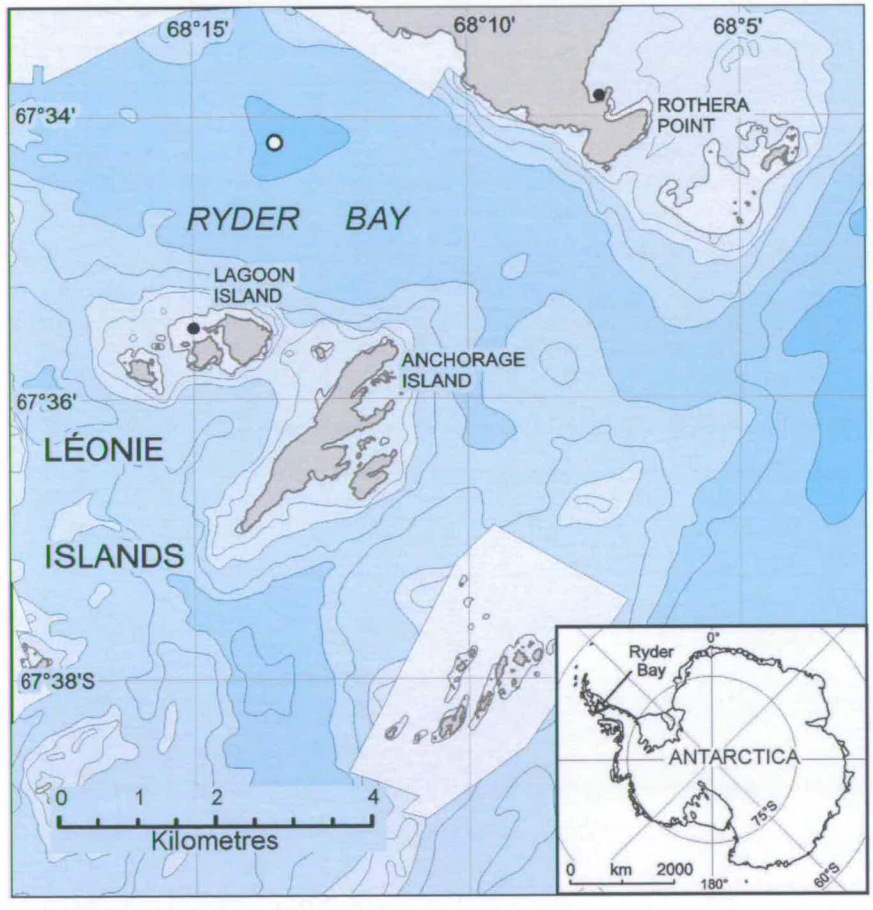


**Figure 5.1. Map of Ryder Bay showing the RaTS site (white circle) and the two other sites used for sea ice sampling (black circles). Map courtesy of the British Antarctic Survey.**

A high resolution time series of surface water samples were taken in Ryder Bay, at the Rothera Time Series study site at 67°34.02'S, 68°14.02'W (Clarke, et al., 2007) during austral spring and summer 2004/2005 and 2005/2006 (Figure 5.1). Low resolution time series sampling was conducted during winter 2005. Sea ice brine and surface water samples at 15 m depth were taken measuring: temperature, salinity, chlorophyll-*a*, $NO_3$, $NH_4$, the partial pressure of carbon dioxide ($pCO_2$), $\delta^{15}N\text{-}NO_3$, POC, PON, and $\delta^{15}N_{PON}$. Routine CTD measurements were also taken at every surface water sampling event to monitor changes in the mixed layer depth. Sinking POC, PON and $\delta^{15}N_{org}$ were analysed from time-series sediment trap material located at two depths at both the RaTS site and a deeper site in Marguerite Bay during the study. Finally, shallow sediment box cores were taken at the RaTS site in January 2005, and were analysed for $\delta^{15}N_{org}$.

### 5.2.2 Sea Ice Sampling

Sea ice brine was sampled using a sack hole drilling method, with samples for $pCO_2$ taken first to minimise atmospheric contamination. Alkalinity samples for $pCO_2$ determination were taken by immersing a 250 ml BOD bottle in the sack hole and sealing the bottle with a plastic stopper ensuring no air bubbles were present. Salinity and temperature were measured using a YSI-500 multi-parameter meter. For particulate carbon and nitrogen measurements, sea ice brine was transferred to acid-clean HDPE carbuoys and taken back to the laboratory for filtration. Sea ice brine samples were filtered through muffle-furnaced (400°C for 4 h) 47 mm GF/F filters, always < 2 h after collection. Aliquots of filtrate from this process was transferred to 50 ml plastic centrifuge tubes and frozen at -20°C for $NO_3$ analysis and used immediately for $NH_4$ analysis. The filters containing particulate material were then dried at 50°C overnight, and stored frozen until analysis.

### 5.2.3 Surface Water Sampling

CTD casts were taken to ~500 m depth using a Sea Bird Electronics 19 Plus SEACAT CTD module. For depth profile measurements of conductivity, temperature and depth a Wet Labs Wetstar module was used. For

measurement of temperature at 15 m, a Sensoren Instrumente Systeme GmbH reversible thermometer was lowered to 15 m, allowed to equilibrate for 2 min before measurements were initiated. Surface water samples were taken using a 5 L Niskin bottle for chlorophyll and $pCO_2$ measurements. Alkalinity samples for $pCO_2$ determination were taken from the Niskin straight into a 250 ml BOD bottle and sealing the bottle with a plastic stopper ensuring that no air bubbles were present. Particulate samples were retrieved using a 12 V dolphin pump and 15 m of silicone tubing weighted down at the end. Water from 15 m was pumped into 10 L HDPE carbuoys for transfer back to the laboratory. Surface water samples were filtered through muffle-furnaced (400°C for 4 h) 47 mm GF/F filters. Aliquots of filtrate from this process was transferred to 50 ml plastic centrifuge tubes and frozen at -20°C for $NO_3$ analysis and used immediately for $NH_4$ analysis. The filters were then dried at 50°C overnight and stored frozen until analysis.

### 5.2.4 $NO_3$, $NH_4$ and $pCO_2$ Determination

Nitrate concentrations were measured in the UK using a Skaler San $^{plus}$ nutrient autoanalyser employing standard coloutimetric techniques (Strickland and Parsons, 1972). Nutrient utilisation (u) was calculated using the seasonal change in surface $NO_3$ concentrations (Lourey and Trull, 2001). Ammonium concentrations were measured on the filtered sea ice and surface water samples using the standard addition method described in (Holmes, et al., 1999) on the day of sample collection. $NO_3$ and $NH_4$ concentrations in sea ice were normalised to 34.5 PSU, the average salinity of the surface waters during this study. Determination of $pCO_2$ was conducted utilising measurements of salinity, temperature, pH and alkalinity. Salinity measurements were taken from the CTD profiles and temperatures were measured using a Sensoren Instrumente Systeme GmbH reversible thermometer. Alkalinity was determined by titration with 0.05 M HCl and the Gran plot method (Almgren, et al., 1983). $pCO_2$ was calculated using constants from (Dickson and Millero, 1987), (Hannson, 1973) and (Mehrbach, et al., 1973) with the CO2SYS programme (Lewis and Wallace, 1998).

### 5.2.5 $\delta^{15}N\text{-}NO_3$ Determination

$\delta^{15}N\text{-}NO_3$ was measured using the bacterial denitrifier method (Casciotti, et al., 2002; Sigman, et al., 2001) during the 04/05 season. Strains of the denitrifying bacteria *Pseudomonas chlororaphis* were used convert the $NO_3$ in sea ice and surface water samples to $N_2O$ in order to measure their $\delta^{15}N$ composition. Stock cultures of *P. chlororaphis* were maintained on tryptic soy agar amended with 10 mM potassium nitrate, and 1mM ammonium sulphate. Working cultures for sample denitrification were cultured in tryptic soy broth amended with 10mM potassium nitrate, 1mM ammonium sulphate and 1ml/L of an antifoaming agent. Prepared medium was decanted into 400 ml aliquots into 500 ml Duran bottles and autoclaved. A starter tube containing 5 ml of the amended tryptic soy broth was inoculated with an individual colony of cells taken from the stock culture and allowed to grow overnight on an orbital shaker. The 500 ml culture vessels containing 400 ml of amended tryptoc soy broth were then inoculated from the starter tube and incubated for 6-11 days on an orbital shaker. On the day of sample preparation, the working culture was divided into 40 ml aliquots and centrifuged for 10 min at 7600 rpm. The supernatant was then decanted and the cells were resuspended in 6 ml of spent medium, resulting in a 7-fold concentration of cells. In order to mimic the matrix effect of seawater, 30 ml of synthetic seawater (33 % NaCl) was added to the 60 ml of cell culture liquid. Using 20 ml crimp lid sample vials, 3 ml of the concentrated bacteria were transferred into each vial. Crimp seal caps were then placed on each sample vial and sealed.

All the vials were degassed at 10 – 20 ml/min for 3 hours using helium (zero grade). The purging gas was introduced through a 26-gauge short needle, inserted through the septum to bubble the medium, and the gas was vented through a 25-gage needle inserted above the liquid level. Once purging was complete, sea ice and surface water samples were injected into the sample vials achieving a final concentration of 10 or 20 nmol N (5 or 10 nmol $N_2O$). For each run, a series of isotope standards (IAEA N3 and USGS-34) were

run throughout the sequence in order to correct raw $^{15}N$ data. After samples and standards were injected into the crimp sealed vials, the vials were incubated overnight to allow complete conversion of nitrate to $N_2O$. The following day, 0.1-0.2 ml of 10N NaOH solution was injected into each sample and standard vial to kill the bacteria. This step also immobilises the bilk of $CO_2$ gas in the sample as dissolved organic carbon. A further 3-4 drops of antifoam B were added to sample vials to prevent foaming during isotopic analysis.

The $\delta^{15}N$ composition of $N_2O$ in the sample vials was then measured using an automated Gas Bench GC-IRMS system. Samples from the 2004/2005 field season were measured in the Sigman Laboratory, Princeton University, Princeton NJ, USA in 2006 (see Casciotti, et al., 2002; Sigman, et al., 2001).

### 5.2.6 Bulk POC/PON and $\delta^{15}N_{PON}$ Determination

Bulk POC, PON and $\delta^{15}N_{PON}$ analyses were conducted using a method similar to Lourey, et al., (2003). Sea ice brine and surface water samples were filtered through muffle-furnaced (440°C for 4 h) 47 mm GF/F filters. The filters were then dried at 50°C overnight and stored frozen until analysis. Prior to analysis, the filters were decarbonated by wetting the filter with Milli-Q water and fuming with HCl for 48h and then drying at 50°C. Filters were analysed for elemental PON and $\delta^{15}N_{PON}$ using a Carlo Erba NA 2500 elemental analyser in-line with a VG PRISM III isotope ratio mass spectrometer. Results are presented in the delta notation versus $N_2$ gas. The analytical precision for the isotopic measurements was 0.2 ‰.

### 5.2.7 Sediment Trap Deployments

Two sediment trap mooring arrays were deployed, with one at the RaTS site and the other at a deeper site in Marguerite Bay to catch sinking particles in concert with the time series water sampling programme. Each mooring consisted of two time-series sediment traps, which were situated at 200 m and 400 m for the RaTS mooring and 200 m and 750 m for the deep site mooring. Each sediment trap was equipped with 21 rotating cups

programmed to rotate at predefined intervals. The strategy employed for cup rotation utilised higher resolution cup turnover during periods of potential sea ice melt and the spring bloom with lower resolution cup rotation during the low flux winter periods. The RaTS site mooring was initially deployed on the 25th January 2005 in 502 m water at 67'34.02°S, 68' 14.02°W. The deep site mooring was deployed on the 24th January 2005 in 841 m water at 67' 55.39°S, 68' 24.15° W. The RaTS mooring and deep mooring were recovered on the 15th February 2006 and the sediment trap bottles were removed and replaced with fresh ones. Both moorings were redeployed on the 17th February 2006. The RaTS mooring was redeployed at a water column depth of 522m at 67' 34.00°S, 68' 14.00°W. The deep mooring was redeployed at a water column depth of 835m at 67' 55.41°S, 68'24.11°W. For a table of sediment trap bottle rotations during the second deployment, refer to Table 6. The moorings were further recovered on 17th December 2006 aboard JCR Cruise 155. The RaTS mooring was successfully retrieved, but unfortunately the deep mooring was lost.

### 5.2.8 Box Cores

A box core was taken from Ryder Bay, nearby to the RaTS site during JCR cruise 112/113 (Brandon, 2005). BC-388 was retrieved at -67.57046°S, -68.22844°W on 24th January 2005 at 505 m water depth. The top 0.5 cm section was used for surface sediment analysis.

### 5.2.9 Sediment Organic Carbon Nitrogen and $\delta^{15}N_{org}$ Determination

One sediment trap cup split and sub-section of the box core were freeze-dried and ground for analysis of particulate components. For POC, PON and $\delta^{15}N_{org}$ analysis, duplicate ~10 mg aliquots of dried, ground sediment were weighed into silver capsules and were acidified with 50 % HCl to remove carbonates and dried at 60°C overnight. Decarbonated samples were then analysed for elemental POC, PON and $\delta^{15}N_{org}$ using a Carlo Erba NA 2500 elemental analyser in-line with a VG PRISM III isotope ratio mass spectrometer. $\delta^{15}N$ results are presented in the delta notation versus $N_2$ gas.

## 5.3 Results

This study presents high-resolution time series analyses of $NO_3$, $\delta^{15}N\text{-}NO_3$ (04/05 only), $NH_4$, POC, PON and $\delta^{15}N_{PON}$, in order to investigate factors influencing the seasonal progression of productivity and $\delta^{15}N_{PON}$ prior to its export to depth. The transfer of this stable isotope signal to sediment traps and the seafloor along with the associated C and N fluxes is then investigated. The reliability of using $\delta^{15}N_{org}$ as a proxy for nitrate utilisation and export production in the coastal Antarctic sea ice environment is then evaluated.

### 5.3.1 Growing Seasons 2004-2006

Sea ice cover, mixed layer depth (MLD), 15 m integrated salinity and chlorophyll a (chl-a) data from growing seasons (04/05 and 05/06) sampled during this study are presented in Figure 5.2. Sea ice cover was variable between the two seasons, occurring from 16$^{th}$ June to 1$^{st}$ November during winter 2004 and 10$^{th}$ June to 25$^{th}$ December during winter 2005. The MLD data in Figure 5.2 show typical seasonality for Ryder Bay, with a deep winter mixed layer and a shallow surface layer in summer, influenced by freshwater from sea ice and glacier melts (Clarke, et al., 2007). The freshwater melt layer stabilises the water column providing an environment favouring growth of diatoms and nutrient utilisation in the photic zone. The presence and retreat of ice during this period and the physical stability of the water column resulted in growing seasons that lasted ~4 months during both growing seasons, but the growing season began and finished ~1 month later during the 05/06 season relative to 04/05, due to extended sea ice cover.

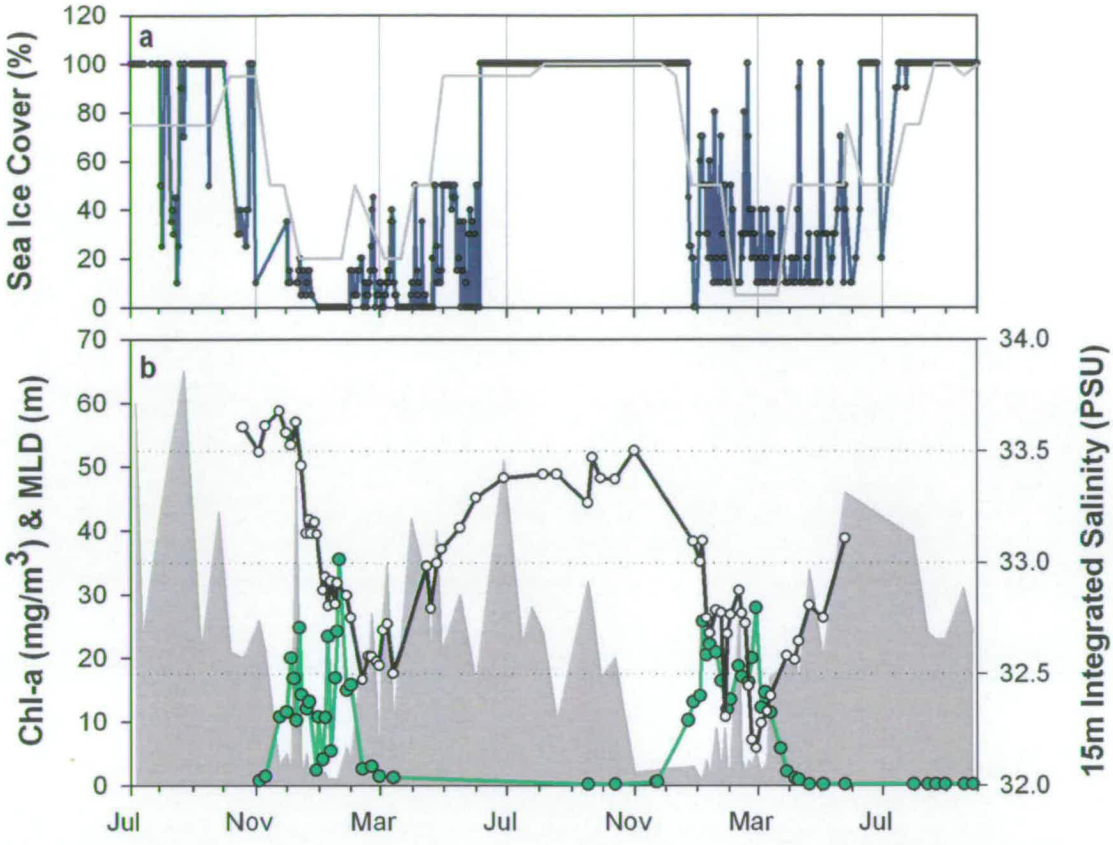


**Figure 5.2. Time series plot of (a) regional sea ice cover (grey line) and local sea ice cover in Ryder Bay based on daily observations (blue lines) and (b) Chl-a (green line), mixed layer depth (grey shaded area) and 15 m integrated salinity (black line) from June 2004 until October 2006.**

### 5.3.2 Sea Ice

Sea ice data are summarised in Appendix 5 and Figure 5.3. PON in sea ice shows clear decreasing trends during each sampling season (Figure 3), similar to chlorophyll and nutrients, probably due to the combined effects of decreasing primary production, freshwater dilution from ice melt increasing the osmotic pressure on sea ice phytoplankton and rates of biodegradation of organic material exceeding that of growth rates. During Dec 2004, sea ice POC declined from 118 µM to 37 µM, during winter 2005 (Sep-Oct) POC ranged between 24 µM and 32 µM, then during Nov and Dec 2005 declined from 43 µM to 20 µM. PON showed similar characteristics with PON declining from 9 µM to 4 µM during Dec 2004, during winter 2005 (Sep-Oct) PON was ~ 4 µM and during Nov and Dec 2005 PON declined from 4 µM to 2 µM. $\delta^{15}N_{PON}$ in sea ice showed an opposite trend to that of PON, with

$\delta^{15}N_{PON}$ increasing from 6.82 to 8.82 ‰ during Dec 04 and from 2.80 ‰ to 9.67 ‰ between Sep and Dec 05.

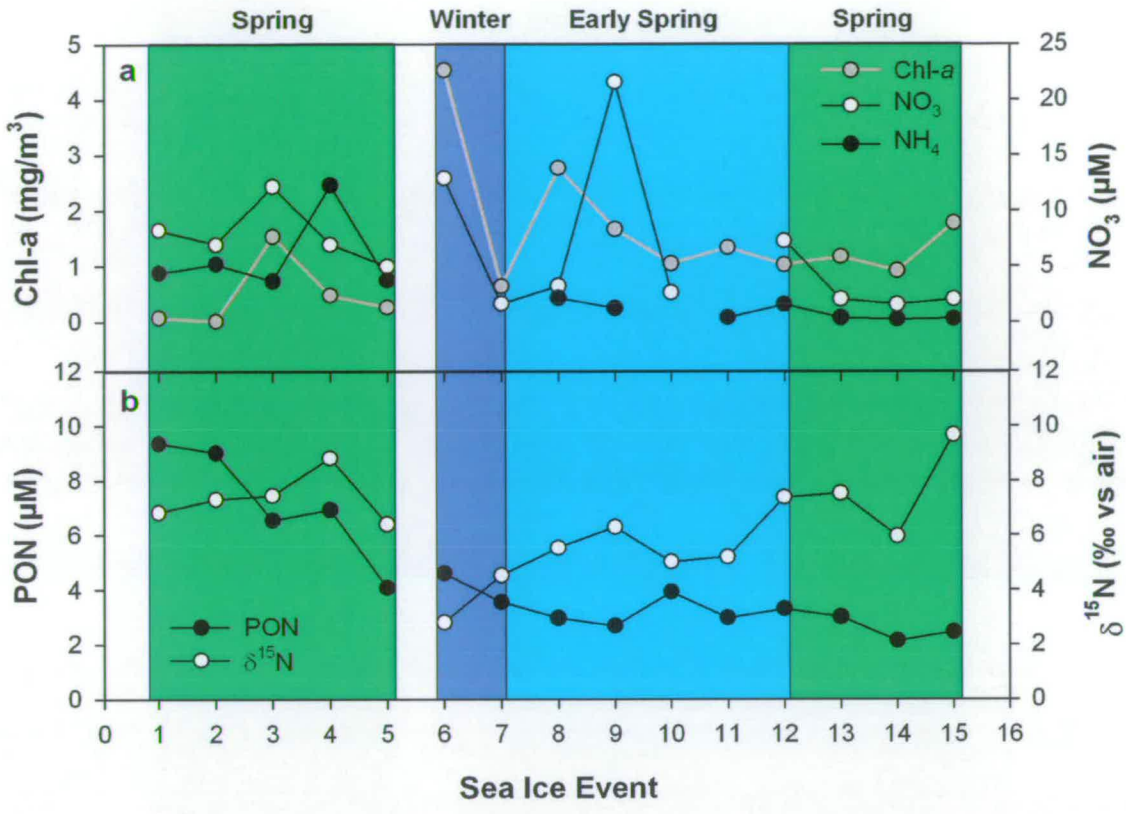


**Figure 5.3. Time-series plots (by event number) of (a) chl-a, nitrate ($NO_3$) and ammonium ($NH_4$) and (b) suspended particulate organic nitrogern (PON) and the nitrogen stable isotope composition of particulate organic nitrogen ($\delta^{15}N$). Shaded areas are indicative of the time periods over the course of the two seasons sampled.**

### 5.3.3 Surface Waters

Surface water time series data exhibit typical pulsed growing seasons during the short sunlit, ice free conditions of austral spring and summer, with the time-series data presented in Appendices 6 and 7. As the sea ice covering the bay began to decay and recede, the spring bloom started (Figure 5.2). Chl-*a* concentrations reached a maximum concentration of 35.55 µg/L. during the 04/05 season and maximum of 27.94 µg/L during the 05/06 season. Both seasons displayed similar characteristics in primary productivity; an initial chl-*a* peak in Nov 04 and Dec 05 during sea ice retreat, followed by a mid season decline, and then a second chl-*a* peak in summer before primary production ceases in mid-February 05 and late

March 06. The surface waters are stabilised by a freshwater lens in the top few m (Clarke, et. al., 2007) due to sea ice and glacier melt, resulting in a shallow Mixed Layer Depth (MLD). The average MLD was 11.36 m during the 04/05 season and 6.15 m during the 05/06 season (Table 5.1). This freshwater lens prevents wind induced vertical mixing. The salinity averaged over the top 15m (Figure 5.2) also displays the seasonal effect of freshwater dilution of the surface ocean, reaching its lowest value during Jan and Feb 2006, indicating higher freshwater input to the surface ocean during the 05/06 season.

Surface water $NO_3$ profiles (Figure 5.4) show a clear seasonal cycle with winter concentrations reaching ~35 µM and high nitrate utilisation is evident during the growing season with concentrations reaching as low as 2.26 µM. $NO_3$ concentrations in surface waters ranged from 3.33 to 26.30 µM during the 04/05 sampling season and from 2.26 to 33.70 µM during the 05/06 sampling season. The relative $NO_3$ utilisation (u) over the two growing seasons averaged 62 % and 69% and reached maxima of 90 % and 93 % during the 04/05 and 05/06 seasons respectively, and is summarised in Table 5.1 along with the above 15 m integrated salinity and MLD data. Despite the freshwater lens that stabilises the water column during the spring and summer (Clarke, et al., 2007), there were still episodic nutrient inputs to surface waters, inferred from increases in $NO_3$ concentrations (Figure 5.4) and occurred at a higher frequency during the 04/05 growing season compared to the 05/06 growing season.

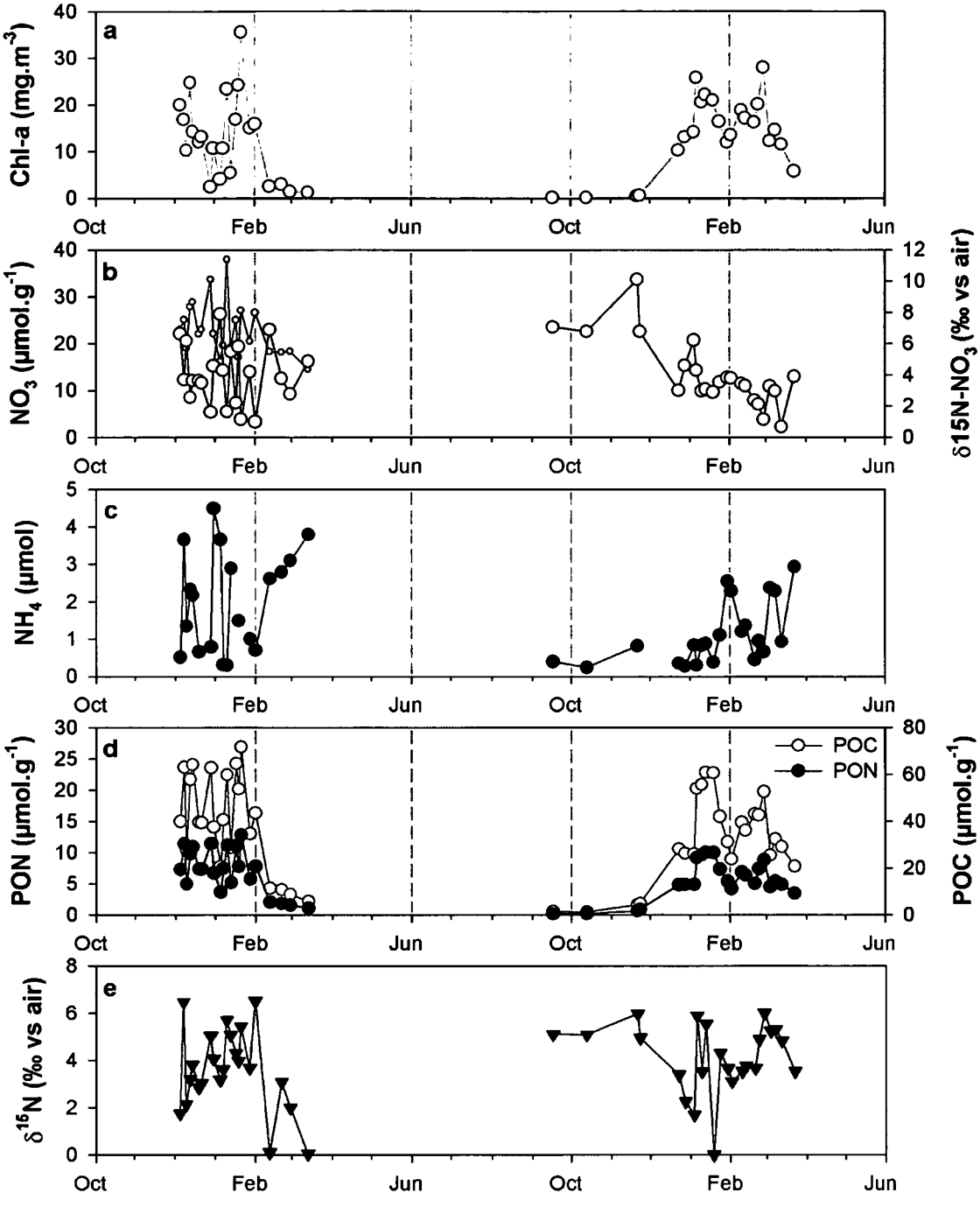


**Figure 5.4. Time series surface water measurements over the 04/05 and 05/06 growing seasons of (a) chl-a (b) $NO_3$ (open circles) and $\delta^{15}N$-$NO_3$ (blue closed circles) (c) $NH_4$ (d) PON and POC and (e) $\delta^{15}N$.**

**Table 5.1. Seasonal averages of salinity, mixed layer depth (MLD), $NO_3$ utilisation (u), $\delta^{15}N\text{-}NO_3$ and $\delta^{15}N_{PON}$.**

| Season | 15 m integrated salinity (PSU) | Average MLD (m) | Average *u* | Average $\delta^{15}N\text{-}NO_3$ (‰ vs air) | Flux Weighted Average $\delta^{15}N_{PON}$ (‰ vs air) |
|---|---|---|---|---|---|
| 04/05 | 33.029 | 11.36 | 0.619 | 7.119 | 4.19 |
| 05/06 | 32.637 | 6.15 | 0.692 | - | 3.96 |

The $\delta^{15}N\text{-}NO_3$ of surface water samples is presented as a time-series profile in Figure 5.4 and as a function of $NO_3$ concentration (ln $NO_3$) in Figure 5.5. $\delta^{15}N\text{-}NO_3$ ranged from 4.35 ‰ (winter value) to 11.37 ‰ during the 04/05 season. The nitrogen stable isotope composition of $NO_3$ shows a clear seasonal response to productivity (Figure 5.4), and has negatively correlation with the ln of $NO_3$ concentration (Figure 5.5), with a slope of -2.061. This slope can be used to estimate the fractionation factor of $NO_3$ during N assimilation, but only if there is an assumption of a closed system (Sigman et al., 1999), however the time series profiles show that $NO_3$ uptake was not occurring in a closed system. The -2.061 slope of the correlation between ln $NO_3$ versus $\delta^{15}N\text{-}NO_3$ is much lower than the 6-8 ‰ fractionation factor estimated by other studies in the Southern Ocean (Sigman et al., 1999; DiFiore, et al., 2006), and is a result of mixing of nitrate depleted surface waters and the nitrate rich UCDW below, reducing the slope of the $\delta^{15}N\text{-}NO_3$ versus ln $NO_3$ plot. Although the water column was more stable during the 05/06 season and displayed progressive $NO_3$ utilisation tending towards a closed system, there is no available $\delta^{15}N\text{-}NO_3$ data to estimate the fractionation factor of $NO_3$ during N assimilation. $NH_4$ concentrations in surface waters also show a seasonal pattern, with winter values as low as 0.24 µM and summer values reaching as high as 4.49 µM. High $NH_4$ concentrations occur during the mid-season decline in biomass likely a result of grazing and then peak again at the end of the season when the phytoplankton and zooplankton in the surface water die and begin to degrade, producing $NH_4$.

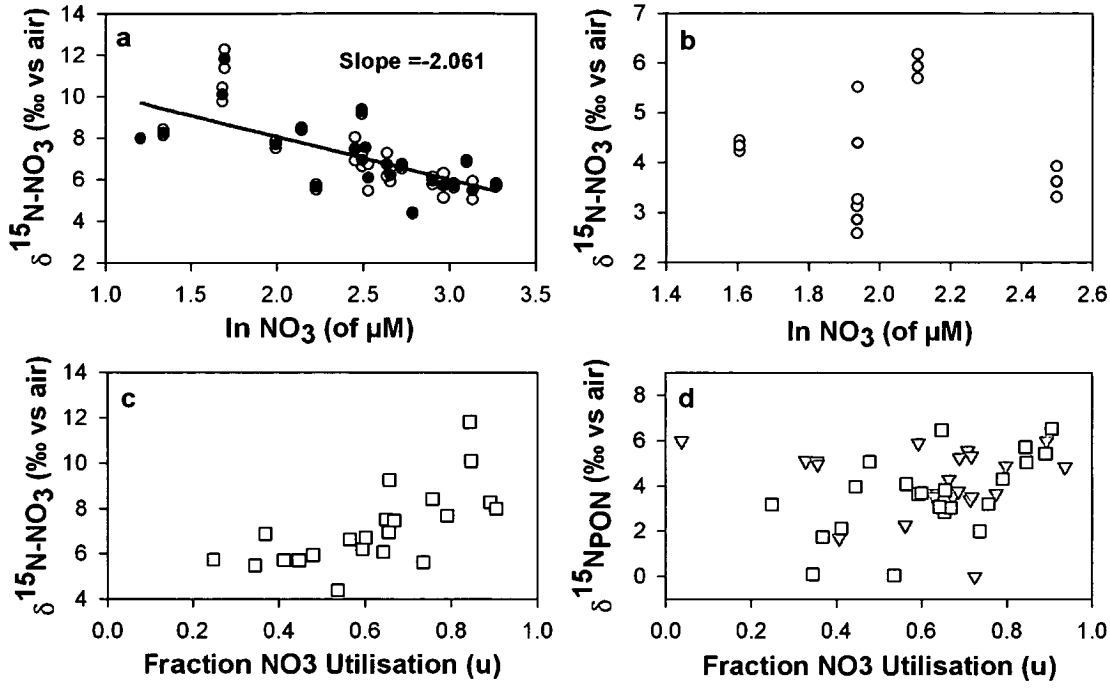


**Figure 5.5. Plots of (a) The surface water ln of nitrate (ln $NO_3$) versus $\delta^{15}N\text{-}NO_3$ during the 04/05 growing season (open circles for replicates and closed circles for mean of replicates) (b) Sea ice ln $NO_3$ versus $\delta^{15}N\text{-}NO_3$) during the 04/05 growing season (open circles for replicates and closed circles for mean of replicates) (c) the fraction of nitrate utilisation (u) versus $\delta^{15}N\text{-}NO_3$) in surface waters and (d) u versus $\delta^{15}N_{PON}$).**

Time-series POC and PON profiles are similar to that of the chlorophyll profiles (Figure 5.4). During the 04/05 season, although the start of the field season was missed, POC peaks with chlorophyll in Dec 04 reaching 64 µM and then in sync with chlorophyll, declines to 21 µM in Jan 05; the mid season decline. The second peak of POC then occurs with chlorophyll in late Jan and early Feb 05 reaching 72 µM, before declining to winter values in Mar 05. During the 05/06 season, winter POC values of ~ 1 µM are observed during Sep and Oct, before increasing with the onset of sea ice retreat in late December, before peaking at 61 µM in mid-Jan 05. The mid-season decline occurred during late Jan and early Feb 05, with POC dropping to 36 µM. The second productivity peak occurring during mid Feb until early March, with

POC peaking at 53 µM before productivity declined at the end of the growing season. PON, as expected, shows very similar characteristics in surface waters over the two growing seasons, peaking with chlorophyll in Dec 04 at 11µM and then in sync with chlorophyll, declines to 4 µM in Jan 05; the mid season decline. The second peak of PON then occurs with chlorophyll in late Jan and early Feb 05 reaching 13 µM, before declining to winter values in Mar 05. During the 05/06 season, winter PON values of ~ 0.2 µM are observed during Sep and Oct, before increasing with the onset of sea ice retreat in late December, before peaking at 10 µM in mid-Jan 05. The mid-season decline occurred during late Jan and early Feb 05, with PON dropping to 4 µM. The second productivity peak occurring during mid Feb until early March, with POC peaking at 9 µM before productivity declined at the end of the growing season. POC/PON ratios are plotted in Figure 5.6 and show that the C/N ratio of particulate organic matter was 5.8, slightly below the Redfield Ratio of 6.6.

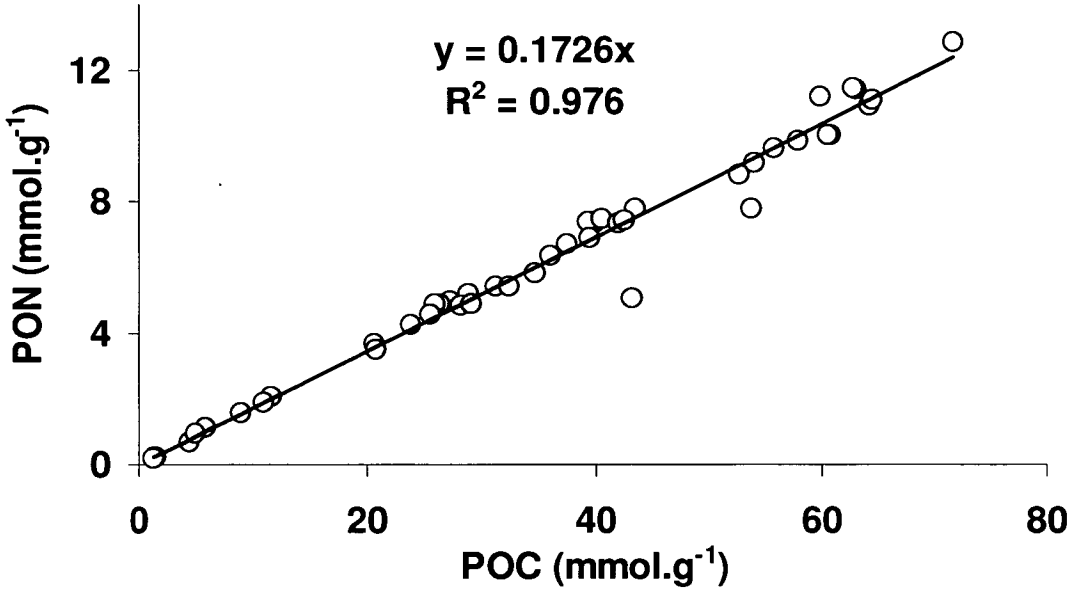


**Figure 5.6. Surface water suspended POC against PON for all samples taken during this study. The fitted linear regression indicates an average C:N ratio of 5.8.**

$\delta^{15}N_{PON}$ profiles for surface waters are also presented in Figure 5.4. $\delta^{15}N_{PON}$ showed an increasing seasonal pattern during the 04/05 growing season, with high variability believed to be brought on by inputs of fresh $NO_3$ into the surface water. When sampling began in Dec 04, the $\delta^{15}N_{PON}$ was initially 1.8 ‰ and then increased to 6.5 ‰ in early Feb 2005. During this period, there is a 'saw-toothed' shape to the profile, where decreases in $\delta^{15}N_{PON}$ occur at the same time as increases in $NO_3$, where fresh nutrients enter the system from vertical or lateral sources and decrease the $\delta^{15}N$ of the $NO_3$ pool. The increases and decreases in $\delta^{15}N_{PON}$ and $NO_3$ during this period are consistent with unstable water column resulting in frequent inputs of nutrient rich water into the surface during phytoplankton growth and N-utilisation. At the end of the growing season, the $\delta^{15}N_{PON}$ decreases to ~ 0 ‰ when phytoplankton growth falls to winter levels. During the 05/06 season, sampling began in Sep 05 under the sea ice, where $\delta^{15}N_{PON}$ was initially 5.1 ‰ and increased to ~ 6 ‰ prior to the onset of sea ice decay and the start of phytoplankton growth in the surface waters in late November, when $\delta^{15}N_{PON}$ decreased to 1.7 ‰ with the onset of the spring bloom before rising again to 5.9 ‰ prior to the mid-season decline in chlorophyll, POC and PON. During the mid-season decline, $\delta^{15}N_{PON}$ dropped to a season low of 0 ‰ before increasing during the second productivity peak and reaching a season maximum of 6 ‰ in late Feb 06. As the 05/06 growing season began to decline in mid Mar 06, $\delta^{15}N_{PON}$ began to decrease in sync with chlorophyll, POC and PON. Although there are subtle increases and decreases in $\delta^{15}N_{PON}$ during the 05/06 growing season, they are nowhere near the same magnitude as the 04/05 season. Similarly, the $NO_3$ profile shows a clearer progression of $NO_3$ depletion, with fewer and more subtle inputs of $NO_3$ into the surface waters. This is consistent with the more stable water column, as described in Section 5.3.1.

Figure 5.5 also presents $NO_3$ utilisation (u) versus $\delta^{15}N\text{-}NO_3$ and $\delta^{15}N_{PON}$ (Figure 5c and 5d respectively). Although there is a positive relationship between u versus $\delta^{15}N\text{-}NO_3$ for the 04/05 season, there is no strong positive

relationship between *u* and $\delta^{15}N_{PON}$. The lack of a strong positive relationship between u and $\delta^{15}N_{PON}$ for either season is caused by the effects of post production degradation processes occurring as a result of grazing by zooplankton and bacteria. This is particularly evident in the samples taken under the sea ice prior to the start of the growing season, where organic matter has a high retention time in the water column for degradation to occur (Lourey, et al., 2003). A further influence may have come from a change in the fractionation factor during N assimilation, but this remains speculative as the main controls on the fractionation factor of N assimilation are poorly constrained (Karsh, et al., 2003; Difiore, et. al., 2006).

### 5.3.4 Sinking Particulate C/N and $\delta^{15}N$

Appendices 8 and 9 and Figure 5.7 presents time-series sediment trap mass fluxes, C and N fluxes and the sinking particulate $\delta^{15}N_{org}$ from the RaTS site and Deep site sediment trap moorings. The sediment traps were deployed on the 16th January, so the initial flux for the 04/05 season can not be accurately quantified. However, from Figure 5.8, fluorescence profiles from the 20th, 21st and 22nd of December 04, there are major peaks in fluorescence at depths below the thermocline, which suggests that this is when the flux of organic matter from the initial productivity peak took place (Clarke et al., 2007). The flux during Dec 04 probably included a significant proportion of the total seasonal flux, as much of this occurs soon after ice break up (Ducklow, et. al., 2007; Garrity, et. al., 2005).

In the RaTS site 200 m and 512 m traps, there were significantly higher mass flux levels and subsequent fluxes of POC and PON during the 04/05 season when there was high levels of nutrient input compared to the 05/06 season where the water column was more stable. In the RaTS 200 m trap during the partial coverage of the 04/05 growing season, dry mass flux from 26th Jan 05 until 1st April 05 totalled 79.3 $g.m^{-2}$, with POC flux totalling 177 mmol $C.m^{-2}$ and PON flux totalling 23 mmol $N.m^{-2}$. In the RaTS 512 m trap over the same period, mass fluxes totalled 42.5 $g.m^{-2}$, with POC flux totalling 92 mmol $C.m^{-2}$

and PON flux totalling 12 mmol $N.m^{-2}$. During the full coverage of the 05/06 growing season, fluxes appear to be much lower than the previous season. In the RaTS 200 m trap, mass fluxes from 1st Feb 06 to 1st Mar 06 totalled 40.9 $g.m^{-2}$, with POC fluxes totalling 54 mmol $C.m^{-2}$ and PON fluxes totalling 8 mmol $N.m^{-2}$. In the RaTS 512 m trap over the same period, mass fluxes totalled 6.4 $g.m^{-2}$, with POC fluxes totalling 12 mmol $C.m^{-2}$ and PON fluxes totalling 2 mmol $N.m^{-2}$.

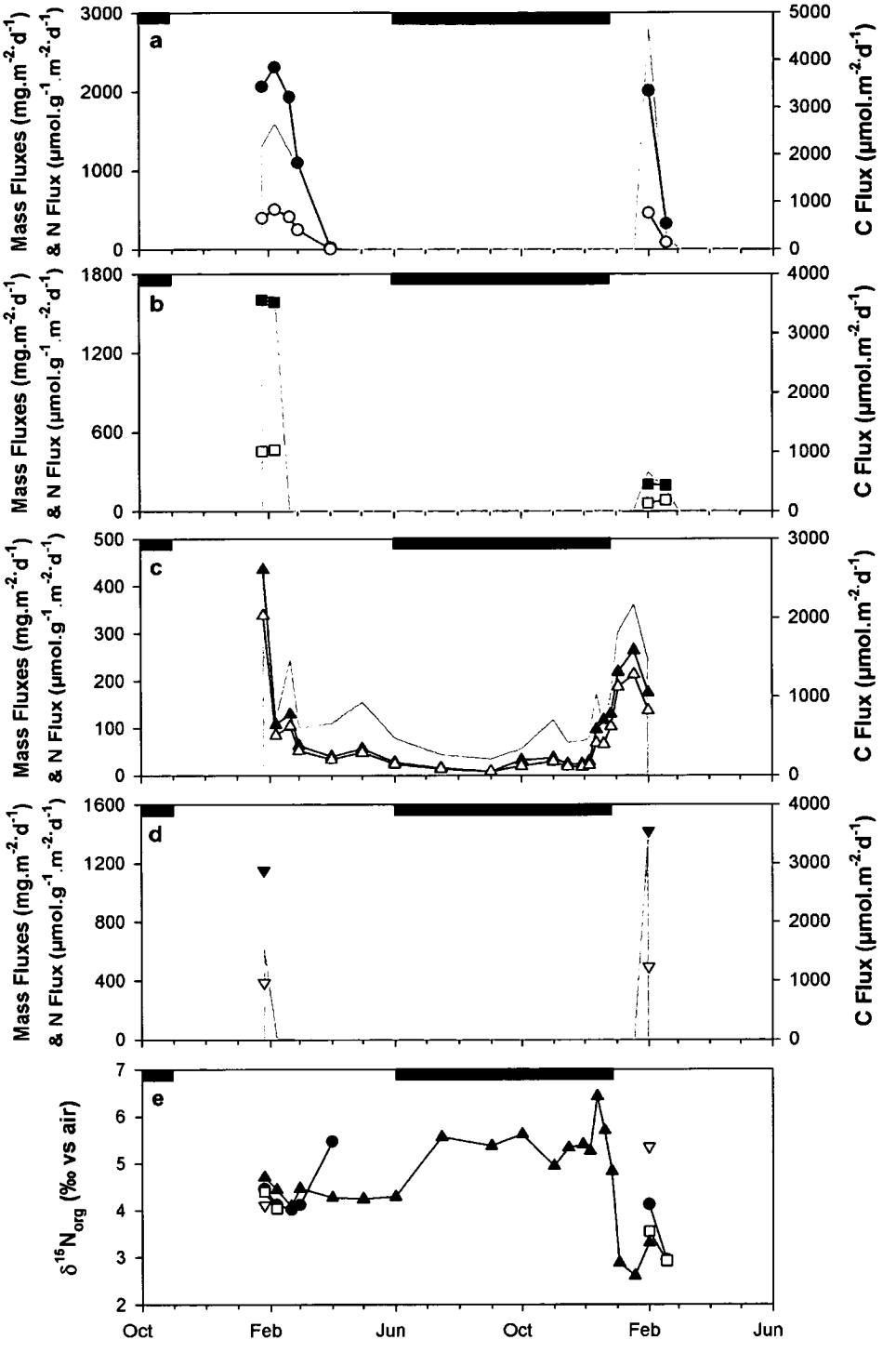


**Figure 5.7. Time-series plots of sediment trap material of mass fluxes (grey shaded area), C flux (closed symbols) and N flux (open symbols) (a) RaTS 200 m trap, (d) RaTS 512 m trap (c) Deep Site 123 m trap (d) Deep Site 745 m trap and (d) the nitrogen stable isotope composition of organic matter ( 15Norg) for the RaTS 200 m trap (closed circles) the RaTS 512 m trap (open circles) the Deep Site 123 m trap (closed triangles) and the Deep Site 745 m trap (open triangles).**

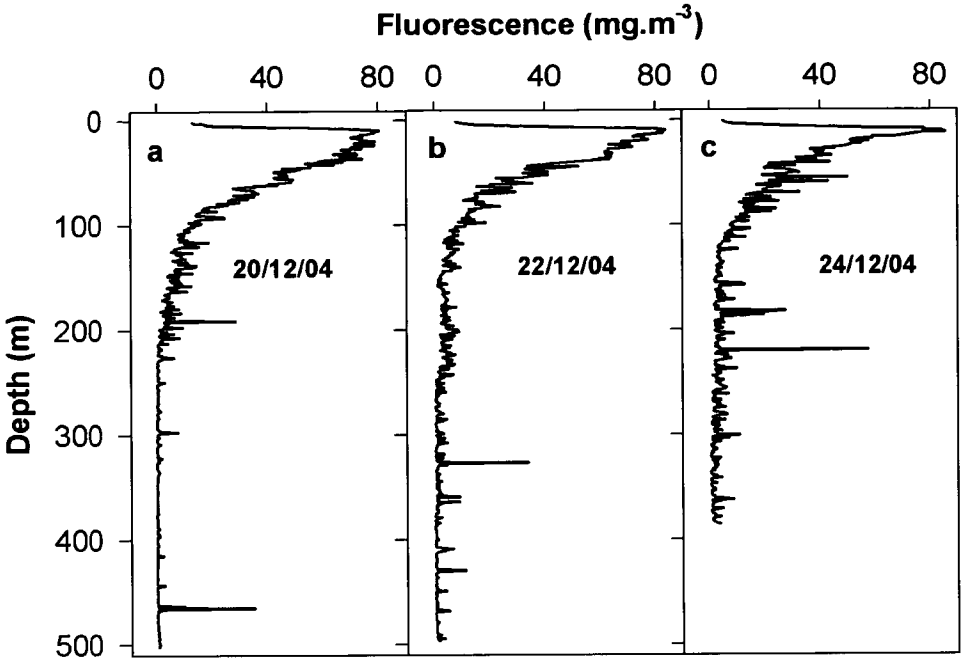


**Figure 5.8. CTD casts of fluorescence for (a) 20/12/04, (b) 22/12/04 and (d) 24/12/04 at the RaTS site.**

In the Deep site 123 m and 745 m traps, there was less of an obvious difference between the two traps from the available data, as there was only partial coverage of the 04/05 season and as the mooring was lost, there is no data for the 05/06 season after mid Feb 06. Without surface water data for this area, it is difficult to constrain the exact levels of productivity, although satellite data (National Ice Centre NOAA) used for this region do show a similar behaviour of sea ice, which exerts control on the timing of the start of the growing season. In the Deep Site 123 m trap during the partial coverage of the 04/05 growing season, mass flux from 26$^{th}$ Jan 05 until 1$^{st}$ April 05 totalled 11.7 g.m$^{-3}$, with POC flux totalling 58 mmol C.m$^{-2}$ and PON flux totalling 8 mmol N.m$^{-2}$. In the Deep Site 745 m trap over the same period, mass fluxes totalled 7.6 g.m$^{-2}$, with POC flux totalling 35 mmol C.m$^{-2}$ and PON flux totalling 5 mmol N.m$^{-2}$. It is worth noting that in the Deep Site 123 m trap, there is continuous coverage of material throughout winter, with POC

and PON flux values consistently low until late December when sea ice begins to decay and recede and the onset of the surface water spring bloom. During the available coverage of the 05/06 growing season, the Deep Site 123 m trap showed significant mass fluxes from 29$^{th}$ Nov 06 to 14$^{th}$ Feb 06, the last time period of available data. During this period, mass fluxes totalled 17 g.m$^{-2}$, with POC fluxes totalling 57 mmol C.m$^{-2}$ and PON fluxes totalling 8 mmol N.m$^{-2}$. In the Deep Site 745 m trap over the same period, mass fluxes totalled 20 g.m$^{-2}$, with POC fluxes totalling 50 mmol C.m$^{-2}$ and PON fluxes totalling 7 mmol N.m$^{-2}$. Average C:N ratios in the two moorings were 6.2 at the RaTS site and 6.9 for the Deep site, which were very close to the Redfield Ratio.

Sediment trap coverage of both seasons also exhibits seasonal patterns of $\delta^{15}N_{org}$. $\delta^{15}N_{org}$ is initially ~ 4.5 ‰ in late Jan 05 and drops to ~ 4.1 ‰ at the start of Apr 05 at the end of the growing season in the 200m RaTS trap. The material trapped at the start of winter 05 (1 Apr – 1 May) then becomes enriched in $^{15}N$ with $\delta^{15}N_{org}$ rising to 5.5 ‰. In the RaTS 512 m trap during this period, stable isotope data is only available until 21$^{st}$ Feb 05 but shows similar characteristics to the 200 m trap with $\delta^{15}N_{org}$ initially 4.4 ‰ in late Jan and early Feb 05 and falling to 4.0 ‰ in Mar 05. During the full coverage of the 05/06 growing season, there were only 2 data points for the RaTS 200 m and RaTS 512 m trap due to the significantly low amount of flux during that growing season. Nonetheless these trap samples display similar features to the latter stages of the 04/05 growing season. In the RaTS 200 m trap $\delta^{15}N_{org}$ is initially 4.1 ‰ in early Feb 06 when the flux first reaches the sediment traps and becomes depleted in $^{15}N$ in late Feb and early Mar 06 where $\delta^{15}N_{org}$ falls to 3.0 ‰. A very similar trend is seen in the RaTS 512 m trap with $\delta^{15}N_{org}$ initially 3.5 ‰ in early Feb 06 and becomes depleted in $^{15}N$ in late Feb and early Mar 06 where $\delta^{15}N_{org}$ falls to 2.9 ‰.

The Deep Site 123 m trap offers more comprehensive coverage of the two growing seasons as there is significant flux throughout winter for elemental

and isotopic analysis, whereas the 745 m trap from the Deep Site mooring offers one data point for each season. During the latter period of the 04/05 season, the 123 m trap shows similar $\delta^{15}N_{org}$ characteristics with $\delta^{15}N_{org}$ initially 4.7 ‰ in late Jan and early Feb 05 and falling to 4.1 ‰ in Mar 05. The small amounts of material trapped between Mar and Jul 05 are consistently ~4.3 ‰ until sea ice cover ensues, when the material under the ice becomes more enriched in $^{15}N$, reaching a maximum value of 6.4 ‰ in late Dec 05 as sea ice begins to decay and recede with the onset of the spring bloom. Then as productivity begins to increase, $\delta^{15}N_{org}$ falls to 2.61 ‰ in late Jan 06 when the initial flux of fresh bloom material reaches the trap. The last data point for this trap, which spans the first half of Feb 06 has a slightly higher $\delta^{15}N_{org}$ value of 3.3 ‰, slightly lower than the same time point for the RaTS traps of 3.5 ‰. The Deep Site 745 m trap exhibits $\delta^{15}N_{org}$ values of 4.1 ‰ from the trap cup covering late Jan and early Feb 05, which is slightly lower than the other three traps and displays the highest value for early Feb 06 of 5.35 ‰, similar to that of material observed in the 123 m trap in late Dec 05.

## 5.4 Discussion

This study presents the first time-series investigation of its kind; in an attempt to assess the major controls on the seasonal nitrogen stable isotope biogeochemistry of the coastal Antarctic sea ice environment. We then assess the reliability of the $\delta^{15}N$ composition of organic matter at the ocean surface, and its subsequent transfer to depth as a tracer for $NO_3$ utilisation. Then link between $NO_3$ drawdown and $CO_2$ drawdown is also assessed to investigate whether increased $\delta^{15}N_{org}$ in sediments can be linked to the lowering of atmospheric $CO_2$ concentrations during glacial cycles as carbon sequestration. Although it is not necessarily suitable to apply the findings here to the open Southern Ocean, where the majority of Antarctic $CO_2$ drawdown may have took place during the onset of glacial periods (Anderson, et al., 2002), they do give insight into the mechanisms that may have occurred and how they affect the $\delta^{15}N$ of organic matter.

### 5.4.1 Sea Ice Nitrogen Isotope Biogeochemistry

The sea ice data presented in this study gives a good indication of the major controls on the composition of organic matter that is eventually released into the water column once sea ice begins to decay and melt. The gradual increase in sea ice $\delta^{15}N_{PON}$ with declining PON at the end of each seasonal cycle of sea ice, coupled with higher C/N ratios (Chapter 4) are consistent with decomposing organic matter within the ice matrix, as $\delta^{15}N$ is known to rise with particle degradation and organic nitrogen is known to decay at a faster rate than carbon (Deniro and Epstein , 1981; Minagawa and Wada, 1984; Saino and Hattori, 1980; 1987). In Figure 5.3, it is clear from the time series profile that the organic matter in sea ice initially has a $\delta^{15}N$ value similar to new production from winter $\delta^{15}N$ values of $NO_3$ (Sigman, et al., 1999), but then grows increasingly enriched in $\delta^{15}N$ with time until the ice disappears. Figure 5.9 presents the concentration of PON plotted against $\delta^{15}N_{PON}$ values for sea ice and surface waters.

It is clear that two very different relationships exist between the two environments, with a weak positive correlation in surface waters, the effect of increased nutrient utilisation and subsequent enrichment of $\delta^{15}N_{PON}$, and a perhaps somewhat surprising negative correlation in sea ice. This negative correlation in sea ice is consistent with the rate of degradation being far greater than that of production of PON. The correlations observed in sea ice are stronger ($R^2$=0.44 during 2004 and $R^2$= 0.47 during 2005) in comparison to the surface waters ($R^2$ = 0.26). This is likely due to the dynamic nature of the surface waters in Ryder Bay, where nutrient inputs, ammonium based production and grazing pressure would have affected the $\delta^{15}N$-$NO_3$ and $\delta^{15}N_{PON}$. There is no evidence of significant nutrient input into the sea ice from underlying water, inferred from the time series data based on $NO_3$ and salinity, which is not surprising considering the closed or semi-closed nature of the sea ice matrix. This leaves high rates of grazing by heterotrophs, bacteria, and possibly foraminifera as the likely source of high degradation

rates and increasing $\delta^{15}N_{PON}$ (Deniro and Epstein, 1981; Minagawa and Wada, 1984; Saino and Hattori, 1980; 1987).

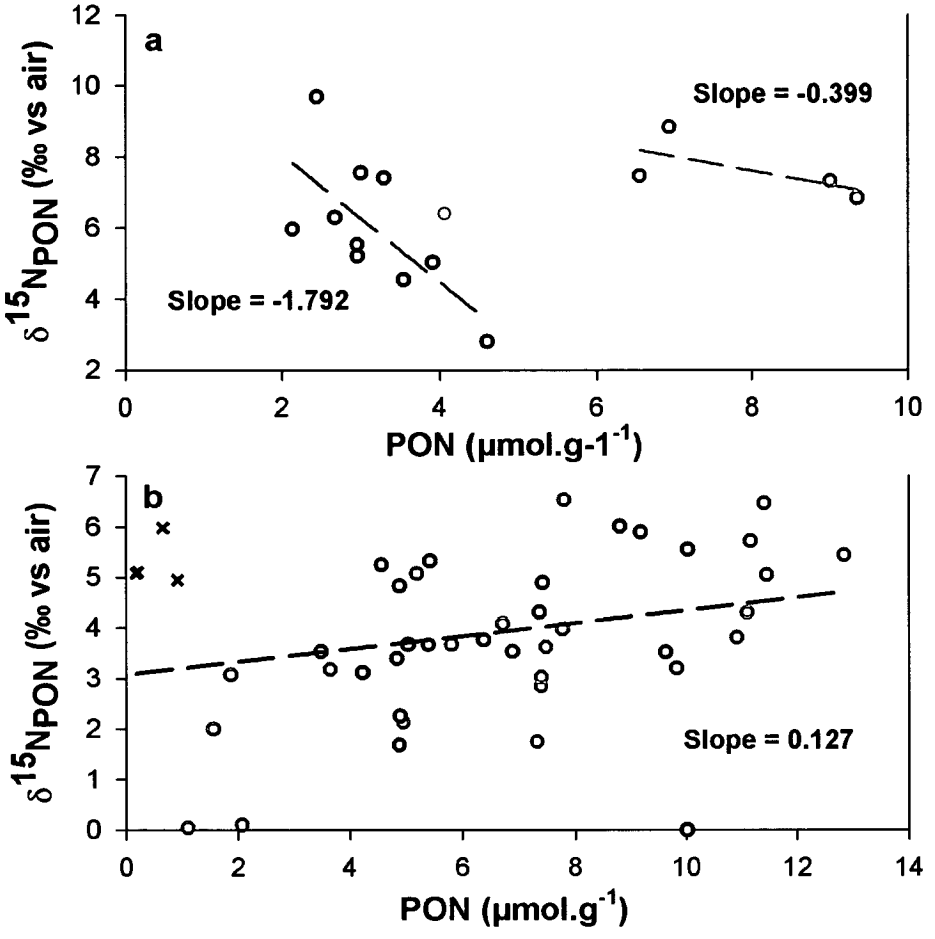


**Figure 5.9. Comparative plots of PON and $\delta^{15}N_{PON}$ for (a) sea ice samples (grey circles for 04/05 season and black circles for 05/06 season) and (b) surface water samples at 15 m (grey circles for 04/05 season and black circles for 05/06 season).**

If high nutrient utilisation was the main cause of increased $\delta^{15}N_{PON}$ in sea ice, we would expect to see similar increases in $\delta^{15}N\text{-}NO_3$. Although $NO_3$ utilisation in sea ice reached up to 95 %, the $\delta^{15}N\text{-}NO_3$ values were not as high as would be expected from intense nutrient utilisation (Sigman, et al., 1999). The lower $\delta^{15}N\text{-}NO_3$ in sea ice may have come from a combination of cell lysis and subsequent nitrogen remineralisation within the ice matrix which would decouple the expected relationship between ln $NO_3$ and $\delta^{15}N\text{-}NO_3$ in

Figure 5.5. The high $O_2$ concentrations in sea ice (generally > 10 mg $O_2$/L) would support the process of nitrification (the oxidation of $NH_4$ to $NO_2$ and then to $NO_3$). High $NH_4$ concentrations were observed in sea ice samples (up to 5 µM) that would provide the necessary substrate for this stepwise oxidation to $NO_3$ and ammonium oxidising bacteria have been observed in sea ice assemblages (Priscu, et al., 1990). In addition, the activity of nitrifying organisms is enhanced if they are attached to surfaces, with sea ice providing surfaces such as ice crystals, polysaccharide gels and other organisms.

High $\delta^{15}N_{PON}$ and high C:N ratios of organic matter in sea ice is therefore attributed to post-production degradation processes occurring in the ice matrix. However, the lack of a similar increase in $\delta^{15}N\text{-}NO_3$ means that the increase in $\delta^{15}N_{PON}$ can not be simply attribute to $NO_3$ utilisation, and must be affected by other processes relating to remineralisation. Therefore the argument that the higher stable isotopic composition of organic matter is produced by higher utilisation of dissolved nutrients in a closed or semi-closed system (Gibson, et al., 1999; Kennedy, et al., 2002), does not appear to be the main factor in this study.

### 5.4.2 Surface Water Nitrogen Isotope Biogeochemistry

The seasonal evolution of surface water $\delta^{15}N_{PON}$ over the two growing seasons highlights the influence that different sea ice regimes can have on the surface water stability and nitrogen stable isotope biogeochemistry in the coastal Southern Ocean. The physical surface water properties (salinity, MLD), nutrient utilisation (u) and the nitrogen stable isotope composition of $NO_3$ and PON are summarised in Table 5.1. The average salinity in the upper 15 m of the water column over the two growing seasons was 0.4 PSU lower during the 04/05 season, indicating there was more freshwater in the system during the heavier sea ice year, which is also consistent with the high frequency observations of brash ice coverage in the bay (Figure 5.2) from daily observations. The effect of this freshwater input into the system is also

seen in the seasonal average mixed layer depths (MLDs). MLD is generally very shallow in Ryder Bay due to a freshwater lens forming in the upper 10 m of the water column, thus stabilising the rest of the water column (Clarke et. al., 2007). The average MLD over the 04/05 season was 11.36 m and over the 05/06 season was 6.15 m. The on average shallower mixed layer depth therefore indicates a more stable surface ocean, with very few incidences of a lowering of the MLD over the growing season due to vertical mixing. Surprisingly, the contrasting conditions in the 04/05 and 05/06 seasons had little impact on the relative and average $NO_3$ utilisation, which were 90 % and 93 % respectively for relative utilisation and 62 % and 69 % respectively for average utilisation.

Figure 5.4 clearly shows the effect frequent inputs of nitrate rich water, seen in the 04/05 season, can have on the $\delta^{15}N_{PON}$ composition of organic matter, with the saw toothed nature of the time-series profile of $\delta^{15}N_{PON}$ and $NO_3$, where the system is tending towards steady state dynamics. In contrast, the 05/06 season $NO_3$ profile reflects a more stable "closed system" effect where $NO_3$ becomes steadily more depleted at the ocean surface over time, with very few incidences of $NO_3$ input. The $\delta^{15}N_{PON}$ profile also displays a more stable seasonal progression, consistent with the closed system model. The early season material underneath sea ice is enriched in $\delta^{15}N$, which in previous studies has been attributed to the effects of biodegradation of particles (Lourey et. al., 2003) and then at the onset of the spring bloom $\delta^{15}N_{PON}$ decreases as utilisation of the fresh UCDW $NO_3$ begins, with the $^{14}N$-$NO_3$ preferentially utilised. There is then progression of $\delta^{15}N_{PON}$ towards higher values over the course of the season, interrupted by negative shifts in $\delta^{15}N_{PON}$ when the low frequency $NO_3$ inputs occur. Although not a fully "closed system" the surface waters were definitely more stable during the 05/06 season, and there are of course other factors affecting $\delta^{15}N_{PON}$ to consider such as grazing, N recycling (Deniro and Epstein, 1981; Minagawa and Wada, 1984; Needoba, et al., 2006 Saino and Hattori, 1980; 1987) and ammonium based production (Altabet, et. al., 1988).

### 5.4.3 Nutrient Sources

Nutrient utilisation and the seasonal evolution of $\delta^{15}N\text{-}NO_3$ and $\delta^{15}N_{PON}$ is relatively easy to predicted based on the assumption of either a fully closed system or a steady state system where nutrient inputs are continuous, if variables such as nutrient utilisation (u) and the fractionation factor ($\varepsilon_p$) are well constrained (Altabet and Francois, 2001; Lourey, et al., 2003; Sigman, et al., 1999b). However, the system in Ryder Bay is more dynamic and thus differs from most of the open Southern Ocean in several ways. Productivity levels and nutrient utilisation are generally much higher in coastal Antarctic regions on the continental shelf (Smith et. al., 1998). There are also episodic injections of nutrients into the surface throughout the growing seasons (Figure 5.4), occurring more frequently during the 04/05 growing season. In order to accurately constrain nitrogen isotope excursions in the surface water, it is essential to know the source of the nutrient rich deeper water that is periodically mixed to the surface.

It is believed that the nutrients of surface waters in Ryder Bay come from Upper Circumpolar Deep Water (UCDW). To test whether these are in fact episodic inputs of UCDW to the surface that mixes nutrient rich water with the partially utilised water already at the surface, a two end-member isotope mass balance model was applied. This model utilises concentrations of $NO_3$ and the $\delta^{15}N\text{-}NO_3$ of the two water masses to model $\delta^{15}N\text{-}NO_3$ of the new water mass after mixing:

$$\delta^{15}N\text{-}NO_{3\,PRED} = f_O(\delta^{15}N\text{-}NO_3^-{}_O) + f_N(\delta^{15}N\text{-}NO_3^-{}_N)$$

Where $f_O$ and $\delta^{15}N\text{-}NO_3^-{}_O$ refer to the fraction of $NO_3$ and the nitrogen stable isotopic composition of $NO_3$ of the partially utilised water mass, and $f_N$ and $\delta^{15}N\text{-}NO_3^-{}_N$ refer to the fraction of $NO_3$ and the nitrogen stable isotopic composition of $NO_3$ of the new UCDW mixing into the surface. The results of this mixing model are presented in Figure 5.10. This model is only applied when there is an increase in $NO_3$ concentration between two measured time

points, and the results are consistent with mixing of UCDW with a $\delta^{15}N\text{-}NO_3$ value of ~ 4.3 ‰ into the surface waters.

The predicted values tend to have lower $\delta^{15}N\text{-}NO_3$ values based on the relationship in Figure 5.10a, which may be due to the fact that the model does not incorporate the possibility that partially $NO_3$ utilised UCDW may be entering the system, and utilisation of $NO_3$ that may have occurred after the mixing but before the discrete measurement.

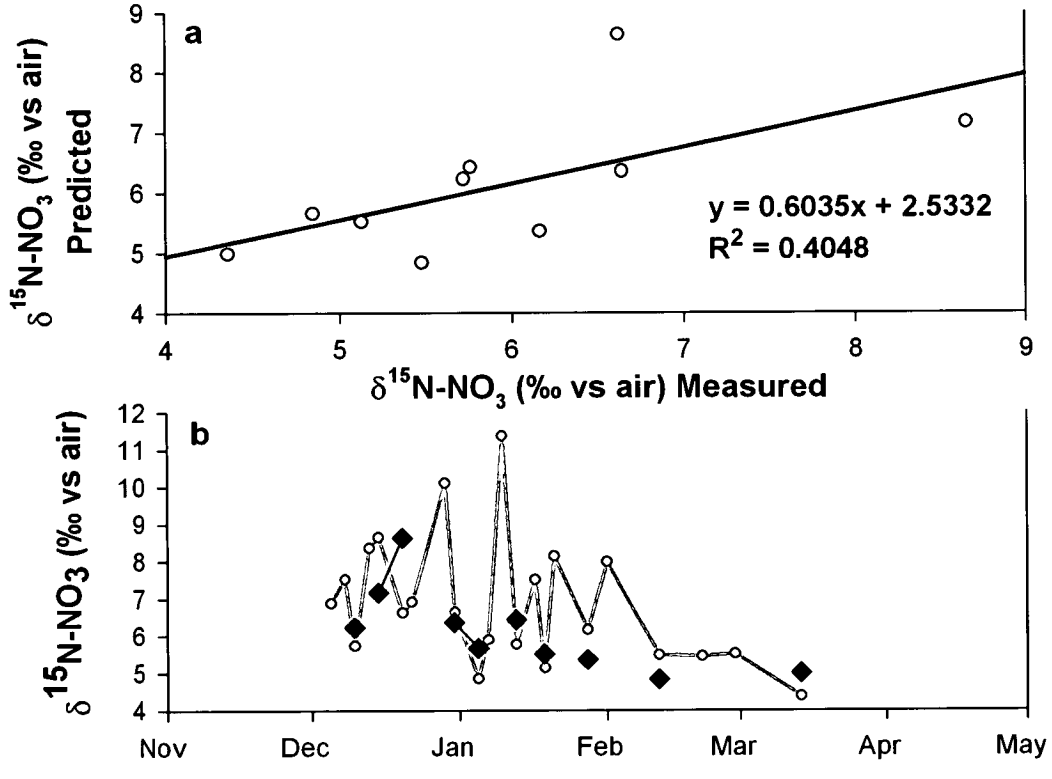


**Figure 5.10. Results from the two end-member isotope mass balance mixing model when NO3 was added to surface waters (a) Measured $\delta^{15}N\text{-}NO_3$ versus predicted $\delta^{15}N\text{-}NO_3$ from the model and (b) Time series profile of measured (grey) versus predicted (black) $\delta^{15}N\text{-}NO_3$.**

### 5.4.4 $NO_3$ Utilisation and $CO_2$ Drawdown

To test the reliability of using $\delta^{15}N_{PON}$ as a tracer for nutrient utilisation in general, Figure 5.11 compares $\delta^{15}N_{PON}$ to $pCO_2$, a common tracer of $CO_2$ utilisation and drawdown. A decrease in $pCO_2$ and an increase in $\delta^{15}N_{PON}$

show nutrient utilisation, and thus the $pCO_2$ profile is plotted in reverse to aid comparison. Figure 5.11a presents a time series profile of $\delta^{15}N_{PON}$ and $pCO_2$, and during the 04/05 season although there are certain periods where similar features are observed between the two parameters, there is generally little agreement between the two profiles, and this is confirmed by the lack of a negative correlation in Figure 5.11b. During the 05/06 season however, the two time series curves show very similar features over the course of the growing season, but again there is no significant correlation observed between the two data sets in Figure 5.11b.

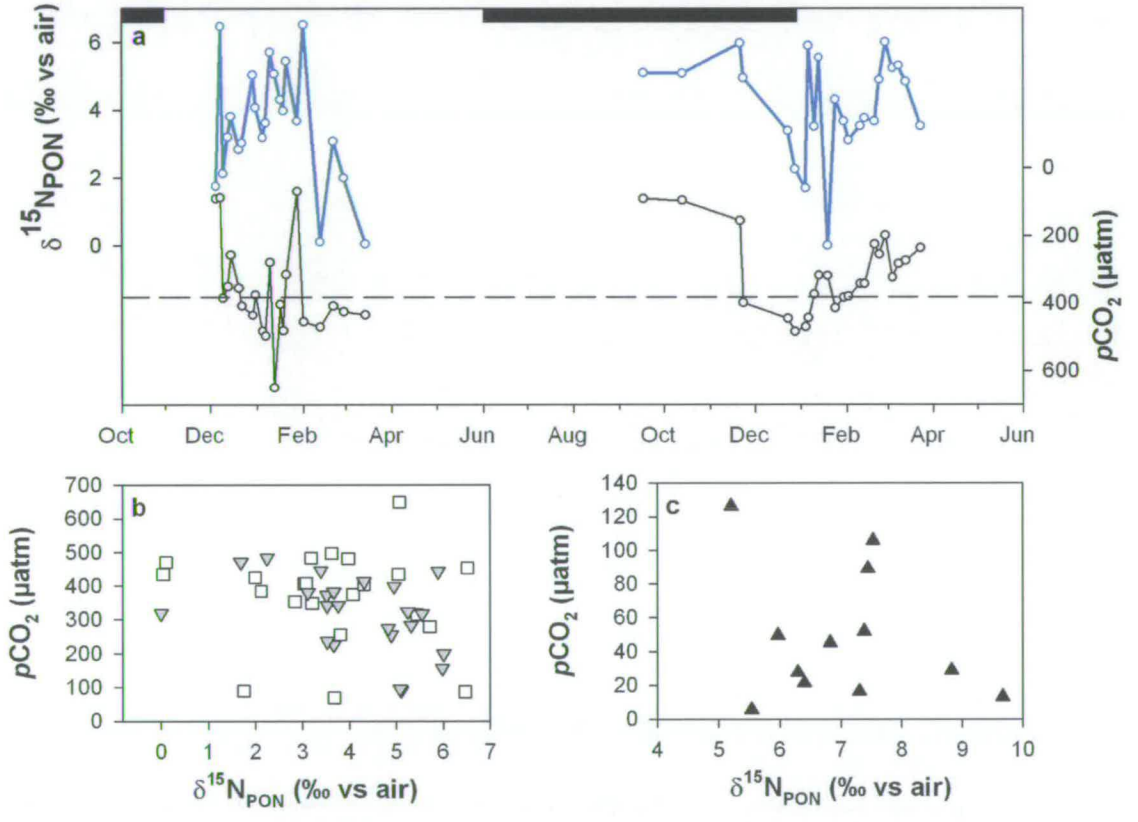


**Figure 5.11. (a) Time-series plot of $\delta^{15}N_{PON}$ and $pCO_2$ in surface waters (b) $\delta^{15}N_{PON}$ versus $pCO_2$ in surface waters during 04/05 season (open circles) and the 05/06 season (closed triangles) and (c) $\delta^{15}N_{PON}$ versus t $pCO_2$ in sea ice**

This decoupling of the two nutrient utilisation proxies is likely due to processes such as air-sea $CO_2$ exchange, where $CO_2$ diffuses from the ocean to atmosphere when surface water $pCO_2$ is high and from atmosphere

to ocean when $pCO_2$ is low. Air-sea exchange of inorganic nitrogen is not considered to have a significant effect on the marine nitrogen cycle. Post-production degradation of PON also decouples the relationship between $\delta^{15}N_{PON}$ and $pCO_2$, where $^{14}N_{PON}$ loss will leave the remaining PON pool enriched in $^{15}N$ through kinetic fractionation, resulting in any assessment of $NO_3$ utilisation from the $\delta^{15}N_{PON}$ composition of organic matter being overestimated. This fundamental decoupling of C and N tracers for utilisation leads to a major uncertainty regarding using $\delta^{15}N$ composition of sediments to infer any processes involving carbon utilisation or export.

### 5.4.5 Sinking Particulate $\delta^{15}N$ and Export Fluxes

The sediment trap time-series profile of $\delta^{15}N_{org}$ shows the same characteristics seen in surface water $\delta^{15}N_{PON}$ (Figures 5.4 and 5.6), albeit the sediment trap changes are lagging surface waters by ~3 weeks. During the latter period of the 04/05 season when sediment trap coverage starts, the surface water $\delta^{15}N_{PON}$ and sediment trap $\delta^{15}N_{PON}$ both vary between 4 and 6 ‰ until productivity and export cease at the end of Feb and March 05 respectively. During Sep until Dec 05, $\delta^{15}N$ values underneath the ice between 5 and 6 ‰ are observed in both surface waters and sediment trap material. These high $\delta^{15}N$ values underneath the ice during winter and early spring are attributed to organic material with a high surface water residence time and are thus composed of heavily degraded PON. $\delta^{15}N_{PON}$ is known to rise with particle degradation (Deniro and Epstein, 1981; Minagawa and Wada, 1984; Saino and Hattori, 1980; 1987), and this effect has been observed in other sediment trap studies in the Southern Ocean (Altabet and Francois, 2001; Lourey et. al., 2003). At the onset of the spring bloom in late Nov 05, the decrease in $\delta^{15}N_{PON}$ to between 2 and 3 ‰ occurs as a result of utilisation of $NO_3$ rich water, and this isotopic shift is also seen in the sediment trap material between mid Dec 05 until early Jan 06 The suspended organic matter then grows enriched in $^{15}N$ once $NO_3$ depletion occurs and this is also seen in the sediment traps until the flux of material ceases at the end of Feb 06. The organic material in the surface waters

during March were not exported to depth, suggesting that this material was retained in the stable surface water and efficiently remineralised, a situation common to this marginal ice zone region (Ducklow et. al., in-press).

Flux weighted average $\delta^{15}N_{org}$ is summarised in Table 5.2, and is consistent with the flux weighted average surface water $\delta^{15}N_{PON}$ value (seasonal flux weighted average values in Table 5.1). These seasonally integrated values from surface waters, sediment traps and surface sediments at the RaTS site are within 0.5 ‰ of one another during the 04/05 season. During the 05/06 season, the seasonally integrated values from surface waters, sediment traps and surface sediments at the RaTS site are within 1 ‰ of one another, excluding the Deep Site 745 m trap of which the material had a $\delta^{15}N_{org}$ value of 5.35 ‰. This trap data consisted of one cup that caught sinking material during January 2005, and considering how deep this trap was situated, the material was likely composed solely of high $\delta^{15}N$ material from underneath the ice.

**Table 5.2. Flux weighted averages of $\delta^{15}N_{org}$ from sediment traps and surface sediment $\delta^{15}N_{org}$ of surface sediments from box cores taken during each season.**

| Season | RaTS 200m Trap $\delta^{15}N_{org}$ (‰ vs air) | RaTS 512m Trap $\delta^{15}N_{org}$ (‰ vs air) | Deep 123m Trap $\delta^{15}N_{org}$ (‰ vs air) | Deep 745m Trap $\delta^{15}N_{org}$ (‰ vs air) | RaTS Surface Sediment $\delta^{15}N_{org}$ (‰ vs air) |
|---|---|---|---|---|---|
| 04/05 | 4.18 | 4.22 | 4.54 | 4.11 | 4.64 |
| 05/06 | 3.89 | 3.18 | 4.11 | 5.35* | 3.88 |

* - Material from one sediment trap cup believed to be composed of material from under sea ice

### 5.4.6 Open versus Closed System $\delta^{15}N$

Figure 5.12 presents the relationship between $\Delta\delta^{15}N$ and the fraction of nitrate removal (u). $\Delta\delta^{15}N$ is the difference between the flux weighted average sinking particulate $\delta^{15}N$ and the initial $\delta^{15}N\text{-}NO_3$ for which 4.8 ‰, a published value for UCDW was used (Sigman et. al., 1999).

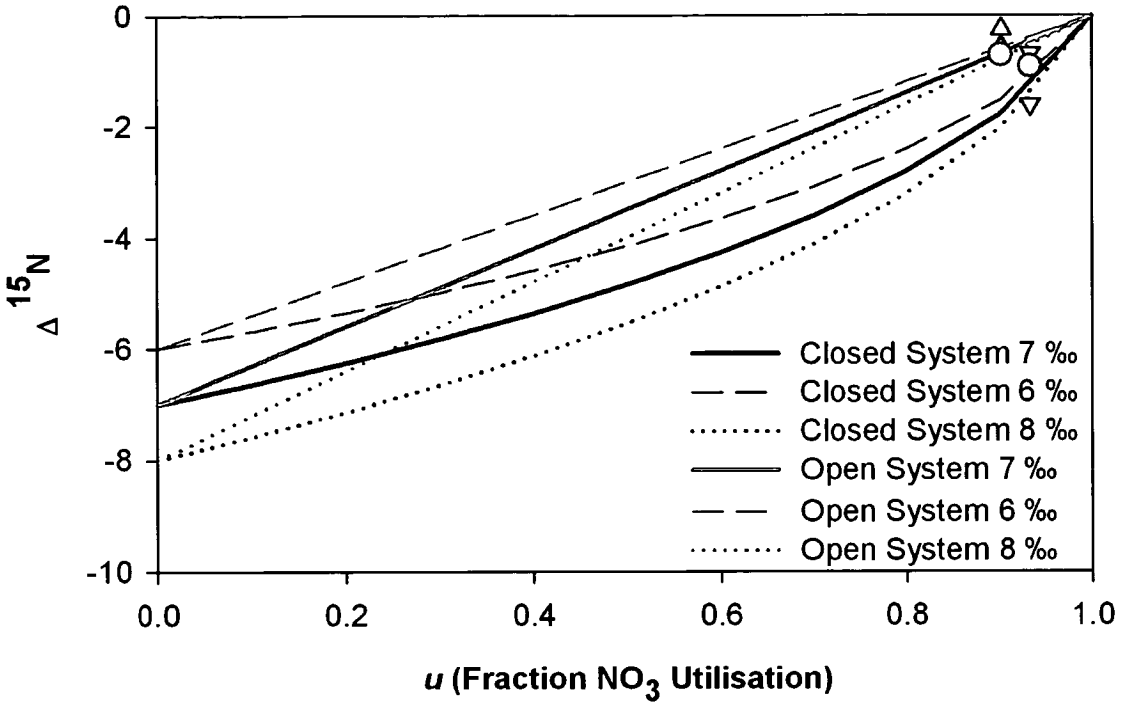


**Figure 5.12. $\Delta\delta^{15}N$ of material collected in time series sediment traps (triangles) and surface sediment $\delta^{15}N$org values from box cores (Circles) from 04/05 season (open symbols) and 05/06 season (closed symbols). Model lines show open system (grey) and closed system (black) nitrate utilisation scenarios, with different fractionation factors published for to the Southern Ocean (6-8 ‰).**

The theoretical relationships for both a closed system and a steady state system of nutrient re-supply for continuous fractionation factors were also modelled (Sigman et. al, 1999b) for previously estimated fractionation factors in the Southern Ocean of 6-8 ‰ (Sigman et al., 1999b; Altabet and Francois, 2001). When comparing the modelled data to the sediment trap and surface sediment data for the RaTS site, the annual sediment data from each season is consistent with the model (i.e. closed system and steady state system) applicable to the hydrographic conditions observed during that season. Data from the 04/05 season, which tended towards the steady state model with high frequency nutrient injections, generally fitted the steady state system model. In contrast, sediment data from the more stratified and stable surface waters of the 05/06 season were consistent with the closed system model (Figure 5.12). Due to the high relative nutrient utilisation observed during

both seasons, it was not possible to make a distinction between the fractionation factors modelled, and it is unclear if these fractionation factors were truly accurate, but the principle of this approach to make the distinction between the two different systems that were operating (closed and steady state) is clear.

These findings show that the fundamental mechanism of the $\delta^{15}N$ proxy for $NO_3$ utilisation works in this environment (i.e. the surface water signal is transferred and preserved in the sediment) with the seasonally integrated values consistent with models of a steady state and closed system for respective seasons. However, it is not appropriate to use the data for inferring changes in carbon drawdown, as the absolute amount of particulate carbon and nitrogen produced for export is controlled by the cumulative amount of available inorganic nutrients over the course of the growing season. This is clearly documented in this study by the fluxes of carbon and nitrogen being significantly higher during the 04/05 season, where the system was approaching the "steady state" model, than the fluxes during the 05/06 season, when the water column was approaching the "closed system" model.

The mechanism controlling these different productivity and export regimes appears to be the extent of sea ice, delivering freshwater to the surface ocean and increasing the stability of the water column. The results from this study therefore weaken the argument that increased $\delta^{15}N$ in glacial Southern Ocean sediments are connected to increased carbon drawdown and lowering of atmospheric $CO_2$ concentrations (Francois and Altabet, 1992; Francois, et al., 1997; Sigman, et al., 1999a), but are consistent with the hypothesis of reduced nutrient delivery to the ocean surface in the glacial Southern Ocean (Francois, et al., 1997; Kumar, et al., 1995).

## 5.5 Conclusions

The following conclusions were drawn from this study:

- Enrichment of $^{15}N$ in sea ice is controlled by post-production decomposition processes rather than the effect of high nutrient utilisation.
- The stability of the surface waters, controlled by sea ice and other sources of freshwater input (e.g. glaciers), plays a significant role in the seasonal evolution of surface water $\delta^{15}N_{PON}$ and total C and N export fluxes.
- The seasonally integrated $\delta^{15}N$ values from sediment traps and surface sediments are consistent with the "steady-state" nitrate utilisation during 04/05 and the "closed system" model during 05/06, reflecting the observed oceanographic characteristics of each season.
- Although the $\delta^{15}N$ value in sediment is consistent with the surface water $\delta^{15}N$ from the models, the proxy for utilisation of nitrate does not reflect the absolute changes in C export fluxes. It is therefore necessary to consider this scenario when making connections between nitrate utilisation and changes in atmospheric $CO_2$.

## 5.6 References

Altabet, M. A. (1988) Variations in nitrogen isotopic composition between sinking and suspended particles: Implications for nitrogen cycling and particle transformations in the open ocean. *Deep Sea Research Part I*, 35, 535-554.

Altabet, M. A., and R. Francois (2001), Nitrogen isotope biogeochemistry of the antarctic polar frontal zone at 170 degrees W, *Deep-Sea Research Part Ii-Topical Studies in Oceanography*, *48*, 4247-4273.

Assayag, N., et al. (2006), Improved method for isotopic and quantitative analysis of dissolved inorganic carbon in natural water samples, *Rapid Communications in Mass Spectrometry*, *20*, 2243-2251.

Brandon, M. (2005), JR112/113 Cruise Report, 12pp.

Carson, D. S., Annet, A, L., Ganeshram, R. S., Crosta, X., Fallick, A. E. and Clarke, A. (in-prep) Factors influencing $\delta^{13}C$ of nutrients and organic matter

in the coastal Antarctic Sea Ice Environment. For submission to *Deep Sea Research Part II: Oceanographic Research Papers.*

Casciotti, K. L., et al. (2002), Measurement of the oxygen isotopic composition of nitrate in seawater and freshwater using the denitrifier method, *Analytical Chemistry, 74*, 4905-4912.

Clarke, A., et al. (2007), Seasonal and interannual variability in temperature, chlorophyll and macronutrients in northern Marguerite Bay, Antarctica, *Deep Sea Research Part II: Oceanographic Research Papers, in press.*

Crosta, X., et al. (2005), Major factors controlling Holocene $\delta^{13}$Corg changes in a seasonal sea-ice environment, Adelie Land, East Antarctica, *Global Biogeochemical Cycles, 19*, doi:10.1029/2004GB002426.

Crosta, X., and A. Shemesh (2002), Reconciling down core anticorrelation of diatom carbon and nitrogen isotopic ratios from the Southern Ocean, *Paleoceanography, 17.*

Deniro, M. J., and S. Epstein (1981), Influence of Diet on the Distribution of Nitrogen Isotopes in Animals, *Geochimica Et Cosmochimica Acta, 45*, 341-351.

Dickson, A. G., and F. J. Millero (1987) A comparison of the equilibrium constants for the dissociation of carbonic acid in seawater media, *Deep Sea Research Part I: Oceanographic Research Papers, 34*, 1733-1743.

Difiore, P. J., Sigman, D. M., Trull, T. W., Lourey, M. J., Karsh, K., Cane, G. and Ho, R (2006) Nitrogen isotope constraints on subantarctic biogeochemistry. *Journal of Geophysical Research*, 111, C08016, doi:10.1029/2005JC003216.

Ducklow, H. W., Erickson, M., Kelly, J., Smith, R. C., Stammerjohn, S. E., Vernet, M. and Karl, D. M. (2007) Particle export from the upper ocean over the continental shelf of the West Antarctic Peninsula: A long-term record, 1992-2006. *Deep Sea Research Part II: Oceanographic Research Papers, in press.*

Francois, R., and M. A. Altabet (1992), Glacial to interglacial changes in surface nitrate utilisation in the Indian sector of the Southern Ocean as recorded by sediment d15N, *Paleoceanography, 7*, 589-606.

Francois, R., et al. (1997), Contribution of Southern Ocean surface-water stratification to low atmospheric CO2 concentrations during the last glacial period, *Nature*, *389*, 929-935.

Garrity, C., Ramseier, R. O., Peinert, R., Kern, S. and Fischer, G. (2005) Water column particulate organic carbon modeled fluxes in the ice-frequented Southern Ocean. *Journal of Marine Systems*, 56, 133-149.

Gibson, J. A. E., et al. (1999), Sedimentation of C-13-rich organic matter from Antarctic sea-ice algae: A potential indicator of past sea-ice extent, *Geology*, *27*, 331-334.

Gleitz, M., et al. (1995), Comparison of Summer and Winter Inorganic Carbon, Oxygen and Nutrient Concentrations in Antarctic Sea-Ice Brine, *Marine Chemistry*, *51*, 81-91.

Hannson, I. (1973), A new set of activity constants for carbonic acid and boric acid in seawater, *deep Sea Research*, *20*, 461-478.

Holmes, R. M., et al. (1999), A simple and precise method for measuring ammonium in marine and freshwater ecosystems, *Canadian Journal of Fisheries and Aquaculture Sciences*, *56*, 1801-1808.

Karsh, K. L., Trull, T. W., Lourey, M. J. and Sigman, D. M. (2003) Relationship of nitrogen isotope fractionation to phytoplankton size and iron availability during the Southern Ocean Iron RElease Experiment (SOIREE), *Limnology and Oceanography*, 48(3), 1058-1068.

Kennedy, H., et al. (2002), Particulate organic matter in Antarctic summer sea ice: concentration and stable isotopic composition, *Marine Ecology-Progress Series*, *238*, 1-13.

Kumar, N., et al. (1995), Increased Biological Productivity and Export Production in the Glacial Southern-Ocean, *Nature*, *378*, 675-680.

Lewis, E., and D. W. R. Wallace (1998), Program developed for CO2 system calculations. ORNL/CDIAC-105. Carbon dioxide information analysis center, Oak Ridge National Laboratory, U.S. Department of Energy, Oak Ridge, Tenesee.

Lourey, M. J., et al. (2003), Sensitivity of delta N-15 of nitrate, surface suspended and deep sinking particulate nitrogen to seasonal nitrate depletion in the Southern Ocean, *Global Biogeochemical Cycles*, *17*.

Mehrbach, C., et al. (1973), Measurement of the apparent dissociation constant of carbonic acid in seawater at atmospheric pressure, *Limnology and Oceanography*, *18*, 897-907.

Minagawa, M., and E. Wada (1984), Stepwise Enrichment of N-15 Along Food-Chains - Further Evidence and the Relation between Delta-N-15 and Animal Age, *Geochimica Et Cosmochimica Acta*, *48*, 1135-1140.

National Ice Centre - National Oceanic and Atmosphere Administration (NOAA). Sattelite Data from Bellingshausen-Asmundsen Sea region satellite data for sea ice cover, 2004-2006. Available http://www.natice.noaa.gov

Needoba, J. A., Marchetti, A., Henry, M. F., Harrison, P. J., Wong, C., Johnson, K. W. and Pedersen, T. F. (2006) Stable nitrogen isotope dynamics of a mesoscale iron enrichment experiment in the NE Subarctic Pacific. *Deep Sea Research II*, 53, 2214-2230.

Priscu, J. C., et al. (1990), Dynamics of Ammonium Oxidizer Activity and Nitrous-Oxide (N2o) within and beneath Antarctic Sea Ice, *Marine Ecology-Progress Series*, *62*, 37-46.

Saino, T., and A. Hattori (1980), N-15 Natural Abundance in Oceanic Suspended Particulate Matter, *Nature*, *283*, 752-754.

Saino, T., and A. Hattori (1987), Geographical Variation of the Water Column Distribution of Suspended Particulate Organic Nitrogen and Its N-15 Natural Abundance in the Pacific and Its Marginal Seas, *Deep-Sea Research Part a-Oceanographic Research Papers*, *34*, 807-827.

Sigman, D. M., et al. (1999a), The isotopic composition of diatom-bound nitrogen in Southern Ocean sediments, *Paleoceanography*, *14*, 118-134.

Sigman, D. M., et al. (1999b), The delta N-15 of nitrate in the Southern Ocean: Consumption of nitrate in surface waters, *Global Biogeochemical Cycles*, *13*, 1149-1166.

Sigman, D. M., et al. (2001), A bacterial method for the nitrogen isotopic analysis of nitrate in seawater and freshwater, *Analytical Chemistry*, *73*, 4145-4153.

Smith, R. C., Baker, K. S. and Vernet, M. (1998) Seasonal and interannual variability of phytoplankton biomass west of the Antarctic Peninsule. *Journal of Marine Systems*, 17, 229-243.

Strickland, J. D. H., and T. R. Parsons (1972), A Practical Handbook of Seawater Analysis, pp. 311. Fisheries Research Board of Canada.

# 6 Particulate Barium Transformations and Fluxes in the Continental Shelf Antarctic Sea Ice Environment


## Abstract

The relationship between excess barium and organic carbon flux to the seafloor has made the use of marine sedimentary excess barite a popular tracer for paleoproductivity in recent decades. There are still, however, large gaps in the understanding of seasonal controls on particulate barium and barite formation in surface waters and at mesopelagic depths. This study presents high-resolution time-series measurements of barium in sea ice, surface waters, sediment traps and surface sediments, to highlight the processes that govern the seasonal flux of excess particulate barium and carbon to the seafloor. High concentrations of excess particulate barium are seen in sea ice, brought on by the continuous recycling of organic matter in the sea ice matrix, which is then released into the water column during sea ice decay and melting. There is then a clear seasonal cycle in the surface water production of particulate barium, with the excess barium pool dominated by "labile" particulate barium during new production. It is during the decay of organic matter during mid-season lags in primary productivity and at the end of the season when production declines that the particulate barium pool becomes dominated by barite. Although this material is a relatively small proportion of the total flux of particulate barium, it does give insight to the processes that eventually lead to the high Ba:C ratio of sinking material, produced as a result of organic carbon degradation and barite supersaturation at mesopelagic depths. The overall flux of excess particulate barium and carbon in sediment traps in this study is consistent with preliminary algorithms produced in previous studies, but we are able to produce a detailed conceptual model of the seasonal progression of particulate barium formation and transformations in the Antarctic sea ice environment.

## 6.1 Introduction

Barite formation in the marine water column and its flux to the seafloor appear linked to surface productivity and carbon export (Bishop, 1988; Dehairs *et al.*, 1992; Dehairs *et al.*, 2000; McManus *et al.*, 1998). Thus the reconstruction of carbon export based on barium content of sediments may provide quantitative information about past changes in primary production (Francois *et al.*, 1997; Ganeshram and Pedersen, 1998; Ganeshram *et al.*, 1995). A host of previous studies utilising sediment traps monitoring fluxes of carbon and barium have produced preliminary algorithms linking the flux of biogenic barium to carbon export production (Dymond *et al.*, 1992; Francois *et al.*, 1995; McManus *et al.*, 2002; Nurnberg *et al.*, 1997). Seasonal and geographic variations in the relationship between carbon and barium fluxes have identified that additional factors influence the flux of barium per unit carbon. Therefore identifying and quantifying these factors is essential to develop a truly reliable paleoproductivity proxy. Studies of the global ocean based on water column profiles of dissolve barium have shown that barium is recycled like nutrients, with lower concentrations at the surface and enrichment at depth. This distribution results from the bio-intermediate nature of barium, with formation of particulate barium at the surface with dissolution at depth, but the exact mechanism of this process is still debated (Bernstein and Byrne, 2004; Bertram and Cowen, 1997; Ganeshram *et al.*, 2003). There is evidence supporting the idea that biogenic microenvironments in sinking detritus provide favourable conditions for barite precipitation through supersaturation resulting from barium and sulphur release from decaying organic matter (Ganeshram *et al.*, 2003; Monnin *et al.*, 1999) and that processes such as trophic processing, faecal pellet packaging and particle aggregation may significantly enhance barite formation. Studies have shown that the relationships between barium and carbon fluxes vary in different oceanic regions (Francois *et al.*, 1995), especially between continental shelf seas, continental margin environments and the open oceans (Dehairs *et al.*, 2000; Francois *et al.*, 1995; McManus *et al.*, 2002). In the polar oceans, little attention has been paid to document the effects of seasonal sea ice cover on

the relationship between barium and carbon fluxes In these environments, ice cover can extend over large portions of the year and controls the timing of the growing season (Eicken, 1992), often resulting in short, episodic spring blooms in association with the melting sea ice. It is unclear how spring blooms and flux of material occurring in episodic 'pulses' may affect the yield of barite per unit carbon in sinking organic matter, but it has been suggested that it may reduce barite fluxes as the organic matter export in these environments occurs too rapidly to allow barite precipitation to attain completion (McManus *et al.*, 2002).

There are no published studies investigating the behaviour of barium in Antarctic sea ice to date, which is surprising considering the influence sea ice has over productivity and particle flux (Arrigo *et al.*, 1997; Garrity *et al.*, 2005; Kim *et al.*, 2005) and the use of barium as a paleoproductivity proxy in the Southern Ocean. Productivity within the sea ice matrix has the potential to produce a Ba:Corg relationship very different to that seen in surface waters. Primary production in sea ice often occurs in a closed or a semi-closed system within brine pockets and brine channels. This closed system effect can retain and degrade large quantities of organic matter produced within the ice matrix, a lot of which may be recycled for further production. Thus the relatively small brine channels and gap layers in sea ice are excellent candidates for barite formation, where barium and sulphur may reach levels high enough for barite precipitation during decay of organic matter. It is therefore essential to understand the biogeochemical cycling of barium in sea ice and monitor the release of barium from decaying and melting sea ice, bearing in mind that sea ice particle can account for a significant proportion of mass flux in the Southern Ocean (Arrigo *et al.,* 1997).

Ganeshram, et al., (2003) developed a useful sequential leaching method for monitoring the behaviour of barium in decaying phytodetritus. This method uses sequential extractions of dilute $HNO_3$ for labile particulate barium, 30 % HCl for barite and hot conc. $HNO_3$ for particulate barium associated with

refractory organic matter. This method was applied to monitor barite growth and behaviour relative to other Ba phases in laboratory phytoplankton decay experiments. The results from the experiments revealed the presence of large pool of labile Ba in the fresh phytoplankton, which during decay was readily released and a proportion converted to barite (see Figure 6.1).

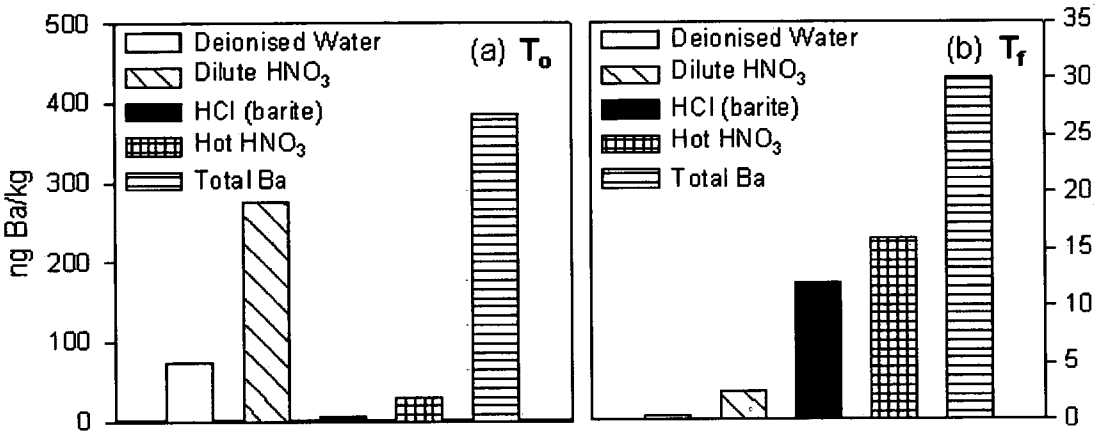


**Figure 6.1. Sequential leaching data showing particulate Ba transformations during decay of phytodetritus, courtesy of Ganeshram et al., (2003). Panels show Ba phases in freshly collected coastal phytoplanktom bloom (a) and after 8 weeks of decay in the dark (b). Note that most Ba resides in the labile fraction (Deionised water + Dilute $HNO_3$ extraction) in the bloom material but mainly in the barite (HCl) and refractory fraction (Hot $HNO_3$) after decay indicating the loss of labile Ba and the production of barite during the decay process.**

This method can easily be transferred to time-series analysis of suspended particulate samples from sea ice and the surface ocean, to monitor the behaviour of barite and other particulate Ba phases over seasonal timescales. This chapter presents a high-resolution study of sea ice and surface water productivity and barium transformations, coupled with time series sediment trap and box cores to monitor the flux and sedimentation of carbon and barium. This study shows that sea ice particulate Ba concentrations are much higher than surface waters and have a higher $Ba_{XS}$:$C_{org}$ ratio. In surface waters, there is a seasonal transition of the particulate barium pool, initially dominated by labile Ba to one dominated by barite as productivity declines and degradation of organic material ensues. Sediment trap data for this region show that the flux of Ba and C are

consistent with previous algorithms produced for the open ocean (Francois *et al.*, 1995; Nurnberg *et al.*, 1997).

## 6.2 Materials and Methods

Field work was conducted from November 2004 until March 2006 based at Rothera Research Station. During the field seasons, samples of sea ice brine were taken around Ryder Bay when sea ice was present and high resolution time series surface water samples were taken in Ryder Bay at the RaTS site (67°34.02'S, 68°14.02'W) during the spring and summer months, (see Figure 6.2) Low resolution sampling occurred during winter 2005.

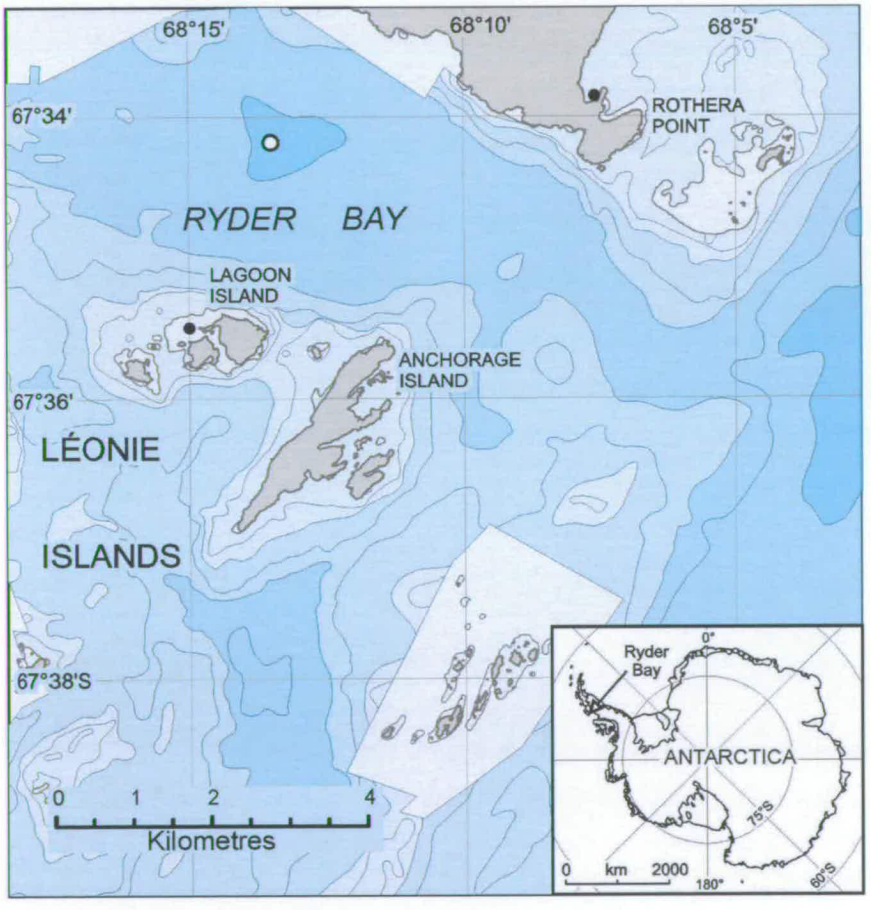


**Figure 6.2. Location of the RaTS site (white circle) of water sampling and the other sites used for sea ice sampling during this study (black circles).**

Mooring arrays containing time-series sediment traps were deployed at the RaTS site and at a nearby deeper site in Marguerite Bay (67°55.39'S, 68° 24.15'W).. Table 6.1 presents mooring site locations and sampling durations for the traps.

**Table 6.1. Details of each sediment trap including, deployment duration, location, water depth and total mass flux.**

| Sediment Trap | Days | Lat. (°S) | Long. (°W) | Water Depth (m) | Start Date | End Date | Total Flux ($mg.m^2.d^{-1}$) |
|---|---|---|---|---|---|---|---|
| RaTS A | 385 | 67.3 | 68.1 | 200 | 26/01/05 | 14/02/06 | 309.307 |
| RaTS B | 385 | 67.3 | 68.1 | 512 | 26/01/05 | 14/02/06 | 121.471 |
| Deep A | 385 | 67.5 | 68.2 | 123 | 26/01/05 | 14/02/06 | 123.992 |
| Deep B | 385 | 67.5 | 68.2 | 745 | 26/01/05 | 14/02/06 | 71.366 |

### 6.2.1 Dissolved Ba Determination

Dissolved barium ($Ba_{dissolved}$) samples were taken from sea ice brine and surface waters at 15m. From sack holes in the sea ice, brine was drawn into an acid clean syringe and transferred to a clean 60 ml HDPE bottle preloaded with 125µL of *Romil ultra-pure* HCl. Samples were stored at +4°C in the dark until analysis. To prepare for analysis, 10 ml of sample was pipetted into a clean 15 ml Savillex© vessel and dried down on a hotplate at 90°C. When dry, ~ 5ml of *Romil ultra-pure* HF and ~0.5ml of Romil ultra-pure 50% (v/v) $HNO_3$ were added to each vessel, the lids were closed and vessels left on a hotplate at 100°C overnight. The lids were then removed and the solutions dried on a hotplate at 90°C. Once dry, ~3ml of *Romil ultra-pure* 50% (v/v) $HNO_3$ was added to each Savillex © vessel, the lids were closed and left on a hotplate at 100°C for 3 hours. The lids were again removed and the solutions were dried on a hotplate at 90°C. Once dry, ~3ml of *Romil ultra-pure* 30% (v/v) HCl was added to each Savillex© vessel, the lids were closed and vessels left on a hotplate at 100°C for 3 hours. The lids were removed and the solution was dried on a hotplate at 90°C. Once dry, the dry sample was resuspended in 10 ml of *Romil ultra-pure* 5% (v/v) $HNO_3$ for analysis.

### 6.2.2 Particulate Barium and Aluminium

Samples for particulate barium and aluminium were taken from sea ice brine and surface waters at 15m. From sack holes in the sea ice, brine was transferred to clean 15 L polypropelene carboys using a clean HDPE 1 L beaker. The samples were transported back to the lab and between 10 and 15 L were filtered through a 142 mm polycarbonate filter with a pore size of 0.45 µM. Surface water samples were pumped from 15 m using a 12 v dolphin pump and 15 m of silicone tubing weighted at the end. The samples were transported back to the lab and between 10 and 15 L were filtered through a 142 mm polycarbonate filter with a pore size of 0.45 µM. After filtration, the filters were folded into quarters and dried in plastic Petri-dishes at 50°C overnight and stored frozen in plastic zip locked bags.

### 6.2.3 Sequential Leaching of Barium

Sequential leaching experiments on 142 mm polycarbonate filters were conducted using a method modified from *Ganeshram, et al.*, (2003). Dry filters were weighed and placed in 60 ml Savillex© vessels. The filters (and filter blanks) were subjected to the following sequential leaching steps and the extracted Ba termed as below in the text:

1. Water: Deionised water was first used to rinse any Ba associated with residual seawater. This step also extracts weakly sorbed Ba and Ba in the cytoplasm released during cell lysis. This step was conducted immediately after sample filtration to remove salts but was not analysed.
2. Dilute nitric acid extraction: 10 % (v/v) *Romil ultra-pure* $HNO_3$ was added to Savillex© vessels and they were kept at room temperature for 5 min to remove readily exchangeable and easily hydrolysable organic-bound Ba. This called the 'labile Ba' fraction
3. Hot hydrochloric acid extraction: 30 % (v/v) *Romil ultra-pure* HCl was added to Savillex© vessels which were kept at 80°C overnight to dissolve barite. This is called the 'barite Ba' fraction

4. Hot nitric acid extraction: 50 % (v/v) *Romil ultra-pure* $HNO_3$ was added to Savillex© vessels which were kept at 80°C overnight to oxidise refractory organic matter and release the associated Ba. This is called the 'refractory Ba' fraction

After each treatment step, the leachate was centrifuged and transferred to a drying vessel (60ml Savillex© vessel) and the extraction vessel was rinsed with *Romil ultra-pure* 5% (v/v) $HNO_3$ with the rinse also transferred to the drying vessel. The leachate was dried at 90°C concurrent with the following leaching strep. Once dry, the leachates were resuspended in 10ml of *Romil ultra-pure* 5% (v/v) $HNO_3$ for analysis.

### 6.2.4 HF Digestion of Material

In order to dissolve all the remaining material in the sample of crustal origin, the samples underwent digestion by HF after the leaching procedure. Immediately after step 4 of the leaching procedure, ~10 ml of *Romil ultra-pure* HF and ~1 ml of *Romil ultra-pure* 50 % (v/v) $HNO_3$ were added to each extraction vessel. The lids were closed and vessels left on a hotplate at 100°C overnight. The lids were then removed and the solutions dried on a hotplate at 90°C. Once dry, ~10ml of *Romil ultra-pure* 50% (v/v) $HNO_3$ was added to each Savillex© vessel, the lids were closed and left on a hotplate at 100°C for 3 hours. The lids were again removed and the solutions were dried on a hotplate at 90°C. Once dry, ~10ml of *Romil ultra-pure* 30% (v/v) HCl was added to each Savillex© vessel, the lids were closed and vessels left on a hotplate at 100°C for 3 hours. The lids were removed and the solution was dried on a hotplate at 90°C. Once dry, the dry sample was resuspended in 10 ml of *Romil ultra-pure* 5% (v/v) $HNO_3$ for analysis. Aliquots of the international standard BC03-1 were routinely digested alongside unknown samples to monitor the efficiency of the digestion procedure, which was better than 95 %.

### 6.2.5 Sediment Trap Material and Surface Sediments

Sediments were dried using a freeze-drier and then ground to a fine powder using a mortar and pestle. Aliquots of dry, ground sediment were weighed

into clean 15 ml Savillex © vessels and underwent the HF digestion protocol described in section 2.4, to completely digest all sedimentary material for analysis.

### 6.2.6 Analysis of Barium and Aluminium

For $Ba_{dissolved}$ samples, the resuspended solutions (5% $HNO_3$) were analysed by inductively coupled plasma mass spectrometry (ICP-MS) at the Scottish Universities Envrionmental Research Centre (SUERC) using a Plasma Quad 2+ ICP-MS. The instrument was calibrated with standard solutions and indium was used as an internal standard added at a rate of 10 ppb. Certified lake water SLRS-4 (CNRC-Canada) was routinely run with seawater samples to cross check the accuracy of the measurements. $Ba_{dissolved}$ samples were diluted by a factor of 20 in Romil ultra-pure 5% (v/v) $HNO_3$ for analysis. The analytical precision for the measurements was generally better than ± 5 %. The resuspended solutions (5% $HNO_3$) from leaching and HF digestions of suspended particles and sediments were analysed by inductively coupled plasma optical emission spectroscopy (ICP-OES) in The School of Geosciences, The University of Edinburgh using a Vista Pro ICP-OES. The instrument was calibrated with standard solutions and indium was used as an internal standard at a rate of 1 ppm. Certified lake water SLRS-4 (CNRC-Canada) was routinely run with seawater samples to cross check the accuracy of the measurements. Leachates were diluted appropriately in *Romil ultra-pure* 5% (v/v) $HNO_3$ for analysis. The analytical precision for the measurements was generally better than ± 2 %.

### 6.2.7 $Ba_{XS}$ Determination

The following formula was used to determine the concentrations of $Ba_{XS}$ in suspended particles and sediments. This fraction is defined as Ba in excess of crustal abundance and expected to consist of organic and barite bound Ba

$$Ba_{XS} = Ba_{Total} - (Ba{:}Al_{Terrigenous} \times Al_{Total})$$

There $Ba_{Total}$ is the total concentration of Ba in the sample, Ba:Al is the crustal ratio of Ba:Al in the region and $Al_{Total}$ is the total concentration of Al in the sample.

### 6.2.8 Suspended Particulate Organic Carbon

Bulk suspended particulate organic carbon (POC) was measured using a method similar to Lourey et al., (2004). Surface water samples were collected using a dolphin pump and silicone tubing from 15 m, water was pumped into acid cleaned HDPE carboys. All water samples were stored in the dark until reaching the lab where they were then processed (<2 h after sampling). Measured volumes of water were filtered through a 47 mm GF/F filter (Whatman 1825 047) using a positive pressure filtration rig custom built by The University of Edinburgh, the system was acid cleaned with HCl prior to each sampling event and was rinsed thoroughly with distilled water between filtrations in any one event. Filters containing particulate material were then dried overnight at 50°C in a clean oven. Once dry, filters were folded in half and stored in aluminium foil at -20°C until analysis. Duplicate filtrations were taken for each sample. To prepare for elemental analysis, filters were removed from the freezer, re-wet with a few drops of Milli-Q water and placed in a dessicator containing an open beaker of HCl for ~48 h to dissolve any carbonates present. The filters were then dried at 50°C for 4 h and cut in half, before excess GF/F filter was removed and the remaining halves of filter material were packed into tin cups for analysis.

POC was analysed using a Carlo Erba NA 2500 elemental analyser using acetanilide as a reference material. Analytical precision for these measurements was consistently better than ± 2 %. Analyses were conducted at the School of Geosciences, The University of Edinburgh.

## 6.3 Results

### 6.3.1 Crustal Ba:Al Determination

As many of the sediment trap and box core Ba:Al ratios were below the generally quoted global average crustal ratio of 0.0075, it is clear that this value is not appropriate for this region of the Western Antarctic Peninsula. Reitz *et al.* (2004) conducted a study of sediment samples from various sites around the global ocean and found many crustal values reported in the past were not necessarily accurate and quoted a global average Ba/Al of 0.0037. A Southern Ocean crustal Ba:Al ratio of 0.0067 was reported for the Weddell Sea (Nurnberg *et al.*, 1997), but again this was significantly above many of the bulk Ba:Al ratios of sediments analysed in this study.

In order to estimate the maximum possible crustal Ba:Al ratio in the Ryder Bay and Marguerite Bay area, Ba was plotted against Al for all samples and linear regression was used to best fit the lowest Ba:Al ratios observed in all sediment samples, this is presented in Figure 6.3. A maximum crustal Ba:Al ratio of 0.0042 was estimated and used to calculate $Ba_{XS}$ throughout this study.

To test the validity of this assumption and the efficiency of the leaching procedure, total leachable Ba from the leaching experiments plotted against the $Ba_{xs}$ concentration calculated from bulk Ba and Al measurements and is also presented in Figure 6.3. A good correlation ($R^2$ = 0.81) is observed between the two concentrations with a slope of 1.28, which suggests that the efficiency of leaching experiments was acceptable and the Baxs mainly consist of organic and barite bound Ba.

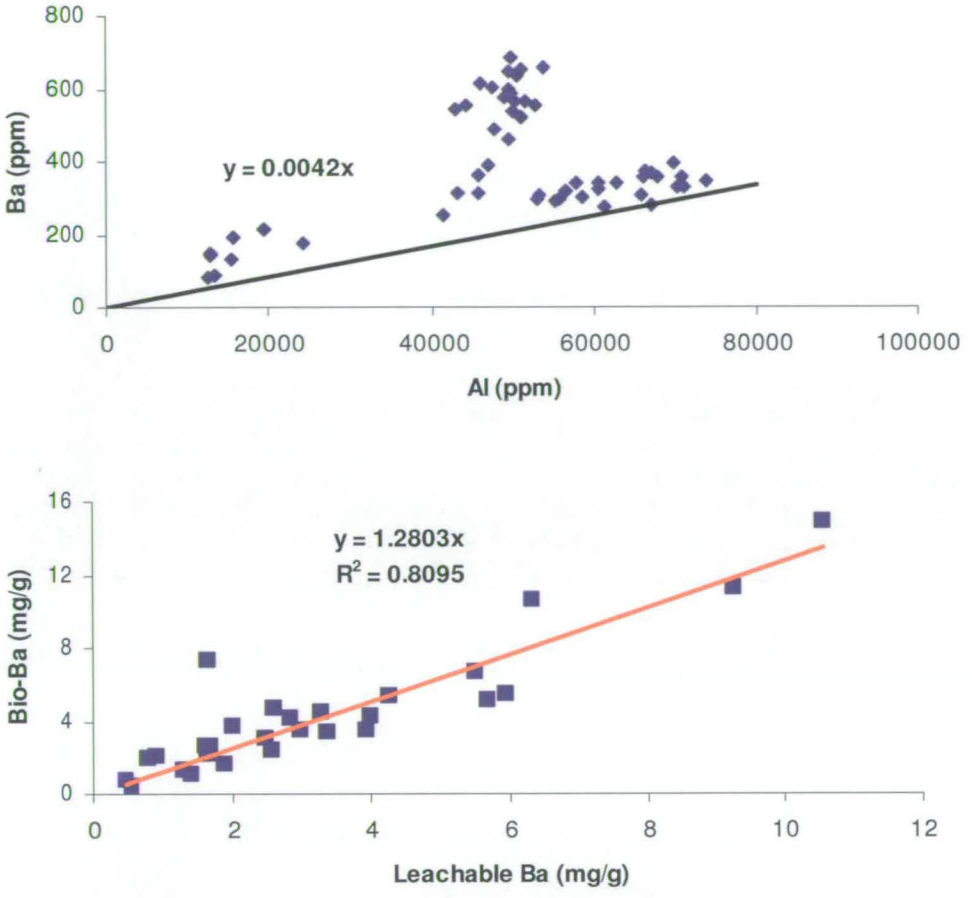


**Figure 6.3. (a) Plot of Al versus Ba to estimate the terrigenous Ba:Al ratio in the Ryder Bay Region. The Ba:Al ration was calculated using the slope of the line fitted to the lowest observed Ba:Al ratio (b) Plot of total leachable Ba from leaching experiments against Bio-Ba calculated from bulk Ba and Al concentrations. The linear regression line is set at an intercept of zero.**

### 6.3.2 Surface Waters and Sea Ice

In Figure 6.4, time series profiles of chl-*a* and $Ba_{XS}$ covering the duration of this study are presented, and surface water Ba and POC data from 15 m are presented in Table 6.2.

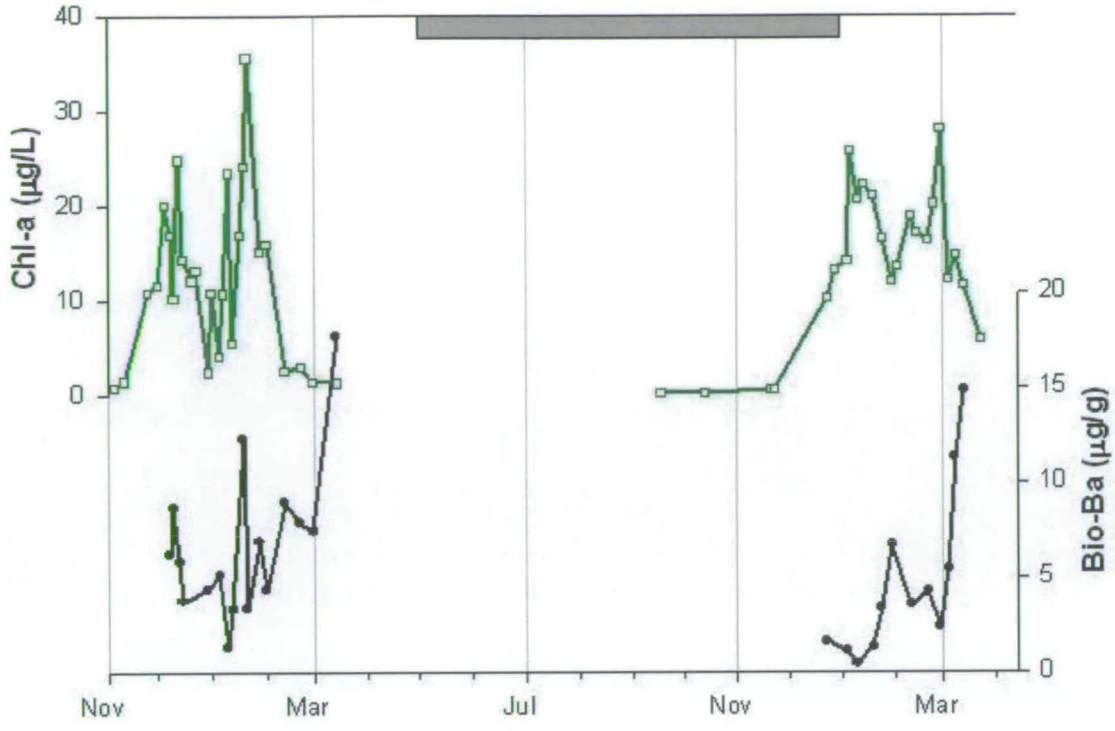


**Figure 6.4. Time series profiles of surface water chlorophyll-a concentrations and biogenic barium ($Ba_{XS}$) over the two growing seasons sampled during this study. Grey bar indicates sea ice coverage.**

$Ba_{XS}$ concentrations in surface waters ranged from 0.71 to 8.59 µg/g during the 04/05 season and from 0.23 to 9.73 µg/g during the 05/06 field season.

Surface water (15 m) POC concentrations ranged from 1580 to 6609 µmol during the 04/05 field season and from 2101 to 5125 µM during the 05/06 field season. $Ba_{XS}$ was produced in the surface waters during the highly productive, short growing season in Ryder Bay.

There is no positive correlation between levels of $Ba_{XS}$ and POC, there is in fact a negative correlation when comparing $Ba_{XS}$:POC against POC, that is presented with a best fit polynomial curve in Figure 5.

**Table 6.2. Surface water dissolved Ba, particulate Ba, particulate Al, $Ba_{XS}$, and POC data from time series study of Ryder Bay at the RaTS site at 15m.**

| Date | Sample | Dissolved Ba (ppb) | Ba ($\mu g.g^{-1}$) | Al ($\mu g.g^{-1}$) | $Ba_{XS}$ ($\mu g.g^{-1}$) | POC ($\mu mol.g^{-1}$) |
|---|---|---|---|---|---|---|
| 08/12/04 | RaTS-002 | 10.14 | 3.44 | 123.47 | 3.75 | 4980.69 |
| 10/12/04 | RaTS-003 | 8.56 | 4.86 | 137.04 | 5.20 | 2929.14 |
| 13/12/04 | RaTS-004 | 9.76 | 3.40 | 43.88 | 3.51 | 4854.33 |
| 15/12/04 | RaTS-005 | 9.72 | 2.14 | 41.40 | 2.25 | 5233.48 |
| 29/12/04 | RaTS-008 | 10.17 | 2.44 | 71.37 | 2.62 | 5217.10 |
| 05/01/05 | RaTS-010 | 8.38 | 2.65 | 160.98 | 3.06 | 2433.60 |
| 10/01/05 | RaTS-012 | 8.78 | 0.71 | 26.55 | 0.77 | 4971.39 |
| 13/01/05 | RaTS-013 | 10.79 | 1.74 | 103.88 | 2.00 | 2468.31 |
| 19/01/05 | RaTS-015 | 9.82 | 6.59 | 311.66 | 7.37 | 4674.73 |
| 21/01/05 | RaTS-016 | 8.74 | 1.84 | 83.16 | 2.05 | 6609.05 |
| 28/01/05 | RaTS-017 | 8.18 | 2.82 | 523.47 | 4.13 | 3108.10 |
| 01/02/05 | RaTS-018 | 8.96 | 2.06 | 216.00 | 2.60 | 6005.41 |
| 12/02/05 | RaTS-019 | 8.67 | 5.14 | 81.57 | 5.35 | 1682.56 |
| 21/02/05 | RaTS-020 | 7.85 | 3.53 | 469.85 | 4.70 | 2068.62 |
| 28/02/05 | RaTS-021 | 8.92 | 3.44 | 408.90 | 4.46 | 1579.83 |
| 14/03/05 | RaTS-022 | 8.67 | 8.59 | 808.67 | 10.61 | 2135.26 |
| 23/12/05 | RaTS-027 | 8.11 | 1.24 | 159.29 | 1.64 | 2648.40 |
| 04/01/06 | RaTS-029 | 8.71 | 0.84 | 111.86 | 1.12 | 2262.64 |
| 10/01/06 | RaTS-031 | 8.84 | 0.23 | 92.59 | 0.46 | 4240.82 |
| 19/01/06 | RaTS-033 | 8.76 | 1.02 | 129.20 | 1.34 | 5124.75 |
| 24/01/06 | RaTS-034 | 8.68 | 2.84 | 219.83 | 3.39 | 4540.56 |
| 30/01/06 | RaTS-035 | 8.97 | 4.84 | 729.75 | 6.66 | 2867.53 |
| 10/02/06 | RaTS-037 | 8.69 | 2.77 | 303.39 | 3.53 | 2926.02 |
| 20/02/06 | RaTS-039 | 8.73 | 1.65 | 1037.97 | 4.25 | 3652.66 |
| 27/02/06 | RaTS-041 | 8.27 | 1.49 | 356.79 | 2.38 | 4274.16 |
| 04/03/06 | RaTS-042 | 8.63 | 2.86 | 1036.29 | 5.45 | 2891.49 |
| 08/03/06 | RaTS-043 | 8.88 | 7.69 | 1443.99 | 11.31 | 2274.85 |
| 13/03/06 | RaTS-045 | 8.54 | 9.73 | 2056.54 | 14.87 | 2100.92 |

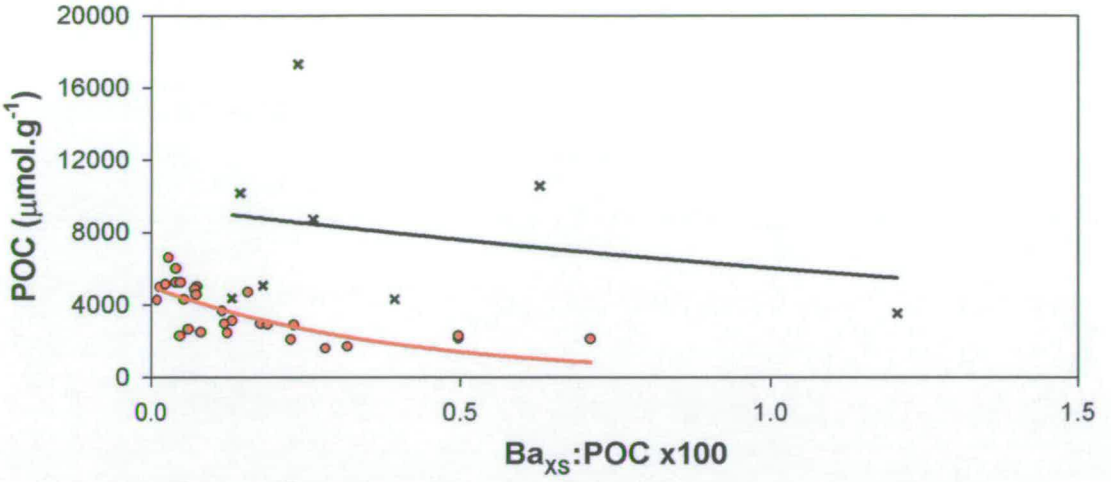


**Figure 6.5. Plot of surface water $Ba_{XS}$:POC against surface water POC concentration. Fitted lines represent decay curves fitted to each data set.**

Sea ice Ba and POC data are presented in Table 6.3, $Ba_{XS}$ concentrations ranged from 5.42 to a very high 64.33 µg/g, which is over 6 times greater than the maximum surface water $Ba_{XS}$ concentration. Sea ice POC concentrations were also generally higher than surface water POC concentrations and ranged from 3522 to 17317 µmol/kg. Like the surface waters, there was a negative correlation between levels of $Ba_{XS}$ and POC, also presented in Figure 6.5 with a best fit polynomial curve.

**Table 6.3. Sea ice dissolved Ba, particulate Ba, particulate Al, $Ba_{XS}$, and POC data from sea ice in Ryder Bay.**

| Date | Sample | Dissolved Ba (ppb) | Ba ($\mu g.g^{-1}$) | Al ($\mu g.g^{-1}$) | $Ba_{XS}$ ($\mu g.g^{-1}$) | POC ($\mu mol.g^{-1}$) |
|---|---|---|---|---|---|---|
| 10/12/04 | SI-001 | 0.765 | 43.17 | 420.64 | 41.40 | 17316.54 |
| 15/12/04 | SI-003 | 1.02 | 17.76 | 690.25 | 14.86 | 10167.26 |
| 17/12/04 | SI-004 | 12.69 | 69.40 | 756.42 | 66.22 | 10556.79 |
| 19/12/04 | SI-005 | 3.76 | 23.66 | 182.27 | 22.90 | 8718.51 |
| 24/11/05 | SI-010 | 2.53 | 6.41 | 147.15 | 5.79 | 4356.47 |
| 28/11/05 | Si-011 | 10.03 | 18.11 | 277.81 | 16.95 | 4298.39 |
| 06/12/05 | Si-013 | 2.85 | 43.35 | 196.14 | 42.52 | 3522.34 |
| 20/12/05 | SI-015 | 1.18 | 10.16 | 234.14 | 9.18 | 5060.28 |

Table 6.4 and Figure 6.6 present sequential leaching experiment data from the RaTS site at 15 m during the 04/05 season, 05/06 season and from sea ice samples used in this study. During the 04/05 season, sampling commenced during the mid-season decline in chl-*a* and POC, a feature also observed during the 05/06 season. Sequential leaching data from 8 Dec 04 until 5 Jan 05 during the decline of the chlorophyll peak, the barite fraction is higher than the labile fraction. Then from the 10 Jan 05 until 1 Feb 05, the labile Ba becomes the more dominant fraction in response to the second chlorophyll peak. Towards the end of the season when productivity declines, the period of 12 Feb 05 until the end of sampling for the 04/05 season (14 Mar 05), barite once again becomes the dominant fraction, reaching a maximum of 68 % of the leachable Ba pool. The Ba associated with refractory organic matter is generally much lower than that of labile Ba and barite, apart from the samples taken 10 Dec 04, and 13 Dec 04 where there is dominant enrichment of refractory Ba. Enrichment of refractory Ba also occurs at the end of the season when productivity declines and barite becomes the dominant fraction. During the 05/06 field season, sampling commenced while sea ice still covered Ryder Bay (see Figure 6.6b). The sequential leaching data show that in surface waters under sea ice and early after its retreat (23 Dec 05 until 4 Jan 06), barite is the dominant Ba fraction reaching 58 % of the leachable Ba pool. When the open water spring bloom begins, the labile Ba fraction generally becomes dominant from 10 Jan 06 until 4 Mar 06 in response to productivity, ranging from 45 to 75 % of the leachable Ba pool, apart from during mid-January when the mid-season decline in chlorophyll occurs and barite becomes the Ba phase at the highest concentration. After 04 Mar 06, the barite fraction begins to increase as productivity starts to decline and from 08 Mar 06 until the end of season sampling (13 Mar 06), barite becomes the dominant portion of total $Ba_{XS}$ reaching 56 % of the leachable Ba pool. The Ba associated with refractory organic matter is generally lower than that of labile Ba and barite, with enrichment of refractory Ba towards the end of the season when productivity declines and barite becomes the dominant fraction. Sequential leaching data

for sea ice samples, presented in Figure 6.6, show concentrations of total leachable Ba in sea ice are an order of magnitude higher than seen in the surface waters. The data also display high variability in the proportions of labile Ba and barite, with refractory Ba contributing a very small proportion of total Ba.

**Table 6.4. Sequential leaching experiment data for surface water and sea ice samples.**

| Date | S1 (10 % $HNO_3$) $Ba_{xs}$ ($\mu g.g^{-1}$) | S2 (Hot 30 % HCl) $Ba_{xs}$ ($\mu g.g^{-1}$) | S3 (Hot 50 % $HNO_3$) $Ba_{xs}$ ($\mu g.g^{-1}$) |
|---|---|---|---|
| Surface Waters | | | |
| 08/12/04 | 0.87 | 0.69 | 0.45 |
| 10/12/04 | 0.66 | 1.50 | 3.53 |
| 13/12/04 | 0.80 | 0.72 | 1.46 |
| 15/12/04 | 0.74 | 0.88 | 0.03 |
| 29/12/04 | 0.64 | 0.92 | 0.06 |
| 05/01/05 | 1.11 | 1.22 | 0.16 |
| 10/01/05 | 0.30 | 0.14 | 0.03 |
| 13/01/05 | 0.47 | 0.33 | 0.01 |
| 19/01/05 | 1.03 | 0.55 | 0.06 |
| 21/01/05 | 0.63 | 0.26 | 0.01 |
| 28/01/05 | 1.57 | 1.07 | 0.21 |
| 01/02/05 | 0.96 | 0.42 | 0.31 |
| 12/02/05 | 0.93 | 3.30 | 0.02 |
| 21/02/05 | 0.89 | 1.39 | 0.30 |
| 28/02/05 | 0.75 | 2.12 | 0.40 |
| 14/03/05 | 1.41 | 4.31 | 0.60 |
| 23/12/05 | 0.80 | 1.10 | 0.01 |
| 04/01/06 | 0.50 | 0.69 | 0.22 |
| 10/01/06 | 0.36 | 0.19 | 0.02 |
| 19/01/06 | 0.95 | 0.30 | 0.06 |
| 24/01/06 | 1.52 | 1.80 | 0.04 |
| 30/01/06 | 3.68 | 1.36 | 0.44 |
| 10/02/06 | 2.95 | 0.80 | 0.18 |
| 20/02/06 | 2.80 | 0.85 | 0.34 |
| 27/02/06 | 1.54 | 0.88 | 0.14 |
| 04/03/06 | 3.32 | 2.03 | 0.58 |
| 08/03/06 | 3.13 | 5.21 | 0.91 |
| 13/03/06 | 3.16 | 5.92 | 1.46 |
| Sea Ice | | | |
| 10/12/04 | 19.33 | 10.96 | 4.36 |
| 15/12/04 | 4.88 | 6.47 | 0.67 |
| 17/12/04 | 46.91 | 14.50 | 1.44 |
| 19/12/04 | 14.39 | 6.20 | 1.55 |
| 24/11/05 | 0.66 | 4.47 | 0.23 |
| 28/11/05 | 9.47 | 7.27 | 0.08 |
| 06/12/05 | 34.91 | 6.99 | 0.37 |
| 20/12/05 | 8.46 | 0.01 | 0.01 |

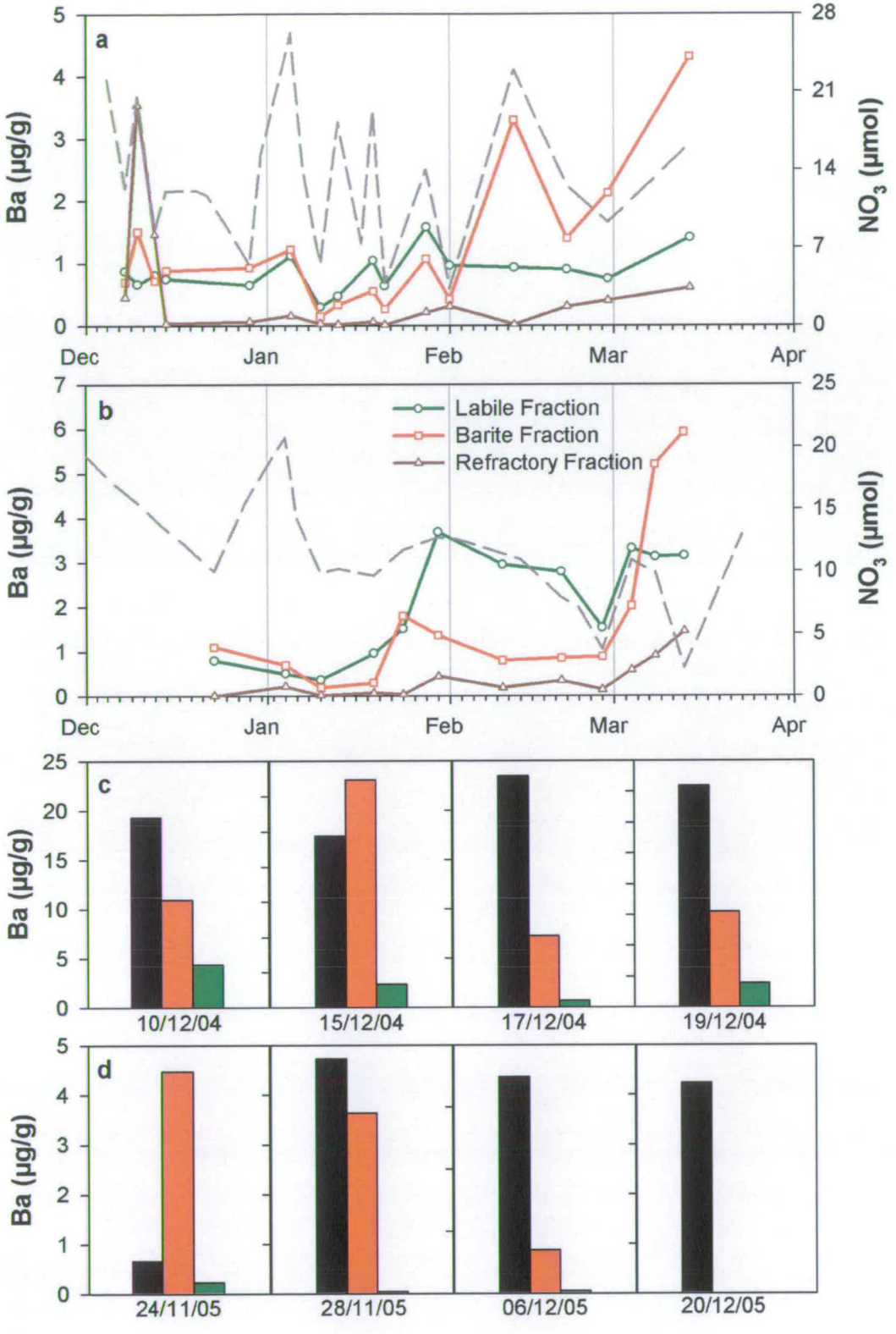


**Figure 6.6. Data from sequential leaching experiments from (a) the 04/05 field season (b) the 05/06 field season, dashed lines represent $NO_3$ concentration (c-d )Data from sequential leaching of sea ice samples (black bars labile fraction, red bars barite and green bars refractory fraction)**

Sea ice samples were collected mainly early in austral spring of the two sampling years when sea ice was still present (Table 6.3; Figure 6.6 black bars) In all but 2 of the sea ice samples (SI-003 and SI-010), the labile portion of Ba is the dominant fraction. In SI-003 and SI-010, barite enrichment is greater than that of labile Ba at 54 and 83 % barite respectively.

Figure 6.7 presents plots of the $Ba_{XS}$:POC ratio and chl-a concentration for surface waters and sea ice. The trends show a decline in $Ba_{xs}$:POC during increases in Chl-a and an increase in $Ba_{xs}$:POC during Chl-a decline. During the 2004/2005 season, $Ba_{XS}$:POC ratios range from 0.02 to 0.50. $Ba_{XS}$:POC ratios stay relatively low during the growing season with subtle increases during periods where chl-a concentration declines. Interestingly the $Ba_{XS}$:POC ratios reach their maximum values at the end of the season when biomass declines and reaches winter values (RaTS-019 to RaTS-022). During the 2005/2006 season, $Ba_{XS}$:POC ratios range from 0.01 to 0.71, with similar features to the 2004/2005 field season. $Ba_{XS}$:POC ratios stay relatively low when there are high standing stocks of chl-a, but increases during periods of biomass decline particularly towards the end of the season. In sea ice, the $Ba_{XS}$:POC ratio ranges from 0.13 to 1.21, and lacks any clear relationship with Chl-a concentrations.

In Figure 6.5, The fitted exponential curves for sea ice and surface waters show that the reduction in POC leads to an increase in $Ba_{XS}$:POC from the system. In addition, the high Baxs:POC samples often have barite as the dominant form of $Ba_{XS}$ and fall during periods of declining biomass in mid season or late in the season when productivity declines (Figure 6.7).

The increase in $Ba_{xs}$ and barite in low POC samples is associated with declining biomass and lends support to the idea of progressive barite enrichment during organic matter decay, so far only documented in laboratory phytoplankton decay experiments (Ganeshram et. al., 2003).

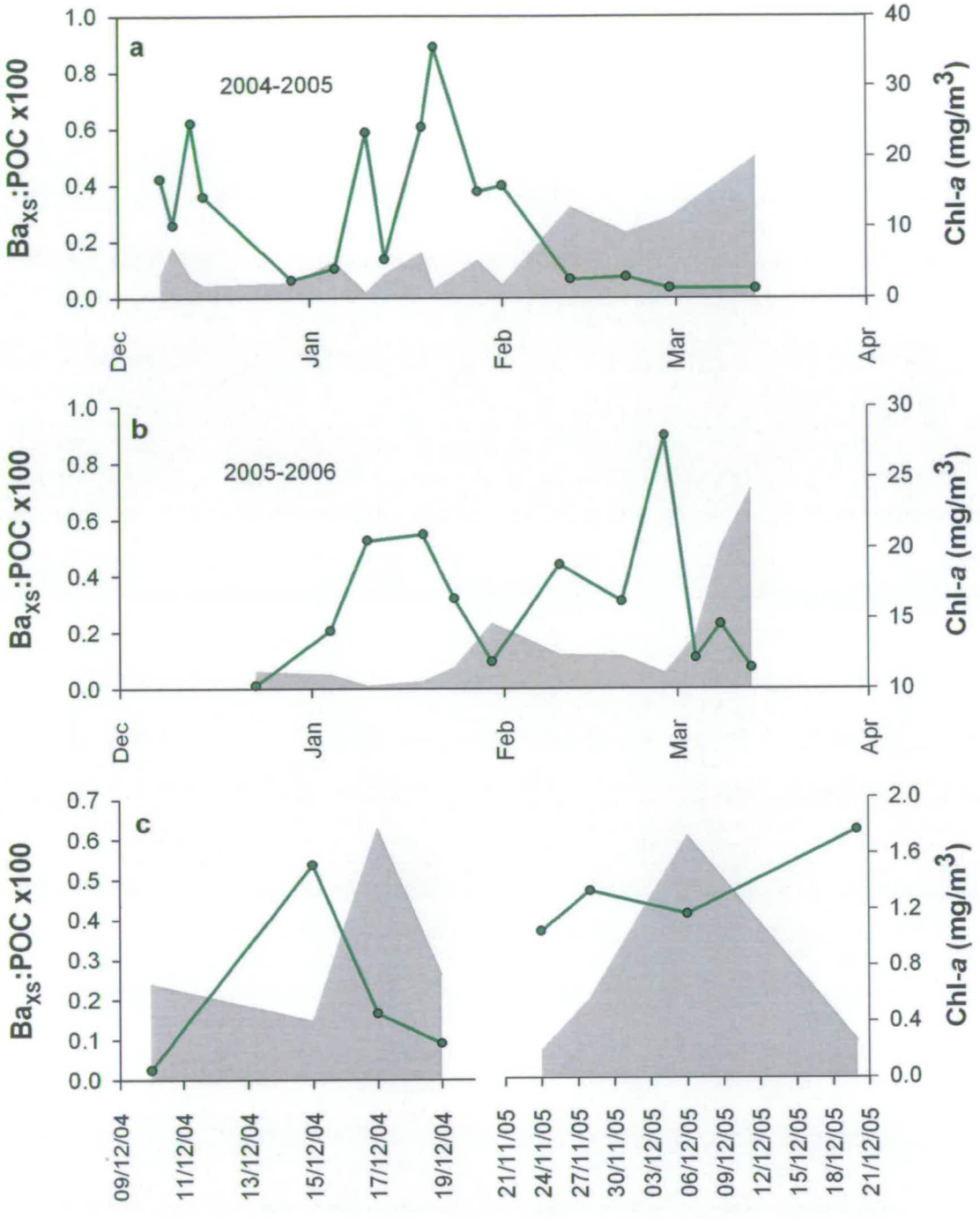


**Figure 6.7. Time series plots of $Ba_{XS}$:POC ratio (grey area) and chl-a concentration (green line) to depict increases in Ba relative to POC during different periods of productivity during the study (a) 2004/2005 season (b) 2005/2006 season and (c) sea ice samples.**

### 6.3.3 Sediment Traps

Time series mass fluxes and fluxes of $Ba_{XS}$ are presented in Figure 6.8 and are summarised in Table 6.5. Mass fluxes exhibit typical high seasonality with high fluxes during austral summer when sea ice retreats and little or no flux during austral winter when productivity and particle flux almost ceases.

The shallow (123m) trap at the deep mooring site does however exhibit significant particle flux throughout winter, likely due to the trap being above the deep winter mixed layer, where the few biogenic particles that are present are not exported to depth. Mass fluxes and $Ba_{XS}$ fluxes show similar trends over the deployment period, which is not surprising as the mass fluxes and carbon content of the sediment are tightly coupled to one another indicating that a high proportion of the material in the sediment cups is of biogenic origin. Mass fluxes in the deep traps are much lower than the fluxes in shallower traps (Table 6.1). This suggests there was no great influence of resuspended or laterally advected material in the deeper sediment traps to affect the signal of vertical flux at these sites.

It has been consistently observed that $Ba_{XS}$ fluxes increase with depth in both sediment trap studies (Dymond *et al.*, 1992) and surface sediment data (Schenau *et al.*, 2001). Annual flux in Table 6.5 generally show the trends expected for change in carbon and $Ba_{XS}$ flux with depth. Carbon fluxes decrease with depth due to loss of $C_{org}$ from biodegradation while sinking. $Ba_{XS}$ fluxes tend to increase with depth, due to barite precipitation in decaying organic matter during sinking, although this increase is not monotonic throughout the water column. There is a reduction in Ba fluxes in the RaTS 512 m trap compared to the deep site 123 m and RaTS 200 m trap. This relationship is also highlighted by the $Ba:C_{org}$ ratio of the traps (Table 6.5).

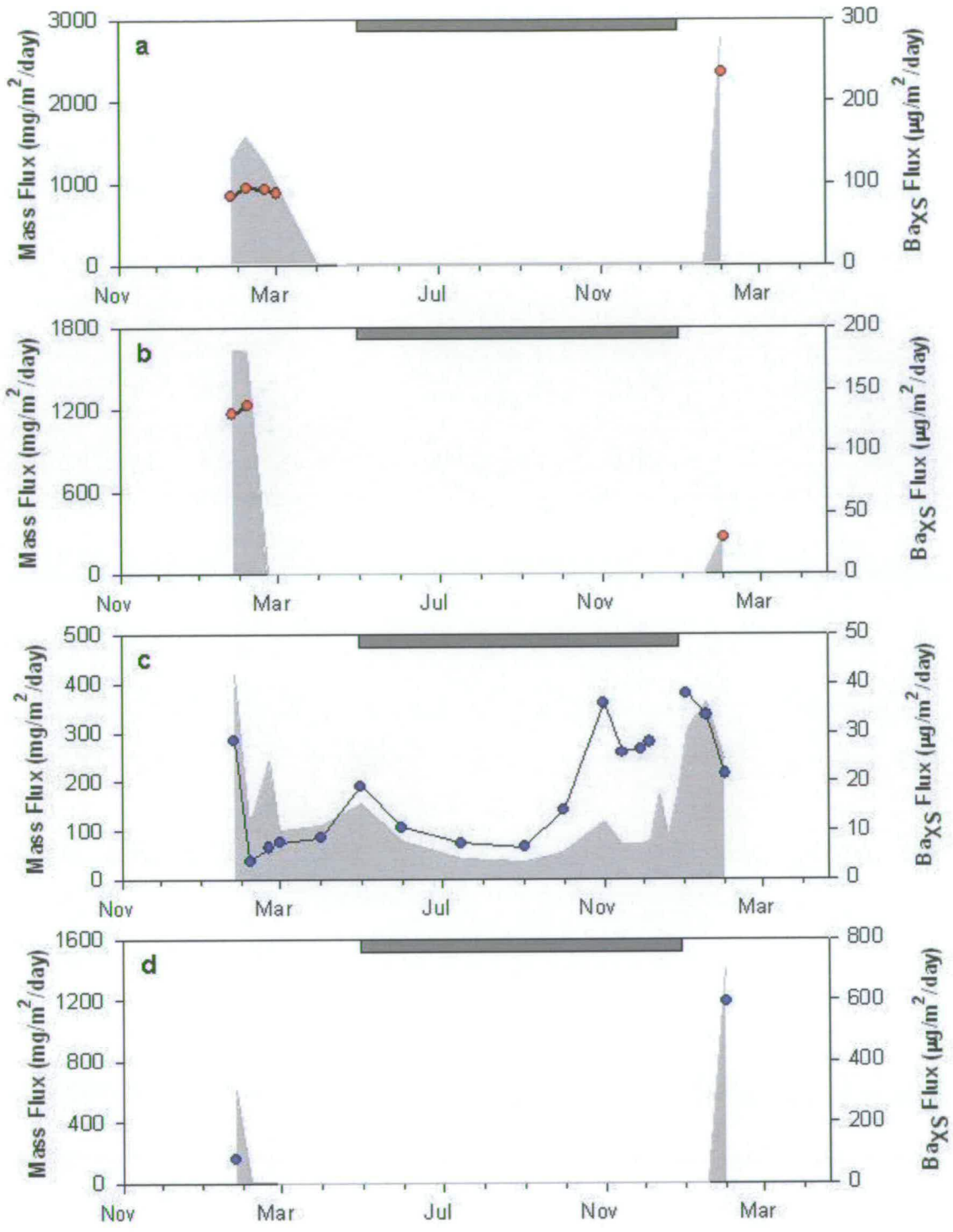


**Figure 6.8. Time series profiles of sediment trap mass fluxes (grey area) and $Ba_{XS}$ fluxes (circles) for (a) The RaTS site 200 m trap (b) RaTS site 512 m trap (c) The deep site 123 m trap and (d) The deep site 745 m trap.**

**Table 6.5. Annual fluxes in sediment traps used for this study. Annual fluxes are calculated from 26 January 2005 until 14 February 2006.**

| Sediment Trap | $C_{org}$ Flux ($\mu mol.g^{-1}.m^{-2}.d^{-1}$) | Ba Flux ($\mu g.m^{-2}/d^{-1}$) | Al Flux ($mg.m^{-2}.d^{-1}$) | $Ba_{XS}$ Flux ($\mu g.m^{-2}.d^{-1}$) | $Ba/C_{org}$ x100 ($\mu g.\mu mol^{-1}$) |
|---|---|---|---|---|---|
| RaTS Site 200m | 6991.76 | 101.33 | 18.54 | 23.51 | 0.336 |
| RaTS Site 512m | 3071.62 | 37.96 | 6.64 | 10.09 | 0.328 |
| Deep Site 123m | 4963.80 | 28.44 | 3.33 | 14.45 | 0.291 |
| Deep Site 745m | 2626.70 | 35.59 | 2.73 | 24.14 | 0.919 |

Figure 6.9 presents the relationship between the flux of $Ba_{XS}$ and the flux of organic carbon in individual trap cups for the shallow and deep traps. Both plots show an expected positive relationship, i.e. increasing $Ba_{XS}$ yield with increasing carbon flux, although there is a high degree of scatter amongst the different traps. From these plots the data from individual cups show that the yield of $Ba_{XS}$ per unit of carbon is higher for the deeper traps than that of the shallower traps. The lack of a tightly coupled $Ba_{XS}$ flux versus $C_{org}$ flux between traps suggests that water depth has an influence on $Ba_{XS}$ yield. This data set, spanning the majority of two seasons, indicates that the $Ba:C_{org}$ varies considerably over seasonal timescales. The main observations from the sediment trap data include; enrichment of $Ba_{XS}$ relative to carbon with depth (Figures 6.9 and 6.10), high seasonality is observed with higher $Ba_{XS}:C_{org}$ ratios occurring in the austral winter and early spring months (Figure 6.10) and the decrease in $Ba:C_{org}$ during periods of very high carbon flux (Figure 6.11).

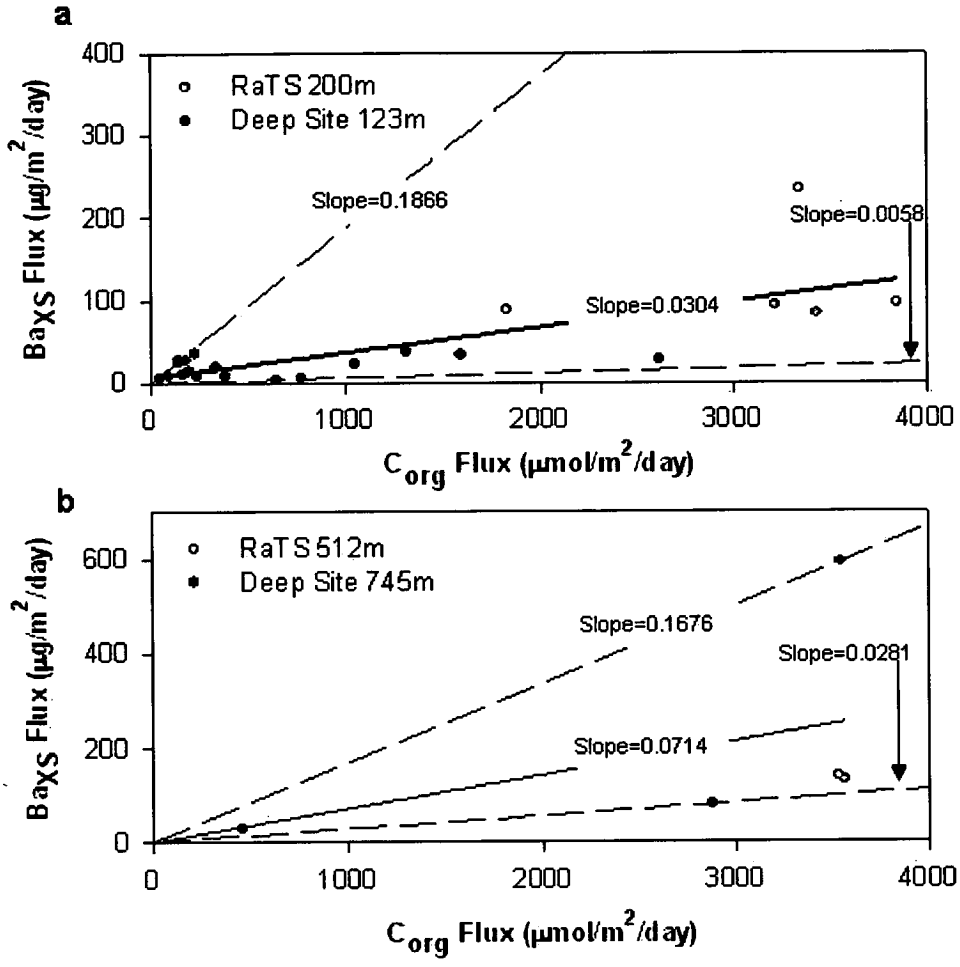


**Figure 6.9. Sediment trap plots of organic carbon flux and $Ba_{XS}$ for (a) The RaTS site 200 m trap and deep site 123 m trap (b) The RaTS site 512 m trap and deep site 745 m trap.**

Although there is a fair amount of scatter in the $C_{org}$ flux versus $Ba_{XS}$ flux (Figure 9), there is an average flux of 30.4 x $10^{-3}$ µg $Ba_{XS}$ per µmol C (with a range of 5.8 x $10^{-3}$ to 186.6 x $10^{-3}$ µg $Ba_{XS}$ per µmol C), whereas in the deeper traps there is an average of 71.4 x $10^{-3}$ µg $Ba_{XS}$ per µmol C (with a range of 28.1 x $10^{-3}$ to 167.6 x $10^{-3}$ µg $Ba_{XS}$ per µmol C). Although there is a >2 fold difference between the average $C_{org}$ flux versus $Ba_{XS}$ flux in the shallow and deep traps, these still fit in with 'typical' global values of 20-50 x $10^{-3}$ µg $Ba_{XS}$ per µmol C (Dymond and Collier, 1996).

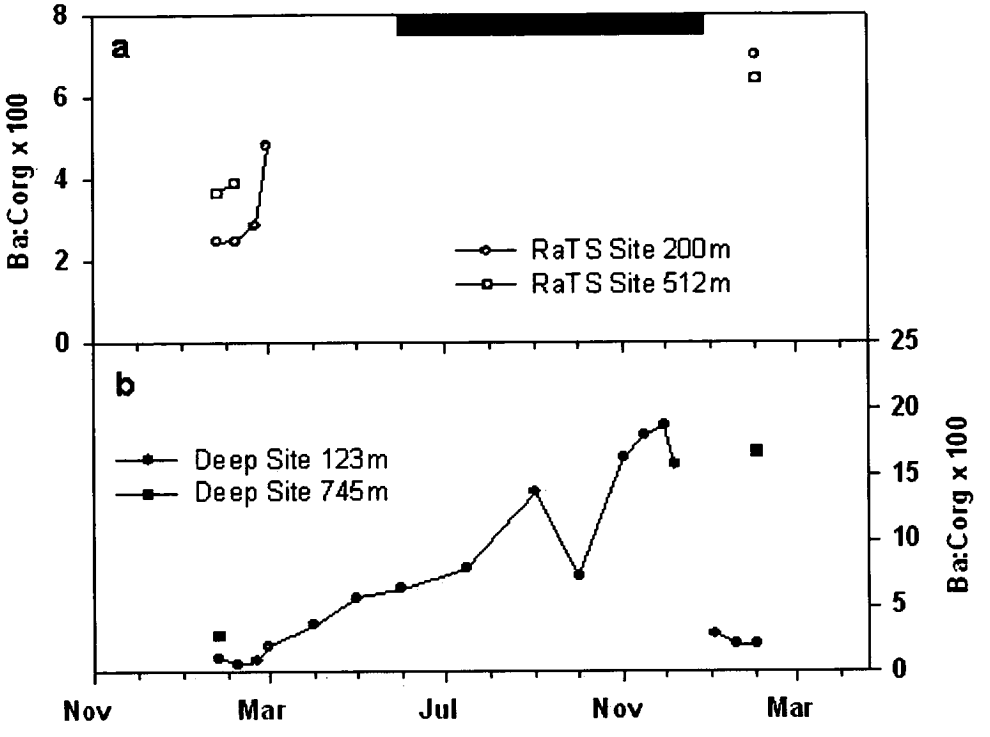


**Figure 6.10. Time series plots of sediment trap Ba:$C_{org}$ ratios for (a) The RaTS mooring sediment traps and (b) The deep site mooring sediment traps.**

Although there is generally an increase in $Ba_{XS}$:$C_{org}$ with depth (Figure 6.10) and differences approach an order of magnitude in some cases, this increase with depth is not always observed. For example, at the onset of sea ice retreat and the spring bloom at the RaTS site, there is a decrease in $Ba_{XS}$:$C_{org}$, whereas in all other sediment trap cups there is an increase with depth. The high seasonality observed in the sediment trap time series has implications for how the flux regime in a seasonally sea ice covered region like Ryder Bay and Marguerite Bay may affect the overall $Ba_{XS}$:$C_{org}$ ratio of sinking particles. These regions are typified by a short growing season where most of the flux of material occurs as a pulse soon after sea ice retreat (Clarke and Leakey, 1996; Clarke *et al.*, 2007; Ducklow *et al.*, 2007). These pulsed blooms are thought to reduce the yield of $Ba_{XS}$ per unit carbon because fast sinking large diatoms or organic matter aggregates are removed from the water column too quickly for the complete formation of particulate barite (McManus *et al.*, 2002). In Figure 6.11 the observation of a reduction in $Ba_{XS}$ yield during high carbon flux is evident from the negative

relationship between $Ba_{XS}$:$C_{org}$ and C flux, for both the shallow and deeper traps.

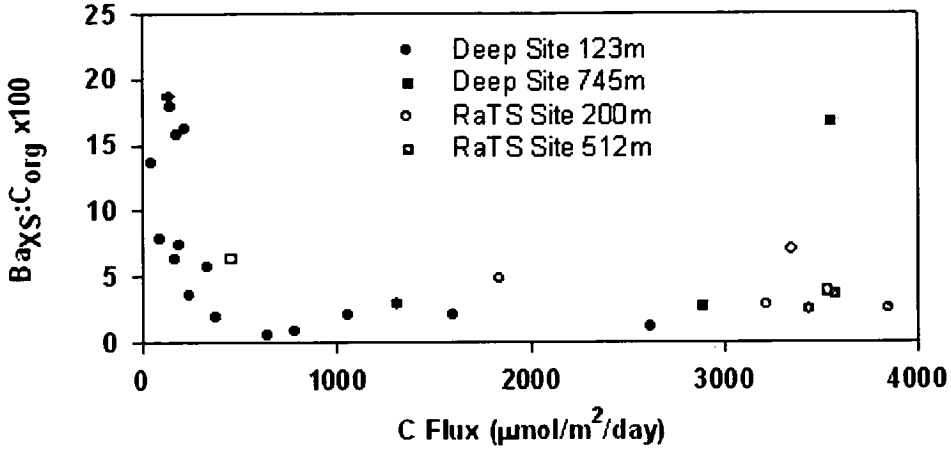


**Figure 6.11. Plot of organic carbon flux versus $Ba_{XS}$:Corg ratio in all sediment traps deployed during this study.**

### 6.3.4 Box Cores

Surface sediment from the RaTS site box core has a $Ba_{XS}$:$C_{org}$ ratio of 0.0570 and from the box core at the deep mooring site the $Ba_{XS}$:$C_{org}$ ratio is 0.3491, which are significant increases from the sediment trap $Ba_{XS}$:$C_{org}$.

## 6.4 Discussion

We present the first time series leaching experiments that monitor the transformations of particulate barium in sea ice and surface waters on a seasonal timescale. Our results show significantly higher standing stocks of $Ba_{XS}$ in sea ice compared to surface waters, the growth of barite in surface waters in association with degrading phytodetritus and an expected increase in the flux of $Ba_{XS}$ to depth with decreasing $C_{org}$ that is consistent with previous published algorithms (Francois *et al.*, 1995).

### 6.4.1 Sea Ice Associated Particulate $Ba_{XS}$

The concentrations of $Ba_{XS}$ in the form of labile particulate Ba, barite and refractory bound Ba (Figures 6.4 and 6.6) in sea ice brine are the first

measurements of their kind and show concentrations an order of magnitude higher than surface waters. The data open up some interesting possibilities regarding the role of sea ice in the formation and flux of particulate barium on a seasonal timescale. This topic has received no attention in the Southern Ocean, which is surprising considering that in seasonally sea ice covered areas productivity associated with sea ice can account for up to 25 % of total production (Arrigo *et al.*, 1997). A recent laboratory experiment (Ganeshram *et al.*, 2003) proved that barite formation occurs as a result of decaying phytoplankton by utilising time series sequential leaching measurements of phytoplankton in carboys. The conditions in this experiment are analogous to the processes that would occur in sea ice as a result of the growth and decay of diatom assemblages within the ice matrix. A continuous cycle of organic matter formation and degradation may partly explain why there is more $Ba_{XS}$ in sea ice compared to surface waters and the high $Ba_{XS}$:$C_{org}$ ratio. Another possible factor influencing the high $Ba_{XS}$ content of sea ice is the effect of transparent exopolymer particles (TEP). Such TEP particles are formed from the coagulation and continuous aggregation of dissolved polysaccharide fibrillar precursors in the DOM pool and are known for promoting aggregation of organic matter and the formation of marine snow during the early stage of phytoplankton decay (Alldredge *et al.*, 1993). Sea ice as a habitat exhibits conditions favourable for significant TEP formation and high concentrations have been measured in the interior of ice floes (Krembs and Engel, 2001; Meiners *et al.*, 2003). It has been hypothesised that the TEP particles in decaying organic matter may provide ion-exchange sites for Ba and may be involved in the precipitation of barite in microenvironments supersaturated with Ba bound to TEP and sulphate released by decaying organic matter (Alldredge *et al.*, 1993; Ganeshram *et al.*, 2003).

Regardless of the mechanisms producing such high $Ba_{XS}$ concentrations in sea ice, the high $Ba_{XS}$:$C_{org}$ ratios in sea ice along with the quantities of readily formed barite have the potential to influence the yield of $Ba_{XS}$ per unit carbon in sinking particles. This possibility, however, is very hard to identify in

sediment trap studies as most of the flux of organic matter from surface water phytoplankton blooms occur during or very shortly after sea ice retreat or melt (Clarke *et al.*, 2007; Garrity *et al.*, 2005), masking the compositional difference of sea ice material. There is evidence from the shallow trap (123m) at the deep mooring site that sea ice associated material may be having an effect on the $Ba_{XS}$:$C_{org}$ composition of sinking particles. During late austral winter and early spring, sea ice can reach the percolation threshold allowing transfer of brine within the ice matrix and ice floes become more porous, resulting in exchange of water and materials between ice brine and the underlying surface water (Perovich *et al.*, 2004). This effect would render the ice matrix as a semi-closed system, rather than a closed system and may permit the flux of material formed or altered in the sea ice to be exported to depth. The highest sediment trap $Ba_{XS}$:$C_{org}$ ratios occur in the 123m deep site trap during late winter and early spring (Figure 6.10), at the time when the ice starts to deteriorate during the onset of spring. Although these high $Ba_{XS}$:$C_{org}$ ratios could result from the effect of higher residence time of particles in the water column during low flux period where barite precipitation may be more efficient, it is also possible that sea ice material may be playing a role. More high resolution sampling of sea ice and underlying surface waters is needed to provide more information on the processes occurring here.

Another interesting possibility yet to be fully investigated, is that barite formation in sea ice may occur through abiotic precipitation of dissolved Ba and dissolved sulphate ($SO_4^{2-}$). Salinity of brine in sea ice can reach concentrations >100 PSU (Gleitz et al, 1995), which could result in brine pockets reaching concentrations of dissolved Ba and $SO_4^{2-}$ high enough to cause such precipitation. This hypothesis works on the same fundamental theory of supersaturation of dissolved Ba and $SO_4^{2-}$ being expelled from decaying organic matter. To test this hypothesis, future material from sea ice could be examined by scanning electron microscopy to observe the morphology of barite crystals present. It has been observed in the past that

abiotic barite crystals are larger, pointier and more irregular in shape compared to barite crystals of biogenic origin (Bertram and Cowen 1997).

### 6.4.2 Surface Water Barium Seasonality

The concentration of $Ba_{XS}$ in the form of labile particulate Ba, barite and refractory bound Ba (Figures 6.4 and 6.6) in surface waters are the first measurements of their kind and show a clear seasonal cycle of $Ba_{XS}$ formation and evolution of the different phases of $Ba_{XS}$ associated with organic matter (Figures 6.4, 6.6 and 6.7). This time-series data set provides important information regarding the processes occurring is surface waters prior to the sinking of particles and formation of the sedimentary $Ba_{XS}$ signature.

Ganeshram et al., (2003) concluded that transformations observed in Ba phases and the growth of barite crystals in decaying phytoplankton cultures, indicate that the decay of organic phytoplankton material is directly involved in the formation of barite. The data presented here from surface water time series leaching experiments is consistent with this mechanism of barite formation, with labile Ba associated with fresh organic matter formed during primary production and the growth of barite during periods where phytoplankton decay occurs. The effects of grazing by zooplankton such as krill and copepods may also enhance the formation of barite in surface waters prior to export. This would occur through processes such as faecal-pellet packaging, which would increase the availability of microenvironments for the retention of Ba and sulphate released during phytoplankton decay to facilitate barite precipitation (Ganeshram *et al.*, 2003).

The seasonal formation of labile Ba during early season primary production and barite formation at the end of the season appears to be influenced by processes associated with sea ice retreat and mixing of water masses. During the 05/06 season the water column was enriched with barite relative to labile Ba (Figure 6.6b) prior to and just after sea ice retreat. This was likely associated with either degradation of fresh phytoplankton material

underneath the ice or with the release of barite rich material from sea ice. It is unlikely that the material underneath the ice was enriched in barite as there was a significant amount of new primary production occurring underneath the ice at this time (Figure 6.4), so that pool of Ba was probably dominated by labile Ba, we therefore attribute the barite enrichment in surface waters early in the season to release of barite enriched material from sea ice. A different situation is observed at the start of sampling during December 2004 during the 04/05 field season. Although sea ice had retreated and the growing season was underway, sampling commenced during a reduction in chlorophyll following the first productivity peak that occurred during November 2004 (Figure 6.5 and 6.7). This may explain why barite was the dominant $Ba_{XS}$ fraction during this period as the recession in chlorophyll may be associated with degradation of phytoplankton providing suitable microenvironments for barite precipitation. It is likely that the observed drops in chlorophyll from both seasons are facilitated by grazing, with such trophic processing enhancing barite formation, but this possibility remains speculative due to lack of grazing data.

The mixing of water masses through upwelling and/or lateral transport also appears to affect the seasonal progression of a $Ba_{XS}$ pool dominated by labile Ba to one dominated by barite. This process can be traced by the behaviour of nutrients such as nitrate. In Figure 7, periods of nutrient utilisation tends to be accompanied by enrichment of labile Ba, indicating biological uptake or abiotic adsorption of Ba onto organic matter followed by degradation of this matter (possibly accelerated by grazing) and growth of the barite fraction. However, the mixing of water masses and resulting nutrient inputs, observed as spikes in the nitrate profiles, suggest that this step-wise process is altered by new material entering the system that is composed of different proportions of the leachable Ba fractions.

### 6.4.3 Sinking Particulate $Ba_{XS}$

An expected enrichment in $Ba_{XS}$ with depth occurs in Ryder Bay and Marguerite Bay (Figure 6.12), consistent with observations seen in many other studies in the open ocean as well as continental shelf or margin environments (Dehairs *et al.*, 1992; Dehairs *et al.*, 2000; Dehairs *et al.*, 1997; Dehairs *et al.*, 1991; Dymond and Collier, 1996; Dymond *et al.*, 1992; Fagel *et al.*, 1999; Fagel *et al.*, 2004; Francois *et al.*, 1995; Jacquet *et al.*, 2006; McManus *et al.*, 1998). However, due to the relatively short deployment period and sediment traps at only two locations, it is difficult to assess the reproducibility of $Ba_{XS}$ flux relative to carbon over longer timescales where sea ice cover and export fluxes can be highly variable (Ducklow *et al.*, 2007; Ducklow *et al.*, 2006), such interannual variability in carbon flux has been implicated in decoupling the $Ba_{XS}$ flux versus carbon flux relationship in other coastal Antarctic environments such as the Ross Sea (McManus *et al.*, 2002).

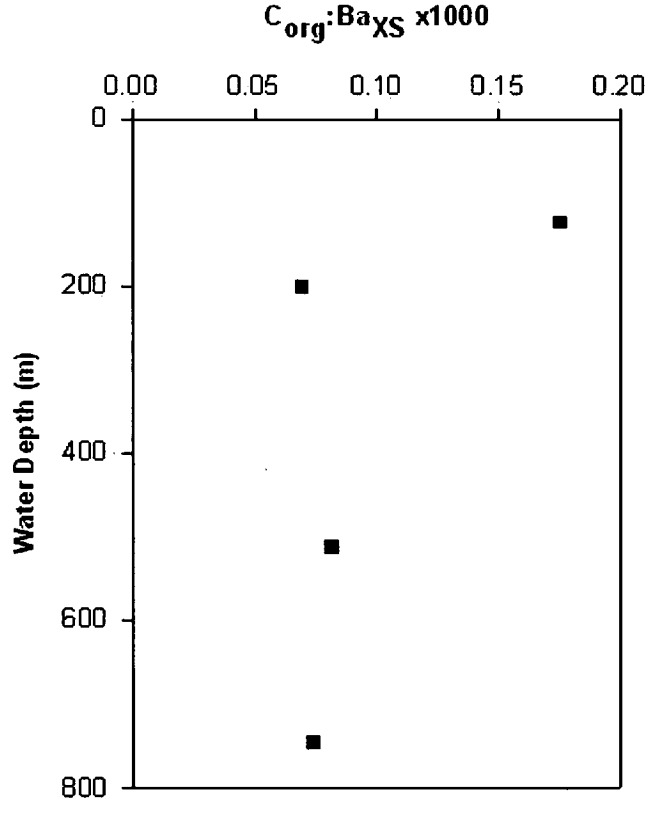


**Figure 6.12. Annual $C_{org}$:$Ba_{XS}$ ratios from sediment traps in this study.**

The key issue surrounding the use of $Ba_{XS}$ in sediments is to be able to confidently relate $Ba_{XS}$ fluxes to organic carbon fluxes, a process that is poorly constrained in continental shelf regions and margins (Fagel *et al.*, 2004; McManus *et al.*, 2002) in contrast to the open ocean (Dymond and Collier, 1996; Francois *et al.*, 1995). Although a high degree of scatter is observed in the $Ba_{XS}$ flux versus $C_{org}$ fluxes in individual trap cups (Figure 6.9), plotting the annual flux of $C_{org}$ and $Ba_{XS}$ in the traps alongside preliminary algorithms published by Francois *et al.* (1995) and Nurnberg *et al.* (1997) show that the flux of $Ba_{XS}$ and $C_{org}$ in this region are consistent with these algorithms (Figure 6.13) .

It appears then, that the algorithms published for the open ocean are indeed suitable for the continental shelf, Antarctic sea ice environment, to reconstruct C flux based on sedimentary $Ba_{XS}$ concentration. However, these results should be treated with caution as other similar environments, such as the Ross Sea (McManus *et al.*, 2002), do not exhibit such a coherent relationship.

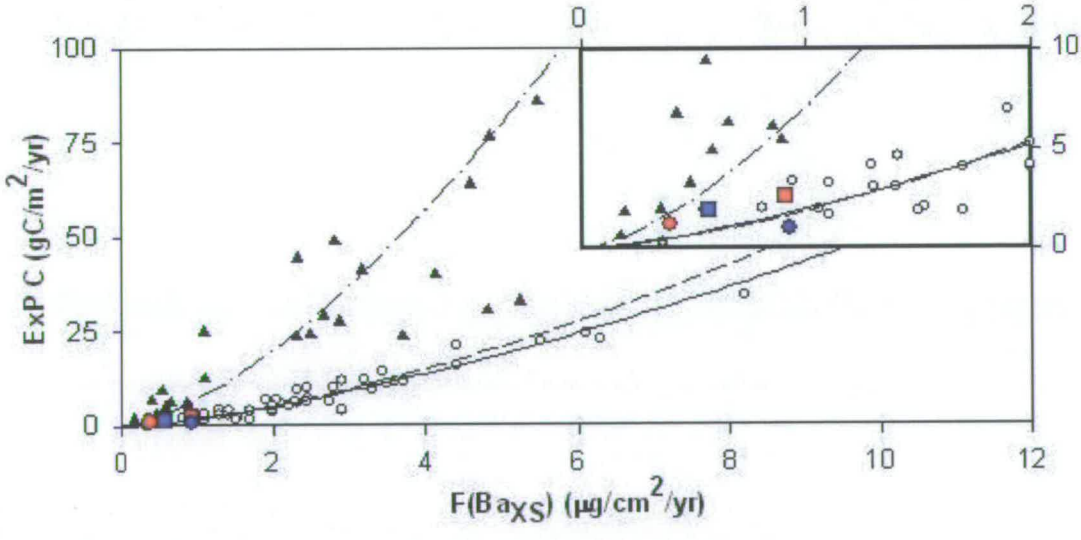


**Figure 6.13. Correlations between sediment trap $Ba_{XS}$ export and carbon export from this study (RaTS 200 m trap red square; RaTS 512 m trap red circle; deep site 123 m trap blue square; deep site 745 m trap blue circle), compared to algorithms from Francois et. al., (1995) (solid line), Nurnberg et. al., (1997) for the open ocean and Dehairs et. al., (1992) for margin algorithm. Insert at top right shows an enlargement of where the data points from this study lie.**

More time series studies in continental shelf Southern Ocean regions are needed to better constrain factors affecting the flux of C and $Ba_{XS}$. Based on our findings, we present a conceptual model of the biogeochemical cycling of Ba in the coastal, Antarctic sea ice environment, which is presented in Figure 6.14 (overleaf).

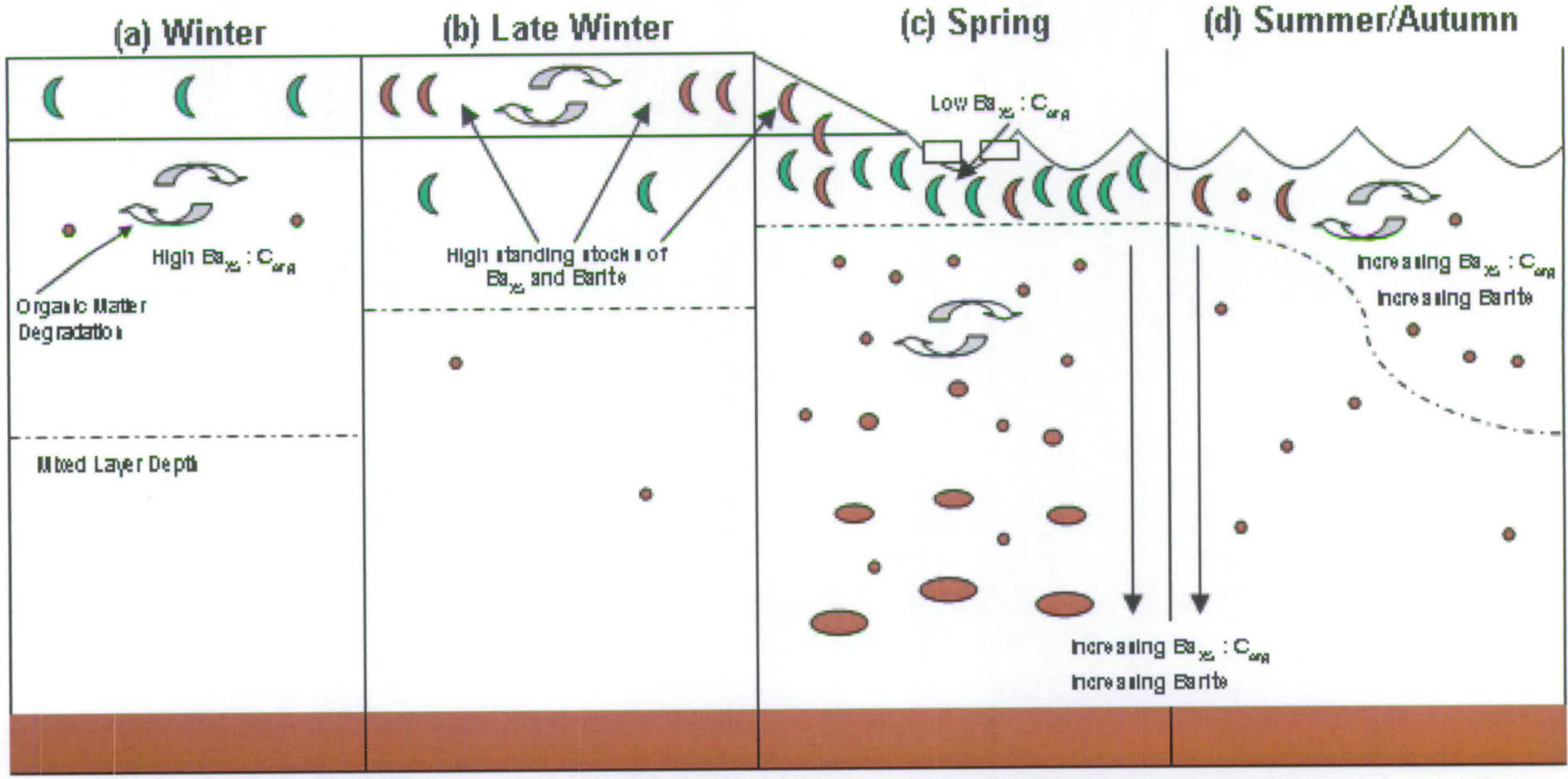


**Figure 6.14. Conceptual model of Ba Cycling in coastal Antarctic sea ice environment.**

The conceptual model presented in Figure 6.14 describes the following processes occurring in the Ba cycle in the coastal Antarctic sea ice environment:

**Winter -** Low levels of fresh production in sea ice matrix (green) with low $Ba_{XS}$:$C_{org}$ composed mainly of labile Ba. A small amount of particulate material is held in the deep winter mixed layer that has a high $Ba_{XS}$:$C_{org}$ ratio from efficient biodegradation of organic material (brown) forming barite through precipitation.

**Late Winter -** During late winter, the biogenic material in sea ice goes through rapid degradation and production cycles, resulting in high standing stocks of $Ba_{XS}$, barite and refractory bound Ba. Primary production starts in surface waters below, where the material has a low $Ba_{XS}$:$C_{org}$ and is composed mainly of labile Ba.

**Spring -** During early spring, the summer shallow mixed layer forms, sea ice retreat seeds highly degraded organic material containing high $Ba_{XS}$, barite and refractory bound Ba to surface waters. This mixes with fresh organic material produced by the spring bloom, which has a low $Ba_{XS}$:$C_{org}$ ratio and is composed mainly of labile Ba. This is the time of high standing stocks of phytoplankton in the shallow mixed layer, and the highest period of export flux where fresh surface water organic material degrades while sinking, forming larger aggregates, and an increase of $Ba_{XS}$:$C_{org}$ with depth occurs due to barite precipitation during organic matter degradation. During the highly productive spring bloom, barite can also be formed in surface waters by degrading organic matter and barite precipitation during periods of grazing and hiatuses in production, resulting in the Ba pool becoming enriched in barite and refractory bound Ba. This period can also be influenced by upwelling of nutrient rich water which can "reset" the step wise process of labile Ba formation and barite precipitation in the euphotic zone.

**Summer/Autumn -** During summer and autumn, production declines and the organic material in surface waters becomes highly degrading resulting in an increase in $Ba_{XS}$:$C_{org}$ and the Ba pool to become dominated by barite through precipitation and enriched in refractory bound Ba.

### 6.4.4 Conclusions

The main conclusions drawn from this study are as follows:

- $Ba_{XS}$ formation in surface waters appears related to productivity, but appears to peak during periods of early decay of phytoplankton when barite is formed.
- Standing stocks of $Ba_{XS}$ in sea ice are consistently an order of magnitude higher than surface waters and display higher than average Ba:POC ratios than surface waters.
- The formation of barite in the water column appears to be linked to the decay of organic matter and precipitation of barite in supersaturated micro-environments.
- The flux of $Ba_{XS}$ relative to carbon in the coastal Antarctic sea ice environment is consistent with algorithms published for the open ocean.
- The conceptual model described in this chapter provides detail on particulate Ba transformations and fluxes in response to sea ice cover and productivity over a full seasonal cycle.

## 6.5 References

Alldredge, A.L., Passow, U., Logan, B.E., 1993. The Abundance and Significance of a Class of Large, Transparent Organic Particles in the Ocean. Deep-Sea Research Part I-Oceanographic Research Papers 40 (6), 1131-1140.

Arrigo, K.R., Worthen, D.L., Lizotte, M.P., Dixon, P., Dieckmann, G., 1997. Primary production in Antarctic sea ice. Science 276 (5311), 394-397.

Bernstein, R.E., Byrne, R.H., 2004. Acantharians and marine barite. Marine Chemistry 86 (1-2), 45-50.

Bertram, M.A., Cowen, J.P., 1997. Morphological and compositional evidence for biotic precipitation of marine barite. Journal of Marine Research 55 (3), 577-593.

Bishop, J.K.B., 1988. The Barite-Opal-Organic Carbon Association in Oceanic Particulate Matter. Nature 332 (6162), 341-343.

Clarke, A., Leakey, R.J.G., 1996. The seasonal cycle of phytoplankton, macronutrients, and the microbial community in a nearshore Antarctic marine ecosystem. Limnology and Oceanography 41 (6), 1281-1294.

Clarke, A., Meredith, M.P., Wallace, M.I., Brandon, M.A., Thomas, D.N., 2007. Seasonal and interannual variability in temperature, chlorophyll and macronutrients in northern Marguerite Bay, Antarctica. Deep Sea Research Part II: Oceanographic Research Papers in press.

Dehairs, F., Baeyens, W., Goeyens, L., 1992. Accumulation of Suspended Barite at Mesopelagic Depths and Export Production in the Southern-Ocean. Science 258 (5086), 1332-1335.

Dehairs, F., Fagel, N., Antia, A.N., Peinert, R., Elskens, M., Goeyens, L., 2000. Export production in the Bay of Biscay as estimated from barium - barite in settling material: a comparison with new production. Deep-Sea Research Part I-Oceanographic Research Papers 47 (4), 583-601.

Dehairs, F., Shopova, D., Ober, S., Veth, C., Goeyens, L., 1997. Particulate barium stocks and oxygen consumption in the Southern Ocean mesopelagic water column during spring and early summer: Relationship with export production. Deep-Sea Research Part Ii-Topical Studies in Oceanography 44 (1-2), 497-516.

Dehairs, F., Stroobants, N., Goeyens, L., 1991. Suspended Barite as a Tracer of Biological-Activity in the Southern-Ocean. Marine Chemistry 35 (1-4), 399-410.

Ducklow, H.W., Erickson, M., Kelly, J., Smith, R.C., Stammerjohn, S.E., Vernet, M., Karl, D.M., 2007. Particle flux from the upper ocean over the continental shelf of the Western Antarctic Peninsula: A long term record,

1992-2006. Deep Sea Research Part II: Topical Studies in Oceanography in press.

Ducklow, H.W., Fraser, W., Karl, D.M., Quetin, L.B., Ross, R.M., Smith, R.C., Stammerjohn, S.E., Vernet, M., Daniels, R.M., 2006. Water-column processes in the West Antarctic Peninsula and the Ross Sea: Interannual variations and foodweb structure. Deep Sea Research Part II: Topical Studies in Oceanography 53 (8-10), 834-852.

Dymond, J., Collier, R., 1996. Particulate barium fluxes and their relationships to biological productivity. Deep-Sea Research Part Ii-Topical Studies in Oceanography 43 (4-6), 1283-&.

Dymond, J., Suess, E., Lyle, M., 1992. Barium in deep-sea sediment: A geochemical proxy for paleoproductivity. Paleoceanography 7 (2), 163-181.

Eicken, H., 1992. The Role of Sea Ice in Structuring Antarctic Ecosystems. Polar Biology 12 (1), 3-13.

Fagel, N., Andre, L., Dehairs, F., 1999. Advective excess Ba transport as shown from sediment and trap geochemical signatures. Geochimica et Cosmochimica Acta 63 (16), 2353-2367.

Fagel, N., Dehairs, F., Peinert, R., Antia, A., Andre, L., 2004. Reconstructing export production at the NE Atlantic Margin: potential and limits of the Ba proxy. Marine Geology 204 (1-2), 11-25.

Francois, R., Altabet, M.A., Yu, E.F., Sigman, D.M., Bacon, M.P., Frank, M., Bohrmann, G., Bareille, G., Labeyrie, L.D., 1997. Contribution of Southern Ocean surface-water stratification to low atmospheric CO2 concentrations during the last glacial period. Nature 389 (6654), 929-935.

Francois, R., Honjo, S., Manganini, S.J., Ravizza, G.E., 1995. Biogenic Barium Fluxes to the Deep-Sea - Implications for Paleoproductivity Reconstruction. Global Biogeochemical Cycles 9 (2), 289-303.

Ganeshram, R.S., Francois, R., Commeau, J., Brown-Leger, S.L., 2003. An experimental investigation of Barite formation in seawater. Geochimica et Cosmochimica Acta 67 (14), 2599-2605.

Ganeshram, R.S., Pedersen, T.F., 1998. Glacial-interglacial variability in upwelling and bioproductivity off NW Mexico: Implications for quaternary paleoclimate. Paleoceanography 13 (6), 634-645.

Ganeshram, R.S., Pedersen, T.F., Calvert, S.E., Murray, J.W., 1995. Large Changes in Oceanic Nutrient Inventories from Glacial to Interglacial Periods. Nature 376 (6543), 755-758.

Garrity, C., Ramseier, R.O., Peinert, R., Kern, S., Fischer, G., 2005. Water column particulate organic carbon modeled fluxes in the ice-frequented Southern Ocean. Journal of Marine Systems 56 (1-2), 133-149.

Jacquet, S.H.M., Dehairs, F., Elskens, M., Savoye, N., Cardinal, D., 2006. Barium cycling along WOCE SR3 line in the Southern Ocean. Marine Chemistry.

Kim, D., Kim, D., Park, J. and Kim, Y., 2005. Interannual variation of particle fluxes in the eastern Branfield Straight, Antarctica: A response to the sea ice distribution. Deep-Sea Research Part I

Krembs, C., Engel, A., 2001. Abundance and variability of microorganisms and transparent exopolymer particles across the ice-water interface of melting first-year sea ice in the Laptev Sea (Arctic). Marine Biology 138 (1), 173-185.

Lourey, M.J., Trull, T.W., Tilbrook, B., 2004. Sensitivity of delta C-13 of Southern Ocean suspended and sinking organic matter to temperature, nutrient utilization, and atmospheric CO2. Deep-Sea Research Part I-Oceanographic Research Papers 51 (2), 281-305.

McManus, J., Berelson, W.M., Klinkhammer, G.P., Johnson, K.S., Coale, K.H., Anderson, R.F., Kumar, N., Burdige, D.J., Hammond, D.E., Brumsack, H.J., McCorkle, D.C., Rushdi, A., 1998. Geochemistry of barium in marine sediments: Implications for its use as a paleoproxy. Geochimica et Cosmochimica Acta 62 (21-22), 3453-3473.

McManus, J., Dymond, J., Dunbar, R.B., Collier, R.W., 2002. Particulate barium fluxes in the Ross Sea. Marine Geology 184 (1-2), 1-15.

Meiners, K., Gradinger, R., Fehling, J., Civitarese, G., Spindler, M., 2003. Vertical distribution of exopolymer particles in sea ice of the Fram Strait (Arctic) during autumn. Marine Ecology-Progress Series 248, 1-13.

Monnin, C., Jeandel, C., Cattaldo, T., Dehairs, F., 1999. The marine barite saturation state of the world's ocean. Marine Chemistry 65, 253-261.

Nurnberg, C.C., Bohrmann, G., Schluter, M., Frank, M., 1997. Barium accumulation in the Atlantic sector of the Southern Ocean: Results from 190,000-year records. Paleoceanography 12 (4), 594-603.

Perovich, D.K., Elder, B.C., Claffey, K.J., Stammerjohn, S., Smith, R., Ackley, S.F., Krouse, H.R., Gow, A.J., 2004. Winter sea-ice properties in Marguerite Bay, Antarctica. Deep-Sea Research Part Ii-Topical Studies in Oceanography 51 (17-19), 2023-2039.

Reitz, A., Pfeifer, K., de Lange, G.J., Klump, J., 2004. Biogenic barium and the detrital Ba/Al ratio: a comparison of their direct and indirect determination. Marine Geology 204 (3-4), 289-300.

Schenau, S.J., Prins, M.A., De Lange, G.J., Monnin, C., 2001. Barium accumulation in the Arabian Sea: Controls on barite preservation in marine sediments. Geochimica et Cosmochimica Acta 65 (10), 1545-1556.

# 7 Reconstructing paleoproductivity throughout the Holocene: A case study from Adélie Land, East Antarctica


## Abstract

Marine sediment cores with high accumulation rates are attractive to ocean and climate scientists, as they present an opportunity to study changes in paleoproductivity, ocean circulation, sea ice extent and seasonality at very high resolution. Piston core MD03-2601, retrieved from a depression in the Dumont D'Urville Trough in East Antarctica presents a 40 m long Holocene core with an average sedimentation rate of 04cm.yr$^{-1}$. However this core, was severely influenced by sediment focusing (ψ). Therefore, to be able to accurately quantify mass fluxes in this region, careful correction using $^{230}$Th normalisation was carried out. Using the corrected preserved fluxes, carbon, opal and excess Ba ($Ba_{XS}$) flux reconstructions were carried out to test the validity of using such proxies on a core heavily affected by ψ. In addition $Mo_{auth}$ and $U_{auth}$ were used to monitor the redox conditions in the sediment, to identify where the $Ba_{XS}$ record may have been compromised as preservation of the $Ba_{XS}$ signal in reducing sediments is highly variable and can decouple from the actual carbon flux this tracer is supposed to record. The results show increased levels of productivity and export production during the mid-Holocene warm period based on the carbon and opal fluxes, with sedimentary conditions becoming periodically reducing during these high flux periods, although the increasing paleo-oxygenation of deep waters during this period probably helped to prevent full anoxia ensuing. The reducing conditions, however, precluded the use of the $Ba_{XS}$ proxy as a quantitative tracer of carbon flux, although it did appear to trace some of the changes in carbon flux over the Holocene. In addition, we observe decoupling of the carbon and opal proxies, with increased opal:carbon ratios during the mid-Holocene warm period occurring as the larger diatoms such as *F. kerguelensis* dominating during this warmer period of reduced sea ice extent. This study therefore highlights how sediment cores heavily affected by ψ can be useful for tracing changes in paleoproductivity at high resolution.

## 7.1 Introduction

Reconstructing past productivity regimes in the Southern Ocean is of great importance in order to understand how it influenced or responded to changes in climate, for example during the different climatic periods of the Holocene (Hodell, et al., 2001; Nielsen, et al., 2004) or on glacial to interglacial timescales (Anderson, et al., 2002; Sigman and Boyle, 2000). A wide variety of elemental and isotopic tracers have been developed and used on the many sediment cores taken in the Southern Ocean to detect changes in various ocean processes including; productivity, nutrient utilisation, sea ice extent, vertical mixing and macronutrient and micronutrient availability (Anderson et al., 1998; Bentaleb et al., 1996; Crosta et al., 2005a; Crosta et al., 1998; Crosta and Shemesh 2002; Crosta et al., 2004; De La Rocha et al., 1998; Elderfield and Rickaby, 2000; Ellwood and Hunter, 2000; Francois and Altabet, 1992; Francois et al., 1997; Kumar et al., 1995; Nurnberg et al., 1997; Robinson et al., 2005; Rosenthal et al., 2000; Wolff et al., 2006).

Core MD03-2601 taken from the Dumont d'Urville trough, East Antarctica, is a 40 m long sequence of laminated diatom ooze that covers the Holocene period and has an exceptionally high sedimentation rate. The goal of this study was to study a suite of paleoproxies on this core in an attempt to accurately constrain paleoproductivity during the different climatic periods of the Holocene. The Holocene period in this region is divided into four general climatic phases: an early Holocene warm period (8.5-11 cal ka BP), an early Holocene cool event (7-8.5 cal ka B.P.), a mid-Holocene warm period (3.5-7 cal ka B.P.), and a late Holocene Neoglacial (1.0-3.5 cal ka B.P), (Crosta et al., 2007).

Cores with a high sedimentation rates are attractive to paleoceanographers as they provide the chance to study sediment records at very high resolution, thus providing the chance to better constrain the interactions between Antarctic atmosphere, oceans, sea ice and glaciers, deep ocean circulation and teleconnections between high and low latitudes. Unfortunately, such

cores are more often than not affected by processes such as sediment focusing that may significantly interfere with reconstructing vertical accumulation rates and subsequent estimations of carbon and opal export and lead to problems constructing an accurate age model. This is a case study to assess the validity of elemental based export flux reconstructions in core MD03-2601.

## 7.2 Proxies

The following proxies for productivity and redox sensitive elements were used for the multi-proxy assessment of this core.

The carbon content of sediment cores has been widely used as a paleoproductivity proxy in the global ocean (Chase et al., 2003; Crosta et al., 2005b; Crosta et al., 2002; Ganeshram et al., 1995). This proxy works on the assumption that the preserved carbon in the sediment can be used in conjunction with the mass accumulation rate (MAR) to calculate the export of carbon to the deep ocean, although great care must be taken when determining the mass accumulation rates (Francois et al., 2004). The carbon proxy should be used carefully as it is use as a paleoproductivity tracer assumes a consistent level of preservation over time, with variable preservation limiting the quantitative value of such reconstructions.

The opal content of sediment cores has also been a popular tool for paleoproductivity reconstructions in the global ocean (Chase et al., 2003; Bareille et al., 1998; Ganeshram and Pedersen, 1998). This proxy works on the same calculation principle as carbon, and is a useful additional tool for studying regions dominated by diatoms to assess the export of silicate from the surface ocean. Once again, care should be taken with this tracer of paleoproductivity as the reconstruction assumes a consistent level of preservation over time though some attempts have been made to correct for differential preservation (Dézileau et al., 2000).

Barite formation in the marine water column and its flux to the seafloor appear linked to surface productivity and carbon export (Bishop 1988; Dehairs et al., 1992; Dehairs et al., 2000; McManus et al., 1998). Thus the reconstruction of carbon export based on barium content of sediments may provide quantitative information about past changes in primary production (Francois *et al.*, 1997; Ganeshram and Pedersen, 1998; Ganeshram *et al.*, 1995). A host of previous studies utilising sediment traps monitoring fluxes of carbon and excess Ba (barium of biogenic origin – $Ba_{XS}$) have produced preliminary algorithms linking the flux of biogenic barium to carbon export production (Dymond *et al.*, 1992; Francois *et al.*, 1995; McManus *et al.*, 2002; Nurnberg *et al.*, 1997). Although relationships between Ba flux and organic carbon flux are poorly constrained in near shore areas (Dehairs et al., 2000; Fagel et al., 1999; Francois et al., 1995), a recent sediment trap study in the Western Antarctic Peninsula (Carson et al., in-prep) has identified that $Ba_{XS}$ and carbon flux show relationships that are consistent with the previously published preliminary algorithms (Dymond and Collier, 1996; Francois et al., 1995). This study therefore uses sedimentary $Ba_{XS}$ as a tracer for changes in carbon flux to the sea floor.

Both Authigenic molybdenum ($Mo_{auth}$) and authigenic uranium ($U_{auth}$) enrichments are associated with the delivery of carbon to the seafloor and dissolved oxygen content at the sediment water interface (McManus, et al., 2006; Morford et, al., 1999; Morford, et al., 2005). When low sedimentary dissolved oxygen leads to reducing conditions, soluble U (VI) is reduced into insoluble U(IV), resulting in $U_{auth}$ precipitation (McManus, et al., 2006). Similarly, $Mo_{auth}$ in reducing sediments is precipitated in the presence of sulphur (Calvert and Pedersen, 1993) where soluble Mo is converted to a more particle reactive thiomolybdate (Erickson and Helz, 2000; Zheng et al., 2000) which are scavenged from sulphur containing organic material, or reacts in association with Fe-S phases (Erickson and Helz 2000; Helz, et al., 1996). In highly reducing and carbon rich sediments, the degree of $Mo_{auth}$ enrichment compared to carbon delivery to the seafloor has been observed

to be much higher than that of $U_{auth}$ (McManus et al., 2006), thought to be as a result of increased sulphur cycling and removal of Mo from pore waters with no change in reduction of U(VI). These redox sensitive elements are therefore used in to trace any changes in redox conditions in core MD03-2601.

## 7.3 Materials and Methods

Piston Core MD03-2601 was retrieved from the Dumont D'Urville Trough, Adélie Land East Antarctica during the Images X cruise in February 2003. The core was retrieved aboard the Marion Dufresne II at 66°03.07'S, 138°33.43'E at a water depth of 746 m (Figure 7.1).

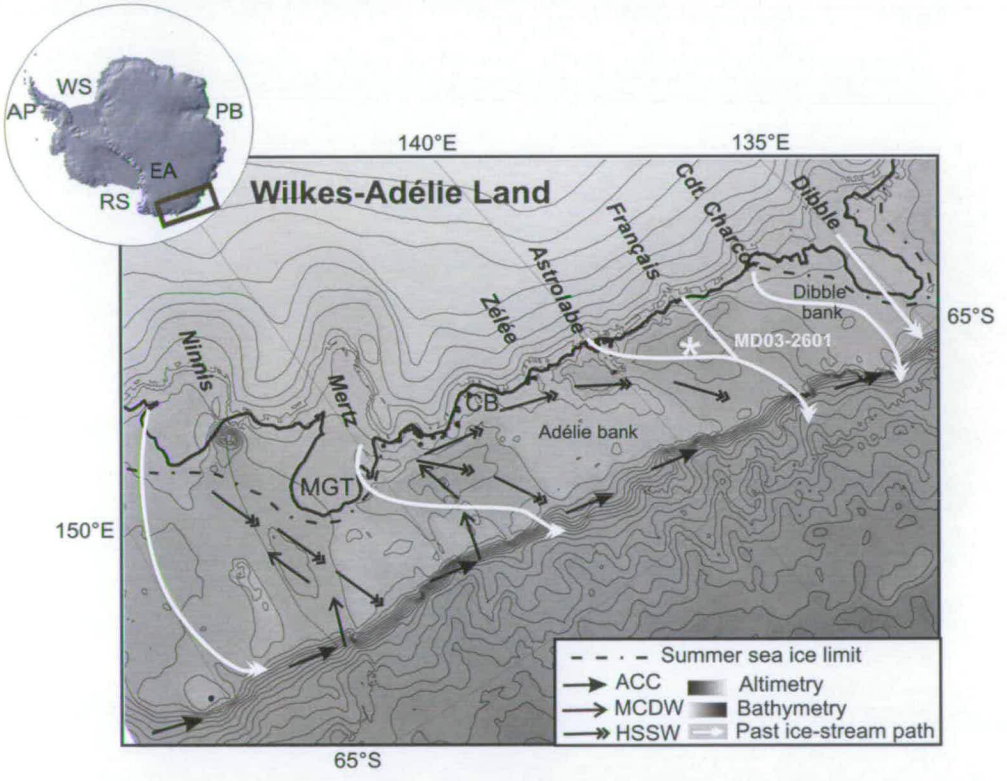


**Figure 7.1. Location of core MD03-2601, limit of summer sea ice, location of glaciers and ice streams, detail of oceanographic currents and different water masses. DDU Dumont d'Urville Base; ACC, Antarctic Circumpolar Current; MCDW, Modified Circumpolar Deep Water, HSSW, High Salinity Shelf Water. Winter sea ice covers the whole oceanic area encompassed by the map.**

The Dumont d'Urville Trough is composed of a number of small depressions reaching a maximum depth of 1000 m (De Santis et al., 2003) that each act

as "funnels" for sinking organic material produced in the area, which improves preservation of phytoplankton cells, that are here mainly composed of diatoms (Wright and van den Enden, 2000). Core MD03-2601 is composed of diatom ooze that alternated between structureless green ooze and green to dark green laminations of millimetre to centimetre thickness (Denis et al., 2006).

### 7.3.1 Age Model

We use the same age model described in Denis et al., (submitted), that used the Calib 5.0 software, the marine calibration Marine04 and a reservoir age of 1300 years as advised for this region. Core MD03-2601 records the last 11-1 cal ka BP period with an average sedimentation rate of 0.4 $cm.yr^{-1}$.

### 7.3.2 Diatom Census Counts

Diatoms were identified were identified every 4 to 8 cm providing a 10 to 20 year resolution (Crosta et al., 2007). Diatom counts followed Schrader and Gersonde (1978) and Laws (1983). More details about slide preparation, diatom identification and are found in Crosta et al., (2004). Around 350 diatom valves were counted in each sample and the relative abundance of each was determined as the fraction of diatom species against total diatom abundance in the sample, here the *Fragilariopsis kerguelensis* are extracted from the total diatom counts.

### 7.3.3 Organic Carbon and Biogenic Opal Measurements

Organic carbon measurements were conducted every 4 cm to 8 cm. The method is described in (Crosta et al., 2005a). Organic carbon content was measured using a Carlo Erba 2500 elemental analyser. Results were checked for internal consistency using calibrated laboratory standards such as Acetanilide, Glycine and Casein. The mean standard deviation of the carbon content is ±0.03%.

Biogenic opal measurements were conducted every 32 cm. Biogenic opal measurements follow a protocol slightly modified from Mortlock and Froelich,

(1989) in which biogenic opal was dissolved in a 0.5 M NaOH solution. Absorbance of the samples was measured each hour for 5 hours to build a dissolution curve (Muller and Schneider, 1993) and then calibrated using five standards of increasing silica concentration and a blank. More details can be found in Crosta et al. (2005a).

### 7.3.4 Elemental Analysis

Elemental analyses were determined using the methods described in (Fitton, et al., 1998) at 32 cm resolution for aluminium (Al), molybdenum (Mo) and barium (Ba). Standard deviations are 0.05 % for Al, 5.8 % for Mo, and 5 ppm for Ba. Although it should be noted that major element precision is governed more by reproducibility in making the glass disc than by counting statistics.

Excess barium, or $Ba_{XS}$ (also known as biogenic barium) was calculated using the following formula (Francois, et al., 1995),

$$Ba_{XS} = Ba_{total} - (Ba/Al_{terrigenous} \times Al_{total})$$

Where $Ba_{total}$ is the total barium content of sediment, $Ba/Al_{terrigenous}$ is 0.0067 for the Southern Ocean (Nurnberg, et al., 1997) and $Al_{total}$ is the total aluminium content of sediment.

Authigenic Mo ($Mo_{auth}$) was calculated using the following formula (Morford and Emerson 1999),

$$Mo_{auth} = Mo_{total} - (Mo/Al_{terrigenous} \times Al_{total})$$

### 7.3.5 Sediment fluxes normalisation

Regions of high sedimentation are often areas that are affected by lateral input of sediment, termed "sediment focusing", and this effect is often intensified by deep water currents (Francois et. al, 2004). In order to reconstructed unbiased biogenic fluxes deposited, we use high-resolution

measurements of $^{230}Th$ (n= 60; Denis et al., submitted) to normalize the opal, carbon and barium percentage contents, following the method developed by Bacon (1984). This method is based on the "assumption that the flux of scavenged $^{230}Th$ reaching the seafloor is know and equal to the rate of $^{230}Th$ production from the decay of $^{234}U$ in the overlying water column" (Francois et al., 2004). Thereby, the normalization of biogenic contents by instantaneous ratio of water column scavenged $^{230}Th$ flux allows an estimation of the mass flux deposition, unbiased by lateral sediment contribution and variations of one component on another, and less impacted by chronological errors (Bacon, 1984; Suman and Bacon; 1989; Francois et al., 2004; Adkins et al., 2006). Thereby, the $^{230}Th$ normalised fluxes resituate the "preserved" vertical fluxes ($^{PR}F_v$) i.e. the material that remained after diagenetic alteration, following :

$$^{PR}F_v = FW / (^{230}Th_{XS})_0$$

Where FW is the rate of $^{230}Th_{XS}$ production in the water column, and therefore its flux to the seafloor, and $(^{230}Th_{XS})_0$ is the measure of $^{230}Th_{XS}$ in the sediment sample.

The preserved vertical rain rate for each sedimentary component was determined using:

$$F_v = {}^{PR}Fv \times fi$$

where fi is the measured weight fraction of the constituent of interest in the sediment (here : opal, organic carbon and biogenic barium).

The application of this approach on active hydrodynamic shallow shelves close to a sea ice system like our study zone can implicate some precaution for using the $^{230}Th$ normalization. The boundary scavenging effect, defined by Spencer et al. (1981), leads to an advection of the $^{230}Th$ radioelement from

low flux zone to high flux zone, inducing an overestimating of radioisotopes inventoried in the sediments underlying high productive areas. Such mechanism can occur in our area from low productive zones as northward to Polar Frontal Zone as well as southward to Marginal Ice Zone, which can scavenge $^{230}$Th via MCDW (Rutgers van der Loeff and Berger, 1993) and/or HSSW (Henderson et al., 1999). Nevertheless, in regions of deep bottom water formation, the renewal of deep waters is more rapid than the residence time of $^{230}$Th (e.g. 40 years), as demonstrated in our area (Rintoul, 1998; Rintoul et al., 1999; Tanhua et al, 2004), leading to loss of $^{230}$Th by northward advection. Therefore, an excess of $^{230}$Th supply by boundary scavenging can be compensate by a loss of $^{230}$Th by high waters renewal, as previously illustrated in the Pacific sector (Chase et al., 2003).

Differential efficiency scavenging of Th has been highlighted in function to rain rate and particles type in several studies (Chase and Anderson, 2004 and references herein). Nevertheless, on the core MD03-2601, the fluxes based on $^{14}$C dates not show variations exceeding a factor 3 and the lithogenic/biogenic ratio differs only by a maximum factor of 1.5 (data not shown). These variations cannot explain the $^{230}$Th changes observed here because one order of magnitude fluxes changes is necessary to affect the scavenging of $^{230}$Th (Francois et al., 1990; Yu, 1994), and any relationships between $^{230}$Th content and different sediment components (opal, $C_{org}$, $N_{org}$ and lithogenic content) are displayed ($r^2 < 0.2$) (data not shown). The position of core MD03-2601 in a shallow environment implicate great detrital and authigenic contributions (respectively, 20 to 55 % and 1 to 23 % of the total $^{230}$Th) in comparison to the scavenged part of $^{230}$Th. Therefore the absolute values of $\Psi$ and of normalized flux reconstructions should be treated with some caution (see error bar on Figure 7.2).

In conclusion, we believe that the $^{230}$Th normalization can be confidently used to document the relative changes of biogenic fluxes over the core site during the Holocene.

## 7.4 Results

Sediment focusing factors (Ψ), classical mass accumulation rates (MAR), $^{230}$Th excess normalised fluxes and diatom abundances are presented in Figure 7.2. The MAR range from 50 to 175 mg/cm$^2$/yr and follow the variations of sediment focusing, whereas the $^{230}$Th normalised MAR show an opposite pattern with much lower values of 2 to 9 mg/cm$^2$/yr. Total diatom abundances follow the same pattern as $^{230}$Th normalised vertical flux, with values ranging from 112 – 2041 x 10$^6$ valves per gram of sediment.

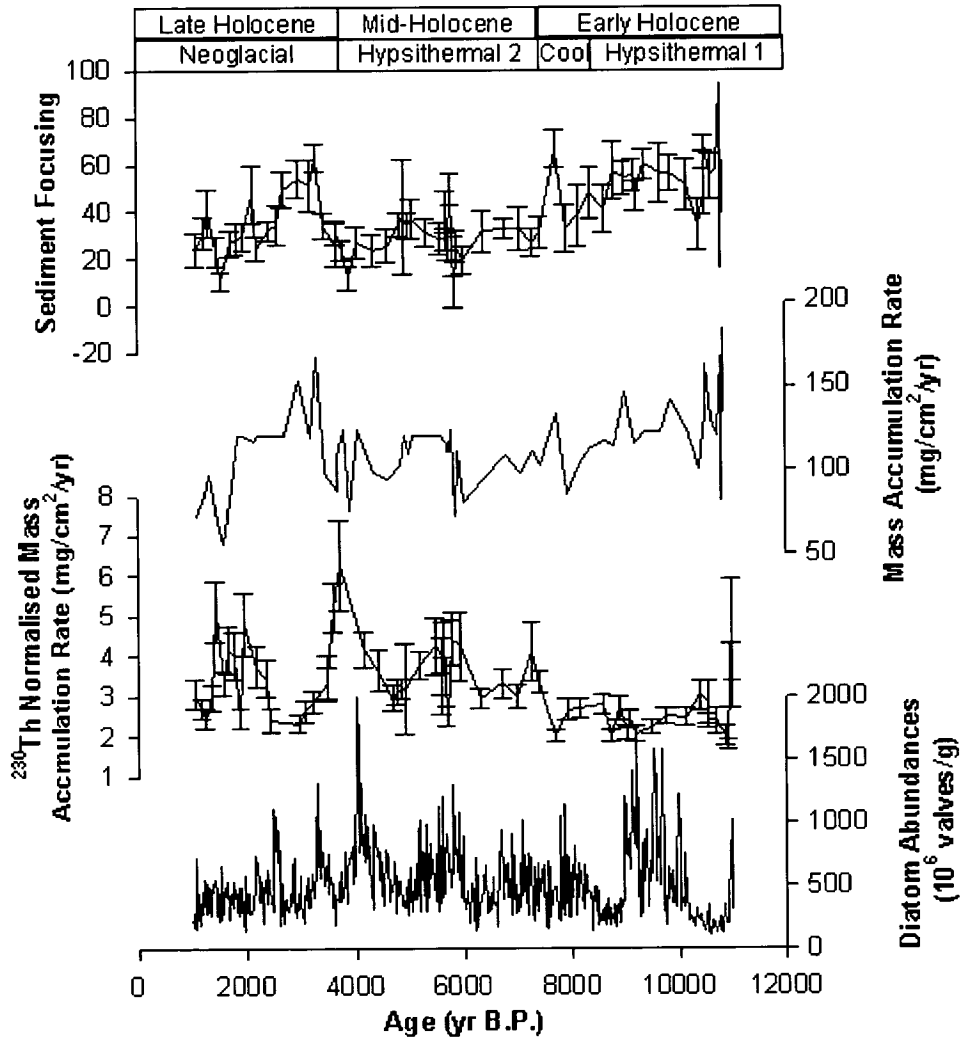


**Figure 7.2. Down-Core profiles of (a) Sediment Focusing (b) Mass accumulation rate, (c) $^{230}$Th normalised mass accumulation rate and (d) Diatom abundances.**

**Boxes at the top of the figure represent the different climatic periods of the Holocene (Denis et al., submitted)**

Carbon and opal data are presented in Figure 7.3. Carbon and opal percentages are plotted alongside $^{230}Th$ normalised vertical flux reconstructions. Carbon and opal percentages show slightly different patterns throughout the Holocene that disappear when they are converted in fluxes by the $^{230}Th$ normalisation. Vertical flux reconstructions of carbon and opal show relatively low values during the early Holocene warm period (11 – 9 cal ka BP), ranging from 0.03 – 0.06 mg/cm2/yr and 0.9 – 2.0 mg/cm2/yr for carbon and opal, respectively. During the cool event (8.5 – 7 cal ka BP), the fluxes of carbon and opal show an increasing trend reaching 0.04 mg/cm2/yr and 1.4 $mg/m^2.yr$ for carbon and opal, respectively.

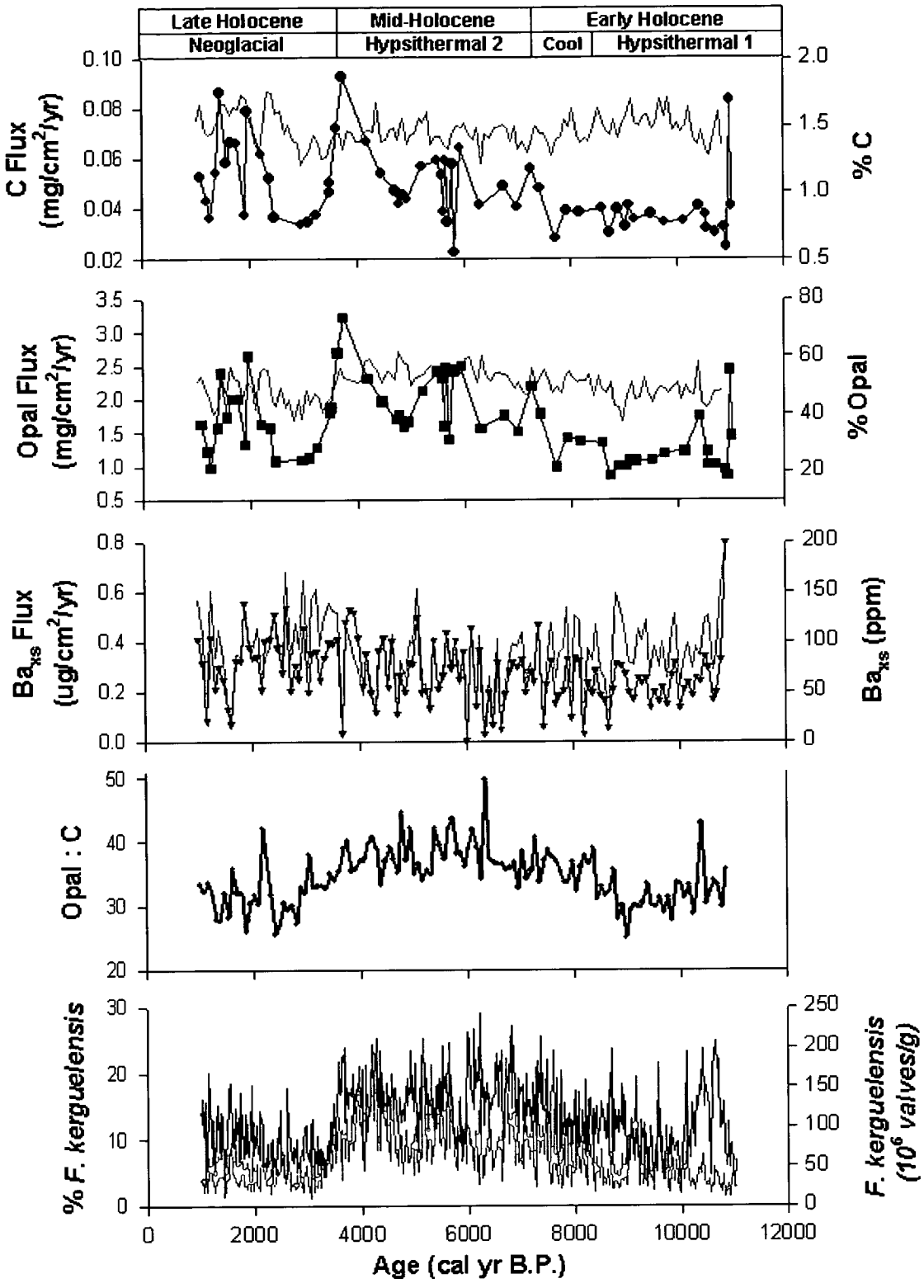


**Figure 7.3. Down-Core profiles of (a) $^{230}$Th normalised carbon flux and % C content of sediment, (b) $^{230}$Th normalised opal flux and % opal content of the sediment, (c) $^{230}$Th normalised $Ba_{XS}$ flux and $Ba_{XS}$ concentration of sediment, (d) opal:C ratios and (e) *% F. kerguelensis* of the total diatom community and *F. kerguelensis* abundances.**

The mid-Holocene warm period (7 – 3.5 cal ka BP) generally show much higher vertical fluxes of carbon and opal ranging from 0.03 – 0.07 mg/cm2/yr and 1.0 – 2.6 mg/cm2/yr, respectively, with two distinct peaks. The late Holocene Neoglacial (3.5 – 1 cal ka BP) are characterised by reduced fluxes as low as 0.03 mg/cm2/yr for carbon and 1.0 mg/cm2/yr BP for opal. There were, however, two flux peaks during the Neoglacial centred at 1.5 and 2.3 cal ka BP, reaching 0.09 mg/cm2/yr for carbon and 3.2 mg/cm$^2$/yr for opal.

$Ba_{XS}$ data are also presented in Figure 7.3 with $Ba_{XS}$ plotted alongside $^{230}Th$ normalised vertical flux reconstructions of $Ba_{XS}$. Normalised $Ba_{XS}$ fluxes range from 0.002 – 0.8 μg/cm$^2$/yr and display different patterns to the carbon and opal reconstructions. In addition to high amplitude variation throughout the core, significant $Ba_{XS}$ flux minima occur at 8.7 during the early Holocene warm period (11-8.5 cal ka BP), 8.2, 8.0 and 7.4 cal ka BP during the cool event (8.5 – 7 cal ka BP), at 6.7, 6.6, 6.5, 6.4, 6.3, 6.2, 6.0, 5.8, 5.3, 4.8, 4.7, 4.6, 4.3 and 3.7 cal ka BP during the mid-Holocene warm period (7 – 3.5 cal ka BP), and at 2.2, 1.6 and 1.2 cal ka BP during the late Holocene Neoglacial (3.5-1 cal ka BP).

Opal:Carbon ratios in Figure 7.3 show maximum values during the mid-Holocene warm period, and generally lower values during the early Holocene warm period and late Holocene Neoglacial. The overall pattern of opal:carbon is similar to the abundances and % of *F. kerguelensis*, also presented in Figure 3.

Figure 7.4 presents the $^{230}Th$ normalised vertical flux reconstructions of $Ba_{XS}$, $Mo_{auth}$, $U_{auth}$ and the $C_{org}$:$Ba_{XS}$ ratio of sediment. The $Mo_{auth}$ and $U_{auth}$ show large variation throughout the Holocene, with each plot displaying a decreasing trend during the mid-Holocene warm period. The $C_{org}$:$Ba_{XS}$ plot displays a fairly consistent flat pattern, apart from distinct peak values occurring in concert with the lows in $Ba_{XS}$ vertical flux reconstructions.

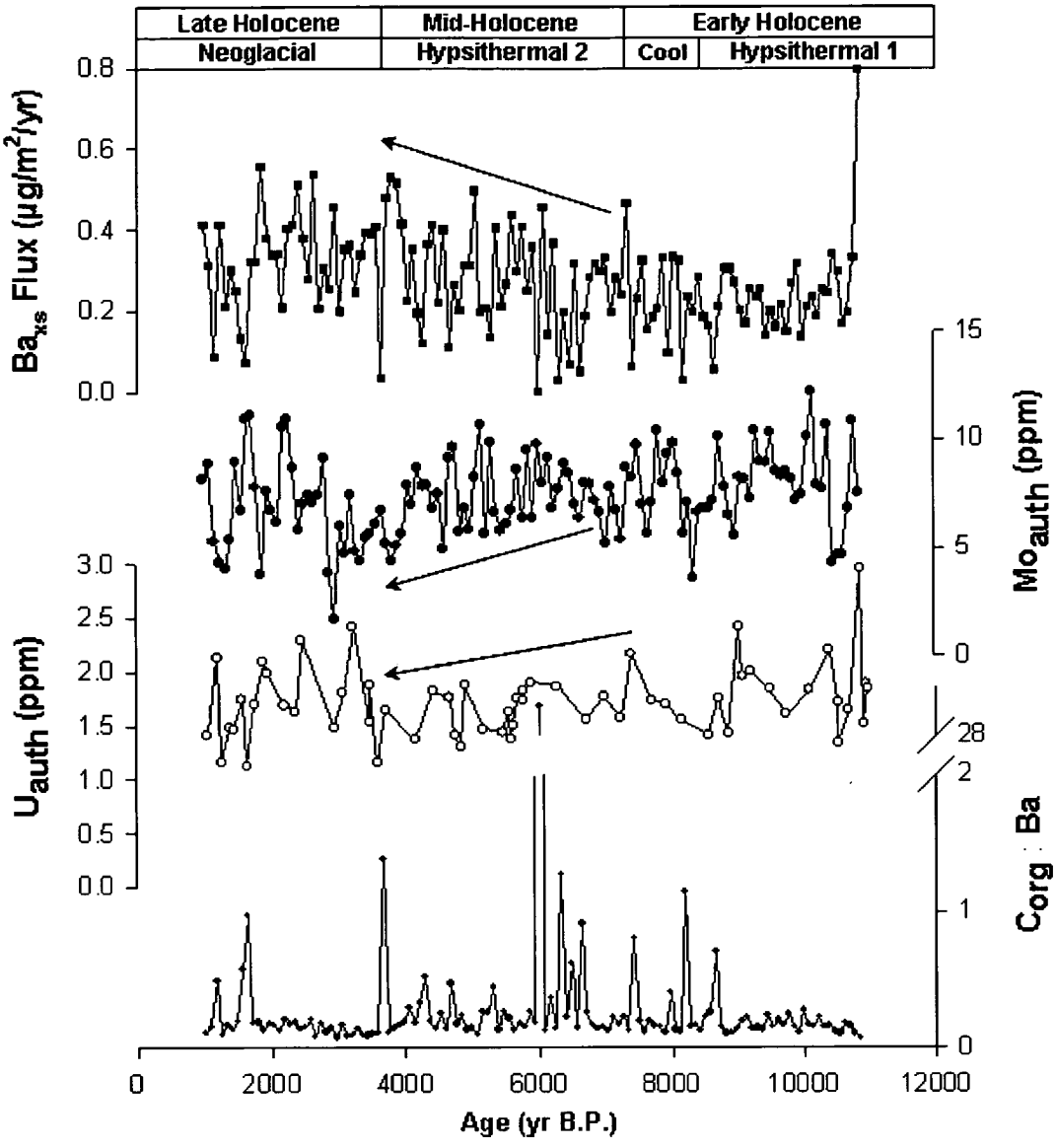


**Figure 7.4. Down-Core profiles of (a) $^{230}$Th normalised $Ba_{XS}$ fluxes, (b) $Mo_{auth}$, (c) $U_{auth}$, and (d) $C_{org}$:Ba ratio of sediment. Lines show increasing $Ba_{XS}$ fluxes and decreasing $U_{auth}$ and $Mo_{auth}$ during the mid-Holocene warm period.**

## 7.5 Discussion

### 7.5.1 Biogenic Flux Reconstructions

Core MD03-2601 has an exceptionally high sedimentation rate (average of 0.4 cm.yr$^{-1}$), implying that it would be an excellent candidate for studying changes in Holocene paleoproductivity at high resolution. However, closer inspection using the $^{230}$Th tracer (Denis et al., submitted) reveals that the

extent of focusing far outweighs the vertical sedimentary fluxes at the core site (Figure 7.2), a common occurrence in such margin systems. This required normalisation by $^{230}Th$ in order to reconstruct the vertical fluxes. The reconstructions of vertical carbon and opal fluxes (Figure 7.3) show good agreement with down-core abundances of diatoms, the major phytoplankton group in this region (Figure 7.2). These records therefore appear to be good indicators of paleoproductivity in the Dumont D'Urville Trough during the Holocene. Despite the uncertainty associated to our quantitative estimations of the vertical biogenic fluxes buried, they agree well with modern studies (Table 7.1). This method of normalisation guarantees the reconstruction of preserved material in the core, but not the total export flux (François et al., 2004). Indeed, modern studies on the continental shelf of Antarctica show that less than 0.2% and 6% of organic carbon and opal, respectively, produced by phytoplankton is permanently buried in the sea bed (Nelson et al., 1996).

The ratios between our buried fluxes of organic carbon and opal with surface production estimated in our area by remote sensing (Arrigo et al., 2003) and water sampling (Beucher et al., 2004) are consistent with the other overall preservation efficiency data (OPE) observed in the coastal and continental shelf zones (CCSZ). The OPE of organic carbon and biogenic silica are relatively high (~0.8% and ~5.5% respectively) but the Si/C ratio in buried sediment (~7 and ~30 as mass and molar ratios, respectively) agrees well with previous studies in the area (Nelson et al., 1996).

The reconstructed $Ba_{XS}$ fluxes do show similar patterns to the opal and carbon profile, but exhibit more variation than the carbon and opal record, and frequent occurrences of $Ba_{XS}$ minima concentrated during the early Holocene cool period and mid-Holocene warm period. The decoupling of the carbon and opal proxies from the $Ba_{XS}$ proxy is thought to be caused by changes to redox conditions in the sediment, that were traced using the redox sensitive elements $Mo_{auth}$ and $U_{auth}$, with enrichment of these elements

linked to organic carbon delivery to the seafloor and reducing conditions in the sediment (McManus et al., 2006).

Table 7.1.

| | | Organic carbon (Flux in molC.$m^{-2}/yr^{-1}$) | | | Opal (Flux in molSi.$m^{-2}/yr^{-1}$) | | |
|---|---|---|---|---|---|---|---|
| **Location** | **Study** | **Production** | **$^{230}$Th-normalised accumulation** | **Overall Preservation Efficiency** | **Production** | **$^{230}$Th-normalised accumulation** | **Overall Preservation Efficiency** |
| Indian Sector - PFZ | Pondaven et al., 2000 | - | - | - | 2.43 | 0.075 | 3.1 |
| Indian Sector - POOZ | Pondaven et al., 2000 | - | - | - | 3.34 | 0.21 | 6.3 |
| Indian Sector - SIZ | Pondaven et al., 2000 | - | - | - | 1.62 | - | - |
| Pacific Sector - PFZ | Nelson et al., 2002 | 6.9 | 0.0012 | 0.017391304 | 0.35 | 0.016 | 4.57 |
| Pacific Sector - POOZ | Nelson et al., 2002 | 8.5 | 0.0017 | 0.020 | 0.95 | 0.048 | 5.05 |
| Pacific Sector - SIZ | Nelson et al., 2002 | 8.7 | 0.0062 | 0.071 | 2.4 | 0.16 | 6.67 |
| Ross Sea - CCSZ | Nelson et al., 1996 | 11.87 | 0.02* | 0.18 | 2.02 | 0.12* | 5.75 |
| DDU - CCSZ ** | Beucher et al., 2004 + this study | - | - | - | 5.184 | **0.275** | **5.30** |
| DDU - CCSZ | Arrigo and Van Dijken, 2003 + this study | 4.64+/-1.15 | **0.473** | **0.85** | - | - | - |

### 7.5.2 Preservation Versus Export/Production Changes

$Mo_{auth}$ and $U_{auth}$ profiles in core MD03-2601 display high variation during the Holocene, but both exhibit a general decreasing trend, especially during the mid-Holocene warm period (Figure 7.4). $Mo_{auth}$ and $U_{auth}$ in core MD03-2601 are affected by both changes to the delivery of carbon to the seafloor and changes to the intensity of deep water currents. Increased export of carbon is evident during the mid-Holocene warm period (Figure 7.3), as is increasing deep water formation reconstructed from sortable silt (Denis et al., submitted), showing an abrupt weakening of deep water formation and bottom water oxygenation at ~7.5 cal ka BP, followed by a steady increase up until 1 cal ka BP. Focusing on the 7.5-4.0 cal ka BP period, the redox proxy data from this study are in agreement with the reconstructed paleo-oxygenation of bottom waters. The long term millennial trends of both $Mo_{auth}$ and $U_{auth}$ show a decreasing trend during this period (Figure 7.4). Therefore, at the Holocene scale, the variations of paleoproductivity evidenced here by $^{230}Th$ normalised biogenic fluxes reflect certainly changes of water column processes (i.e. production/remineralisation/export) than differential preservation at the sediment/water interface.

However, on shorter centennial time-scales there are episodic enrichments of both $Mo_{auth}$ and $U_{auth}$ that were likely caused by higher delivery of organic material to the seafloor, resulting in reducing conditions irrespective of active deep water ventilation. When organic sediment loads to the seafloor drive conditions towards anoxia, the enrichment of $Mo_{auth}$ relative to carbon can increase by up to 5 times compared to oxic conditions thought to be as a result of more intense sulphur cycling, where little or no change is observed in $U_{auth}$ (McManus et al., 2006). This is consistent with many of the sharp peaks in $Mo_{auth}$ in core MD03-2601, especially during the mid-Holocene warm period, not occurring in concert with peaks in $U_{auth}$. It should be noted that the sortable silt proxy from Denis et al (submitted) and $U_{auth}$ were measured at lower resolution than the $Mo_{auth}$, so the $Mo_{ath}$ may capture

higher resolution changes in sediment redox chemistry but does not allow direct comparison with SS and $U_{auth}$.

### 7.5.3 $Ba_{XS}$ Proxy Sensitivity

Reducing conditions severely compromise the preservation of barite in marine sediments (McManus et al., 1998; Schenau et al., 2001) and such conditions appear to have affected the $Ba_{XS}$ proxy in this core. This precludes the assumption made with the $Ba_{XS}$ proxy that preservation in the sediment record is predictable or consistent. Preservation in oxic sediments is usually very good as pore waters are generally considered to be saturated with dissolved Ba, resulting in low barite dissolution (Dymond et al., 1992). However in reducing sediments, sulphate reduction during the oxidation of organic matter will reduce sulphate concentrations in sediments to a value that promotes remobilisation of Ba through dissolution of barite ($BaSO_4$), resulting in increased dissolved Ba concentrations in sediment pore waters (McManus et al., 1998; Schenau et al., 2001). This can also lead to re-precipitation of barite below the sulphate reduction layer, which may skew both sections (sulphate reducing and oxic sediment below) for latter day reconstruction.

Although the $Mo_{auth}$ and $U_{auth}$ data are consistent with periods of reducing conditions during the Holocene, thus precluding a quantitative reconstruction of paleoproductivity using the $Ba_{XS}$ proxy, there is still some qualitative value in the data. During the early Holocene cool event and mid-Holocene warm period there is a general increasing trend in the reconstructed flux of $Ba_{XS}$, when the redox sensitive proxies $Mo_{auth}$ and $U_{auth}$ show a general decreasing trend. This observation is consistent with an increase in deep water currents and ALBW formation (Denis et al., submitted), and suggests that preservation of barium improved in the presence of better oxygenation of sediments. In Figure 4, the $C_{org}$:Ba ratio shows distinct peaks when the $Ba_{XS}$ fluxes display minima and the $Mo_{auth}$ display maxima. These peaks in $C_{org}$:Ba agree are consistent with reduced preservation of Ba during periods of sub-oxic diagenesis and sulphate reduction and lend support to the interpretation

of the redox sensitive proxies. Any interpretation based on $Ba_{XS}$, however, should therefore be treated with caution due to the lack of constraint on the variable preservation of $Ba_{XS}$ in sediments as a result of sedimentary oxygen deficiencies.

### 7.5.4 Opal:$C_{org}$ Decoupling

The opal:carbon ratio in Figure 3 highlights how opal and carbon decouple from one another as export proxies during the Holocene in the Dumont D'Urville Trough. The concave shape of the down-core profile shows that the opal:carbon ratio significantly increased during the early Holocene cool event, reached peak values during the mid-Holocene warm period, and then declined towards the onset of the late-Holocene Neoglacial. Opal:carbon ratios in diatoms can be affected by diatom species (Abelmann, et al., 2006; Smetacek, et al., 2004), growth rates (Assmy et al., 2006; Assmy et al., 2007), and iron availability (Armand, et al., 2008; Hutchins and Bruland 1998; Mosseri et. al., 2008; Takeda, 1998). The high productivity and particle flux suggest that iron was not limited, and iron sources are not thought to have limited productivity during the Holocene (Vaillancourt et al., 2003), at least early on in the growing season, with sources including Aeolian transport, melting ice, coastal sediments and transport of Upper Circumpolar Deep Water (UCDW) across the shelf (Sambrotto et al., 2003). Larger diatom species such as *F. kerguelensis* (Figure 7.3) display an almost identical pattern to the down-core variations in opal:carbon ratios. This shift in diatoms is a result of the climate driven shortening of sea ice coverage in early spring and lengthening of the phytoplankton growing season (Crosta et al., 2005) leading to *F. kerguelensis* out-competing the sea ice associated *Fragilariopsis curta* as the dominant diatom species. The *F. kerguelensis* profile is similar to other large diatom species but *F. kerguelensis* is presented here as it is the dominant larger diatom species during the mid-Holocene warm period (Crosta et al., 2007). *Fragilariopsis kerguelensis* is considered a slow growing species (Assmy, et al., 2006; Assmy, et al., 2007) and it's robust structure compared to the more fragile, pennate or needle-like diatom species gives it a higher opal:carbon ratio (Armand et al., 2008). In

addition, field studies in the Southern Ocean observed the highest recorded opal:carbon ratio in diatom blooms heavily dominated by *F. kerguelensis* (Queguiner et al., 1997). In addition to the longer growing seasons of the mid-Holocene warm period giving rise to dominance of *F. kerguelensis*, the slower and but longer period of diatom growth resulted in higher silicification of *Fragilariopsis* species and *Corethron pennatum* (Denis et al., 2006), perhaps exacerbating the effect on the opal:carbon ratios than just a change in diatom community composition.

Although we can not rule out differential preservation in this core based on the inferred differences in redox conditions, it is not suspected that the opal or carbon content of core MD03-2601 was significantly affected by variable preservation along the Holocene. Strong changes in degradation would have affected the opal:carbon ratios, with opal preferentially degrading over carbon (DeMaster et al., 1996) as opal is well preserved in diatom dominated environments of rapid export. However, the opal:carbon ratio appears to be principally affected by changes to diatom species (see above) and shows no variation consistent with the redox ($Mo_{auth}$ and $U_{auth}$) or deep water ventilation proxies (Denis et al., submitted). Similarly, the carbon:nitrogen ratio is around 7-8 all core long (data not shown). Heavier degradation of organic material would have increased the carbon:nitrogen ratio when preferential degradation of organic nitrogen during diagenesis occurred (Ganeshram et al., 1999; Hedges et al., 1986; Rosenfeld, 1981).

## 7.6 Conclusions

This study of core MD03-2601 was a useful case to identify how useful paleoproductivity proxies are for reconstructing export flux in regions of high sediment focusing.

Normalisation of the traditional mass accumulation rate calculations with $^{230}Th$ provides more the estimation of the preserved vertical fluxes. In despite of error bars associated to the $^{230}Th$ normalisation method, the reconstructed biogenic fluxes are in agreement with modern studies.

After ruling out changes in preservation affecting the carbon and opal flux reconstructions, we believe that the variations of preserved fluxes are representative of produced/exported biogenic flux variations in the Dumont D'Urville trough. Our data show higher fluxes of carbon and opal during the mid-Holocene warm period, and during the late Holocene Neoglacial period.

Although the down core $Ba_{XS}$ profile traces some of the changes in carbon flux, this paleoproductivity proxy fails as a quantitative indicator of carbon export due to changes in the redox conditions of the sediment that were inferred using the redox sensitive elemental proxies Mo and U.

The increase in opal:carbon ratios during the mid-Holocene optimum is linked to changes in the diatom assemblages towards larger diatom species, such as *F. kerguelensis* that export more opal per unit carbon. These species dominated due to the extended open water conditions during this climatic period.

## 7.7 References

Anderson, R. F., et al. (2002), The Southern Ocean's biological pump during the Last Glacial Maximum, Deep-Sea Research Part Ii-Topical Studies in Oceanography, 49, 1909-1938.

Anderson, R. F., et al. (1998), Late-Quaternary changes in productivity of the Southern Ocean, Journal of Marine Systems, 17, 497-514.

Armand, L. K., Cornet-Barthaux, V., Mosseri, J. and Queguiner, B. (2008) Late summer diatom biomass and community structure on and around the naturally iron-fertilised Kerguelen Plateau in the Southern Ocean. *Deep-Sea Research II*, 55, 653-676.

Bacon, M. P., and R. F. Anderson (1982), Distribution of thorium isotopes between dissolved and particulate forms in the deep sea, Journal of Geophysical Research 87, 2045–2056.

Bareille, G. et al. (1998), Glacial-interglacial changes in the accumulation rates of major biogenic components in Southern Indian Ocean sediments, Journal of Marine Systems, 17, 527-539.

Bentaleb, I., et al. (1996), Organic carbon isotopic composition of phytoplankton and sea-surface pCO2 reconstructions in the Southern Indian Ocean during the last 50,000 yr, Organic Geochemistry, 24, 399-410.

Beucher, C., P. Tréguer, A.M. Hapette, R. Corvaisier, N. Metzl, JJ. Pichon (2004) Intense summer Si recycling in the surface Southern Ocean, Geophysical Research Letters, 31, L09305, doi: 10.1029/2003GL018998.

Bishop, J. K. (1988) The barite-opal-organic carbon association in oceanic particulate matter. *Nature*, 332, 341-343.

Calvert, S. E., and T. F. Pedersen (1993), Geochemistry of recent oxic and anoxic marine sediments: implications for the geological record, Marine Geology, 113, 67-88.

Carson, D. S., et al. (in-prep) Particulate barium transformations and fluxes in the coastal Antarctic sea ice environment. *For submission to Deep Sea Research.*

Chase, Z., et al. (2003), Accumulation of biogenic and lithogenic material in the Pacific sector of the Southern Ocean during the past 40,000 years, Deep-Sea Research Part Ii-Topical Studies in Oceanography, 50, 799-832.

Crosta, X., et al. (1998), Application of modern analog technique to marine Antarctic diatoms: Reconstruction of maximum sea-ice extent at the last glacial maximum, Paleoceanography, 13, 284-297.

Crosta, X., and A. Shemesh (2002), Reconciling down core anticorrelation of diatom carbon and nitrogen isotopic ratios from the Southern Ocean, Paleoceanography, 17.

Crosta, X., et al. (2002), Late quaternary variations of elemental ratios (C/Si and N/Si) in diatom-bound organic matter from the Southern Ocean, Deep-Sea Research Part Ii-Topical Studies in Oceanography, 49, 1939-1952.

Crosta, X., et al. (2004), Late Quaternary sea ice history in the Indian sector of the Southern Ocean as recorded by diatom assemblages, Marine Micropaleontology, 50, 209-223.

Crosta, X., et al. (2005a), Major factors controlling Holocene d13Corg changes in a seasonal sea-ice environment, Adelie Land, East Antarctica, Global Biogeochemical Cycles, 19, doi:10.1029/2004GB002426.

Crosta, X., et al. (2005b), Nutrient cycling in the Indian sector of the Southern Ocean over the last 50,000 years, Global Biogeochemical Cycles, 19, doi:10.1029/2004GB002344.

Crosta, X., Debret, M., Denis, D., Courty, M.A. and Ther, O. (2007) Holocene long- and short-term climate changes off Adélie Land, East Antarctica. Geochemistry, Geophysics, Geosystems, 8(11), Q11009, doi: 10.1029/2007GC001718.

Crosta, X., Denis, D. and Ther, O. (2008) Sea ice seasonality during the Holocene, Adelie Land, East Antarctica. Marine Micropaleontology, 66, 222-232.

De La Rocha, C. L., et al. (1998), Silicon-isotope composition of diatoms as an indicator of past oceanic change, Nature, 395, 680-683.

De Santis, L., et al. (2003), Seismo-stratigraphic analysis of the Wilkes Land continental margin (East Antarctica): Influence of glacially driven processes on the Cenozoic deposition, Deep Sea Research Part II: Topical Studies in Oceanography, 50, 1563-1594.

Dehairs, F., Baeyens, W. and Goeyens, L. (1992) Accumulation of suspended barite at mesopelagic depths and export production in the Southern Ocean. *Science,* 258, 1332-1335.

Dehairs, F., et al. (2000), Export production in the Bay of Biscay as estimated from barium - barite in settling material: a comparison with new production, Deep-Sea Research Part I-Oceanographic Research Papers, 47, 583-601.

DeMaster, D. J., et al. (1996), Preservation efficiencies and accumulation rates for biogenic silica and organic C, N, and P in high-latitude sediments: The Ross Sea, Journal of Geophysical Research-Oceans, 101, 18502-18518.

Denis, D., et al. (2008), Glacier and deep current dynamics and their imprints on Holocene sedimentary record, Adelie Land, East Antarctica Margin, *Submitted to Quaternary Science Reviews.*.

Denis, D., et al. (2006), Seasonal and subseasonal climate changes recorded in laminated diatom ooze sediments, Adelie Land, East Antarctica, The Holocene, 16, 1137-1147.

Dézileau, L. et al. (2000), Evidence for strong sedment redistribution by bottom currents along the southeast Indian Ridge, Deep-Sea Research I, 47, 1899-1936.

Dymond, J., et al. (1992), Barium in deep-sea sediment: A geochemical proxy for paleoproductivity, Paleoceanography, 7, 163-181.

Dymond, J., and R. Collier (1996), Particulate barium fluxes and their relationships to biological productivity, Deep-Sea Research Part Ii-Topical Studies in Oceanography, 43, 1283-&.

Elderfield, H., and R. E. M. Rickaby (2000), Oceanic Cd/P ratio and nutrient utilization in the glacial Southern Ocean, Nature, 405, 305-310.

Ellwood, M. J., and K. A. Hunter (2000), Variations in the Zn/Si record over the last interglacial glacial transition, Paleoceanography, 15, 506-514.

Erickson, B. E. and Helz, G. R. (2000) Molybdenum (VI) speciation in sulfidic waters: stability and lability of thiomolybdates. *Geochimica et Cosmochimica Acta*, 64, 1149-1158.

Fagel, N., et al. (1999), Advective excess Ba transport as shown from sediment and trap geochemical signatures, Geochimica Et Cosmochimica Acta, 63, 2353-2367.

Fagel, N., et al. (2004), Reconstructing export production at the NE Atlantic Margin: potential and limits of the Ba proxy, Marine Geology, 204, 11-25.

Fitton, J. G., et al. (1998), Volcanic rocks from the Southeast Greenland Margin at 63oN: Composition, petrogenesis, and mantle sources, Proceedings of the Ocean Drilling Programme, Scientific Results, 152, 331-350.

Francois, R., and M. A. Altabet (1992), Glacial to interglacial changes in surface nitrate utilisation in the Indian sector of the Southern Ocean as recorded by sediment d15N, Paleoceanography, 7, 589-606.

Francois, R., et al. (1997), Contribution of Southern Ocean surface-water stratification to low atmospheric CO2 concentrations during the last glacial period, Nature, 389, 929-935.

Francois, R., et al. (2004), Th-230 normalization: An essential tool for interpreting sedimentary fluxes during the late Quaternary, Paleoceanography, 19, PA1018, doi:1010.1029/2003PA000939.

Francois, R., et al. (1995), Biogenic Barium Fluxes to the Deep-Sea - Implications for Paleoproductivity Reconstruction, Global Biogeochemical Cycles, 9, 289-303.

Ganeshram, R. S., et al. (1995), Large Changes in Oceanic Nutrient Inventories from Glacial to Interglacial Periods, Nature, 376, 755-758.

Ganeshram, R. S., and T. F. Pedersen (1998), Glacial-interglacial variability in upwelling and bioproductivity off NW Mexico: Implications for quaternary paleoclimate, Paleoceanography, 13, 634-645.

Hutchins, D. A. and Bruland, K. W. (1998) Iron-limited diatom growth and Si:N uptake ratios in a coastal upwelling regime. *Nature*, 393, 561-564.

Helz, G. R., Miller, C. V., Charnock, J. M., Mosselmans, J. F. W., Pattrick, R. A. D., Garner, C. D., and Vaughan, D. J. (1996) Mechanisms of molybdenum removal from the sea and its concentration in black shales: EXAFS evidence. *Geochimica et Cosmochimica Acta*, 60, 3631-3642.

Hodell, D. A., et al. (2001), Abrupt cooling of Antarctic surface waters and sea ice expansion in the South Atlantic sector of the Southern Ocean at 5000 cal yr BP, Quaternary Research, 56, 191-198.

Hughen, K. A., et al. (2004), Marine04 Marine radiocarbon age calibration, 26-0 ka BP, Radiocarbon, 46, 1059-1086.

Kumar, N., et al. (1995), Increased Biological Productivity and Export Production in the Glacial Southern-Ocean, Nature, 378, 675-680.

Laws, R. A. (1983), Preparing strewn slides for quantitative microscopical analysis: A test using calibrated microspheres, Micropaleontology, 24, 60-65.

McManus, J., et al. (1998), Geochemistry of barium in marine sediments: Implications for its use as a paleoproxy, Geochimica Et Cosmochimica Acta, 62, 3453-3473.

McManus, J., Dymond, J., Dunbar, R. B. and Collier, R. W. (2002) Particulate barium fluxes in the Ross Sea. *Marine Geology*, 184, 1-15.

McManus, J., Berelson, W. M., Severmann, S., Poulson, R. L., Hammond, D. E., Klinkhammer, G. P. and Holm, C. (2006) Molybdenum and uranium geochemistry in continental margin sediments: Paleoproxy potential. *Geochimica et Cosmochimica Acta*, 70(18), 4643-4662.

Menden-Deuer, S. and E.J. Lessard (2000), Carbon to volume relationships for dinoflagellates, diatoms and other protist plankton, Limnology and Oceanography, 45(3), 569-579.

Morford, J. L. and Emerson, S. (1999) The geochemistry of redox sensitive trace metals in sediments. *Geochimica et Cosmochimica Acta*, 63, 1735-1750.

Morford, J. L., Emerson, S. R., Breckel, E. J. and Kim, S. H. (2005) Diagenesis of oxyanions (V, U, Re and Mo) in pore waters and sediments from a continental margin. *Geochimica et Cosmochimica Acta*, 69, 5021-5032.

Mortlock, R. A., and P. N. Froelich (1989), A Simple Method for the Rapid-Determination of Biogenic Opal in Pelagic Marine-Sediments, Deep-Sea Research Part a-Oceanographic Research Papers, 36, 1415-1426.

Mosseri, J., Queguiner, B, Armand. L. and Cornet-Barthaux, V. (2008) Impact of iron on silicon utilization by diatoms in the Southern Ocean: A case study of Si/N cycle decoupling in a naturally iron-enriched area. *Deep-Sea Research II*, 55, 801-819.

Muller, P. J., and R. Schneider (1993), An Automated Leaching Method for the Determination of Opal in Sediments and Particulate Matter, Deep-Sea Research Part I-Oceanographic Research Papers, 40, 425-444.

Nielsen, S. H. H., et al. (2004), Holocene climate in the Atlantic Sector of the Southern Ocean: controlled by insolation or oceanic circulation?, Geology, 32, 317-320.

Nurnberg, C. C., et al. (1997), Barium accumulation in the Atlantic sector of the Southern Ocean: Results from 190,000-year records, Paleoceanography, 12, 594-603.

Queguiner, B., Treguer, P., Peeken, I. and Scharek, R. (1997) Biogeochemical dynamics and the silicon cycle in the Atlantic sector of the Southern Ocean during austral spring 1992. *Deep-Sea Research II*, 44, 69-89.

Robinson, R. S., et al. (2005), Diatom-bound N-15/N-14: New support for enhanced nutrient consumption in the ice age subantarctic, Paleoceanography, 20.

Rosenthal, Y., et al. (2000), Southern Ocean contributions to glacial-interglacial changes of atmospheric pCO(2): An assessment of carbon isotope records in diatoms, Paleoceanography, 15, 65-75.

Sambrotto, R. N., Matsuda, A., Vaillancourt, R., Brown, M., Langdon, C., Jacobs, S. S. and Measures, C. (2003) Summer plankton production and nutrient consumption patterns in the Mertz Glacier Region of East Antarctica. *Deep-Sea Research II*, 50, 1393-1414.

Schenau, S. J., et al. (2001), Barium accumulation in the Arabian Sea: Controls on barite preservation in marine sediments, Geochimica Et Cosmochimica Acta, 65, 1545-1556.

Sigman, D. M., and E. A. Boyle (2000), Glacial/interglacial variations in atmospheric carbon dioxide, Nature, 407, 859-869.

Suman, D. and Bacon, M. P. (1989) Variations in Holocene sedimentation in the North American Basin determines from 230Th measurements. *Deep Sea Research. Part A,* 36, 869-878.

Takeda, S. (1998) Influence of iron availability on nutrient consumption ratio of diatoms in oceanic waters. *Nature*, 393, 774-777.

Vaillancourt, R. D., Sambrotto, R. N., Green, S. and Matsuda, A. (2003) Phytoplankton biomass and photosynthetic competency in the summertime Mertz Glacier Region of East Antarctica. *Deep-Sea Research II*, 50, 1415-1440.

Wolff, E. W., et al. (2006), Southern Ocean sea-ice extent, productivity and iron flux over the past eight glacial cycles, Nature, 440, 491-496.

Wright, S. W., and R. L. van den Enden (2000), Phytoplankton community structure and stocks in the East Antarctic marginal ice zone (BROKE survey,

January-March 996) determined by CHEMTAX analysis of HPLC pigment signatures, Deep Sea Research Part II: Topical Studies in Oceanography, 47, 2363-2400.

Zheng, Y., Anderson, R. F., van Geen, A. and Kuwabara, J. (2000) Authigenic molybdenum formation in marine sediments: a link to pore water sulphide in the Santa Barbara Basin. *Geochimica et Cosmochimica Acta*, 64, 4165-4178.

# 8 Conclusions

The results of this study have identified some of the key mechanisms controlling present day biogeochemical processes that affect productivity and export production in the coastal Antarctic sea ice environment. Understanding more about such processes in sea ice, surface waters and the sediment surface that affect geochemical signatures that are preserved in sediments, lead us towards developing more accurate reconstructions of the past surface ocean (productivity, export production, sea ice cover, etc) based on isotopic and elemental inspection of Southern Ocean sediment cores. Understanding such mechanisms may also lead to an understanding of how reduced sea ice extent in the future, a result of the warming Western Antarctic Peninsula, may effect the seasonality of this environment.

In addition to the work in Ryder Bay and Marguerite Bay, the validity of carbon, opal, and $Ba_{XS}$ proxies as tracers of changes in productivity in a continental shelf Antarctic sediment core heavily affected by sediment focusing was carried out. This investigation showed that using careful correction of lateral inputs of material ($^{230}Th$), and applying redox sensitive element proxies ($Mo_{auth}$ and $U_{auth}$), changes in Holocene productivity and export production could be confidently reconstructed, and the results are consistent with the regional climatic phases known to have existed during the last 12,000 years.

## 8.1 Productivity and Particle Flux

The two growing seasons had certain similar characteristics:

- A ~4 month duration
- A two peak chlorophyll, POC and PON characteristic
- High levels of nutrient utilisation

However, there were also significant differences between the two seasons:

- Extended sea ice cover caused the growing season to start ≥1 month later for the 05/06 season compared to the 04/05 season;

- More freshwater delivered to the surface during the 05/06 season resulted in a more stratified water column;
- Significantly lower particle flux occurred during the 05/06 growing season.

Gaps in available data have precluded a full comparison between the two seasons, but nonetheless several conclusions may still be drawn from this study.

High standing stocks of POC and PON in sea ice suggest that organic matter from sea ice may contribute to not only the seeding of the spring bloom in this region, but may also contribute to the particle flux in this environment. Sea ice not only exerts control on the timing of the spring bloom, but in conjunction with glacier melt, the freshwater input appears to significantly affect the stability of the water column and the characteristics of the growing season. More freshwater input appears to reduce the delivery of nutrients to the surface water, resulting in cumulatively less nutrients being available for utilisation over the course of the season. This therefore reduces the total amount of production and export over the growing season, reducing the drawdown of major nutrients such as $CO_2$, $NO_3$ and $PO_4$.

The two peak characteristic of each growing season may be explained by grazing pressures during the mid-season decline in biomass and elevation of $NH_4$. This appears to lead to elevated levels of regenerated production during the latter period of the growing season. Estimated export efficiency at this site is very low, consistent with other studies in this region. This is as a result of efficient grazing on new primary production, and the relatively long retention time of material in the stratified water column, that leads to increased remineralisation and regenerated production during the latter stages of the growing season.

Seasonal progression of carbon:nitrogen ratios and opal:carbon ratios in sinking particles show increases with depth and elevated levels during winter. The increasing carbon:nitrogen ratios with depth and during winter are related to degradation and remineralisation of organic matter, as organic nitrogen is preferentially degraded over organic carbon.

The elevated opal:carbon ratios with depth may be affected in a similar way by degradation, but also may be due to the smaller diatom species (e.g. *Corethron pennatum*), that have a lower opal:carbon ratio not being exported as efficiently as larger diatoms that have a higher opal:carbon ratio. The higher opal:carbon ratios in winter, however, are likely a result of efficient degradation of carbon, compared to opal, of the slow growing, convalescing, diatom communities that exist under sea ice.

## 8.2 Carbon and $\delta^{13}C$ in the Coastal Antarctic Sea Ice Environment

$\delta^{13}C$, although classically used as a proxy for surface water $pCO_2$, shows extreme variability over the course of a season in both sea ice and surface waters, with the amplitude of changes ~10 ‰, almost the entire marine range of $\delta^{13}C$ seen in the global ocean.

Sea ice $\delta^{13}C_{POC}$ appears to be controlled more by post-production decomposition processes and not a high degree of nutrient utilisation as other studies may have inferred and there is no evidence of this material contributing to the seasonal flux of material in sediment traps.

$[CO_{2(aq)}]$ and $\delta^{13}C\text{-}CO_2$ do not appear to influence $\delta^{13}C_{org}$, instead the ~10 ‰ shifts seen in surface waters appear driven by seasonal shifts in diatom assemblages and the subsequent shift to lower SA:V ratios of the assemblages during the isotopic shifts, possibly exacerbated by changes to internal diatom biochemical pathways for carbon fixation and changing growth rates.

Although much of the surface suspended material (including certain diatom species) are not exported to depth, the $\delta^{13}C$ composition of surface suspended organic carbon is faithfully transferred to depth.

Sediment $\delta^{13}C$ is therefore not a reliable proxy for $pCO_2$, unless changes in diatom assemblages, documented in sediments or sediment cores, can be used to assess the subsequent changes in $\varepsilon_p$ during surface water productivity. This would require a large programme of laboratory and field work to accurately document $\varepsilon_p$. based on each diatom species or group.

### 8.3 Nitrogen and $\delta^{15}N$ in the Coastal Antarctic Sea Ice Environment

This study documents that although sinking $\delta^{15}N_{org}$ can be used to reconstruct the degree of $NO_3$ utilisation in surface waters, it is not appropriate to directly link this proxy to the quantity of carbon exported from surface waters. In addition, the enrichment of $^{15}N$ in sea ice is controlled by post-production decomposition processes rather than the effect of high nutrient utilisation, but there is no evidence from the $\delta^{15}N$ of sediment trap material that this heavily influenced the composition of the seasonal flux.

The two contrasting growing seasons observed in this study led to significantly different amounts of organic carbon and nitrogen to be exported from the euphotic zone, but each season displayed similar levels of % nutrient utilisation. It was the stability of the surface waters, controlled by sea ice and other sources of freshwater input (e.g. glaciers) that played the major role in the seasonal evolution of surface water $\delta^{15}N_{PON}$ and total C and N export fluxes. During the 04/05 seaons, the dynamic nature of the surface waters resulted in high frequency inputs of nutrients to the surface as a result of delivery of UCDW through upwelling or vertical mixing providing more nutrients for conversion into organic matter and subsequent export. The 05/06 season, in contrast, consisted of a more stable water column with very few small inputs of nutrients to the surface and material was retained at the surface for longer.

These apparently "steady state" dynamics (04/05 season) and "closed system dynamics" (05/06) season were then tested using the $\Delta\delta^{15}N$ predictive model. The seasonally integrated $\delta^{15}N$ values from sediment traps and surface sediments are consistent with the "steady-state" nitrate utilisation during 04/05 and the "closed system" model during 05/06, reflecting the observed oceanographic characteristics of each season.

Although the $\delta^{15}N$ value in sediment is consistent with the surface water $\delta^{15}N$ and nutrient utilisation from the models, the proxy for utilisation of nitrate does not reflect the absolute changes in C export fluxes. It is therefore necessary to consider this scenario when making connections between nitrate utilisation and changes in atmospheric $CO_2$.

## 8.4 Barium Biogeochemistry in the coastal Antarctic Sea Ice Environment

The results from this investigation into the biogeochemical cycling of Ba in the coastal Antarctic sea ice environment provides important information on the seasonal evolution of the different pools of $Ba_{XS}$ (the labile fraction, barite, and $Ba_{XS}$ associated with refractory organic matter) in response to productivity in sea ice, surface waters and during export of material to depth.

Standing stocks of $Ba_{XS}$ in sea ice are consistently an order of magnitude higher than surface waters and display higher than average Ba:POC ratios than surface waters. Although there is no direct evidence to link this to material exported in sediment traps, it is hard to ignore such high amounts of $Ba_{XS}$ that may affect the $Ba_{XS}$ versus C flux algorithm used to reconstruct carbon export. Shallower sediment traps placed underneath sea ice may aid our understanding of the fate of this material, but it is very difficult to successfully deploy shallow sediment traps in this environment due to the frequency of icebergs that may collide with such equipment.

$Ba_{XS}$ formation in surface waters definitely appears related to productivity, but appears to peak during periods of early decay of phytoplankton when barite is formed and becomes the dominant pool of $Ba_{XS}$. This is observed during the mid-growing season declines in biomass (associated with grazing) and at the end of the season when productivity ceases and the remaining material in surface waters is degraded. These observations give us a good understanding of the seasonal cycle of surface water Ba and C, the precursor material that then sinks and becomes further enriched in $Ba_{XS}$ and depleted in carbon before settling on the sediment surface.

This study therefore provides compelling evidence that the formation of barite in the water column is a result of decaying organic matter and precipitation of barite in supersaturated micro-environments, as described in earlier works.

Although previous studies on the continental shelf of Antarctica and continental margin environments have failed to observe relationships between $Ba_{XS}$ and C flux, this study provides data showing that the flux of $Ba_{XS}$ relative to carbon in the coastal Antarctic sea ice environment is consistent with algorithms published for the open ocean.

Based on this data, a conceptual model for the biogeochemical cycling of Ba on a seasonal timescale was developed and consists of the following:

(a) **Winter -** Low levels of fresh production in sea ice matrix (green) with low $Ba_{XS}$:$C_{org}$ composed mainly of labile Ba. A small amount of particulate material is held in the deep winter mixed layer that has a high $Ba_{XS}$:$C_{org}$ ratio from efficient biodegradation of organic material (brown) forming barite through precipitation.

(b) **Late Winter -** During late winter, the biogenic material in sea ice goes through rapid degradation and production cycles, resulting in high standing stocks of $Ba_{XS}$, barite and refractory bound Ba. Primary

production starts in surface waters below, where the material has a low $Ba_{XS}$:$C_{org}$ and is composed mainly of labile Ba.

(c) **Spring** - During early spring, the summer shallow mixed layer forms, sea ice retreat seeds highly degraded organic material containing high $Ba_{XS}$, barite and refractory bound Ba to surface waters. This mixes with fresh organic material produced by the spring bloom, which has a low $Ba_{XS}$:$C_{org}$ ratio and is composed mainly of labile Ba. This is the time of high standing stocks of phytoplankton in the shallow mixed layer, and the highest period of export flux where fresh surface water organic material degrades while sinking, forming larger aggregates, and an increase of $Ba_{XS}$:$C_{org}$ with depth occurs due to barite precipitation during organic matter degradation. During the highly productive spring bloom, barite can also be formed in surface waters by degrading organic matter and barite precipitation during periods of grazing and hiatuses in production, resulting in the Ba pool becoming enriched in barite and refractory bound Ba. This period can also be influenced by upwelling of nutrient rich water which can "reset" the step wise process of labile Ba formation and barite precipitation in the euphotic zone.

(d) **Summer/Autumn** - During summer and autumn, production declines and the organic material in surface waters becomes highly degrading resulting in an increase in $Ba_{XS}$:$C_{org}$ and the Ba pool to become dominated by barite through precipitation and enriched in refractory bound Ba.

## 8.5 Summary of Proxy Findings in Ryder Bay

The application of $\delta^{13}C$ , $\delta^{15}N$ and barium in the coastal Antarctic sea ice environment has opened this environment up to thorough geochemical inspection. The findings however, do question the validity of some of these proxies for paleo-$pCO_2$ concentrations ($\delta^{13}C$), nutrient utilisation ($\delta^{15}N$) and carbon export (Ba) both on the continental shelf of Antarctica and the open Southern Ocean.

In this environment shifts in diatom assemblages on a seasonal timescale affect the fractionation factor of carbon fixation so that the $\delta^{13}C$ of freshly produced and sinking organic matter, does not relate to the concentration of $CO_2$ in the surface ocean, the fundamental relationship that this proxy is based on. This raises the question as to whether historical changes in $\delta^{13}C$ in Southern Ocean sediments was in fact a shift in dissolved $CO_2$, or perhaps subtle changes in diatom assemblages as a response to environmental factors.

In addition, the $\delta^{15}N$ of organic matter does trace the relative utilisation of $NO_3$ on a seasonal timescale, when the surface ocean is in either a closed system or open system in terms of nutrient dynamics. However, the $\delta^{15}N$ fails to recognise the significant differences in absolute quantities of exported organic matter (i.e. nutrient drawdown) that has similar $\delta^{15}N$ values. This weakens the argument connecting nutrient utilisation and $CO_2$ drawdown during glacial to interglacial cycles that is often used in paleoceanographic papers on the Southern Ocean to explain changes in atmospheric $CO_2$ concentrations.

Ba, however, does seem to work as a proxy for organic carbon export, when data from this study are applied to the classic correlations used to produce the current preliminary algorithm for using Ba to estimate C export (Figure 6.13). This study also enhances our knowledge of Ba cycling in surface waters, the precursor to intense barite formation in sinking organic matter, on a seasonal timescale. The Ba data also open up the possibility that barite is formed by abiotic precipitation in sea ice brine channels, although this remains speculative without further data on barite crystal morphology.

Further studies in Ryder Bay, to prolong the time-series presented in this work, should provide more robust conclusions for the arguments raised throughout this thesis.

## 8.6 Reconstructing Paleoproductivity in Core MD03-2601

The study of core MD03-2601 was a useful case to identify how useful paleoproductivity proxies are for reconstructing export flux in regions of high sediment focusing.

Normalisation of the traditional mass accumulation rate calculations with $^{230}Th$ provides more the estimation of the preserved vertical fluxes. After ruling out changes in preservation affecting the carbon and opal flux reconstructions, it is believed that the variations of preserved fluxes are representative of produced/exported biogenic flux variations in the Dumont D'Urville trough. The data show higher fluxes of carbon and opal during the mid-Holocene warm period, and during the late Holocene Neoglacial period.

Although the down core $Ba_{XS}$ profile traces some of the changes in carbon flux, this paleoproductivity proxy fails as a quantitative indicator of carbon export due to changes in the redox conditions of the sediment that were inferred using the redox sensitive elemental proxies $Mo_{auth}$ and $U_{auth}$.

The increase in opal:carbon ratios during the mid-Holocene optimum is linked to changes in the diatom assemblages towards larger diatom species, such as *F. kerguelensis* that export more opal per unit carbon. These species dominated due to the extended open water conditions during this climatic period.

It therefore seems that high accumulation rate sediment cores can be useful for studying past paleoproductivity changes at high resolution, as long as the effects of sediment focusing can be constrained and removed from any reconstructions. In addition, high flux environments may be subject to reducing conditions perpetuating at the sediment surface, so it is essential to also apply proxies that identify this process, especially when using redox sensitive tracers such as Ba.

## 8.7 Future Considerations

Although this project has provided useful information on the biogeochemical cycling of elemental and isotopic tracers of productivity and particle flux, the study only lasted for two growing seasons. The coastal Antarctic sea ice environment is characteristically subject to high inter-annual variability, as documented in the RaTS biological programme and the Palmer LTER programme (referenced throughout this thesis). Therefore, in order to fully constrain the effects that the physical, biological and chemical characteristics of a growing season have on the geochemical proxies investigated here, a longer time-series is essential. Over time this should dilute the effect of inter-annual variability and confirm or disprove some of the conclusions drawn from this two year study on the elemental and isotopic biogeochemical cycling in this dynamic environment. Funding has been granted to continue the sea ice, surface water and sediment trap time series for the next 3 years. This will allow the generation of further data similar to that presented in this project to improve our understanding of how the biogeochemical cycling of carbon, nitrogen, opal and barium responds to growing seasons that are controlled by factors such as sea ice, water column properties, grazing and future climate change.

# 9 Appendices

## 9.1 Appendix 1. Full list of sampling events during the 2004/2005 field season.

| Event | Date | Location and Depth |
|---|---|---|
| RaTS-001 | 05/12/2004 | RaTS Site – 15m |
| RaTS-002 | 08/12/2004 | RaTS Site – 15m |
| RaTS-003 | 10/12/2004 | RaTS Site – 15m |
| RaTS-004 | 13/12/2004 | RaTS Site – 15m |
| RaTS-005 | 15/12/2004 | RaTS Site – 15m |
| RaTS-006 | 20/12/2004 | RaTS Site – 15m |
| RaTS-007 | 22/12/2004 | RaTS Site – 15m |
| RaTS-008 | 29/12/2004 | RaTS Site – 15m |
| RaTS-009 | 31/12/2004 | RaTS Site – 15m |
| RaTS-010 | 05/01/2005 | RaTS Site – 15m |
| RaTS-011 | 07/01/2005 | RaTS Site – 15m |
| RaTS-012 | 10/01/2005 | RaTS Site – 15m |
| RaTS-013 | 13/01/2005 | RaTS Site – 15m |
| RaTS-014 | 17/01/2005 | RaTS Site – 15m |
| RaTS-015 | 19/01/2005 | RaTS Site – 15m |
| RaTS-016 | 21/01/2005 | RaTS Site – 15m |
| RaTS-017 | 28/01/2005 | RaTS Site – 15m |
| RaTS-018 | 01/02/2005 | RaTS Site – 15m |
| RaTS-019 | 12/02/2005 | RaTS Site – 15m |
| RaTS-020 | 21/02/2005 | RaTS Site – 15m |
| RaTS-021 | 28/02/2005 | RaTS Site – 15m |
| RaTS-022 | 14/03/2005 | RaTS Site – 15m |

## 9.2 Appendix 2. Full list of sampling events during the 2005/2006 field season.

| Event | Date | Location and Depth |
|---|---|---|
| RaTS-023 | 17/09/2005 | RaTS Site – 15m |
| RaTS-024 | 13/10/2005 | RaTS Site – 15m |
| RaTS-025 | 21/11/2005 | ~1m underneath sea ice sampling site |
| RaTS-026 | 23/11/2005 | ~1m underneath sea ice sampling site |
| RaTS-027 | 23/12/2005 | ~1m underneath sea ice sampling site |
| RaTS-028 | 28/12/2005 | RaTS site 2 – 15m |
| RaTS-029 | 04/01/2006 | RaTS site 2 – 15m |
| RaTS-030 | 06/01/2006 | RaTS site 2 – 15m |
| RaTS-031 | 10/01/2006 | RaTS site 2 – 15m |
| RaTS-032 | 13/01/2006 | RaTS site – 15m |
| RaTS-033 | 19/01/2006 | RaTS site – 15m |
| RaTS-034 | 24/01/2006 | RaTS site – 15m |
| RaTS-035 | 30/01/2006 | RaTS site – 15m |
| RaTS-036 | 02/02/2006 | RaTS site – 15m |
| RaTS-037 | 10/02/2006 | RaTS site – 15m |
| RaTS-038 | 13/02/2006 | RaTS site – 15m |
| RaTS-039 | 20/02/2006 | RaTS site 2 – 15m |
| RaTS-040 | 23/02/2006 | RaTS site – 15m |
| RaTS-041 | 27/02/2006 | RaTS site – 15m |
| RaTS-042 | 04/03/2006 | RaTS site – 15m |
| RaTS-043 | 08/03/2006 | RaTS site – 15m |
| RaTS-044 | 13/03/2006 | RaTS site 2 – 15m |
| RaTS-045 | 23/03/2006 | RaTS site – 15m |

## 9.3 Appendix 3. List of sea ice sampling events during the 2004/2005 and 2005/2006 field seasons.

| Sea Ice Event (2004/2005) | Date | Sea Ice Event (2005/2006) | Date |
|---|---|---|---|
| SI-001 | 10/12/2004 | SI-006 | 17/09/2005 |
| SI-002 | 13/12/2004 | SI-007 | 13/10/2005 |
| SI-003 | 15/12/2004 | SI-008 | 21/11/2005 |
| SI-004 | 17/12/2004 | SI-009 | 23/11/2005 |
| SI-005 | 19/12/2004 | SI-010 | 24/11/2005 |
| | | SI-011 | 28/11/2005 |
| | | SI-012 | 01/12/2005 |
| | | SI-013 | 06/12/2005 |
| | | SI-014 | 09/12/2005 |
| | | SI-015 | 20/12/2005 |

## 9.4 Appendix 4. List of Measured Parameters out with the RaTS programme measured for surface water and sea ice samples.

| Measured Parameters in Surface Waters and Sea Ice |
|---|
| Conductivity, temperature and Depth |
| Chlorophyll a and pheaopigment |
| Dissolved inorganic carbon (DIC and $pCO_2$) |
| Stable isotopic composition of DIC ($\delta^{13}$C-DIC) |
| Bulk particulate organic carbon (POC) |
| Stable isotopic composition of POC ($\delta^{13}$Corg) |
| Dissolved organic carbon (DOC) |
| Dissolved inorganic nitrogen ($NO_3$, $NO_2$, $NH_4$) |
| Stable isotopic composition of $NO_3$ ($\delta^{15}$N-$NO_3$, $\delta^{18}$O-$NO_3$) |
| Stable isotopic composition of $NH_4$ ($\delta^{15}$N-$NH_4$) |
| Bulk particulate organic nitrogen (PON) |
| Stable isotopic composition of PON ($\delta^{15}$Norg) |
| Dissolved inorganic nitrogen (DON) |
| Major Particulate Elements |
| Minor Particulate Elements |
| Dissolved Barium (Dissolved Ba) |
| Particulate Barium (Particulate Ba) |

## 9.5 Appendix 5. Sea ice time-series N data from the 04/05 and 05/06 growing season.

| Sea Ice Event (Date) | $NO_3$ (µmol) | $\delta^{15}N\text{-}NO_3$ (‰ vs air) | $NH_4$ (µmol) | Chl-*a* ($mg.m^{-3}$) | PON ($\mu mol.g^{-1}$) | $\delta^{15}N_{PON}$ (‰ vs air) |
|---|---|---|---|---|---|---|
| 001 | 3.90 | 5.92 | 2.08 | 0.07 | 9.35 | 6.82 |
| 002 | 1.62 | 2.85 | 1.21 | 0.01 | 9.00 | 7.31 |
| 003 | 5.77 | 3.62 | 1.72 | 1.54 | 6.55 | 7.44 |
| 004 | 2.63 | 4.39 | 4.66 | 0.47 | 6.93 | 8.82 |
| 005 | 2.29 | 4.34 | 1.72 | 0.26 | 4.07 | 6.40 |
| 006 | 13.47 | - | - | 4.53 | 4.60 | 2.80 |
| 007 | 1.70 | - | - | 0.64 | 3.55 | 4.53 |
| 008 | 2.15 | - | 1.43 | 2.77 | 2.96 | 5.54 |
| 009 | 9.08 | - | 0.51 | 1.66 | 2.68 | 6.29 |
| 010 | 1.43 | - | - | 1.04 | 3.92 | 5.01 |
| 011 | - | - | 0.37 | 1.33 | 2.97 | 5.21 |
| 012 | 3.79 | - | 0.82 | 1.02 | 3.30 | 7.39 |
| 013 | 1.06 | - | 0.19 | 1.17 | 3.01 | 7.53 |
| 014 | 0.98 | - | 0.13 | 0.91 | 2.14 | 5.97 |
| 015 | 1.14 | - | 0.16 | 1.77 | 2.45 | 9.67 |

## 9.6 Appendix 6. Surface water time series N data for the 04/05 growing season.

| Date | $NO_3$ (µmol) | $\delta^{15}N\text{-}NO_3$ (‰ vs air) | $NH_4$ (µmol) | Chl-*a* ($mg.m^{-3}$) | PON ($\mu mol.g^{-1}$) | $\delta^{15}N_{PON}$ (‰ vs air) |
|---|---|---|---|---|---|---|
| 05/12/2004 | 22.13 | 6.88 | 0.51 | 20.03 | 7.31 | 1.75 |
| 08/12/2004 | 12.33 | 7.52 | 3.66 | 16.84 | 11.41 | 6.46 |
| 10/12/2004 | 20.57 | 5.72 | 1.35 | 10.24 | 4.94 | 2.13 |
| 13/12/2004 | 8.52 | 8.36 | 2.33 | 24.76 | 9.83 | 3.20 |
| 15/12/2004 | 12.06 | 8.65 | 2.17 | 14.30 | 10.91 | 3.81 |
| 20/12/2004 | 12.09 | 6.62 | 0.66 | 12.05 | 7.39 | 2.84 |
| 22/12/2004 | 11.61 | 6.90 | | 13.16 | 7.39 | 3.03 |
| 29/12/2004 | 5.40 | 10.10 | 0.79 | 2.44 | 11.45 | 5.04 |
| 31/12/2004 | 15.25 | 6.64 | 4.49 | 10.73 | 6.71 | 4.07 |
| 05/01/2005 | 26.30 | 4.85 | 3.66 | 4.10 | 3.66 | 3.18 |
| 07/01/2005 | 14.25 | 5.89 | 0.31 | 10.67 | 7.47 | 3.62 |
| 10/01/2005 | 5.48 | 11.37 | 0.30 | 23.42 | 11.16 | 5.71 |
| 13/01/2005 | 18.25 | 5.76 | 2.89 | 5.44 | 5.19 | 5.07 |
| 17/01/2005 | 7.35 | 7.51 | | 16.88 | 11.10 | 4.30 |
| 19/01/2005 | 19.40 | 5.13 | 1.49 | 24.16 | 7.77 | 3.97 |
| 21/01/2005 | 3.85 | 8.13 | | 35.55 | 12.84 | 5.43 |
| 28/01/2005 | 13.98 | 6.16 | 1.01 | 15.01 | 5.80 | 3.68 |
| 01/02/2005 | 3.33 | 7.98 | 0.70 | 15.88 | 7.80 | 6.52 |
| 12/02/2005 | 22.96 | 5.48 | 2.62 | 2.58 | 2.07 | 0.10 |
| 21/02/2005 | 12.52 | 5.44 | 2.80 | 2.95 | 1.87 | 3.07 |
| 28/02/2005 | 9.25 | 5.51 | 3.10 | 1.38 | 1.57 | 1.99 |
| 14/03/2005 | 16.25 | 4.36 | 3.80 | 1.25 | 1.10 | 0.04 |

## 9.7 Appendix 7. Surface water time-series N data for the 05/06 growing season.

| Date | $NO_3$ (µmol) | $NH_4$ (µmol) | Chl-*a* ($mg.m^{-3}$) | PON ($\mu mol.g^{-1}$) | $\delta^{15}N_{PON}$ (‰ vs air) |
|---|---|---|---|---|---|
| 17/09/2005 | 23.54 | 0.40 | 0.12 | 0.23 | 5.10 |
| 13/10/2005 | 22.58 | 0.24 | 0.14 | 0.19 | 5.08 |
| 21/11/2005 | 33.70 | 0.81 | 0.50 | 0.67 | 5.98 |
| 23/11/2005 | 22.57 | | 0.60 | 0.92 | 4.95 |
| 23/12/2005 | 10.00 | 0.35 | 10.24 | 4.84 | 3.39 |
| 28/12/2005 | 15.32 | 0.27 | 13.07 | 4.89 | 2.25 |
| 04/01/2006 | 20.75 | 0.84 | 14.13 | 4.88 | 1.69 |
| 06/01/2006 | 14.27 | 0.30 | 25.74 | 9.17 | 5.89 |
| 10/01/2006 | 9.87 | 0.83 | 20.51 | 9.63 | 3.52 |
| 13/01/2006 | 10.23 | 0.88 | 22.16 | 10.02 | 5.54 |
| 19/01/2006 | 9.65 | 0.38 | 20.95 | 10.01 | 0.00 |
| 24/01/2006 | 11.73 | 1.11 | 16.39 | 7.36 | 4.30 |
| 30/01/2006 | 12.73 | 2.54 | 11.92 | 5.39 | 3.67 |
| 02/02/2006 | 12.59 | 2.28 | 13.48 | 4.23 | 3.11 |
| 10/02/2006 | 11.45 | 1.20 | 18.79 | 6.87 | 3.53 |
| 13/02/2006 | 10.97 | 1.36 | 17.09 | 6.36 | 3.76 |
| 20/02/2006 | 7.90 | 0.45 | 16.21 | 5.04 | 3.67 |
| 23/02/2006 | 7.07 | 0.95 | 20.07 | 7.42 | 4.89 |
| 27/02/2006 | 3.78 | 0.66 | 27.94 | 8.81 | 6.00 |
| 04/03/2006 | 10.91 | 2.37 | 12.21 | 4.56 | 5.24 |
| 08/03/2006 | 9.90 | 2.28 | 14.61 | 5.42 | 5.31 |
| 13/03/2006 | 2.26 | 0.93 | 11.49 | 4.89 | 4.83 |
| 23/03/2006 | 12.96 | 2.93 | 5.79 | 3.49 | 3.53 |

## 9.8 Appendix 8. Sediment Trap flux data and $\delta^{15}N_{org}$ from the RaTS Site throughout the duration of this study.

| Cup Opening Date | Mass Flux 200m (mg.m$^{-2}$/d$^{-1}$) | POC Flux 200m (µmol.m$^{-2}$/d$^{-1}$) | PON Flux 200m (µmol.m$^{-2}$/d$^{-1}$) | $\delta^{15}N_{org}$ 200m (‰ vs air) | Mass Flux 512m (mg.m$^{-2}$/d$^{-1}$) | POC Flux 512m (µmol.m$^{-2}$/d$^{-1}$) | PON Flux 512m (µmol.m$^{-2}$/d$^{-1}$) | $\delta^{15}N_{org}$ 512m (‰ vs air) |
|---|---|---|---|---|---|---|---|---|
| 26/1/05 | 1296.38 | 3430.39 | 394.19 | 4.46 | 1637.47 | 3564.67 | 457.58 | 4.40 |
| 7/2/05 | 1581.77 | 3845.11 | 503.55 | 4.12 | 1628.48 | 3524.76 | 465.53 | 4.04 |
| 21/2/05 | 1244.37 | 3214.52 | 410.79 | 4.02 | 2.13 | - | - | - |
| 1/3/05 | 1020.72 | 1826.84 | 246.98 | 4.12 | 0.84 | - | - | - |
| 1/4/05 | 21.58 | 31.41 | 4.65 | 5.47 | 0.13 | - | - | - |
| 1/5/05 | 0.10 | - | - | - | 0.19 | - | - | - |
| 1/6/05 | 0.02 | - | - | - | 0.06 | - | - | - |
| 15/7/05 | 0.30 | - | - | - | 0.32 | - | - | - |
| 1/9/05 | 0.23 | - | - | - | 0.40 | - | - | - |
| 1/10/05 | 0.07 | - | - | - | 0.16 | - | - | - |
| 1/11/05 | 0.23 | - | - | - | 0.19 | - | - | - |
| 15/11/05 | 0.23 | - | - | - | 0.17 | - | - | - |
| 29/11/05 | 0.45 | - | - | - | 0.34 | - | - | - |
| 6/12/05 | 0.70 | - | - | - | 1.17 | - | - | - |
| 13/12/05 | 2.17 | - | - | - | 0.81 | - | - | - |
| 20/12/05 | 1.20 | - | - | - | 0.61 | - | - | - |
| 27/12/05 | 1.33 | - | - | - | 0.79 | - | - | - |
| 3/1/06 | 0.32 | - | - | - | 0.16 | - | - | - |
| 18/1/06 | 0.58 | - | - | - | 4.84 | - | - | - |
| 1/2/06 | 2789.23 | 3341.96 | 457.90 | 4.12 | 294.93 | 453.08 | 60.00 | 3.55 |
| 18/2/06 | 140.39 | 537.00 | 84.97 | 2.95 | 174.89 | 438.47 | 65.66 | 2.92 |

## 9.9 Appendix 9. Sediment Trap flux data and $\delta^{15}N_{org}$ from the Deep Site throughout the duration of this study.

| Cup Opening Date | Mass Flux 123m (mg.m$^{-2}$/d$^{-1}$) | POC Flux 123m (µmol.m$^{-2}$/d$^{-1}$) | PON Flux 123m (µmol.m$^{-2}$/d$^{-1}$) | $\delta^{15}N_{org}$ 123m (‰ vs air) | Mass Flux 745m (mg.m$^{-2}$/d$^{-1}$) | POC Flux 745m (µmol.m$^{-2}$/d$^{-1}$) | PON Flux 745m (µmol.m$^{-2}$/d$^{-1}$) | $\delta^{15}N_{org}$ 745m (‰ vs air) |
|---|---|---|---|---|---|---|---|---|
| 26/1/05 | 419.00 | 2612.19 | 338.10 | 4.71 | 614.22 | 2880.83 | 388.43 | 4.11 |
| 7/2/05 | 115.15 | 645.11 | 85.07 | 4.45 | 12.47 | - | - | - |
| 21/2/05 | 241.91 | 775.87 | 104.03 | 4.10 | 4.25 | - | - | - |
| 1/3/05 | 100.35 | 380.76 | 52.61 | 4.47 | 0.46 | - | - | - |
| 1/4/05 | 109.27 | 238.48 | 33.93 | 4.28 | 0.30 | - | - | - |
| 1/5/05 | 154.41 | 335.63 | 48.05 | 4.24 | 0.36 | - | - | - |
| 1/6/05 | 78.83 | 166.59 | 23.44 | 4.29 | 0.11 | - | - | - |
| 15/7/05 | 43.18 | 93.75 | 13.62 | 5.56 | 0.11 | - | - | - |
| 1/9/05 | 34.17 | 48.43 | 8.40 | 5.37 | 0.13 | - | - | - |
| 1/10/05 | 55.59 | 193.49 | 20.10 | 5.62 | 0.05 | - | - | - |
| 1/11/05 | 117.64 | 220.43 | 29.35 | 4.94 | 0.29 | - | - | - |
| 15/11/05 | 69.63 | 144.10 | 18.41 | 5.33 | 0.29 | - | - | - |
| 29/11/05 | 71.93 | 141.85 | 17.99 | 5.40 | 0.39 | - | - | - |
| 6/12/05 | 77.29 | 177.17 | 21.68 | 5.27 | 0.70 | - | - | - |
| 13/12/05 | 172.87 | 579.64 | 68.36 | 6.43 | 1.54 | - | - | - |
| 20/12/05 | 88.55 | 699.69 | 65.92 | 5.69 | 1.76 | - | - | - |
| 27/12/05 | 174.90 | 776.65 | 103.49 | 4.83 | 1.18 | - | - | - |
| 3/1/06 | 302.03 | 1309.09 | 187.45 | 2.88 | 0.54 | - | - | - |
| 18/1/06 | 360.64 | 1587.73 | 213.14 | 2.61 | 0.31 | - | - | - |
| 1/2/06 | 242.59 | 1049.52 | 136.88 | 3.31 | 1413.38 | 3545.23 | 493.32 | 5.35 |